Insights into the comparative biological roles of *S. cerevisiae* nucleoplasmin-like FKBPs Fpr3 and Fpr4

by

Neda Savic
B.Sc. Portland State University, 2012

A Dissertation Submitted in Partial Fulfillment
of the Requirements for the Degree of

DOCTOR OF PHILOSOPHY

in the Department of Biochemistry and Microbiology

Supervisory Committee

Insights into the comparative biological roles of *S. cerevisiae* nucleoplasmin-like FKBPs Fpr3 and Fpr4

by

Neda Savic
B.Sc. Portland State University, 2012

Supervisory Committee

Dr. Christopher J. Nelson, Supervisor
Department of Biochemistry and Microbiology

Dr. Juan Ausio, Departmental Member
Department of Biochemistry and Microbiology

Dr. Caren C. Helbing, Departmental Member
Department of Biochemistry and Microbiology

Dr. Peter C. Constabel, Outside Member
Department of Biology

Abstract

The nucleoplasmin (NPM) family of acidic histone chaperones and the FK506-binding (FKBP) peptidyl proline isomerases are both linked to chromatin regulation. In vertebrates, NPM and FKBP domains are found on separate proteins. In fungi, NPM-like and FKBP domains are expressed as a single polypeptide in nucleoplasmin-like FKBP (NPL-FKBP) histone chaperones. *Saccharomyces cerevisiae* has two NPL-FKBPs: Fpr3 and Fpr4. These paralogs are 72% similar and are clearly derived from a common ancestral gene. This suggests that they may have redundant functions. Their retention over millions of years of evolution also implies that each must contribute non-redundantly to organism fitness. The redundant and separate biological functions of these chromatin regulators have not been studied. In this dissertation I take a systems biology approach to fill this knowledge gap.

First, I refine the powerful synthetic genetic array (SGA) method of annotating gene-gene interactions, making it amenable for the analyses of paralogous genes. Using these 'paralog-SGA' screens I define distinct genetic interactions unique to either Fpr3 or Fpr4, shared genetic interactions common to both paralogs, and masked genetic interactions which are direct evidence for processes where these enzymes are functionally redundant. I provide transcriptomic evidence that Fpr3 and Fpr4 cooperate to regulate genes involved in polyphosphate metabolism and ribosome biogenesis. I identify an important role for Fpr4 at the 5' ends of protein coding genes and the non-transcribed spacers of ribosomal DNA. Finally, I show that yeast lacking Fpr4 exhibit a genome instability phenotype at rDNA, implying that this histone chaperone regulates chromatin structure and DNA access at this locus. Collectively, these data demonstrate that Fpr3 and Fpr4 operate separately, cooperatively and redundantly to regulate a variety of chromatin environments. This work is the first comprehensive and comparative study of NPL-FKBP chaperones and as such represents a significant contribution to our understanding of their biological functions.

Table of Contents

List of Tables

List of Figures

List of Abbreviations

5-FOA	5-fluoroorotic acid
A. fumigatus	*Aspergillus fumigatus*
A. nidulans	*Aspergillus nidulans*
ADA	Ada2-Ada3-Ada4/Gcn5-Sgf29 histone acetyltransferase
Ada2	transcriptional adaptor 2
Ada3	transcriptional adaptor 3
Ahc1	ADA histone acetyltransferase component 1
Ahc2	ADA histone acetyltransferase component 2
Air1	arginine methyltransferase-interacting RING finger protein 1
ALCL	acute anaplastic large cell lymphoma
ALK	anaplastic lymphoma kinase
AML	acute myeloid leukemia
Ani1	*Sz. pombe* CENP-A N-terminal domain isomerase 1
Ani2	*Sz. pombe* CENP-A N-terminal domain isomerase 2
APL	acute promyelocytic leukemia
ARF	alternative reading frame tumor suppressor protein
Arp7	actin related protein 7
Arp9	actin related protein 9
ARS	autonomous replication sequence
ASF1	anti-silencing function 1
ATP	adenosine triphosphate
ATPase	adenosine triphosphatase
Bim1	binding to microtubules 1
Bre2	brefeldin A sensitivity 2
BTHB	basic tilted helical bundle
BWA	Burrows-Wheeler aligner
C. albicans	*Candida albicans*
C. elegans	*Caenorhabditis elegans*
C. glabrata	*Candida glabrata*
C. neoformans	*Cryptococcus neoformans*
Cdc14	cell division cycle 14
CDK4	cyclin-dependent kinase 4
CE	core element
CENP-A	centromere protein A
ChIP	chromatin immunoprecipitation
CKII	casein kinase II
Cls4	calcium sensitive 4
c-MYC	cellular myelocytomatosis
cryoEM	cryogenic electron microscopy
CsA	cyclosporin A
Cse4	chromosome segregation 4
Ctk	carboxy-terminal domain kinase
Ctk1	carboxy-terminal domain kinase 1
Ctk2	carboxy-terminal domain kinase 2
Ctk3	carboxy-terminal domain kinase 3
CUT	cryptic unstable transcript
CYP33	cyclophilin 33

CYPA	cyclophilin A
D. hansenii	*Debaryomyces hansenii*
D. melanogaster	*Drosophila melanogaster*
D. rerio	*Danio rerio*
Dcc1	defective in sister chromatid cohesion 1
DE	differentially expressed
Dis3	homolog of *Sz. pombe* Dis3 (chromosome disjunction 3)
DMA	deletion mutant array
DNA	deoxyribonucleic acid
E. cuniculi	*Encephalitozoon cuniculi*
E. gossypii	*Eremothecium gossypii*
EMDB	electron microscopy data base
ERC	extrachromosomal rDNA circle
ESCRT	endosomal sorting complex required for transport
ETS1	external transcribed spacer 1
ETS2	external transcribed spacer 2
FDR	false discovery rate
FK506	tacrolimus
FKBP	FK506 binding protein or FK506 sensitive proline rotamase
FKBP12	FK506 sensitive proline rotamase 12
FKBP25	FK506 sensitive proline rotamase 25
FKBP3	FK506 sensitive proline rotamase 3 (gene)
FKBP5	FK506 sensitive proline rotamase 5
Fob1	fork blocking less 1
FPR3	FK506-sensitive proline rotamase 3 (gene)
Fpr3	FK506-sensitive proline rotamase 3 (protein)
FPR4	FK506-sensitive proline rotamase 4 (gene)
Fpr4	FK506-sensitive proline rotamase 4 (protein)
G. gallus	*Gallus gallus*
G. zeae	*Gibberella zeae*
GAG	Group antigens (gene)
Gcn4	General control nonderepressible 4
Gcn5	General control nonderepressible 5
GO	gene ontology
H. sapiens	*Homo sapiens*
HAT	histone acetyltransferase
Hda1	histone deacetylase 1
HDAC	histone deacetylase
HEXIM1	hexamethylene bis-acetamide-inducible protein 1
HMG1	3-hydroxy-3-methylglutaryl-coenzyme a reductase 1 (gene)
HMG2	3-hydroxy-3-methylglutaryl-coenzyme a reductase 2 (gene)
Hos2	Hda one similar 2
Hos3	Hda one similar 3
HOX	homeobox (gene)
IGS1	ribosomal intergenic spacer 1
IGS2	ribosomal intergenic spacer 2
Irr1	irregular cell behavior 1
ITS1	internal transcribed spacer 1
K. lactis	*Kluyveromyces lactis*
KAT	lysine acetyltransferase
KDM	lysine demethylase

Kip2	kinesin related protein 2
KMT	lysine methyltransferase
LSU	large ribosomal subunit
LTR	long terminal repeat
MATa	mating type locus a
MATα	mating type locus α
MIPS	Munich information center for protein sequences
MLL1	mixed lineage leukemia 1
MOPS	(3-(N-morpholino)propanesulfonic acid)
mRNA	messenger ribonucleic acid
mTOR	mechanistic target of rapamycin
mTRP	minimal *TRP1* promoter
Mtr3	mRNA transport 3
Mtr4	mRNA transport 4
N. crassa	*Neurospora crassa*
Net1	nucleolar silencing establishing factor and telophase regulator 1
Ngg1	necessary for glucose repression of gal10 related his3-g25 promoter
Nlp	nucleoplasmin like protein
NLS	nuclear localization signal
NMR	nuclear magnetic resonance
Nop53	nucleolar protein 53
Nph	nucleophosmin
NPL	nucleoplasmin-like
NPL-FKBP	nucleoplasmin-like FK506 binding protein
NPM	nucleoplasmin/nucleophosmin
NPM1	nucleophosmin 1/ nucleolar protein NO38
NPM2	nucleoplasmin 2
NPM3	nucleophosmin 3/ nucleolar protein NO29
NTS1	non-transcribed spacer 1
NTS2	non-transcribed spacer 2
OD	optical density
PASK	poly-acidic serine and lysine
PCR	polymerase chain reaction
PDB ID	RCSB (Research Collaboratory for Structural Bioinformatics) protein databank identification
PET	paired end tag
PHD3	plant homeodomain 3
PHO8	phosphate metabolism 8 (gene)
POL	RNA-directed DNA polymerase, also known as reverse transcriptase
Poly(A)	poly-adenine
PPI	peptidyl proline isomerase
PTM	post-translational modification
RARα	retinoic acid receptor alpha
RFB	replication fork block
RNA Pol I	RNA polymerase I
RNA Pol II	RNA polymerase II
RNA Pol III	RNA polymerase III
RNA	ribonucleic acid
RNA-seq	RNA sequencing
RPKM	reads per kilobase of transcript per million mapped reads

RPL5	ribosomal protein L5
RPL6A	ribosomal protein of the large subunit 6 A
RPL6B	ribosomal protein of the large subunit 6 B
r-proteins	ribosomal proteins
RRM	RNA recognition motif
Rrn3	regulation of RNA polymerase I 3
rRNA	ribosomal ribonucleic acid
Rrp4	ribosomal RNA processing 4
Rrp40	ribosomal RNA processing 40
Rrp41	ribosomal RNA processing 41
Rrp42	ribosomal RNA processing 42
Rrp43	ribosomal RNA processing 43
Rrp45	ribosomal RNA processing 45
Rrp46	ribosomal RNA processing 46
Rrp6	ribosomal RNA processing 6
RT-qPCR	reverse transcription quantitative polymerase chain reaction
Rtt102	regulator of Ty1 transposition 102
S. cerevisiae	*Saccharomyces cerevisiae*
SAGA	Spt-Ada-Gcn5 acetyltransferase
SD	synthetic defined
Sdc1	Set1/COMPASS homolog of Dpy30 from *C. elegans* 1
Set1	SET domain-containing 1
Set1/COMPASS	suppressor (of position effect variegation), enhancer of zeste, and trithorax domain containing protein 1/ complex of proteins associated with set 1
Set2	SET domain-containing 2
SGA	synthetic genetic array
Sgf29	SAGA associated factor 29
Shg1	Set1/COMPASS hypothetical G
Sir2	silent information regulator 2
SLIK	SAGA-like
Smc3	stability of minichromosomes 3
Snf11	sucrose non-fermenting 11
Snf2	sucrose non-fermenting 2
Snf5	sucrose non-fermenting 5
Snf6	sucrose non-fermenting 6
snoRNA	small nucleolar ribonucleic acid
SOD2	superoxide dismutase 2 (gene)
Spp1	Set1/COMPASS PHD finger protein 1
SSL	synthetically sick or synthetically lethal
SSU	small ribosomal subunit
Swd1	Set1/COMPASS WD40 repeat protein 1
Swd2	Set1/COMPASS WD40 repeat protein 2
Swd3	Set1/COMPASS WD40 repeat protein 3
SWI/SNF	switch/sucrose non-fermentable
Swi1	switching deficient 1
Swi3	switching deficient 3
Swp29	SWI/SNF-associated protein 29
Swp73	SWI/SNF-associated protein 73
Swp82	SWI/SNF-associated protein 82
Sz. pombe	*Schizosaccharomyces pombe*

T1	terminator 1
T2	terminator 2
TBP	TATA binding protein
TFIIIA	transcription factor for RNA Pol III A
TFIIIB	transcription factor for RNA Pol III B
TFIIIC	transcription factor for RNA Pol III C
Tom1	temperature dependent organization in mitotic nucleus/ trigger of mitosis 1
TPR	tetratricopeptide repeat
TRAMP5	Trf5-Air1-Mtr4 polyadenylase 5
Trf5	topoisomerase one-related function 5
tRNA	transfer ribonucleic acid
UAF	upstream activating factor
UE	upstream element
URA3	Uracil requiring 3 (gene)
Ura3	Uracil requiring 3 (protein)
WT	wild type
X. tropicalis	*Xenopus tropicalis*
Y. lipolytica	*Yarrowia lipolytica*
YPD	yeast extract-peptone-dextrose

Acknowledgements

First and foremost, I would like to express my sincere gratitude to my supervisor, Dr. Chris Nelson, for his continuous guidance, support, and encouragement over the entire course of my doctoral dissertation research.

I would also like to thank the members of my committee, Drs. Juan Ausio, Peter Constabel, and Caren Helbing for their valuable advice and insightful comments throughout my PhD research project.

I would like to acknowledge Dr. Perry Howard and the members of his lab (both past and present) for their helpful advice during our many shared lab meetings, and the lab of Dr. Alisdair Boraston for the use of equipment critical to several of my experiments.

The research presented in this dissertation would not have been possible without the input of our collaborators, Drs. Martin Hirst and Misha Bilenky, from the Michael Smith Laboratories at the University of British Columbia.

I would also like to thank my fellow labmates: David Dilworth, Geoff Gudavicious, Andrew Leung, Drew Bowie, and Francy Jardim for reagents, practical advice, and the many years that we have spent working alongside each other. I would like to express my gratitude to the many undergraduate students that I have had the pleasure of co-supervising: David Rattray, Brenna Stanford, Mike Situ, Marie Perry, Shawn Shortill, Courtney Gauthier, Anthony Hinde, Bjoern Knutson, Mia Frier, and Joseph Dobbs. For bringing outside perspectives to my research, I would like to thank my fellow graduate students from the biochemistry and microbiology department: Nick Brodie, Gillian Dornan, Kevin Yongblah, Monica Mesa, and Björn Fröhlich. It has been a pleasure to have worked with such a great group.

Finally, I would like to thank my parents, my brother, and my grandparents for their continuous encouragement and support throughout the entirety of my education. I am especially grateful for the support of my parents and brother during the writing of this dissertation. This accomplishment would never have been possible without them.

Dedication

This dissertation is dedicated to my family.
Thank you for the years of encouragement and support.

Chapter 1
Introduction

1.1 General Introduction

The DNA molecule lies at the center of all processes critical for life. Growth, development, homeostasis, and repair all require careful coordination and control of information coded for within the DNA template. Balancing the efficient storage of DNA within the limited space of a cell while maintaining controlled access to the information stored within it, poses a fundamental challenge. Consequently, cells have evolved complex mechanisms for orchestrating DNA storage and accessibility[1].

Eukaryotic cells solve the genome storage/accessibility problem with a multi-level system of DNA packaging in the nucleus. At the primary level of this system lies the nucleosome core particle: a repeating functional unit[2,3] consisting of 147 DNA base pairs superhelically wound (approximately 1.75 turns) around an octamer of core histone proteins[4,5]. A canonical histone octamer is composed of two heterodimers of histones H2A and H2B, and a heterotetramer of histones H3 and H4[6]. Variable length stretches of linker DNA flank each nucleosome core particle[7] and may associate with additional factors such as linker histones[8], allowing nucleosomes to interact with each other and assemble into polymorphic higher order arrays[7,8]. This nucleoprotein complex of histones and DNA is called chromatin, and is further organized into distinct topological domains[9], loops[10] and other larger scale architectural features[11]. Large segments of chromatin and even entire chromosomes occupy defined spatial territories in the nucleus[12]. This hierarchical system of packaging DNA into chromatin allows eukaryotic cells to condense, organize, and store DNA in the nucleus.

Nucleosomes restrict access to underlying DNA sequences. Therefore, the processes of gene transcription, DNA repair, and DNA replication all enlist nuclear factors to overcome the steric barrier of chromatin. Although the electrostatic forces which hold histones and DNA in a nucleosome are very stable[13], nucleosomes are not static structures[14]. Rather, they are highly dynamic and can exist in, and transition between, multiple compositional and conformational states[15]. Access to DNA can be facilitated spontaneously through rapid DNA unwrapping and

rewrapping around the nucleosome[16,17]. Factors such as the underlying DNA template sequence[18,19], the presence of variant histones in place of canonical ones[20], and charge altering post-translational modifications on histones[21,22] all influence spontaneous DNA accessibility. However, the properties of nucleosomes must be actively regulated. This is accomplished through the recruitment of chromatin modifying factors such as: i) enzymes which place or remove post-translational marks on histones; ii) chromatin remodelers which drive nucleosome sliding along DNA; or iii) histone chaperones which assemble or disassemble nucleosomes with canonical and variant histones. Thus, eukaryotic cells employ multiple mechanisms to fine tune chromatin states and facilitate controlled access to DNA.

This dissertation sets out to compare the biological functions of two related chromatin modifying proteins in yeast: Fpr3 and Fpr4. Based mostly on *in vitro* observations, these modifiers are classified as both histone chaperones and histone post-translational modifiers. However, at the onset of this dissertation project the breadth of biological processes that employ these chromatin regulator factors was unclear, as was their functional relationship to each other.

In this chapter, I will begin by presenting an overview of the different classes of chromatin modifying proteins. I will focus on three pertinent families of chromatin modifiers: the nucleoplasmin (NPM) family of histone chaperones, the FK506-binding protein (FKBP) family of histone post-translational modifiers, and nucleoplasmin-like FKBPs (NPL-FKBPs). Emphasis will be placed on the structural and functional features of these proteins. I will focus on the *Saccharomyces cerevisiae* (budding yeast) NPL-FKBPs, Fpr3 and Fpr4, and will present evidence for both the functional divergence and similarity of these enzymes. After discussing their connection to ribosome biogenesis, I will end this chapter by presenting the research objectives of my dissertation.

1.2 Chromatin and its modifications

Eukaryotic cells have evolved multiple systems for actively modulating nucleosome dynamics and controlling chromatin architecture. This regulation involves complex interplay between hundreds of proteins, but the modes of action can be broken down into three major categories: i) chemical modification of DNA, ii) histone post-translational modifications, and iii) nucleosome remodelers and chaperones (Figure 1). The best studied chemical DNA modification is the covalent addition of a methyl group to the carbon 5 position of the cytosine ring[23]. While this modification can directly affect the curvature of the DNA molecule[24] and thus its stability and position on histones[25,26], it is best understood as a marker to recruit effector molecules

indirectly[27]. As DNA methylation is absent in budding yeast, the organism of study in this dissertation, it will not be further discussed.

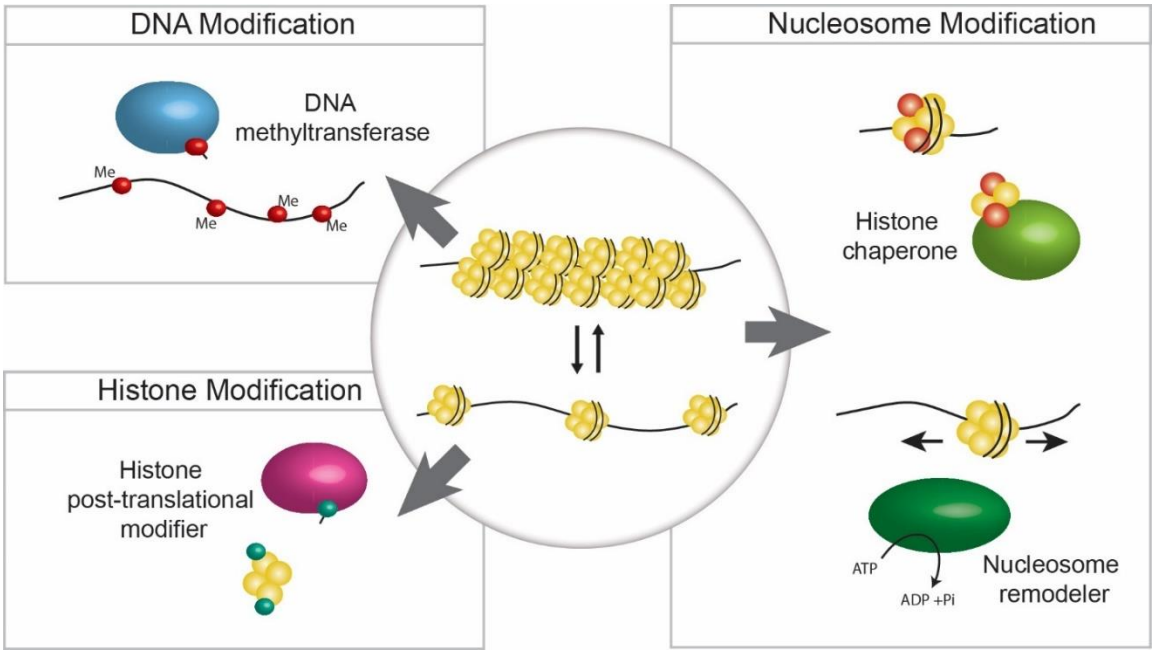

Figure 1. Multiple modes of chromatin regulation control DNA accessibility.
Chromatin regulators include: DNA methyltransferases (top left), which covalently modify the DNA template; histone post-translational modifiers (bottom left), which add or remove modifications on histones; histone chaperones (top right), which facilitate changes in nucleosome assembly and content; and ATP driven nucleosome remodelers (bottom right), which modify nucleosome positioning.

I summarize the key concepts in the remaining two modes of chromatin regulation in the following sections. I discuss the ADA histone acetyltransferase and the Set1/COMPASS methyltransferase complexes as examples of histone modifiers, and the SWI/SNF complex as an example of a nucleosome remodeler. Each of these complexes are of direct relevance to the data generated in this dissertation. The NPM-family of histone chaperones, of central importance to this dissertation, is discussed in a separate section. For additional examples of chromatin regulators, I direct the reader to the following review articles on histone post-translational modifiers[28,29], histone chaperones[30,31], and nucleosome remodelers[32,33].

1.2.1 The ADA histone acetyltransferase complex

Altering the chemical properties of histones with post-translational modifications (PTMs) affects chromatin architecture and DNA accessibility. Generally, PTMs are deposited at specific amino acid residues both within the histone cores[34] and on their unstructured terminal tails[29] by

writer enzymes. Covalent histone PTMs include functional groups (methyl, acetyl, and phosphate)[35,36], small polypeptides (ubiquitin and other small ubiquitin like polypeptides)[37,38], sugars (N-acetylglucosamine)[39], and lipids (palmitic acid)[40]. The location and chemical properties of these marks can drastically alter histone-histone[41], histone-DNA[42], nucleosome-nucleosome[43], and nucleosome-regulatory protein interactions[44]. Histone PTMs may affect these interactions *directly* through altering the charge of the residue[45] or *indirectly* via the attraction of or repulsion of effector proteins[44]. To regulate post-translational modifications, cells employ a wide repertoire of enzymes. This diverse group of proteins can direct the addition[46], removal[47] , or alteration[48,49] of histone PTMs to actively regulate chromatin.

Histone lysine acetylation involves the addition an acetyl moiety from acetyl coenzyme A onto the ε-amino group of a histone lysine residue[50]. This modification neutralizes the basic (positive) charge of a lysine and directly weakens or disrupts interactions of the acetylated histone with surrounding negatively charged DNA[45,51]. Histone acetylation, particularly on nucleosomes at gene promoters[52,53] and 5' ends[53,54], is generally associated with increased DNA accessibility[55] and transcriptional activation[56,57]. Histone acetyltransferases (HATs), more appropriately also referred to as lysine acetyltransferases (KATs) because they also target non-histone proteins[58], catalyze the addition of this histone PTM[59].

The yeast ADA complex is a histone acetyltransferase consisting of six components: a Gcn5 catalytic subunit, and five accessory subunits (Ada2, Ngg1/Ada3[60,61], Sgf29[62], Ahc1[60], and Ahc2[62]). The Gcn5, Ada2, Ngg1, and Sgf29 components of this complex constitute a core HAT module which is also present in two related histone acetyltransferases: the SAGA and SLIK complexes[62]. *In vitro,* the Gcn5 catalytic subunit displays potent HAT activity on free histones, with a preference for lysines 9 and 14 on histone H3 and lysines 8 and 16 on histone H4[46]. However, on nucleosomal histones[61] and *in vivo*[63], additional components of the core HAT module are necessary to potentiate histone acetyltransferase activity. A transcriptional activator (Gcn4) recruits the Gcn5 core HAT module to gene promoters[64]. There, it hyperacetylates surrounding histone residues and generates an accessible chromatin environment associated with transcriptional activation[64]. Gcn5 targets the promoters of actively transcribed protein coding genes[65,66], and microarray gene expression data indicate that it regulates the expression of approximately 4% of yeast genes[67,68].

Histone deacetylases (HDACs) remove or *erase* PTMs placed by acetyltransferases such as the ADA complex. Examples of these enzymes include the yeast histone deacetylases Hda1, Hos2, and Hos3. Hda1 deacetylates multiple lysine residues on histones H3 and H2B[69] and consequently functions as a transcriptional repressor at genomic loci including the ribosomal

DNA[70]. Histone deacetylases Hos2 and Hos3, deacetylate residues on histones H3 and H4[71] and on all four canonical histones[72] respectively and, repress the transcription of ribosomal protein coding genes[70]. By modulating histone acetylation, HATs and HDACs play and important role in actively controlling DNA accessibility to regulate processes such as transcription.

1.2.2 The Set1/COMPASS histone methyltransferase complex

Histone lysine methylation involves the transfer of up to three methyl moieties from S-adenosyl-L-methionine to the ε-amino group of a histone lysine residue[50]. This generates four potential methyl states (unmethylated, monomethylated, dimethylated, and trimethylated) at a given lysine[50]. Importantly, methylation does not alter the positive charge of a lysine side chain, rather, it is best understood as a feature recognized by methyl-lysine binding effector proteins[28,29]. Lysine methylation has been associated with both activation[52,73] and repression of transcription [74,75], and the site, methyl state, and genomic context each affect the ultimate impact of this mark. Lysine methyltransferases (KMTs) facilitate the deposition of methyl marks on histones [28,29].

The yeast Set1/COMPASS complex is a KMT composed of eight components[76]. It consists of a functionally essential core (composed of Swd1, Swd3, and the methyltransferase Set1) and five additional subunits (Shg1, Sdc1, Spp1, Bre2, and Swd2)[76]. During active transcription, the Set1/COMPASS complex associates with elongating RNA polymerase II (RNA Pol II)[77], where it catalyzes the (mono-, di-, and tri-) methylation of lysine 4 on histone H3 (H3K4)[75,78]. RNA Pol II C-terminal domain kinases Ctk1, Ctk2, and Ctk3 (Ctk complex) regulate Set1/COMPASS directed H3K4 mono- di- and tri- methylation patterns[79]. The Set-1/COMPASS complex and its regulators contribute to the formation of a methylation gradient along the length of an actively transcribed gene, where histones near the transcription start site are trimethylated and those at the terminator are monomethylated[53]. This gradient may function as a marker of transcriptional frequency[80]. RNA-seq and microarray genome expression experiments in *S. cerevisiae* indicate that Set1 contributes to both positive and negative regulation of transcription from many yeast loci, including phosphate responsive genes and genes involved in ribosome biogenesis[81,82].

Histone lysine demethylases (KDMs) remove or *erase* mono- di- or tri- methylation marks placed by KMTs such as the Set1/COMPASS complex[28,29]. As these enzymes are not of direct relevance to the data presented in this dissertation, I direct the reader to [83] for a comprehensive overview of their functions. By modulating histone lysine methylation, the activities of KMTs and KDMs contribute to chromatin regulation.

1.2.3 The SWI/SNF nucleosome remodeling complex

Nucleosome remodelers (also known as chromatin remodelers), regulate chromatin architecture and DNA accessibility by repositioning nucleosomes using energy derived from ATP hydrolysis[32,84]. A defining feature of these enzymes is the presence of an ATPase DNA translocase domain which drives DNA repositioning relative to the histone octamer[32,84]. Chromatin features such as histone PTMs (particularly on histone tails) can modulate the activity of nucleosome remodelers[85].

The SWI/SNF nucleosome remodeler in yeast is a complex consisting of: a catalytic core (composed of Arp7, Arp9 and the Snf2 ATPase)[86], a histone octamer contact module (composed of Snf5 and Swp82)[87], and a number of accessory proteins (Swi1, Swi3, Snf11, Rtt102, Snf6, Swp73, and Swp29)[88]. A bromodomain on the Snf2 ATPase subunit targets SWI/SNF to acetylated nucleosomal histone H3 and H4 tails[89] . Here it may either translocate DNA to facilitate nucleosome sliding[90,91] or disassemble nucleosomes and evict histones[86,92]. Genome wide microarray expression studies have shown that the SWI/SNF complex is associated both with transcriptional activation and repression[68,93] and affects the expression of approximately 6% of yeast genes[68]. Genes positively regulated by Snf2 include acid phosphatase and Matα specific genes[93]. At gene promoters, histone acetylation in conjunction with SWI/SNF directed chromatin remodeling is generally associated with transcriptional activation[94,95]. Known SWI/SNF promoter targets include some Gcn4 regulated promoters[96,97] and the *PHO8* promoter[98] The activities of multiple classes of ATP dependent nucleosome remodelers contribute to active chromatin regulation.

1.3 The nucleoplasmin (NPM) family of histone chaperones

Histone chaperones contribute to chromatin regulation by controlling the folding[99], localization[100], and supply[101] of free histones, and by facilitating the ordered deposition of histones onto DNA[102]. Among the first of these enzymes to be discovered[102], were members of the nucleophosmin/nucleoplasmin (NPM) family[103]. This family of chaperones appears to be conserved throughout metazoans. NPM family proteins have been found in humans (*H. sapiens*)[103], chicken (*G. gallus*)[103–105] , western clawed frog (*X. tropicalis*)[103,104] , zebrafish (*D. rerio*)[103,104,106], and fruit flies (*D. melanogaster*)[103].

The NPM family is divided into four major sub-groups: NPM1, NPM2, NPM3, and invertebrate NPM-like (Figure 2 A)[103]. Tissue specific protein expression analyses based on immunohistochemical staining indicate that NPM1 and NPM3 are present in all human tissues, while NPM2 expression is enhanced in the brain and thyroid[107,108]. All members of the NPM

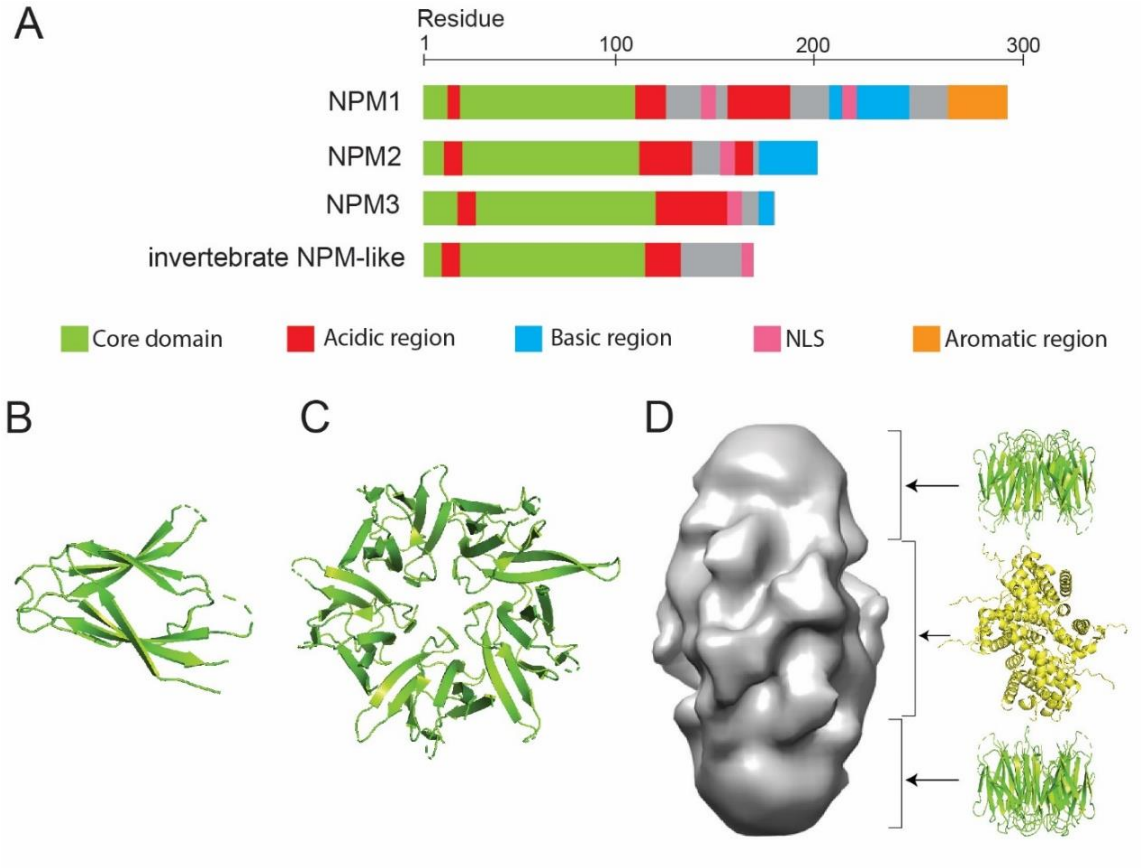

Figure 2. Nucleoplasmin family histone chaperones are characterized by a conserved core domain. (A) Characteristic domain architectures of the four nucleoplasmin family sub-groups: NPM1, NPM2, NPM3 and invertebrate NPM-like. *Xenopus* Npm1 (also known as NO38), *Xenopus* Npm2 (also known as nucleoplasmin), *Xenopus* Npm3 (also known as NO29), and *Drosophila* Nlp are presented as examples. The N-terminal core domains (green) and acidic patches (red) are conserved between all four sub-groups. Approximate amino acid lengths are indicated. (B) Crystal structure of the N-terminal core of *Xenopus* Npm2 (PDB ID:1K5J)[109]. (C) Crystal structure of the pentamer assembled from core domain monomers of *Xenopus* Npm2 (PDB ID:1K5J)[109] (top view). (D) CryoEM structure of the *Xenopus* Npm2 pentamer in complex with the histone octamer (EMDB accession number EMD-0323)[110]. Positions of the *Xenopus* Npm2 pentamers and histone octamer are indicated with crystal structures at the right (Npm2: side view and colored green (PDB ID:1K5J)[109] , histone octamer: colored yellow (PDB ID:1AOI)[5]). Structures were rendered using the PyMOL Molecular Graphics System, Version 2.0 Schrödinger, LLC.

family share a conserved N-terminal core domain with a characteristic nucleoplasmin fold and differ in features at their less conserved C-terminal ends (Figure 2 A)[103,111]. The NPM core domain forms an eight stranded β-barrel with jellyroll fold topology and is followed by a region rich in acidic residues containing a nuclear localization sequence (NLS)[109,111–113] (Figure 2 B). Crystal structures of NPM family protein core domains from human[114,115], *X. tropicalis*[109,113], and *D. melanogaster*[112] indicate that five monomer subunits form a donut shaped pentamer (Figure 2 C). A recent CryoEM study of *Xenopus* nucleoplasmin (Npm2) has revealed that, in addition to interacting with both histone H2A-H2B and H3-H4 dimers, two Npm2 pentamers can form a complex with the complete histone octamer (Figure 2 D)[110]. Phosphorylation and exposure of the

acidic C-terminal regions of Npm2 were found to be essential for stabilizing interactions with the octamer[110].

1.3.1 NPM1

NPM sub-group proteins (NPM1-NPM3) are implicated in numerous biological functions in metazoan cells including ribosome biogenesis[116], mitotic spindle assembly[117], transcription regulation[118], chromatin remodeling[119], and histone storage[120]. The most extensively studied NPM family protein is NPM1 (also known as nucleophosmin, numatrin and B23 in mammals, and NO38 in amphibians)[111]. The best described function of this protein is in ribosome biogenesis. In mammalian cells NPM1 immunoprecipitates with nucleolin[121], an acidic histone chaperone which is involved in ribosomal RNA (rRNA) processing during the early stages of ribosome biogenesis[122]. NPM1 also associates with 28S rRNA[123] and physically interacts with a complex of ribosomal proteins and RNA helicases[124] required for rRNA processing[125]. NPM1 is necessary for the nuclear export of RPL5, a large ribosomal subunit protein[126]. Additionally, NPM1 exhibits ribonucleolytic activity *in vitro* and facilitates rRNA maturation[127,128].

NPM1 also plays a role in microtubule spindle dynamics. Human NPM1 immunoprecipitates with CENP-A, a centromere specific histone H3 variant associated with kinetochore assembly[129]. Immunofluorescence microscopy experiments in human cells also reveal that during mitosis NPM1 localizes to the mitotic microtubule spindle poles[130] and is necessary for correct spindle organization and kinetochore-microtubule attachment[117].

NPM1 has been implicated in transcription regulation both indirectly and directly. NPM1 indirectly plays a role in the regulation of gene expression through physical interactions with: RNA polymerase regulators such as the HEXIM1 negative regulator of RNA Pol II[118], transcription factors such as c-MYC[131], and chromatin modifiers such as mammalian GCN5[132] and the SWI/SNF complex[119]. NPM1 has also been implicated transcription regulation through direct interactions with gene promoters. The C-terminal domain of NPM1 binds G-quadruplex secondary DNA structures[133] formed within the GC-rich promoter of the manganese superoxide dismutase encoding *SOD2* gene[133,134]. There, it induces *SOD2* expression in a dose dependent manner[135]. In addition to the regulation of RNA Pol II promoters, NPM1 has also been implicated regulating RNA Pol I transcription. Chromatin immunoprecipitation experiments indicate that it associates with RNA Pol I transcribed ribosomal DNA (rDNA) and contributes to rRNA expression[116,136].

1.3.2 NPM2 and NPM3

Xenopus Npm2 (also known as nucleoplasmin) is the most abundant nuclear protein in oocytes where it stores pools of free histone H2A-H2B prior to fertilization[102,120,137]. *Xenopus* egg extracts immunodepleted for Npm2 fail to induce sperm nuclear decondensation[138], and the exchange of sperm specific DNA binding basic proteins (protamines) with canonical histone H2A-H2B[139]. This decondensation and chromatin remodelling step normally occurs immediately after fertilization. Collectively these experiments implicate Npm2 in both histone storage, and nucleosome remodeling during the early stages of amphibian embryogenesis. Post translational modifications, including phosphorylation, of residues within the C-terminal acidic regions of Npm2 may regulate its histone binding and deposition activity by modulating Npm2-histone interactions[140]. Although the functions of NPM2 proteins in mammalian cells are still not fully understood, *Npm2*-null mice embryos exhibit nuclear defects which indicate that at least some embryogenesis related roles of NPM2 may be conserved in mammalian cells[141].

Relatively little is known about the functions of the NPM3 and invertebrate NPM-like subfamily proteins. Human NPM3 may interact with NPM1 and play a shared role in regulating ribosome biogenesis[123], while *Drosophila* NPM-like proteins, Nph and Nlp, have been implicated in sperm chromatin remodeling[142]. *In vitro*, *Drosophila* Nph can facilitate the assembly of core histones onto DNA[143], while both Nph and Nlp promote the dissociation of protamines from reconstituted model sperm chromatin[142]. Taken together, the NPM family histone chaperones (NPM1-NPM3) participate in multiple biological processes, their precise mechanisms of action both with respect to chromatin and elsewhere; however, are not yet fully understood.

1.3.3 NPM family histone chaperones in disease

Mutations in genes encoding NPM1 and NPM3 proteins are linked to blood and bone cancers. Heterozygous insertions in the *NPM1* gene are found in approximately 30% of adult acute myeloid leukemia (AML) patients[144–146]. These insertions result in mutant NPM1 proteins which dislocate from the nucleolus to the cytoplasm[144–146]. Mutant NPM1 interacts with both wild type NPM1[147] and ARF, a tumor suppressor protein involved in p53-dependent cell cycle arrest[148]. These interactions are thought to drive the early events of leukemogenesis by sequestering wild type NPM1 and ARF away from the nucleus to the cytoplasm[147]. This may have two compounding deleterious consequences. The first, perturbation of the tumor suppressive functions of ARF, and the second, loss of function defects in NPM1 mediated regulation of ribosome biogenesis or chromatin architecture[149].

NPM1 translocations can also generate oncogenic fusion proteins[149,150]. Approximately one third of acute anaplastic large cell lymphoma (ALCL) patients have a fusion between the C-terminus of NPM1 and the catalytic domain of the ALK tyrosine kinase[151]. This results in a constitutively active NPM1-ALK chimera kinase[152], that drives oncogenesis by multiple mechanisms[150]. Similar fusion events between *NPM1* and a retinoic acid receptor gene (*RARα*) have been reported in acute promyelocytic leukemia (APL)[153]. Although its role in oncogenesis is less understood, NPM3 is upregulated in some soft tissue myxoinflamatory fibroblastic sarcomas[154]. The fact that NPM family histone chaperones are mutated or differentially expressed in multiple cancers prompts further interest in a more complete understanding of their biology.

1.4 Prolyl isomerization

A peptide bond between two amino acids can exist in two structural states: *cis* and *trans*[155,156]. In the *cis* state the alpha carbons (C^{α}) of both amino acids face the same direction, and the dihedral angle (ω) between them is 0° (Figure 4 A). In the *trans* state they face opposite directions and ω is 180° (Figure 4 A). Due to steric clashes between side chains (R groups), almost all of the peptide bonds found in proteins are present in the *trans* confirmation[157]. Because proline cannot freely rotate about the C^{α}-N bond (Figure 4 B), peptide bonds preceding a proline (X-P) are subjected to steric clashes in both *cis* and *trans* states (Figure 4 C). The lower energy differences between X-P *cis* and *trans* peptide bonds vs between X-non-proline *cis* and *trans* peptide bonds[158], make *cis* X-P peptide bonds more stable and common than *cis* X-non-proline bonds[157,159]. The isomerization state (*cis* vs *trans*) of a given peptidyl-prolyl bond has drastic implications on the local conformation of a polypeptide and on the three dimensional structure of a protein[160] (Figure 4 D).

Although proline containing polypeptides can interconvert between isomeric forms on their own, a relatively high energy barrier (~20kcal/mole)[161] limits this rate of interconversion to the order 10s-100s of seconds[162]. This makes proline isomerization the rate limiting step in protein folding[163,164] and presents a biological problem. Peptidyl-prolyl isomerases (PPIs) are ubiquitous enzymes dedicated to accelerating this slow exchange of *cis-trans* states to timescales compatible with biology. For example, in *in vitro* protein refolding experiments, in the absence of PPIs the refolding of urea denatured mouse immunoglobin light chain takes approximately 200 seconds[165]. Upon the addition of 1.6μM of a PPI extracted from pig kidney, refolding time is decreased by sevenfold[165]. PPIs are found across all domains of life and are present in most major compartments of the cell[166–168].

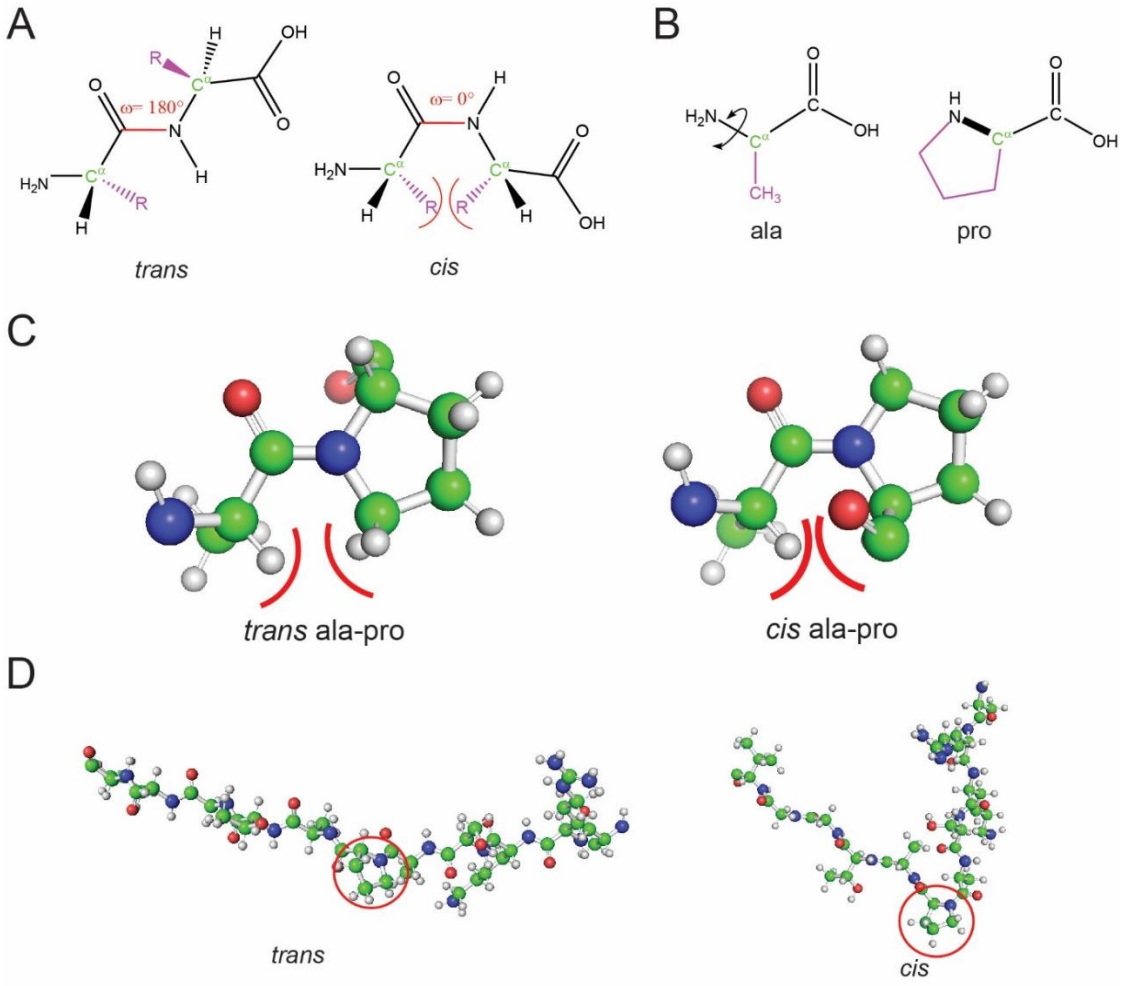

Figure 3. Peptidyl-prolyl bonds can exist in *cis* or *trans* orientation.
(A) Dipeptide in *trans* and *cis* conformations with dihedral angles (ω) indicated. Peptide bonds are shown in red, C^{α} carbons are green, and side chain groups (R) are purple. Steric clashes between R groups in *cis* conformation are indicated with red arcs. (B) Amino acids such as alanine can rotate freely about the C^{α}-NH_2 bond. Proline cannot rotate about this bond (indicated in bold). (C) Alanine-peptidyl proline dipeptides in *trans* and *cis* states. Steric clashes in both orientations are indicated with red arcs. (D) The orientation of peptidyl-prolyl bonds can result in a drastic change in structure of the resulting polypeptide. Ten amino acids flanking a peptidyl-proline in *cis* and *trans* state. The central proline residue is circled. Chemical structures were rendered using PerkinElmer ChemDraw Prime 16.0. Ball and stick structures were rendered using the PyMOL Molecular Graphics System, Version 2.0 Schrödinger, LLC.

1.4.1 Peptidyl-prolyl isomerases

Eukaryotic PPIs are classified into three structurally distinct protein families: cyclophilins[166–169], parvulins[166,168], and FK506 binding proteins (FKBPs)[170,171]. The cyclophilin and FKBP families of PPIs were originally identified in the 1980s as the intracellular targets of the immunosuppressive drugs cyclosporin A (CsA)[172] and tacrolimus (FK506)[173,174] respectively. Parvulin family PPIs were uncovered in the early 1990s and were not characterized by binding to

a class of immunosuppressant drugs, but rather by their homology to a small PPI originally isolated from *E. coli*[175,176]. The number of PPIs in an organism generally increases with its complexity. The human genome encodes seventeen cyclophilins, thirteen FKBPs, and only two parvulin family proteins while the *S. cerevisiae* genome encodes eight cyclophilins, four FKBPs, and a single parvulin[177].

Each PPI family is defined by a structurally distinct catalytic domain. Many PPIs also possess additional accessory domains which facilitate cellular localization and contribute to protein function[168,177–179]. Cyclophilin family PPIs are defined by an ~18kDa catalytic cyclophilin-like-domain consisting of an 8 stranded anti-parallel β-sheet sandwich capped at both ends by two α-helices (Figure 4 A)[180–182]. The parvulin family ~10kDa catalytic domain consists of a central 4 stranded anti-parallel flattened β-barrel surrounded by 4 α-helices (Figure 4 B)[183]. FKBP family PPIs possess at least a single repeat of a ~12kDa catalytic FKBP domain[171]. This domain consists of a central α-helix flanked by a 5 stranded anti-parallel β-sheet (Figure 4 C)[184–186]. As they are not the focus of this dissertation, I direct the reader to the following reviews for more information on the structure and functions cyclophilins[187,188] and parvulins[189,190].

Despite their different folds, the α-helices and β-sheets in all three PPI families form a shallow, solvent exposed, hydrophobic pocket[191] which facilitates catalytic activity, and in cyclophilins and FKBPs also serves as the binding site of the immunosuppressant enzymatic inhibitors CsA[181,182] and FK506[185,192] respectively. In FKBPs, this hydrophobic pocket is lined by a conserved array of 6-9 aromatic amino acids at the protein's active site[184–186], and in addition to binding FK506, also binds other macrolide family immunosuppressive drugs such as, ascomycin (FK520), and rapamycin (Figure 4 D and E)[173,174,184,185,192].

Despite decades of structural, biochemical, and computational studies, a definitive consensus on the catalytic mechanism of PPIs has not yet been reached. It is generally accepted that all three families catalyze isomerization without amide bond breakage, by stabilizing an intermediate structure where the proline is rotated halfway between *cis* and *trans* states ($\omega \sim 90°$)[193–196]. However, there is computational and structural evidence that these partially rotated intermediate structures adopt different turns in FKBP mediated catalysis vs cyclophilin mediated catalysis, suggesting divergent catalytic mechanisms[195,197]. Many models for the catalytic mechanism of *cis-trans* isomerization have been proposed thus far[194]. A recent study of isomerization in a prokaryotic FKBP has proposed a catalysis model in which the residue N-terminal to the peptidyl-prolyl bond is anchored to the FKBP catalytic pocket[198]. This anchoring is facilitated via hydrogen bonds with the FKBP β-strand residues, and side chain interactions with the hydrophobic pocket[198]. Thus stabilized, the residues C-terminal to the peptidyl-prolyl bond (and

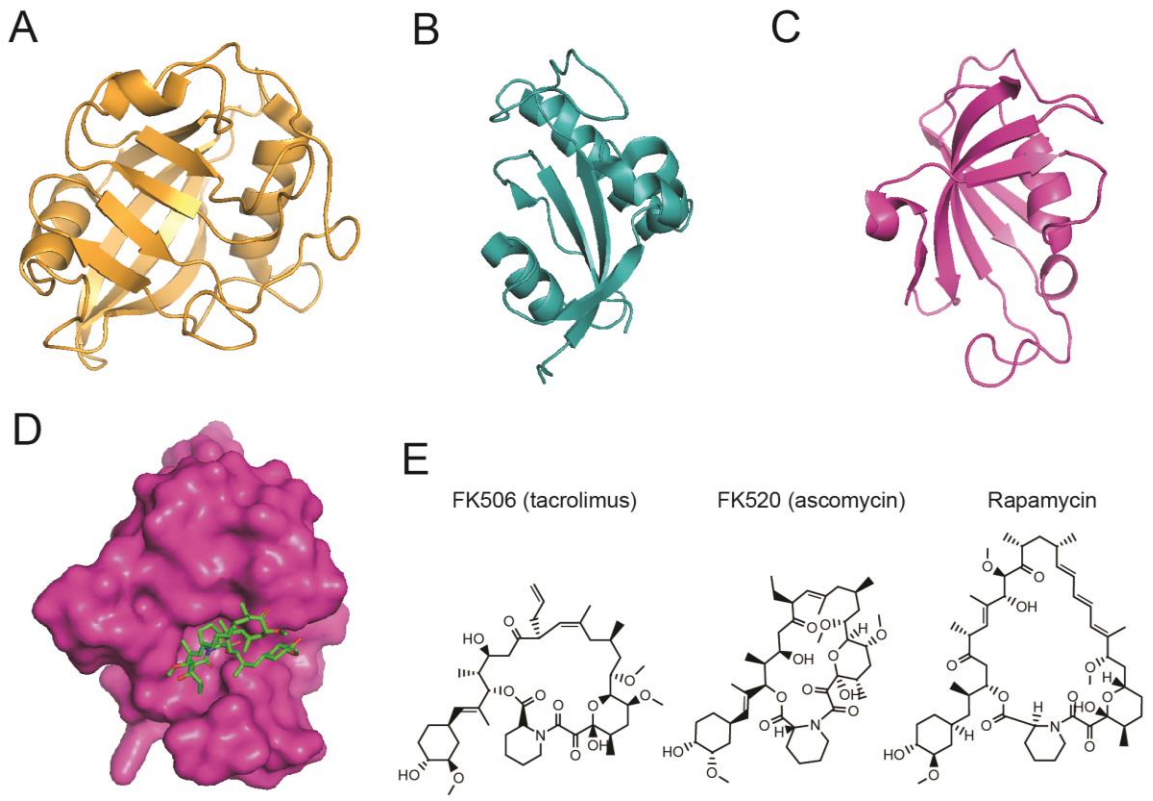

Figure 4. FKBP family PPIs catalyze *cis-trans* peptidyl-prolyl isomerization.
(A) Crystal structure of the archetypal human cyclophilin CYPA (PDB ID: 3K0M)[199]. (B) Crystal structure of the human parvulin PIN1 (PDB ID: 1NMW)[200]. (C) Crystal structure of human FKBP12 (PDB ID: 2PPN)[186] which consists of a single the archetypal FKBP catalytic domain. (D) Rapamycin bound to the catalytic pocket of human FKBP12 (PDB ID: 2DG3)[201]. (E) Chemical structures of macrolide class immunosuppressants: tacrolimus (FK506); tacrolimus analog ascomycin (FK520); and rapamycin. Crystal structures were rendered using the PyMOL Molecular Graphics System, Version 2.0 Schrödinger, LLC. Chemical structures were rendered using PerkinElmer ChemDraw Prime 16.0.

the proline side chain) can then twist to facilitate isomerization by adapting a partially rotated intermediate form[198]. Other factors, such as intra-substrate hydrogen bonding interactions between the amide hydrogen and imide nitrogen of the partially rotated intermediate may also contribute to stabilizing this transition state[194,195]. Several cytoplasmic fungal FKBPs possess a conserved proline residue in a protruding loop adjacent to the hydrophobic active site, which raises the interesting possibility that self-isomerization may contribute to regulating their function[202].

Despite the fact that the immunosuppressants CsA and FK506 are structurally unrelated molecules[203–205], both inhibit T-cell proliferation via the formation of an immunosuppressant-PPI-calcineurin ternary complex. Immunosuppression by FK506 involves the binding of FK506 to the hydrophobic catalytic pocket of the cytosolic FKBP, FKBP12[206]. The resulting FK506-FKBP12 forms a ternary complex with the calcium-dependent phosphatase calcineurin[206,207]. Thus bound,

calcineurin phosphatase activity is inhibited[206] which prevents the transcription of interleukin-2 and other cytokines that regulate T-cell activity and consequently immune response[208–210]. Immunosuppression by CsA occurs through a similar mechanism in which CsA binds to the cytosolic cyclophilin, CYPA and forms a ternary complex with calcineurin[206]. Interestingly, immune suppression by rapamycin occurs through a distinct pathway from that of FK506[211]. Rather than forming a complex with calcineurin, rapamycin bound FKBP12 forms a ternary complex with the mechanistic target of rapamycin (mTOR) kinase[212,213]. This inhibits its catalytic activity and consequent central regulatory role in multiple signalling pathways associated with immune effector response[214]. Because treatment of cyclophilins/FKBPs with immunosuppressant inhibitors results in gain of function phenotypes, the proline targets of these enzymes cannot be inferred from inhibition-based assays and are thus poorly understood. This necessitates the development of alternative readout systems to study their catalytic activities *in vivo*.

1.4.2 Prolyl-isomerases as a molecular switch: the CYP33-MLL1 case study

Prolyl isomerases have been implicated in multiple functions including: de-novo protein folding[215], protein refolding[216], and serving as a molecular switch to induce a conformationally dependent change of function[217,218]. The best studied example of peptidyl-prolyl isomerization functioning as a molecular switch in the nucleus, is the cyclophilin 33 (CYP33) mediated regulation of the mixed lineage leukemia (MLL1) histone H3K4 methyltransferase. MLL1 can function as both an activator and repressor of *HOX* gene expression during hematopoiesis[217,219]. It consists of multiple domains, including a central PHD3 histone trimethylation reader domain joined by a short (6 residue) linker sequence to a bromodomain[217]. Through the *cis-trans* isomerization of a proline residue (P1629) located in the linker region of MLL1, CYP33 induces a structural rearrangement in the PHD3 and bromodomains[217]. This rearrangement reveals a previously occluded binding surface within MLL1 which binds the non-catalytic RNA recognition motif (RRM) domain of CYP33[217]. RRM binding to the PHD3 domain of MLL1 may alter the binding affinity of PHD3 to trimethylated histones, thus mediating the functional transition of MLL1 from a transcriptional activator to a repressor of *HOX* gene expression[217,220]. CYP33 mediated regulation of MLL1 is evidence that PPIs regulate protein function *in vivo* through targeted proline isomerization events. Although less is known about FKBP regulated proline isomerization, a recent study has implicated the FKBP5 mediated isomerization of a

CDK4 proline in myoblast differentiation[218], which lends additional emerging support to the importance of proline isomerization events in regulating protein function.

1.4.3 Yeast nuclear FKBPs target histones

In addition to regulating protein function by serving as a molecular switch, peptidyl-proline isomerization has also been implicated in chromatin biology by acting as a non-covalent histone post-translational modification. The catalytic domains of fungal nuclear FKBPs can interact with nucleosomes[221], and have been implicated in peptidyl-proline isomerization events on both canonical[222,223] and variant[224,225] histones.

Fungal nuclear FKBP catalytic domains possess four conserved, basic surface patches rich in lysine residues[221]. Recombinant FKBP mutants in which these charged patches have been neutralized fail to associate with nucleosomal DNA *in vitro*, indicating that these highly charged surfaces mediate FKBP interactions with chromatin[221].

The FKBP domain of the *S. cerevisiae* nuclear FKBP, Fpr4, can isomerize synthetic peptides centered around three proline residues found on canonical histone H3 (prolines 16, 30, and 38)[222,223]. Catalytically inactive point mutants of the Fpr4 FKBP domain are associated with an increase in the Set2 mediated methylation of a lysine residue (K36) adjacent to histone H3 proline 38[223]. This, together with the fact that mutation of proline 38 on histone H3 decreases methylation of lysine 36, is evidence that Fpr4 mediated *cis-trans* isomerization of proline 38 acts as a histone post-translational modification to control Set2 methylation of lysine 36[223] . Although the exact mechanism of action remains to be determined, Fpr4 isomerization has been implicated in regulating the kinetics of transcriptional activation *in vivo*[223] .

In addition to targeting canonical histone H3, fungal nuclear FKBPs can also isomerize prolines on histone variants. Catalytically inactive point mutants of the *S. cerevisiae* nuclear FKBP, Fpr3, prevent the degradation of the Cse4 histone H3 variant *in vivo*[224]. The fact that Cse4 proline 134 point mutants of also fail to degrade, is evidence that Fpr3 mediated isomerization of Cse4 proline 134 is necessary for the degradation of this histone variant *in vivo*[224]. In *Sz. Pombe* the nuclear FKBPs Ani1 and Ani2 physically associate with proline 15 on the N-terminal domain of centromeric histone H3 variant CENP-A[225]. Deletion mutants of *ANI1* (Δ*ani1*) and *ANI2* (Δ*ani2*) are associated with similar chromosome missegregation phenotypes to those seen in mutants of CENP-A proline 15[225]. This implicates Ani1 and Ani2 mediated isomerization of CENP-A proline 15 in *Sz. Pombe* chromosome segregation[225]. Taken together, these studies provide evidence for the importance of FKBP mediated proline isomerization events in histone post-translational modification and in chromatin biology.

1.4.4 Vertebrate nuclear FKBPs

Some predominantly nuclear FKBPs in humans, *G. gallus*, *X. tropicalis*, and *D. rerio* possess an N-terminal basic tilted helical bundle (BTHB) domain and a C-terminal FKBP catalytic domain (Figure 5 A)[171,177,226,227]. The BTHB domain consists of a compact bundle of 5 α-helices[228] (Figure 5 B) and facilitates binding to double stranded RNA[229] and DNA[230,231]. Human FKBP25 (also referred to by its gene name *FKBP3*)[226,228,231,232], physically associates with ribosomal proteins[229,233], ribosome biogenesis factors[229,233], transcription factors[231,234,], and chromatin modifiers including histone deacetylases HDA1 and HDA2[234] and the histone chaperone nucleolin[119,233,235]. Despite this association with chromatin modifiers and nuclear proteins, the impact of FKBP25 on gene expression and in chromatin biology is limited. For example, an RNA-seq analysis of HEK293 cells depleted of FKBP25 showed only subtle changes in overall gene expression[236]. This suggests that the impact of FKBP25 in transcriptional regulation is minimal[236]. However, a limitation of this analysis was that it was designed as an exploratory assay and only performed in a single cell line and biological replicate[236]. FKBP25 has been implicated in other DNA centric processes such as mitotic spindle dynamics[236]. During mitosis the catalytic FKBP domain of FKBP25 directly binds microtubules, promoting their polymerization and stability, and associates with the mitotic spindle apparatus to regulate entry into mitosis. While the limited amount of work in this area restricts any major conclusions, it is possible that vertebrate nuclear FKBPs may have evolved different roles in chromatin regulation compared to their invertebrate counterparts.

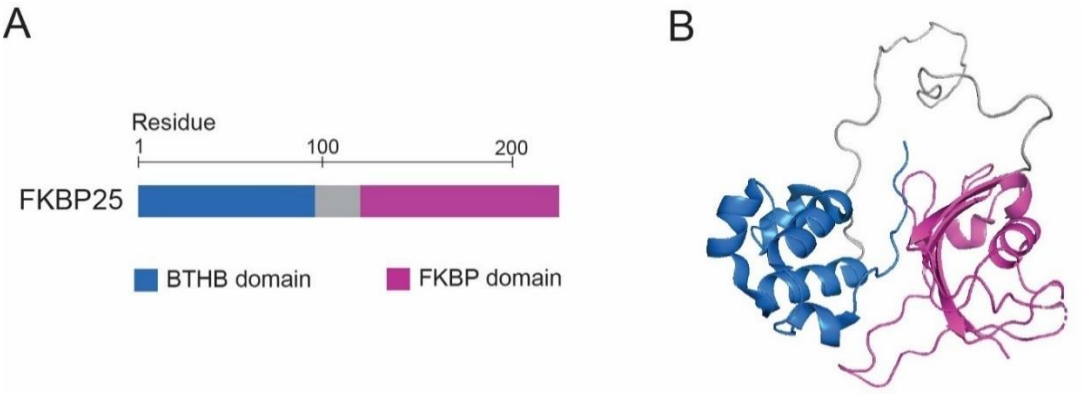

Figure 5. Vertebrate nuclear FKBPs possess an N-terminal basic tilted helical bundle (BTHB) domain.
(A) Characteristic domain architecture of vertebrate nuclear FKBPs. Human FKBP25 is presented as an example. The N-terminal basic tilted helical bundle (BTHB) domain (dark blue), FKBP domain (purple), and approximate amino acid lengths are indicated. (B) NMR structure of full length human FKBP25 (PDB ID: 2MPH)[231]. BTHB domain is colored dark blue and FKBP domain is colored purple. Structures were rendered using the PyMOL Molecular Graphics System, Version 2.0 Schrödinger, LLC.

1.5 The Nucleoplasmin-like FKBPs

Nucleoplasmin-like FKBPs (NPL-FKBPs) are a family of histone chaperones/post-translational modifiers found in plants[179,237], insects[177,238], and fungi[178]. They share features with both metazoan NPM family histone chaperones[103,111], and vertebrate nuclear FKBPs[226]. The N-terminal domains of NPL-FKBPs possess the pentameric nucleoplasmin fold characteristic of the NPM histone chaperone family[239] (Figure 6 and appendix Figure 38). This domain is followed by a highly charged region, rich in stretches of acidic and basic amino acids[177,178,237,238,240], and a C-terminal FKBP domain structurally related to that found in vertebrate nuclear FKBPs[171] (Figure 6 and appendix Figure 38). Like metazoan NPM-family proteins and vertebrate nuclear FKBPs, NPL-FKBPs are predominantly localized to the nucleus[177–179,237,238]. Taken together, the NPL-FKBP family is a hybrid class of proteins with structural similarities to both NPMs and nuclear FKBPs. In the following sections I present an overview of the NPM, nuclear FKBP, and NPL-FKBP repertoires of plants, insects, and fungi.

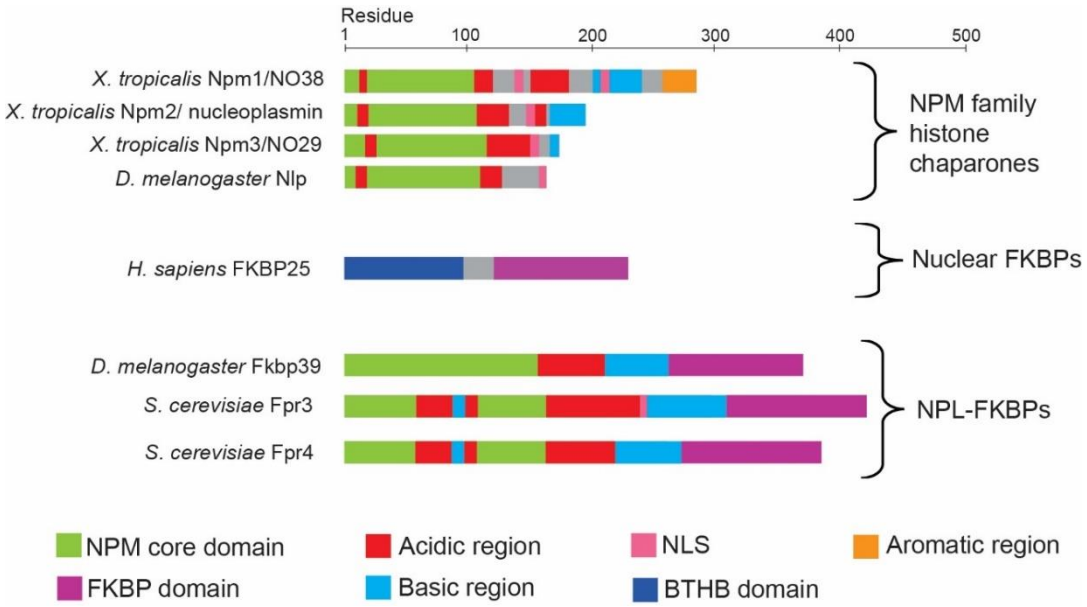

Figure 6. NPL-FKBPs share features of both NPM family histone chaperones and nuclear FKBPs. Characteristic domain architectures of the metazoan NPM family of histone chaperones, vertebrate nuclear FKBPs, and plant, fungi, and Drosophila NPL-FKBPs. The NPM core domain which possesses the nucleoplasmin fold and characteristic central stretches of acidic and basic residues are common to both NPM family chaperones and NPL-FKBPs. The FKBP catalytic domain is common to both nuclear FKBPs and NPL-FKBPs. Approximate amino acid lengths are indicated.

1.5.1 Nucleoplasmin-like FKBPs in plants and insects

Insect genomes do not have genes encoding NPM1, NPM2, and NPM3 sub-group proteins. Similarly, nuclear FKBPs with an N-terminal BTHB domain are absent. In their place are more

distantly related NPM-like proteins (see Figure 2 A)[111] and nuclear NPL-FKBPs. Insect NPM-like proteins are characterized by a single nucleophosmin-like core domain, while NPL-FKBPs consist of an N-terminal NPM-like (NPL) domain and a C-terminal FKBP domain (Figure 7). The fruit fly (*D. melanogaster*) genome codes for two NPM-like proteins: Nph, Nlp[103] and one NPL-FKBP, Fkbp39[177,238] (Figure 7).

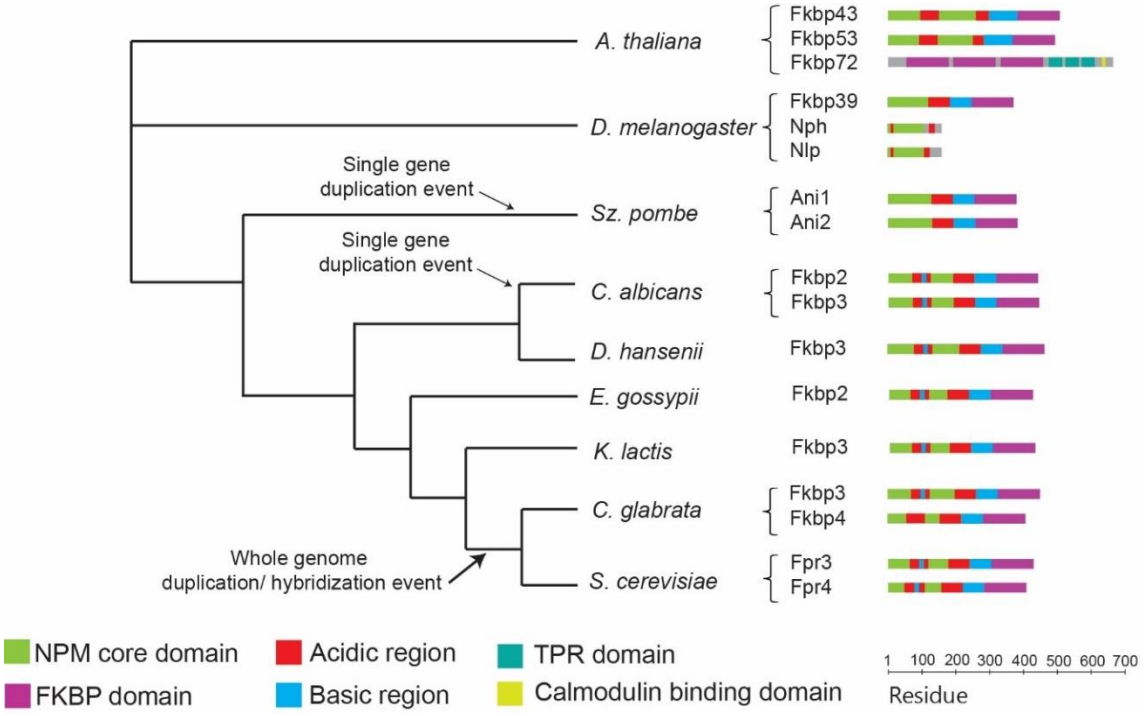

Figure 7. Overview of NPMs, nuclear FKBPs, and NPL-FKBPs in select insects, plants, and fungi. Common taxonomic tree (left) adapted from[178] depicting evolutionary relationships between several representative insects, plants, and fungi. Branch lengths are not proportional to evolutionary distances. Fungi are ordered as previously reported[178]. Domain architecture diagrams (right) of NPM family histone chaperones, nuclear FKBPs, and NPL-FKBPs found in each representative organism. Approximate amino acid lengths are indicated.

Plant genomes appear to lack genes encoding NPM family proteins but code for several nuclear FKBPs, including NPL-FKBPs similar to fruit fly Fkbp39. The thale cress (*A. thaliana)* genome encodes for three FKBPs predicted to be at least partially nuclear[179,237](Figure 7). Thale cress FKBP72 consists of three repeats of the FKBP motif followed by a tetratricopeptide (TPR) and calmodulin binding domain[237] (Figure 7). Thale cress FKBP43 and FKBP53 have nucleoplasmin like N-terminal domains and a single FKBP motif at their C-termini[237](Figure 7). They likely resulted from a gene duplication event[179]. Thus, insects possess NPM-like and NPL-FKBP proteins while plants lack NPMs but possess NPL-FKBPs and other nuclear FKBPs.

1.5.2 Nucleoplasmin-like FKBPs in fungi

Like plant genomes, fungal genomes also lack NPM family protein genes but code for NPL-FKBPs. Interestingly, not all fungi have NPL-FKBPs: *Y. lipolytica*, *A. nidulans*, *A. fumigatus*, *N. crassa*, *G. zeae*, and *C. neoformans* lack NPL-FKBPs, while *E. cunuculi* lacks FKBPs altogether[178]. Thus, despite being highly conserved across many eukaryotes, NPMs, nuclear FKBPs, and NPL-FKBPs are not universal.

The *K. lactis, E. gossypii* and *D. hansenii* genomes possess a single NPL-FKBP coding gene, while *C. albicans*, *Sz. pombe*, *C. galbrata,* and *S. cerevisiae* encode duplicate NPL-FKBPs[178] (Figure 7). The *C. albicans* and *Sz. Pombe* duplicates (Fkbp2/Fkbp3 and Ani1/Ani2 respectively) likely resulted from single gene duplication events which occurred at some point in their evolution (Figure 7). The *C. galbrata* and *S. cerevisiae* duplicates (Fkbp3/Fkbp4 and Fpr3/Fpr4 respectively) arose from a single whole genome duplication[241] or hybridization event[242] in a common ancestor prior to their divergence (Figure 7). The presence of duplicate NPL-FKBP genes across distantly related fungi and plants suggests that in many organisms there is an evolutionary advantage to having two genes encoding NPL-FKBPs.

1.5.3 Gene duplication events

In fungal evolutionary history, a major whole genome duplication[243,244] or genome hybridization event[242] is thought to have occurred in a common ancestor of *S. cerevisiae* and *C. galbrata* after the divergence of *K. lactis* (Figure 7)[243,244]. This event resulted in the doubling of every chromosome. In *S. cerevisiae,* a period of rapid genomic reorganization[245] and genome loss[246] is thought to have immediately followed this event. Most of the resulting duplicated genes, or paralogs, were thus lost from the genome. The NPL-FKBPs, *FPR3* and *FPR4,* are two genes that were among the 10%-13% retained on the genome over the subsequent course of evolution[247]. Under conditions of growth in rich media and at optimal temperatures, both genes are individually and collectively non-essential for survival[248]. However, there is evidence that the absence of both genes results in a non-lethal reduction in fitness[249]. *FPR3* and *FPR4* show synteny with duplicated genes upstream and downstream of them. The paralogs *HMG1* and *HMG2*, which code for 3-hydroxy-3-methylglutaryl-coenzyme A reductases, are found approximately 1200bp and 600bp upstream of *FPR3* and *FPR4* respectively (Figure 8). The *RPL6A* and *RPL6B* paralogs code for large ribosomal subunit proteins and are located 1800bp and 1000bp downstream of *FPR3* and *FPR4* respectively (Figure 8).

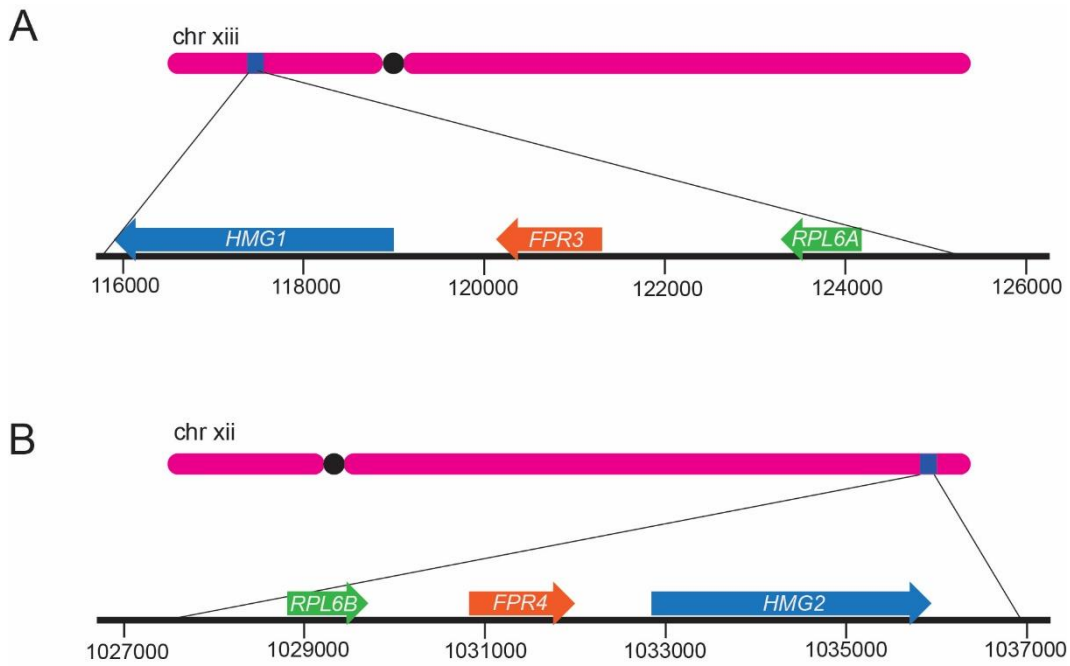

Figure 8. *FPR3* and *FPR4* display synteny in *S. cerevisiae*.
(A) Diagram of chromosome xiii with a close-up view of *FPR3* and two flanking genes (*HMG1* and *RPL6A*). (B) Diagram of chromosome xii with a close-up view *FPR4* and two flanking genes (*HMG2* and *RPL6B*).

Duplicate genes play an important role in protein and species evolution[250–252]. While the most common fate of duplicates is the accumulation of deleterious mutations over time and eventual loss[253–255], biology has learned to harness the value of these events through multiple mechanisms.

Immediately after a duplication event, a second gene copy can contribute to biological robustness by simply increasing dosage. This is particularly relevant for highly expressed genes; two well-studied examples of these include the histone coding genes[256] and ribosomal protein genes[257]. The fact that duplicates are more likely to have negative genetic interactions with each other than with non-duplicate genes[258], and that duplicated genes are less likely to produce severe fitness defects when deleted than non-duplicates[259] is evidence that many paralogs must have at least some degree of functional redundancy which contributes to biological robustness .

Duplicated genes also allow for an initial relaxation of selective constraints and provide an opportunity for evolutionary innovation and divergence[244,255]. Thus, since the earliest observations of duplications on chromosomes[260,261] and redundant genes [262–266], models have been proposed implicating gene duplication events as complex drivers of evolution[267–278]. I recommend [270] as an excellent review of the models proposed thus far.

Major models of post-duplication gene evolution include the neofunctionalization[271,273,277] and subfunctionalization model[274,275]. In the neofunctionalization model, one of the duplicate genes

accumulates positive, gain-of-function, mutations resulting in the development of new divergent functions[271,273,277]. In the subfunctionalization model, one duplicate acquires either gain- or loss-of-function mutations which result in an optimization or subdivision respectively of the functions originally performed by the unduplicated ancestral gene[274,275]. Because evolutionary forces act continuously, and can drive both the maintenance of duplicate genes with redundant functions and their functional divergence over time, experimentally assessing the degree of functional redundancy between duplicates is challenging.

1.6 Yeast Fpr3 and Fpr4

The paralogous yeast genes *FPR3* and *FPR4* code for two highly similar proteins, Fpr3 and Fpr4[248,279–281]. These proteins have common features which indicate a potential to carry out redundant functions. They also have unique features which indicate that over time the two may have diverged to carry out additional novel roles. In the following sections I present an overview of the features of these proteins and discuss evidence for their functional similarity and divergence.

1.6.1 Protein features of Fpr3 and Fpr4

At the overall level of their amino acid sequences, Fpr3 and Fpr4 proteins are approximately 60% identical and 72% similar (Figure 9 A). They share similar domain architectures (Figure 9 A). At their N-termini, both proteins have an NPM-like core domain consisting of the characteristic 8 stranded β-barrel with jellyroll fold topology (Figure 9 B)[239]. Unlike the metazoan NPM core however, the core domains of many fungal NPM-like proteins (including Fpr3 and Fpr4) contain an insertion of approximately 60 amino acids between the β4 and β5 strands[221,239]. This insertion, bisecting the NPM-like core domain, is comprised of stretches of acidic and basic residues. It is predicted to form a loop protruding away from the core (Figure 9 B)[221]. Like other NPM family histone chaperones, the nucleoplasmin core domains of Fpr3 and Fpr4 have the intrinsic propensity to form oligomers[109,239,282] (Figure 9 C).

The core NPM-like domain of both proteins is followed by a highly acidic region and a basic region (Figure 9 A) that forms a linker between the NPM-like and FKBP domains. These degenerate highly charged stretches are the most variable regions between Fpr3 and Fpr4. *In vitro,* the central acidic region of Fpr4 was found to be both necessary and sufficient for mediating interactions with free histones[221]. Both Fpr3[283] and Fpr4[284,285] have *in vitro* histone chaperone activity, facilitating the deposition of core histones onto closed circular DNA. In Fpr4,

this activity was found to reside solely in the N-terminal NPM core and central acidic domains (amino acids 1-220)[284,285].

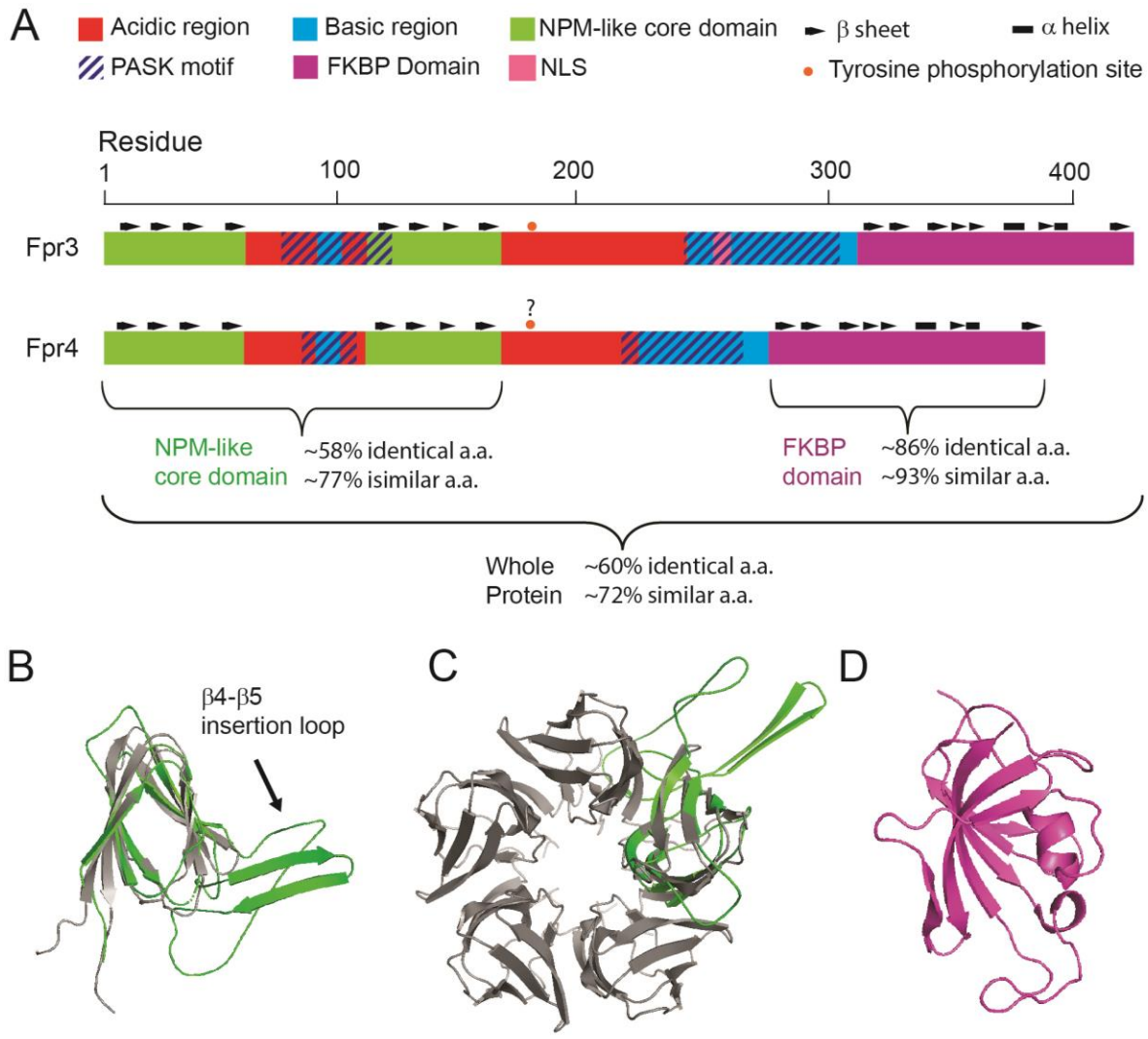

Figure 9. Fpr3 and Fpr4 share domain architectures.
(A) Domain architecture diagrams of Fpr3 and Fpr4. Approximate amino acid lengths are indicated. (B) Predicted structure of the yeast Fpr4 NPM domain (amino acids 1-168) in green overlaid on a single chain of the NMR structure of the NPM domain of *Drosophila* Fkbp39 (PDB ID: 4CA9) in gray[239]. The β4-β5 insertion loop which divides the NPM core domain in two is rich in acidic and basic residues as well as poly-acidic serine and lysine residue polyphosphorylation (PASK) motifs[286]. (C) Predicted structure of the yeast Fpr4 NPM domain (amino acids 1-168) in green overlaid on the NMR structure of the oligomerized NPM domain of Drosophila Fkbp39 (PDB ID: 4CA9) in gray[239] Overlaid figure adapted from[221]. (D) NMR structure of the Fpr4 PPI domain (PDB ID: 4BF8)[222].

Both proteins have a highly conserved C-terminal FKBP peptidyl-prolyl isomerase domain[222] (Figure 9 A). The FKBP domain of Fpr4 (Figure 9 D) has activity towards prolines 16, 30, and 38 of histone H3[222,223] and can interact with nucleosomes[221].

Fpr3 and Fpr4 appear to share similar post-translational modifications. Both proteins were recently found to be lysine polyphosphorylated, along with several ribosome biogenesis factors, at characteristic poly-acidic serine and lysine residue (PASK) motifs[286]. In Fpr3 and Fpr4 these motifs are located in and around basic regions, both within the NPM insertion loop and in the highly charged linker preceding the FKBP domain (Figure 9 A). Although the precise polyphosphorylated residues are not known, the addition of this post-translational modification would have drastic implications on the biochemical properties and functions of both of these proteins.

In *S. cerevisiae*, tyrosine phosphorylation is extremely uncommon and very few tyrosine phosphorylated proteins have been identified thus far[287]. Interestingly, Fpr3 is among this limited set. It is phosphorylated at tyrosine 184 by casein kinase II (CKII)[288–290] and dephosphorylated by phosphoprotein phosphatase Ptp1[291] (Figure 9 A). Although the biological significance of this modification remains to be fully understood[291–293], it has been proposed to control Fpr3 localization[291]. Whether Fpr4 is similarly tyrosine phosphorylated has not been explored; however, it remains a possibility as the target tyrosine residue appears to be conserved in both proteins.

1.6.2 Evidence for Fpr3 and Fpr4 functional similarity

Large scale protein interaction studies have revealed that Fpr3 and Fpr4 interact with each other physically[294]. This suggests that they may operate together. They also interact with a subset of common proteins, including histones H3 and H4 and a number of ribosome biogenesis factors such as Nop53[294,295]. Recently, the FKBP domain of Fpr4 has also been shown to bind nucleosomes through four lysine rich basic patches on its surface[221]. Although the ability of the Fpr3 FKBP domain to bind nucleosomes has never been tested directly, the fact that the amino acid sequences of the two domains are approximately 86% identical suggests that Fpr3 likely shares this ability.

Finally, both Fpr3 and Fpr4 can act as multi-copy suppressors of temperature sensitivity and mating defects resulting from the absence of the Tom1 E3 ubiquitin ligase[296,297]. This ligase ubiquitinates multiple substrates, including the ADA histone acetyltransferase complex, to target them for degradation by the proteosome[298]. Taken together, the many common features shared by Fpr3 and Fpr4 are evidence that they may have at least some degree of functional redundancy.

1.6.3 Evidence for Fpr3 and Fpr4 functional divergence

There is also evidence that Fpr3 and Fpr4 are not equivalent. Large scale protein interaction studies have uncovered subsets of physical interactors that appear to be unique to each protein[294]. Fpr3 uniquely physically interacts with factors required for mitotic sister chromatid cohesion (such as Dcc1, Irr1, and Smc3) and microtubule binding proteins (such as Bim1 and Kip2)[294]. Fpr4 also interacts with a unique subset of proteins; however, the ontological enrichments within this smaller subset are less clear[294].

Fpr3 has been identified as a regulator of chromosome dynamics at mitotic[294,299] and meiotic[300,301]centromeres. During meiosis, it enhances recombination checkpoint delay[300] and prevents meiotic chromosome synapsis initiation at centromeres[301]. To my knowledge, there have been no reports describing similar data for Fpr4. Both Fpr3 and Fpr4 regulate the protein levels of a centromeric histone H3 variant, Cse4[224], *in vivo*. Single gene deletion mutants of both Δ*fpr3* and Δ*fpr4* were associated with increased endogenous protein levels of Cse4 and increased Cse4 protein stability[224]. However, the level of Cse4 stabilization in Δ*fpr3* mutants was higher than that in Δ*fpr4* mutants indicating that these enzymes do not contribute equally to this biological process. Taken together these interactions and reports are evidence that Fpr3 and Fpr4 may have begun to functionally diverge over the course of evolution.

1.7 Ribosome Biogenesis

Both Fpr3 and Fpr4 localize to the nucleus and are enriched in the nucleolus for most of the cell cycle[279–281,302]. Fpr4 also physically associates with a variety of genomic loci, including the nucleolar ribosomal DNA (rDNA) chromatin[223,284]. Although the functions of these enzymes within this sub-nuclear body are not clear, they may be linked to the chromatin mediated regulation of transcription from rDNA. Evidence for this includes the fact that the N-terminal domain of Fpr4 (amino acids 1-284) is sufficient for silencing a reporter gene integrated within the rDNA locus[284]. Additionally, Fpr4 has been implicated in transcription induction kinetics through the isomerization of prolines on the amino tail of histone H3[223]. Notably, plant NPL-FKBPs related to *S. cerevisiae* Fpr3 and Fpr4 seem to have similar impacts on chromatin remodeling and transcription regulation at rDNA[240]. In the following sections I present an overview of rDNA chromatin regulation and ribosomal RNA processing and quality control. Each of these processes are of direct relevance to the data generated in my dissertation.

1.7.1 The nucleolus and rDNA chromatin regulation

The nucleolus is a membraneless sub-nuclear body consisting of ribosomal RNA coding genes (rDNA) and associated ribosome biogenesis proteins (including rRNA transcription machinery, rRNA processing factors, and pre-ribosomes)[303]. In *S. cerevisiae*, rDNA is located on the long arm of chromosome 12 and consists of 100-200 repeated genes organized in tandem[304] (Figure 10). A single rDNA tandem repeat is 9.1kb long and consists of two transcript coding regions. *RDN37* codes for the 35S pre-rRNA transcript and is transcribed by RNA pol I, while *RDN5* codes for the 5S pre-rRNA transcript transcribed by RNA pol III[304,305] (Figure 10). These rRNA coding regions are separated by two intergenic spacer sequences : *NTS1* (also known as *IGS1*) and *NTS2* (also known as *IGS2*)[304] (Figure 10).

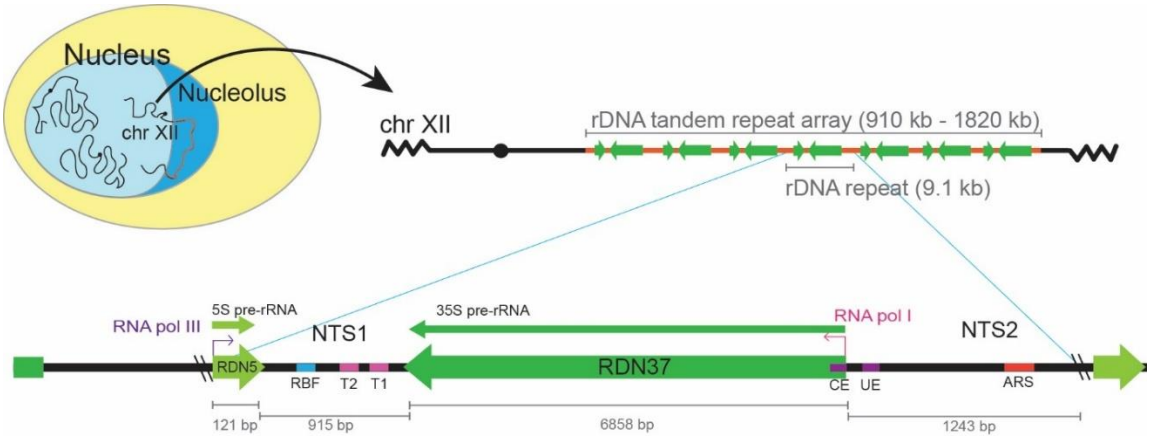

Figure 10. The nucleolus contains tandem repeats of ribosomal RNA genes
S. cerevisiae nucleolus and the features of chromosome 12 (chr XII). Abbreviations: replication fork binding site (RBF); terminator 1 (T1); terminator 2 (T2); promoter core element binding site (CE); promoter upstream element binding site (UE); autonomous replication sequence (ARS).

The *NTS* loci of the rDNA tandem array contain several important features (Figure 10). The *NTS1* sequence contains two elements downstream of the 35S coding region that serve as terminators of transcription (T1 and T2)[306]. Approximately 90% of RNA Pol I transcribed rRNA transcripts terminate at the first element[306]. Transcripts that escape the initial termination sequence terminate at the second "fail-safe" termination site[306]. The *NTS1* locus also includes a replication fork barrier (RFB) site downstream of the 35S sequence. This feature inhibits the progression of the DNA replication fork in the direction opposite to 35S rDNA transcription[307], allowing rDNA replication to proceed essentially unidirectionally and preventing collisions between DNA and RNA polymerases[307]. The *NTS2* locus contains an autonomous replication site (ARS) which functions as a unidirectional origin of replication[307]. Additionally, it contains

binding sites for two cis-regulatory elements (the upstream element (UE) and the core element (CE)) which enhance transcription of the 35S rRNA[308].

Growing cells have an enormous demand for proteins, and consequently ribosomes, to produce them[309]. Accordingly, a significant proportion of transcription is devoted to the energetically demanding process of ribosome biogenesis[309,310]. At least 60% of RNA Pol II transcribed mRNAs code for ribosomal proteins (r-proteins) and ribosome biogenesis or assembly factors, while approximately 80% of the total RNA in yeast is comprised of rRNAs[309]. Multiple tandem rDNA repeats facilitate high levels of rRNA transcription and are among the most heavily transcribed sequences both in yeast and other eukaryotes[309].

Due to their repetitive nature, however, tandem rDNA repeats are also highly sensitive to recombination events. These events result in the excision of circular rDNA species from the genomic array called extrachromosomal rDNA circles (ERCs), and conversely loss of DNA from chromosome 12[311,312]. ERCs are maintained in the cell and, due to the presence of the ARS site within *NTS2*, replicate along with the genomic DNA each time the cell divides[312,313]. Through a mechanism that may involve tethering to the nuclear pore complex[314], ERCs are retained in the mother cell upon cell division and accumulate in her exponentially after each round of DNA replication[312,313]. Here they may titrate essential replication factors[315] and contribute to replicative yeast senescence[311,312].

To balance the need for a high degree of expression with the need to limit recombination, rDNA is maintained in a mixed chromatin environment consisting of transcriptionally active and inactive repeats. Only approximately 50% of the tandem repeats in a given rDNA array are actively transcribed[316] and are thus present in an environment devoid of nucleosomes, known as euchromatin. The remaining 50% of rDNA repeats are transcriptionally inactive, or silenced[316]. The chromatin state (active or silenced) of a given rDNA gene is not fixed and can switch stochastically[317,318].

Silencing at rDNA originates at the *NTS1* and *NTS2* loci via one of two parallel pathways (for details of which I direct the reader to the following review[319]). In the Sir2 dependent pathway, the Fob1 protein binds to the RFB site where it recruits a complex consisting of the Sir2 histone deacetylase, Net1, and Cdc14 proteins[320,321]. Sir2 subsequently deacetylates lysines 9 and 14 on histone H3 and lysine 16 on histone H4 at proximal nucleosomes[322] promoting tight nucleosome packing and the generation and spread of an inaccessible DNA-protein environment[323], known as heterochromatin, around this locus[319]. In the Sir2 independent pathway, Fob1 interacts with condensin[324] which localizes the rDNA to the nuclear periphery[319,325] where it is sequestered away

from recombination proteins and transcription factors. The Sir2 independent pathway may function specifically during certain stages of mitosis when Sir2 is not present in the nucleus[319].

1.7.2 rRNA processing and quality control

S. cerevisiae cytoplasmic ribosomes consist of two subunits composed of rRNA and r-proteins. The 40S small subunit (SSU), where mRNA and tRNAs are brought together, consists of 18S rRNA and 33 r-proteins (Figure 11)[326]. The 60S large subunit (LSU), where the peptidyl transferase reaction occurs, consists of 5S rRNA, 5.8S rRNA, 25S rRNA, and 46 r-proteins (Figure 11)[326].

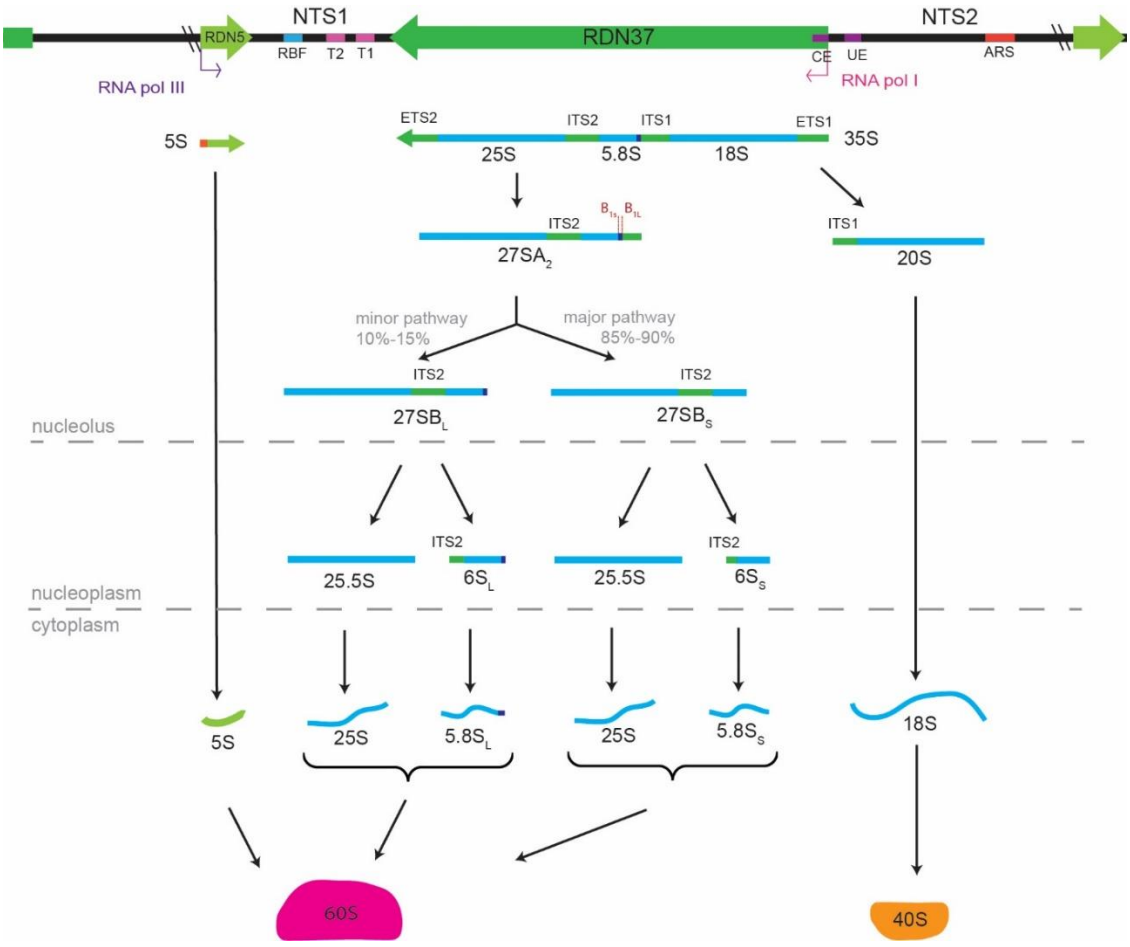

Figure 11. Ribosome biogenesis in yeast.
Pathway of yeast pre-rRNA processing from the nucleolus to the cytosol adapted from Woolford and Baserga's 2013 review[327].

Ribosome biogenesis requires the careful coordination of multiple factors including all three RNA polymerases (Pol I, Pol II, and Pol III), r-proteins, and ribosome biogenesis factors. Protein

phosphorylation plays an important role in ribosome biogenesis[328], and many ribosome biogenesis factors contain PASK motifs and are polyphosphorylated *in vivo*[286]. For details on the process of ribosome biogenesis, I direct the reader to the following reviews of ribosome biogenesis in yeast[327] and in humans[329].

In brief, yeast ribosome biogenesis begins with the transcription of rRNA in the nucleolus. The 18S, 5.8S, and 25S rRNAs originate from an initial 35S pre-rRNA transcript[304] (Figure 11). Transcription of 35S pre-rRNA requires RNA pol I and four transcription factors: the UAF upstream activating factor (which binds the UE), the TATA binding protein (TBP) (which binds the promoter TATA box), the core factor (which binds the CE), and the protein Rrn3[330–333].

The 35S pre-rRNA transcript is both co- and post- transcriptionally cleaved, folded, and modified as it is exported from the nucleolus to the cytoplasm (Figure 11)[327]. First, the 5' and 3' external transcribed spacers (ETS1 and ETS2 respectively) are removed[334]. Next, a cleavage within an internal transcribed spacer ITS1 separates this transcript into a 20S and a $27SA_2$ pre-rRNA precursor[335]. Processing of $27SA_2$ pre-rRNA proceeds via two alternative pathways. Approximately 85%-90% of transcripts are cleaved at a B_{1S} site at the 5'end, while the remaining 10%-15% are cleaved at a B_{1L} site[336–338]. The resulting precursors ($27SB_S$ and $27SB_L$ respectively) differ by 6 nucleotides and result in two variant 5.8S rRNAs[339,340]. The functions of these variants remain unknown. Subsequent cleavages and processing within the nucleosol and cytoplasm result in the formation of mature 18S, 5.8S, and 25S rRNAs.

Transcription of 5S rRNA begins with the recruitment of RNA Pol III to the promoter, and requires three transcription factors: TFIIIA (which is specific to the internal promoter of 5S genes), TFIIIB, and TFIIIC[341]. A cleavage at its 5' end in the cytoplasm results in the mature transcript[342]. Modifications placed by small nucleolar riboproteins (snoRNPs) and associations with r-proteins occur both co- and post- transcriptionally and facilitate correct ribosomal folding, processing, and function[327].

Because ribosome biogenesis is a complex process, it is subject to stringent quality control mechanisms. RNA exosome complexes contain exonucleases and function to degrade defective rRNAs and pre-rRNAs[343,344]. The nuclear exosome in *S. cerevisiae* consists of six proteins (Rrp41, Rrp42, Rrp43, Rrp45, Rrp46, and Mtr3) which form a barrel-like structure with a central pore called the PH ring[345,346] (Figure 12 A). At the pore entry site are three additional proteins (Rrp4, Rrp40, and Csl4) which form a cap, and a 5'-3' exonuclease (Rrp6)[345–347] (Figure 12 A). At the pore exit site is a second catalytic subunit: Dis3, which has both endonuclease and 3'-5' exonuclease activity[345,346,348] (Figure 12 A).

The nuclear exosome degrades a wide variety of transcripts in addition to rRNAs and pre-rRNAs: including tRNAs[349,350], telomeric RNAs[351], small nucleolar (snoRNAs)[344], mRNAs[352], and cryptic unstable transcripts (CUTs)[353–355] . However, in order to efficiently initiate degradation, it requires that the targeted transcript have a short stretch of 4-6 poly-adenines at its 3'end[344]. This short poly(A) tail is thought to facilitate binding of the target to the exosome and initiate degradation. The yeast TRAMP5 complex functions to recognize and polyadenylate transcripts for degradation in the nuclear exosome[356]. It consists of: a non-canonical poly(A) polymerase (Trf5) which catalyzes the addition of the short poly(A) tail; an RNA binding protein (Air1) thought to contribute to its interaction with the target; and a helicase (Mtr4) which unwinds secondary structures on the target[357] (Figure 12 B). How the TRAMP5 complex recognizes target transcripts is still not fully understood but rRNA target recognition may be based on ribosome biogenesis kinetics[358]. The TRAMP5 complex immunoprecipitates with rDNA which suggests that it may act as a co-transcriptional rRNA surveillance mechanism[359].

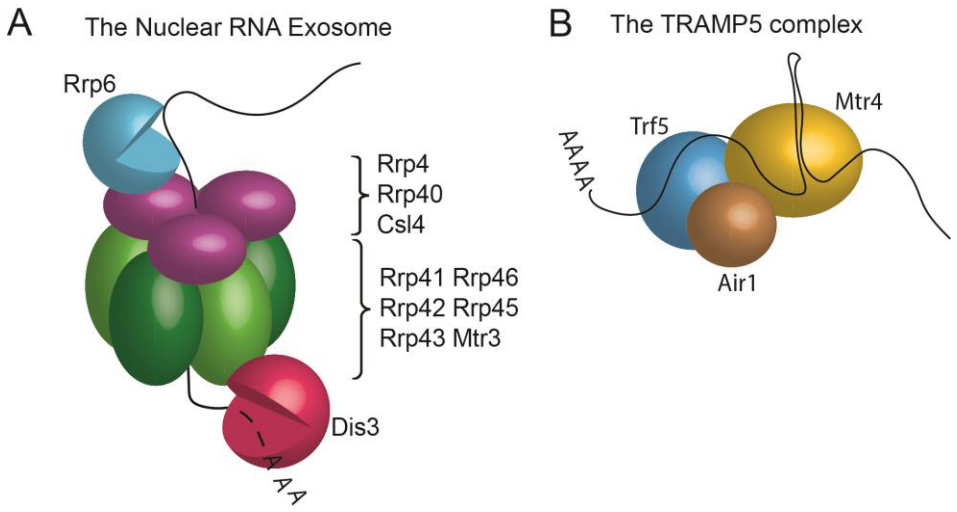

Figure 12. The nuclear RNA exosome and TRAMP5 complexes.

(A) Schematic of the nuclear RNA exosome adapted from Wolin et al. 2012 review [360] (B) Schematic of the TRAMP5 complex adapted from Wolin et al. 2012 review [360]

1.8 Research Objectives

NPM-family histone chaperones and FKBP prolyl-isomerases are both involved in chromatin regulation. In insects, plants, and fungi key features of both of these enzymes are present in the NPL-FKBP family of histone chaperones/chromatin remodelers. Many model organisms, including *Saccharomyces cerevisiae*, have two NPL-FKBPs derived from the duplication of a common ancestral gene. Although great strides have been made in our understanding of the

structural and biochemical properties of these enzymes, much remains to be discovered regarding their biological functions and mechanisms of action. The roles of their prolyl-isomerase functions, in particular, have proven especially elusive and intriguing. A comprehensive understanding of the biological processes and pathways sensitive to NPL-FKBPs in insects, plants and fungi such as *S. cerevisiae*, will provide valuable insights into the functions of related enzymes in mammals and will contribute to an improved understanding of their roles in disease etiology.

At the onset of this dissertation project, the comparative biological functions of the *S. cerevisiae* NPL-FKBPs, Fpr3 and Fpr4, were poorly understood. While their retention over millions of years of evolution implied that both enzymes contributed to organism fitness and were thus not equivalent, their high degree of structural similarity also indicated the potential for functional redundancy. The overarching objective of my research has been to characterize the separate and redundant biological functions of these chromatin regulators using a systems biology approach.

Given the collective evidence for both shared and separate functions, I hypothesized that Fpr3 and Fpr4 are in the process of functionally diverging, and thus simultaneously operate separately, cooperatively and redundantly to regulate a variety of chromatin environments.

To test this hypothesis, I began by refining the powerful synthetic genetic array (SGA) method of annotating gene-gene interactions, by making it amenable to the analyses of paralogous genes. My logic was that these genetic interactions would serve as distinct phenotypic fingerprints, that reveal instances of paralog redundancy and cases for distinct and separate functions (i.e. neofunctionalization). These experiments are presented in Chapter 2.

The genetic interaction data generated in Chapter 2 prompted me to look deeper into the impact of Fpr3 and Fpr4 on the transcriptome. In Chapter 3, I provide transcriptomic evidence in support of shared, separate, and redundant functions of Fpr3 and Fpr4, and show that these enzymes cooperate to regulate genes involved in polyphosphate metabolism and ribosome biogenesis. Furthermore, I identify an important role for Fpr4 at the 5’ ends of protein coding genes and the non-transcribed spacers of ribosomal DNA.

In Chapter 4, I show that yeast lacking Fpr4 also exhibit a genomic instability phenotype at ribosomal DNA, consistent with the model that this histone chaperone regulates chromatin structure and DNA access at this locus. Collectively, the data presented in this dissertation represent the first comprehensive and comparative study of NPL-FKBP chaperones in yeast and as such provide a significant contribution to our understanding of their biological functions.

Chapter 2
Genetic interactions reveal comparative functions of Fpr3 and Fpr4

This chapter was adapted in part from the publication:

Savic, N., Shortill, S. P., Bilenky, M., Dobbs, J. M., Dilworth, D., Hirst, M., Nelson, C.J. Histone Chaperone Paralogs Have Redundant, Cooperative, and Divergent Functions in Yeast. *Genetics*. **213(4),** 1301-1316 (2019).

Contributions pertaining to data presented in this chapter: Experiments and data analysis were performed by NS under the supervision of CJN with the following exceptions: SS assisted with the biological replicate of the SGA screen data included in this chapter under the supervision of NS. SS performed the validation spotting assays in Figure 18 A and B.

2.1 Introduction

Both NPM family proteins and nuclear FKBPs are clinically relevant in humans. However, due to the complexity of human biological systems, their functions remain poorly understood. Insect, plant, and fungal NPL-FKBPs share similarities to human NPMs and nuclear FKBPs via their NPM-like and FKBP domains respectively (see Figure 9). Thus, understanding the functions of NPL-FKBPs in simpler model eukaryotes will provide a foundation for understanding the roles of their human orthologues. However, a challenge to the study of NPL-FKBPs in classic unicellular model organisms (*S. cerevisiae* and *Sz. pombe*) is that these proteins appear as paralogs in these organisms (see Figure 7)[178,179].

At the onset of this dissertation, information about the comparative functional biology of the *S. cerevisiae* NPL-FKBP paralogs, Fpr3 and Fpr4, was limited. *In vitro,* the NPM-like domain of Fpr4 was known to build chromatin by chaperoning histones onto DNA[283–285]. The FKBP domains of both proteins were known to have prolyl-isomerase activity towards prolines on histone tails[222–224]. Less was known about the functions of these enzymes *in vivo*. When present on high copy number plasmids, both enzymes suppress temperature sensitivity and mating defects associated with mutants of the Tom1 E3 ubiquitin ligase[296]. Additionally, Fpr3 was implicated in chromosome dynamics at mitotic[294,299]and meiotic[300,301]centromeres, while Fpr4 was linked to

chromatin and transcription at rDNA[223,284]. Collectively, these data suggested that Fpr3 and Fpr4 may carry out both common and divergent functions. However, a dedicated and comparative systems-level analysis had never been performed on them.

Genetic interactions occur when mutations in two or more genes produce a phenotype in combination with each other that is different than would be expected given the effects of each mutation individually[361,362]. Aggravating (or synthetic) genetic interactions involve multi-gene mutants with *more* extreme phenotypes than expected, while alleviating (or suppressor) genetic interactions involve mutants with *less* extreme phenotypes than expected[361]. Because functionally related genes tend to genetically interact with each other[363], genes with known functions can provide insight into interacting genes with unknown functions. Synthetic genetic interactions identify compensatory biological pathways and complexes, while suppressor interactions identify gene products involved in concert or in the same biological pathway[361]. Synthetic genetic array (SGA) analysis is a high-throughput screening approach[364–366] for systematically constructing multi-gene deletion mutants and scoring their relative fitness to identify genetic interactions.

Chromatin modifiers, such as the histone chaperone *ASF1* and the histone post-translational modifier *HDA1*, display clear chromatin-related genetic interactions in SGA screens[249,367]. Prior to the work presented in this dissertation however, the published genetic interactomes of *FPR3* and *FPR4*[249,367–370] included few chromatin-related genes. This is surprising given their *in vitro* histone chaperone[283–285] and histone prolyl-isomerase activities[222,223], their physical association with chromatin[223,284], and effect on transcription activation kinetics[223]. A possible explanation for this lack of interactors is functional redundancy between Fpr3 and Fpr4. The high similarity of these enzymes may allow them to compensate for each other; this compensation would be expected to mask *FPR3* and *FPR4* interactions in conventional SGA screens. In support of this explanation, *Δfpr3* and *Δfpr4* single gene deletion mutants are viable and lack fitness related phenotypes[248] , but double deletion *Δfpr3Δfpr4* mutants display a reduced fitness (synthetic sick) phenotype[249]. However, several species of fungi related to *S. cerevisiae* also possess duplicate NPL-FKBPs, either through parallel or convergent evolution (Figure 7). This argues against the complete redundancy of these enzymes and predicts that each paralog must provide a unique function. To test the validity of these models, I developed *Paralog-SGA* which is an adaptation of the conventional yeast SGA approach specially designed to dissect the genetic interactions of paralogs.

In this chapter, I present data from a set of comprehensive Paralog-SGA screens which provide insights into the comparative biology of *S. cerevisiae* Fpr3 and Fpr4. These data support both the redundant and unique function models. I find that Fpr3 and Fpr4 have divergent genetic

interaction profiles with respect to genes involved in centromeric chromatin function (unique to Fpr3) and replicative cell aging (unique to Fpr4). Furthermore, I identify a genetic interaction profile shared between Fpr3 and Fpr4 with genes involved in chromatin remodeling. This implies an unexpected cooperative function of these histone modifiers. I show that the TRAMP5 RNA exosome becomes essential only in *Δfpr3Δfpr4* yeast, providing direct evidence for functional redundancy of these paralogs in the negative regulation of RNAs. Taken together, these experiments represent the first comprehensive functional analysis of Fpr3 and Fpr4 *in vivo* and provide an explanation for why such highly conserved proteins are retained.

2.2 Results

2.2.1 Paralog-SGA reveals distinct genetic interaction fingerprints for duplicated genes

Conventional *S. cerevisiae* SGA screens[365,366] are designed to identify the genetic interactions of a single query gene. They involve crossing a single gene deletion mutant query to the 4976-strain yeast non-essential deletion mutant array (DMA). Sporulating the resultant diploids allows unlinked alleles to segregate, while subsequent selection steps isolate double deletion meiotic progeny. The colony sizes of these double deletion mutants are then scored as a proxy for fitness to identify interacting genes (Figure 13). Negative aggravating, or synthetic sick/lethal (SSL) genetic interactions are identified by double deletion mutants with lower than expected fitness phenotypes. Positive alleviating, or suppressor genetic interactions are identified by double deletion mutants with higher than expected fitness. One limitation to this conventional approach, is that paralogs of the query may functionally compensate for the deleted query and mask a subset of interactions associated with redundant functions.

Most genetic interactors of *FPR3* and *FPR4* published before the onset of this dissertation work were uncovered using a conventional SGA approach[249,367–370]. The most comprehensive conventional SGA study to date has identified: 28 non-essential genes as negative and 21 non-essential genes as positive significant interactors of *FPR3*, and 74 non-essential genes as negative and 29 non-essential genes as positive significant interactors of *FPR4*[367,371]. An analysis of the ontologies enriched among these interacting genes using a web based cluster interpreter for yeast[372] reveals no significantly enriched molecular functions, biological processes, cellular components, or protein complexes (at a *p*-value cut-off of $\leq 10^{-4}$). The lack of chromatin related genetic interactors in these screens is especially surprising given their *in vitro* histone

chaperone[283–285] and prolyl isomerase activities[222,223], and their *in vivo* physical association with chromatin[223,284] and effect on transcription kinetics[223].

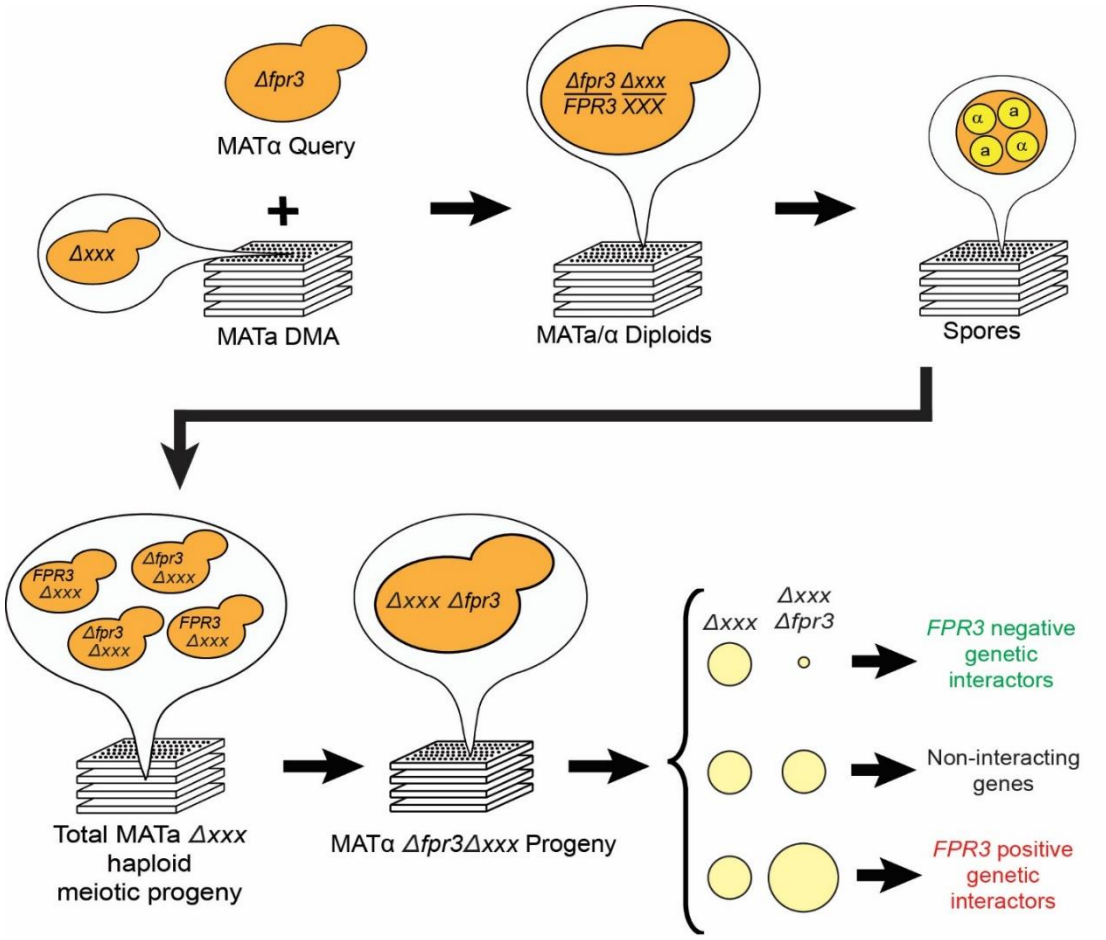

Figure 13. Conventional synthetic genetic array workflow.
Schematic of key steps in the conventional synthetic genetic array workflow adapted from Tong, A. and Boone, C. (2006)[365]. *FPR3* is used as an example query gene. A MATα haploid single deletion *Δfpr3* query strain is crossed to the MATa *Δxxx* DMA collection. The resulting MATa/α diploids are subjected to sporulation, allowing all unlinked alleles to segregate randomly. A mixed population of total MATa *Δxxx* meiotic progeny spores are germinated. Subsequent selection steps allow for the isolation of all *Δfpr3Δxxx* progeny. Phenotypic features such as colony sizes are assessed as a proxy for cell fitness. Genetic interactions are identified by comparing the fitness (*i.e.* colony area) of each double deletion mutant colony to the corresponding single deletion *Δxxx* control colony. Negative aggravating, or synthetic sick/lethal genetic interactions are identified by double mutants with significantly decreased colony sizes relative to the controls. Positive alleviating, or suppressor genetic interactions are identified by double mutants with significantly increased colony sizes relative to the controls.

In contrast, conventional SGA analysis of known chromatin modifiers, such as the histone chaperone *ASF1* and the histone deacetylase *HDA1*, reveals a significant number of interacting genes directly associated with chromatin. For example, the 332 significant negative genetic interactors of *ASF1*, include a significant enrichment of genes with ontologies such as: histone deacetylation (p=1.808x10^{-6}), HDA1 complex (p=9.572x10^{-5}) and CAF-1 complex

(p=9.572x10^{-5})[367,371]. A possible explanation for the absence of chromatin related *FPR3* and *FPR4* genetic interactors in conventional SGA screens is that the high similarity of these enzymes allows them to functionally compensate for each other. Thus, in conventional SGA screens based on single gene deletion query mutants, this compensation would mask a subset of their genetic interactions. Evidence that paralogous genes may functionally compensate for each other includes the fact that paralogs are more likely to have negative genetic interactions with each other than with non-paralog genes[258], and the fact that single gene deletion mutants of a paralogous gene tend to have less severe fitness defects than single gene deletion mutants of a non-paralogous gene[259].

To capture masked genetic interactions and comprehensively determine biological processes sensitive to Fpr3 and Fpr4, I designed and performed a paralog specific modified SGA screen (Figure 14, see materials and methods at the end of this chapter). The modified *Paralog-SGA* workflow involves crossing a dual-query *Δfpr3Δfpr4* double mutant to the DMA. Spores generated from this single cross are manipulated in parallel to create double (*Δfpr3Δxxx* and *Δfpr4Δxxx*) and triple (*Δfpr3Δfpr4Δxxx*) mutant sets of meiotic progenies. Importantly, to avoid the slow growth phenotype of *Δfpr3Δfpr4* dual deletion mutants and their vulnerability to spontaneous alleviating suppressor mutations, the query strain harbours a 'rescuing' episomal *URA3* plasmid with a functional *FPR4* gene. This plasmid is maintained until the final step of the screen when counter-selection with 5- fluoroorotic acid (5-FOA) creates the *Δfpr4* null status. The colony sizes of each double and triple mutant are then compared to the sizes of their corresponding total haploid population controls and represented as a fitness ratio. Based on the total spread of fitness ratios within each screen set, cut-off thresholds are established using the Balony image analysis software package[373] to identify positive and negative genetic interactions. Mutants with fitness ratios below a lower threshold cut-off (l) represent synthetic sick and lethal interactions between the query gene(s) and gene *XXX* from the DMA. Mutants with fitness ratios above an upper threshold cut-off (u) represent suppressor interactions. A summary of each genetic screen is provided in the form of an "S-curve" that plots the fitness ratio of each double or triple mutant (Figure 15).

Using automatically estimated l and u cut-off thresholds and default Balony hit parameters (i.e. reproducibility in 3/3 sets and p-values < 0.05), I detected 534 synthetic sick/lethal (l=0.914) interactions for *FPR3* (Figure 15 A) and 216 synthetic sick/lethal (l=0.923) interactions for *FPR4* (Figure 15 B). These numbers represent 10.7% and 4.3% respectively of the 4976 non-essential genes present in our MATa yeast deletion collection. The higher number of interactors uncovered via this paralog-SGA approach compared to the number of interactors uncovered by conventional

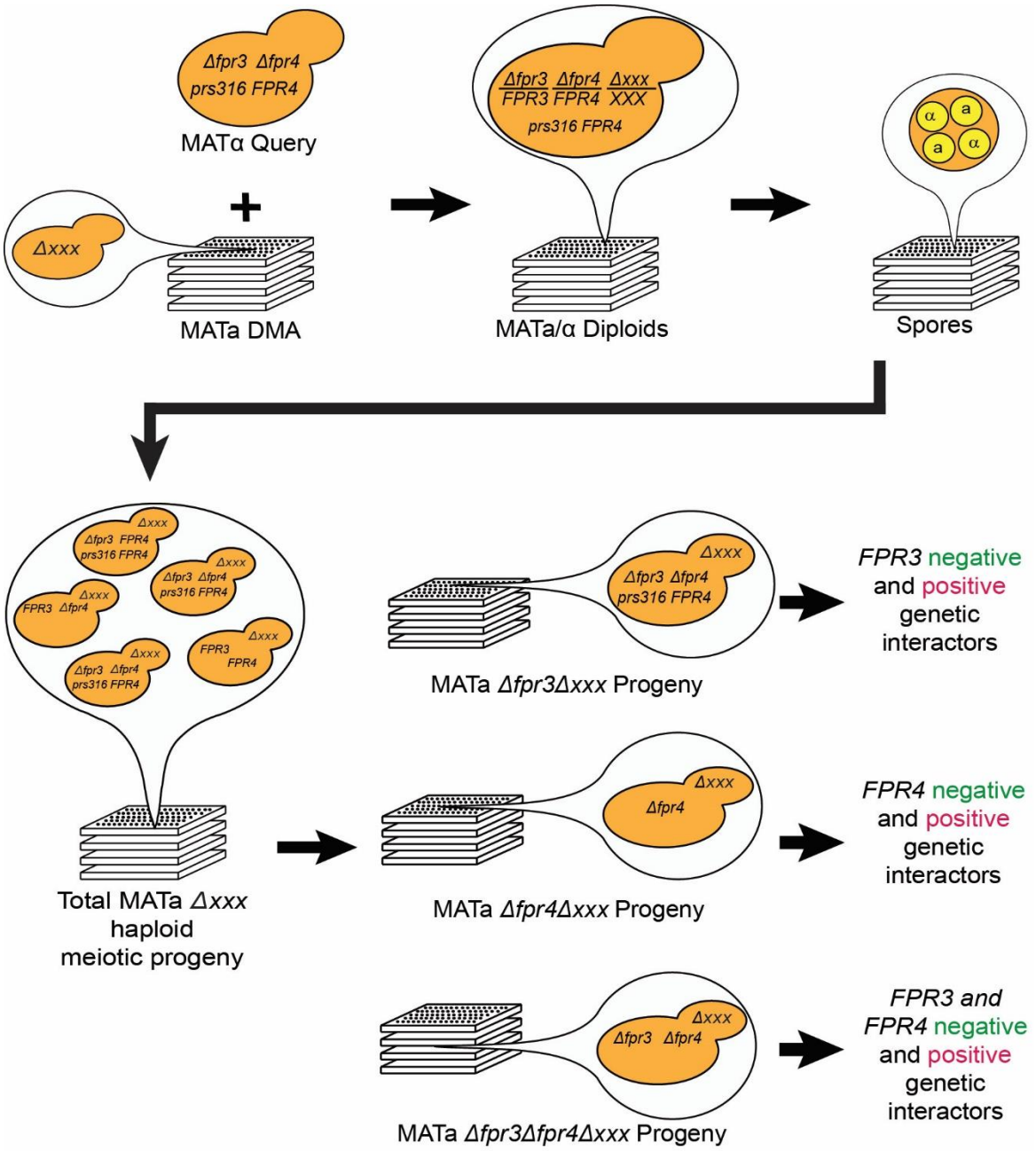

Figure 14. Paralog synthetic genetic array (Paralog-SGA) workflow.
Schematic of key steps in the paralog synthetic genetic array workflow. A MATα haploid double deletion *Δfpr3Δfpr4* query strain, harboring *FPR4* on an episomal plasmid (pRS316-FPR4), is crossed to the MATa *Δxxx* DMA. The resulting MATa/α diploids are subjected to sporulation allowing all unlinked alleles and episomal plasmid to segregate randomly. A mixed population of total MATa *Δxxx* meiotic progeny spores are germinated. Subsequent selection steps allow for the parallel isolation of all *Δfpr3Δxxx* progeny, *Δfpr4Δxxx* progeny, and *Δfpr3Δfpr4Δxxx* progeny. Colony sizes (measured as pixel area) are then scored as a proxy for cell fitness. Genetic interactions are identified by assessing the ratio of normalized sizes of each multi-gene progeny mutant colony to the corresponding total haploid meiotic progeny population *Δxxx* control colony. Negative aggravating, or synthetic sick/lethal genetic interactions correspond to multi-gene progeny mutant colonies with significantly decreased sizes relative their corresponding controls (i.e. ratios << 1). Positive alleviating, or suppressor genetic interactions correspond to multi-gene progeny mutant colonies with significantly increased sizes relative their corresponding controls (i.e. ratios >>1).

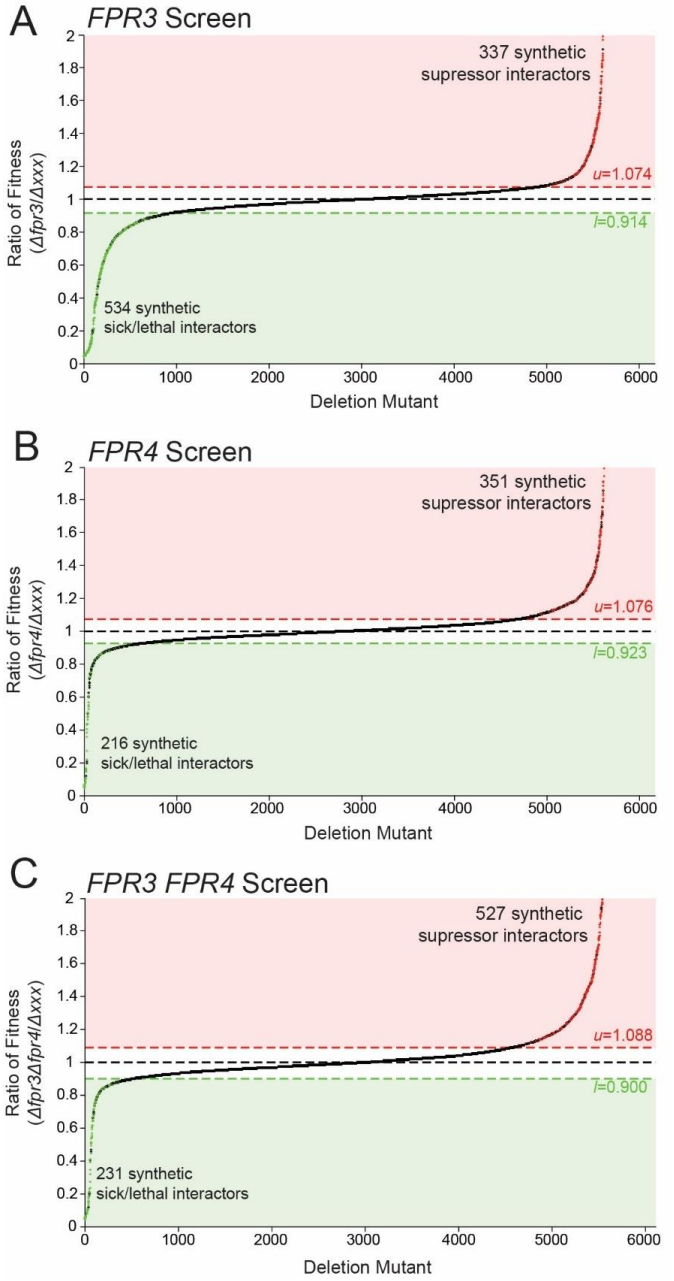

Figure 15. Paralog-SGA reveals negative and positive genetic interactors of *FPR3* and *FPR4*
S-curves summarizing the ratios of fitness corresponding to each multi-gene deletion mutant generated from: (A) the *FPR3* screen, (B) the *FPR4* screen, and (C) the *FPR3 FPR4* screen. Ratios of fitness were calculated with the Balony image analysis software package[373] by dividing the normalized mean area occupied by each experimental multi-gene deletion mutant colony (in pixels) by the normalized mean area occupied by its corresponding total meiotic progeny control colony (in pixels). Each ratio is represented as a single dot. Green dots indicate synthetic sick and lethal phenotypes, red dots indicate suppressor phenotypes, and black dots indicate no interaction or a ratio that does not satisfy default Balony hit paraleters. Total numbers of interacting genes are indicated on the plots. The total numbers of interacting genes do not include linked genes and count genes present in multiple copies on the DMA only once. Upper (*u*) and lower (*l*) cutoff thresholds are represented by red and green dashed horizontal lines respectively.

SGA[367,371] may be due to several fundamental differences in screen design and data processing. The most important difference likely being the presence of the low copy rescuing plasmid harboring *FPR4* in the paralog-SGA query (Figure 14). The use of different normalization algorithms, and significance cut-off thresholds in the scoring of genetic interactors in conventional vs. paralog SGA screens, may also have contributed to the differences in the overall number of interactors uncovered. The fact that *FPR3* negatively interacts with more than twice as many non-essential genes compared to *FPR4* in these paralog-SGA screens, immediately indicated that these two enzymes are not functionally equivalent and that the deletion of *FPR3* imparts more genetic vulnerabilities on cells than the deletion of *FPR4*.

The dual gene screen, designed to uncover masked genetic interactions, identified only 231 synthetic sick/ lethal *Δfpr3Δfpr4Δxxx* triple mutants (l=0.900) (Figure 15 C). Notably, there are fewer synthetic sick or lethal *Δfpr3Δfpr4Δxxx* mutants than *Δfpr3Δxxx* mutants, which suggests that Fpr4 is toxic in the absence of Fpr3. In other words, the slow growth of many *Δfpr3Δxxx* deletion strains may be due to Fpr4 partially engaging in Fpr3-regulated processes. In triple *Δfpr3Δfpr4Δxxx* mutants, lack of toxic Fpr4 eliminates this subset of indirect interactions and results in a lower total number of synthetic sick/lethal interactors.

2.2.2 *FPR3* and *FPR4* have separate, shared, and redundant genetic interactions including with genes involved in chromatin biology

To gain insights into the comparative biology of Fpr3 and Fpr4, I performed a gene ontology analysis on the negative genetic interactors that were a) unique to the *FPR3* screen, b) unique to the *FPR4* screen, c) common to both *FPR3* and *FPR4* screens, and d) masked; or only present in the *FPR3FPR4* double mutant screen. I identified 456 and 138 genetic interactors that were unique to either *FPR3* or *FPR4* respectively (Figure 16 top). Thus, the number and nature of these genetic interactions demonstrates that these paralogs are not functionally equivalent. I also uncovered 78 genes that interacted with both *FPR3* and *FPR4* (Figure 16 top). These interactions indicate that there are also specific contexts of paralog cooperativity, i.e. situations where both proteins are required for function. Finally, my analysis identified 75 masked interactors (Figure 16 bottom). Deletion of these genes only impacted the fitness *Δfpr3Δfpr4* double mutant yeast. Thus, these interacting genes presumably describe processes where the two paralogs are functionally redundant.

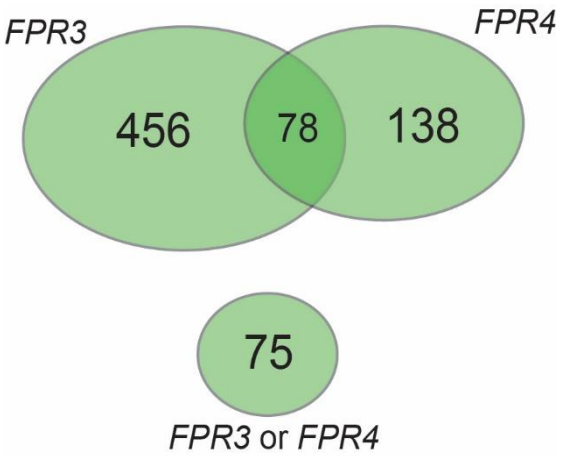

Figure 16. *FPR3* and *FPR4* have unique, cooperative, and redundant synthetic sick/lethal genetic interactions.
Venn diagrams indicating the numbers of unique and cooperative (top) and redundant (bottom) synthetic sick/lethal genetic interactors uncovered from the Paralog-SGA analysis.

Ontologies enriched among the 456 unique synthetic sick and lethal genetic interactors of *FPR3* are listed in appendix Table 1. The *p*-values associated with each ontology were calculated automatically by the FunSpec program[372], and represent the probability that the intersection of the 456 interacting genes with any given ontology occurs by chance. Notable ontologies with *p*-values below an arbitrary cut-off of $p \leq 10^{-4}$ include biological processes such as: mitochondrial translation ($p<10^{-14}$); mitotic sister chromatid cohesion ($p=1.42\text{x}10^{-5}$); protein lipoylation ($p=2.06\text{x}10^{-5}$); ubiquitin-dependent protein catabolic process via the multivesicular body sorting pathway ($p=2.45\text{x}10^{-5}$); establishment of mitotic spindle orientation ($p=5.98\text{x}10^{-5}$); and mitochondrial genome maintenance ($p=9.20\text{x}10^{-5}$) (Figure 17).

Special attention was given in the analysis to interacting genes coding for complex components (Figure 17). Here the arbitrary *p*-value cut-off was set to a higher $p \leq 10^{-2}$. Among *FPR3* specific interactors were genes coding for components of: the large and small mitochondrial ribosomal subunits ($p<10^{-14}$ and $p=7.49\text{x}10^{-7}$ respectively); the mitochondrial pyruvate dehydrogenase complex ($p=1.16\text{x}10^{-3}$); the cytochrome bc1 complex ($p=3.11\text{x}10^{-3}$); and the ESCRT II endosomal sorting complex ($p= 3.06\text{x}10^{-4}$) (Figure 17). Also identified were all three components of the carboxy-terminal domain protein kinase 1 (Ctk1) complex ($p=3.06\text{x}10^{-4}$), and four components of the Swr1 chromatin remodeler ($p=9.00\text{x}10^{-3}$). These interactions support at least some potentially chromatin centric roles for Fpr3. Complexes involved in chromosome segregation, such as the astral microtubule ($p=6.48\text{x}10^{-6}$), kinetochore ($p=1.14\text{x}10^{-4}$), and the Mrc1/Tof1/Csm3 complex ($p=3.06\text{x}10^{-4}$), were also uncovered among genetic interactors unique to *FPR3* but not *FPR4*. These systems-level data support reports which indicate that Fpr3, but not

Fpr4, regulates mitotic and meiotic chromosome dynamics, including those associated with centromeres[224,300,301].

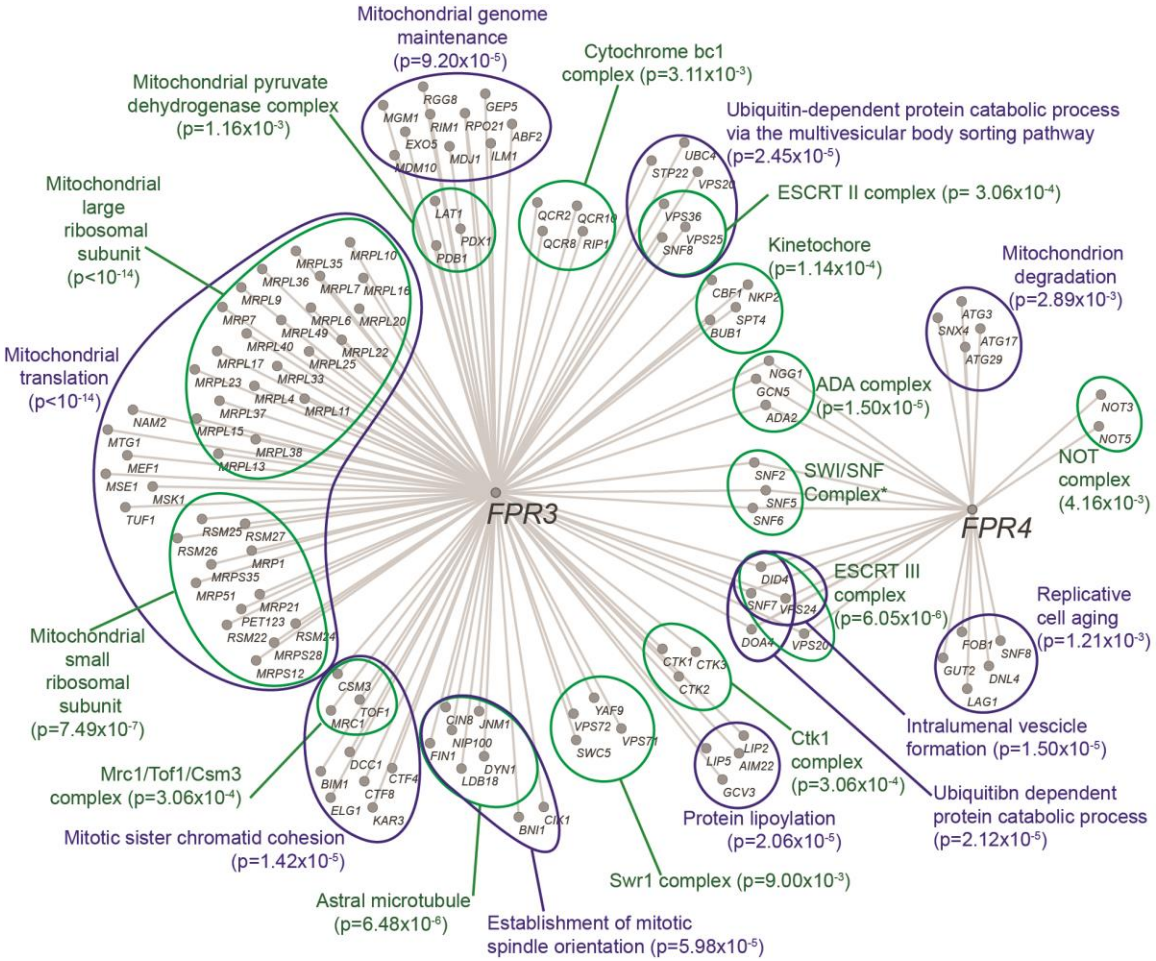

Figure 17. Synthetic sick/lethal genetic interactors reveal that Fpr3 and Fpr4 have separate and cooperative functions.
Network diagram summarizing the synthetic sick/lethal genetic interactions of *FPR3* and *FPR4* as identified in Paralog-SGA screens. Genes displaying a negative interaction (grey circles) are clustered based on common biological processes (blue) or membership in annotated protein complexes (green). * *SNF2*, *SNF5*, and *SNF6* were identified as hits in the *FPR4* screen only, but displayed a synthetically sick phenotype with both Δ*fpr3* and Δ*fpr4* mutations in confirmatory spotting assays (see Figure 18). Interaction network was generated using the Cytoscope open source software platform[374]. Lines between genes indicate a negative genetic interaction.

Although the paralog screens uncovered 138 *FPR4* specific genetic interactions, they fell into limited ontology categories (see appendix Table 2). At an arbitrary *p*-value cut-off of $p \leq 10^{-4}$, there were no ontologies related to biological processes among *FPR4* unique genetic interactors. However, at a higher cutoff ($p \leq 10^{-2}$), the processes of mitochondrion degradation ($p=2.89\text{x}10^{-3}$) and replicative cell aging ($p=1.21\text{x}10^{-3}$) emerged (Figure 17). The enrichment of genes associated with replicative cell aging among *FPR4* unique interactors is of particular interest given the link between this aging process and chromatin mediated rDNA stability[375], and will be further

explored in Chapter 4 of this dissertation. These interactions thus support a role for Fpr4 in this process that is not shared by Fpr3. The only protein complex ontologies enriched among *FPR4* unique negative interactors were two of the nine components of the Ccr4-NOT transcription regulator complex ($4.16x10^{-3}$) (Figure 17), which has been implicated in multiple steps of mRNA regulation[376]. Taken together, the number and nature of negative genetic interactions from single query screens suggests a model where Fpr3 and Fpr4 have at least some separate biological functions for which they are not interchangeable. This model predicts that Fpr4 cannot fulfil some biological functions of Fpr3, particularly those in meiotic and mitotic chromosome dynamics, and mitochondrial ribosome biology, while Fpr3 cannot substitute for the more limited roles of Fpr4 in processes related to replicative cell aging.

Genetic interactions shared between *FPR3* and *FPR4* would be expected only if both paralogs were required for efficient execution of the biological process. Ontologies enriched among the 78 shared synthetic sick/lethal genetic interactors are listed in appendix Table 3. Notable biological processes, with *p*-values below an arbitrary cut-off of $p \leq 10^{-4}$, included intralumenal vesicle formation ($p=1.50x10^{-5}$), and ubiquitin dependent protein catabolic process involving the multivesicular body sorting pathway ($p=2.12x10^{-5}$) (Figure 17). Complex related ontologies enriched among common interactors of Fpr3 and Fpr4 included the ESCRT III endosomal sorting complex ($p=6.05x10^{-6}$), the Ada2/Gcn5/Ada3 (ADA) histone acetyltransferase complex ($p=1.50x10^{-5}$), and the SWI/SNF chromatin remodeling complex (Figure 17). Shared genetic interactions with key components of the ADA complex (*ADA2* and *NGG1*) and the SWI/SNF remodeler (*SNF2*, *SNF5* and *SNF6*) were independently confirmed using spotting assays (Figure 18). The processes and complexes enriched among shared genetic interactors indicate that Fpr3 and Fpr4 cooperate in performing some biological functions. This proposed cooperativity is supported by the fact that Fpr3 and Fpr4 co-purify[294] and have the intrinsic propensity to form oligomers[109,239,282]. Furthermore, the shared interactions with known chromatin modifiers are genetic evidence that Fpr3 and Fpr4 cooperatively regulate chromatin. In the absence of either paralog, cells become reliant on the SWI/SNF remodeler and the ADA histone acetyltransferase for robust growth.

2.2.3 The TRAMP5 nuclear exosome is a masked genetic interactor of *FPR3* and *FPR4*

Genes essential to *Δfpr3Δfpr4* double mutant yeast but not to *Δfpr3* or *Δfpr4* single mutants indicate processes where these paralogs are functionally redundant. I refer to these interactions as ‘masked’. My Paralog-SGA screening approach revealed 75 such genetic interactions (Figure 16

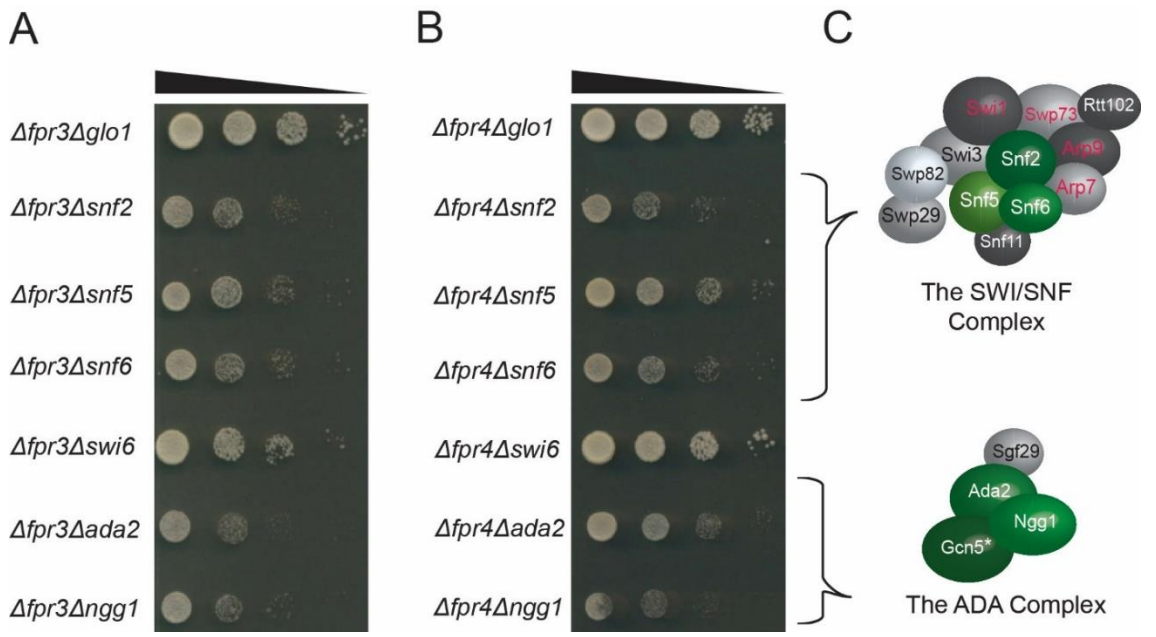

Figure 18. *FPR3* and *FPR4* each display a negative genetic interaction with genes encoding ADA and SWI/SNF complex components.
Ten-fold serial dilution spotting assays of double deletion mutants of (A) *Δfpr3* or (B) *Δfpr4* and genes coding for components of the SWI-SNF complex (*Δsnf2*, *Δsnf5*, and *Δsnf6*) and the ADA complex (*Δada2* and *Δngg1*). Double mutants of Δ*glo1* and Δ*swi6* were included as controls and represent genes which do not display a genetic interaction with *FPR3* or *FPR4*. All strains were generated from the SGA cross and are shown after 2 days of growth at 30ºC on selective media (for the *Δfpr3* double deletion mutants :SD-media lacking histidine, arginine, lysine, leucine, and uracil and containing canavanine and thialysine both at a final concentration of 50mg/L, and G418 and clonNAT both at a final concentration of 200mg/L, for the *Δfpr4* double deletion mutants :SD-media lacking histidine, arginine, and lysine and containing canavanine and thialysine both at a final concentration of 50mg/L, and G418 and clonNAT both at a final concentration of 200mg/L and 5-fluoroorotic acid at a final concentration of 1000mg/L). (C) Schematic of the SWI/SNF complex (top) and ADA complex (bottom). Complex components coded for by shared synthetic sick/lethal genetic interactors of *FPR3* and *FPR4* are colored green. Complex components coded for by genes that are not synthetic sick or lethal genetic interactors are colored gray. Red text labels indicate components of the complex encoded by essential genes or genes not present in our DMA collection. * indicates that *GCN5* was identified as a genetic interactor of both *FPR3* and *FPR4* in the screens. However, the validation spotting assays for *Δgcn5* are not shown here.

bottom). Ontologies enriched among these masked genetic interactors are listed in appendix Table 4. At a *p*-value cut-off of $p \leq 10^{-4}$, there were no biological processes ontologies enriched among masked interactors. At a higher cutoff ($p \leq 10^{-2}$), enriched biological processes terms included: mitochondrial membrane organization ($p=1.24 \times 10^{-4}$), mitochondrial proton-transporting ATP synthase complex assembly ($p=5.26 \times 10^{-3}$), fructose metabolic process ($p=1.81 \times 10^{-3}$), cellular calcium ion homeostasis ($p=4.24 \times 10^{-3}$), and a set of terms related to nuclear polyadenylation dependent RNA catabolic processes ($p \leq 5.26 \times 10^{-3}$). These terms are derived from similar gene ontology annotations of the *TRF5*, *AIR1*, and *RRP6* genes (Figure 19). The only complex related ontology associated with masked negative interactors was the TRAMP5 non-

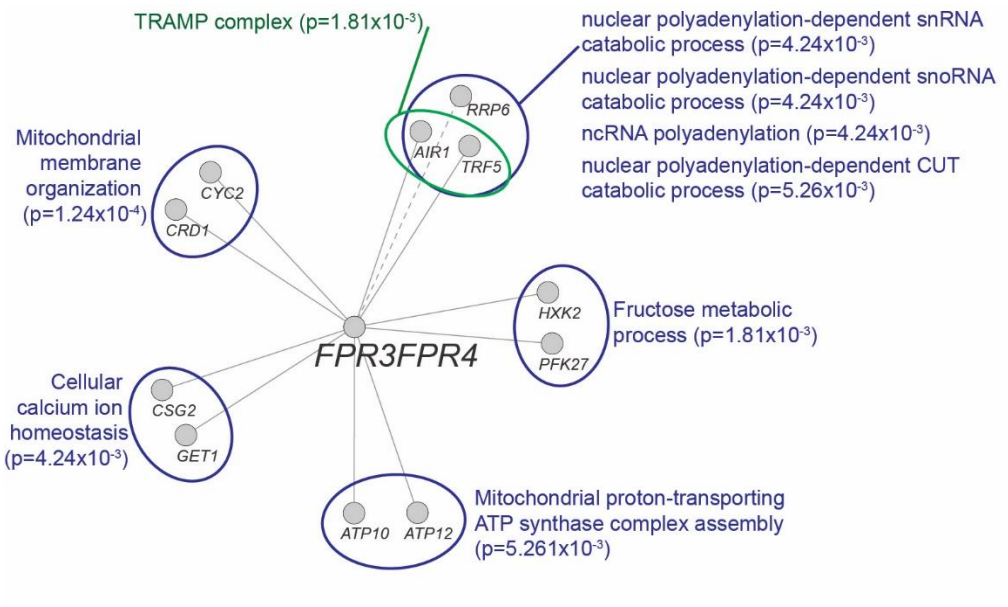

Figure 19. Masked synthetic sick/lethal genetic interactors reveal that Fpr3 and Fpr4 have redundant functions.
Network diagram summarizing the masked synthetic sick/lethal genetic interactions of *FPR3* and *FPR4* as identified in Paralog-SGA screens. Genes displaying a negative interaction (grey circles) are clustered based on common biological processes (blue) or membership in annotated protein complexes (green). Interaction network was generated using the Cystoscope open source software platform[374]. Lines between genes indicate a negative genetic interaction. Dashed network edge line indicates that the associated genetic interaction was at the threshold of significance using default Balony hit parameters and was confirmed independently of the Paralog-SGA screen.

canonical polyadenylation complex (i.e. TRAMP complex (p=1.81x10^{-3})) (Figure 19). This protein complex is an RNA surveillance factor that recognizes and polyadenylates a variety of RNA transcripts to target them for degradation by the nuclear RNA exosome [344,377–379] (Figure 20 A). Two non-essential genes encoding components of this complex, *TRF5* and *AIR1*, were among notable masked interactors in *Δfpr3Δfpr4* double mutant yeast (Figure 20 B). A third non-essential gene, encoding the nuclear exosome exonuclease *RRP6*, was at the threshold of significance using default Balony settings (Figure 20 B). I independently validated these genetic interactions by scoring the fitness of *Δfpr3Δfpr4Δrrp6* and *Δfpr3Δfpr4Δtrf5* yeast using growth assays with mutant populations generated from the paralog-SGA cross (Figure 20 C). These assays confirmed that triple mutants of both *Δfpr3Δfpr4Δrrp6* and *Δfpr3Δfpr4Δtrf5* displayed reduced proliferation rates compared to their corresponding total haploid meiotic progeny controls (which consisted of a mixed population of all *Δtrf5* and *Δrrp6* cells generated from the cross) (Figure 20 C). The masked negative genetic interaction with the TRAMP5 complex members could be explained by a model where Fpr3 and Fpr4 have redundant biological functions involving the negative regulation of RNAs. In such a model, cells lacking Fpr3/Fpr4

and TRAMP5 would accumulate these target RNAs, which could lead to slow growth and the observed synthetic sickness.

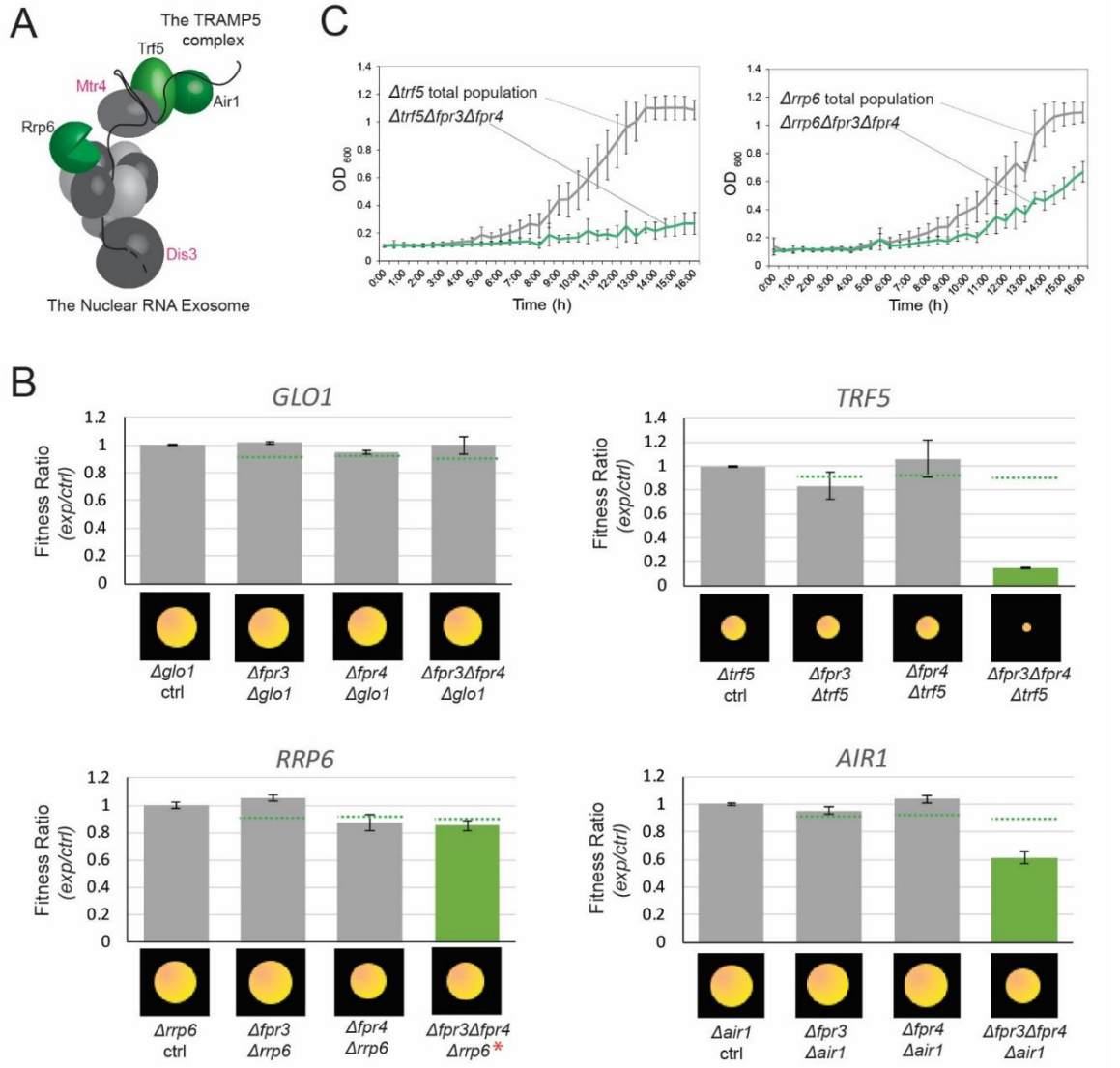

Figure 20. The TRAMP5 nuclear RNA exosome is a masked genetic interactor of *FPR3* and *FPR4*. (A) Schematic of the TRAMP5 complex (top right) and the nuclear RNA exosome (bottom left) adapted from Wolin et al. 2012[360]. Complex components encoded by masked negative genetic interactors of *FPR3* and *FPR4* are colored green. Red text labels indicate components of complex coded for by essential genes. (B) Plots of fitness ratios (normalized mean experimental colony size/ normalized mean control colony size) of indicated *Δfpr3Δxxx*, *Δfpr4Δxxx*, and *Δfpr3Δfpr4Δxxx* mutants. Mutants of *Δglo1* are included as an example of a non-interacting gene. Ratios significantly below the lower fitness ratio cut-off threshold (*l*) automatically estimated by Balony for each screen (dashed green line) are indicated with green bars. Error bars indicate standard deviation of three technical replicates. * indicates that 2/3 replicates for the *Δfpr3Δfpr4Δrrp6* deletion mutant were below the cut-off threshold. Balony software generated images of each mutant normalized to the plate median colony size are illustrated along the x-axis. (C) Growth curves depicting optical density at 600nm (OD_{600}) vs time (h) for select triple deletion mutants and corresponding total haploid meiotic progeny control populations. Error bars indicate standard deviation of three technical replicates.

2.2.4 Suppressor genetic interactors support chromatin-centric functions for Fpr3 and Fpr4

Loss of function mutations which alleviate fitness defects in combination with each other are called suppressor mutations. The positive genetic interactions associated with suppressor mutants can provide information about genes involved in concert or in the same biological processes or pathways[361]. Therefore, the suppressor genetic interactions uncovered by the paralog-SGA screens (Figure 15) are also descriptive of the function(s) of Fpr3 and Fpr4. To examine these interactions, I again used automatically estimated *l* and *u* thresholds and default Balony hit parameters (i.e. reproducibility in 3/3 sets and *p*-values < 0.05), to score and identify positive suppressor interactors of *FPR3* and/or *FPR4*. That is, genes whose disruption results in increased growth rates of *Δfpr3*, *Δfpr4*, and *Δfpr3Δfpr4* mutants (Figure 15).

I identified 337 suppressor (*u*=1.074) interactions in the *FPR3* screens (Figure 15 A) and 351 suppressor (*u*=1.076) interactions in the *FPR4* screens (Figure 15 B). Of these, 218 interactions were unique to *FPR3*, 232 were unique to *FPR4*, and 119 were common to both *FPR3* and *FPR4* (Figure 21 top). The dual gene screen identified 527 *Δfpr3Δfpr4Δxxx* triple mutants (*u*=1.088) with improved phenotypes relative to their corresponding *Δxxx* controls (Figure 15 C). Of these, 191 mutants revealed masked suppressor genetic interactions. Deletion of these *XXX* genes suppressed the growth defect of *Δfpr3Δfpr4* double mutant yeast but not either *Δfpr3* or *Δfpr4* single mutants (Figure 21 bottom). Thus, as with synthetically sick/lethal genetic interactors, suppressor interactions support the fact that Fpr3 and Fpr4 are not equivalent and have unique, cooperative, and redundant roles.

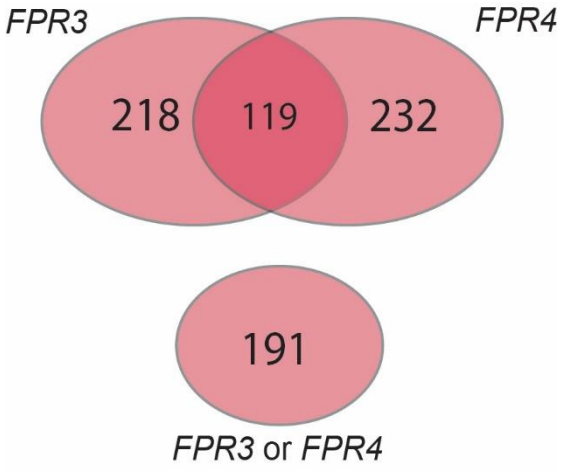

Figure 21. *FPR3* and *FPR4* have unique, cooperative, and redundant suppressor genetic interactions. Venn diagrams indicating the numbers of unique and cooperative (top) and redundant (bottom) suppressor genetic interactors uncovered from the Paralog-SGA analysis.

A gene ontology analysis of the 218 suppressors unique to *FPR3* is presented in appendix Table 5. At an arbitrary *p*-value cut-off of $p \leq 10^{-4}$, there were no biological processes enriched among these genes. At a higher *p*-value cut-off ($p \leq 10^{-2}$) the only biological process revealed was chromatin silencing at telomere ($p=4.76 \times 10^{-4}$) (Figure 22). Complex related ontologies included: three of the eight subunits of the SET1/COMPASS histone methyltransferase complex[380] ($p=1.62 \times 10^{-3}$), and the vacuolar membrane EGO complex which plays a role in microautophagy[381] ($p=3.01 \times 10^{-3}$) (Figure 22). The relationship between Fpr3 and suppressors associated with telomeric chromatin silencing may be related to the Fpr3 mediated regulation of centromeric chromosome dynamics. In both *S. cerevisiae*[382] and *Sz. Pombe*[383], chromatin regulators involved in telomeric silencing have also been implicated in homologous recombination and chromosome segregation during meiosis. One possibility is that in cells lacking Fpr3, defects in the generation of centromeric chromatin during meiosis necessitate the centromeric recruitment of additional chromatin modifiers which are also necessary for telomeric silencing. One example of such a common factor is the *S. cerevisiae* histone methyltransferase Dot1, which is necessary for both telomeric silencing[384] and meiotic sister chromatid recombination[382]. The resultant change in telomeric dosage of these dual function regulators may produce defects in telomeric silencing or structure which render the activity of other telomeric silencing factors toxic. Thus, double mutants of *FPR3* and genes encoding these now toxic telomeric silencing proteins grow better than mutants of *FPR3* alone, explaining the positive genetic interactions between these genes.

Ontologies enriched among the 232 suppressor interactors unique to *FPR4* are presented in appendix Table 6. Biological processes associated with these interactions (with *p*-values below the arbitrary cut-off of $p \leq 10^{-4}$) included translation ($p=9.69 \times 10^{-6}$) and ribosomal small subunit assembly ($p=6.99 \times 10^{-5}$) (Figure 22). Notable complex related ontologies included: the cytosolic large and small ribosomal subunits ($p=7.72 \times 10^{-6}$ and $p=1.14 \times 10^{-3}$ respectively), and the NUP107-160 nuclear pore outer ring complex[385] ($p=1.25 \times 10^{-3}$) (Figure 22). The relationship between Fpr4 and suppressors encoding components of the nuclear pore complex may be associated with replicative cell aging, given the recent discovery that misassembled nuclear pore complexes accumulate in replicatively aged cells and result in defects in nucleocytoplasmic exchange[386]. If cells lacking Fpr4 are especially sensitive to replicative cell aging, then double mutants lacking both Fpr4 and these nucleoporins may avoid aging related defects in nucleocytoplasmic exchange and thus grow better than single mutants lacking Fpr4 alone. Although much remains to be understood about the relationship between Fpr3 and Fpr4 and these suppressor interactors,

collectively, these unique interactions support the model that Fpr3 and Fpr4 perform some separate biological functions for which they are not interchangeable.

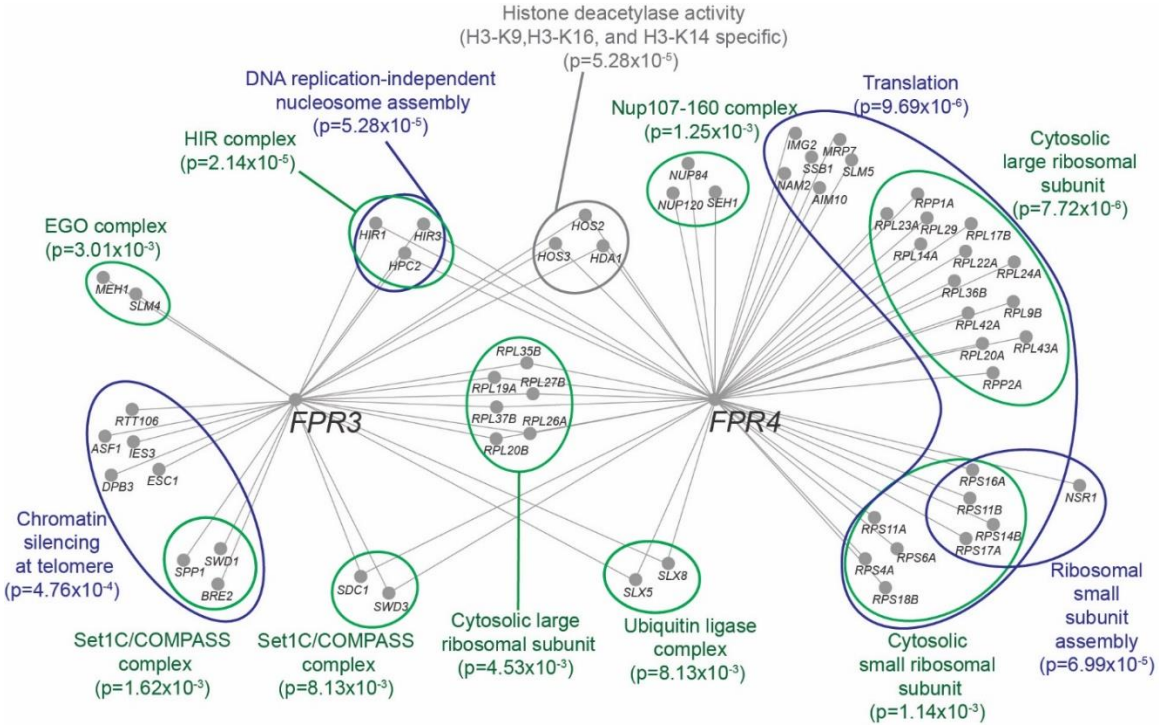

Figure 22. Suppressor genetic interactors support separate and cooperative functions for Fpr3 and Fpr4

Network diagram summarizing the suppressor genetic interactions of *FPR3* and *FPR4* as identified in Paralog-SGA screens. Genes displaying a positive interaction (grey circles) are clustered based on common biological processes (blue), common molecular functions (grey), and membership in annotated protein complexes (green). Interaction network was generated using the Cystoscope open source software platform[374]. Lines between genes indicate a positive genetic interaction.

Ontologies enriched among the 119 suppressor interactors shared between *FPR3* and *FPR4* are presented in appendix Table 7. The only biological process in this list with $p \leq 10^{-4}$ was DNA replication independent nucleosome assembly ($p=5.28\text{x}10^{-5}$) (Figure 22). Notable complex related ontologies included two additional components of the SET1/COMPASS complex ($p=8.13\text{x}10^{-3}$)[380], additional protein components of the cytosolic large ribosomal subunit ($p=4.53\text{x}10^{-3}$), and components of the (Slx5-Slx8 SUMO targeted) ubiquitin ligase complex ($p=8.13\text{x}10^{-3}$)[387] (Figure 22). Shared suppressor ontologies with the lowest *p*-values included several genes encoding histone deacetylases ($p=5.28\text{x}10^{-5}$) and components of the HIR replication-independent nucleosome assembly complex ($p=2.14\text{x}10^{-5}$) (Figure 22). Double mutants of *Δfpr3* or *Δfpr4* and three genes coding for NAD+ independent histone deacetylases (*HOS2*, *HDA1*, and *HOS3*) displayed significantly improved fitnesses relative to their corresponding controls (Figure 23 A). Likewise, double mutants of *Δfpr3* or *Δfpr4* and three of

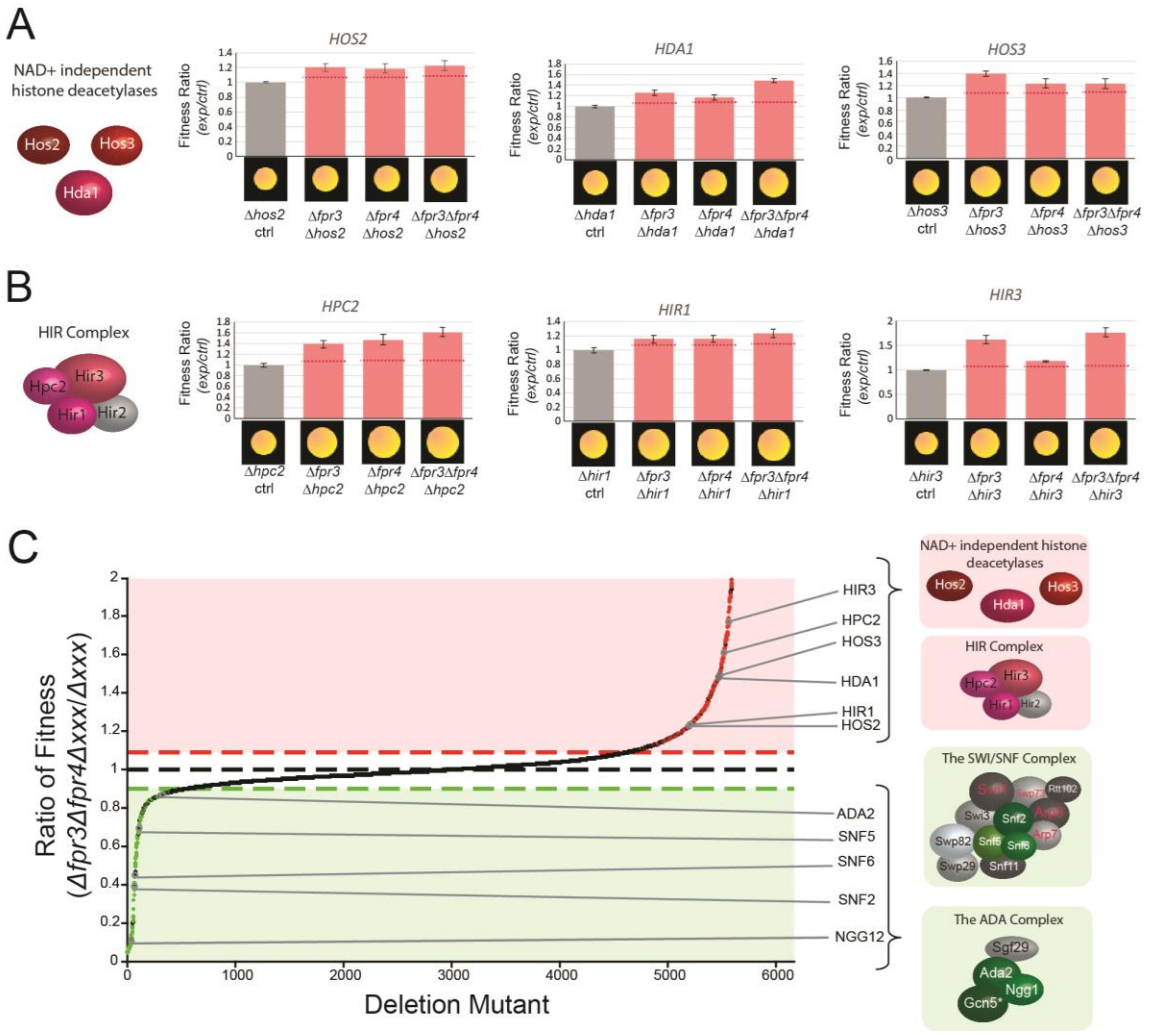

Figure 23. Suppressor genetic interactions support chromatin-centric functions of Fpr3 and Fpr4. (A) Schematic of Hos2, Hda1, and Hos3 (left). Plots of fitness ratios (normalized mean experimental colony size/ normalized mean control colony size) of indicated *Δfpr3Δxxx*, *Δfpr4Δxxx*, and *Δfpr3Δfpr4Δxxx* mutants (right). Ratios significantly above the upper fitness ratio cut-off threshold (*u*) automatically estimated by Balony for each screen (dashed red line) are indicated with red bars. Error bars indicate standard deviation of three technical replicates. Balony software generated images of each mutant normalized to the plate median colony size are illustrated along the x-axis. (B) Schematic of the HIR complex (left). Plots of fitness ratios (normalized mean experimental colony size/ normalized mean control colony size) of indicated *Δfpr3Δxxx*, *Δfpr4Δxxx*, and *Δfpr3Δfpr4Δxxx* mutants (right). Ratios significantly above the upper fitness ratio cut-off threshold (*u*) automatically estimated by Balony for each screen (dashed red line) are indicated with red bars. Error bars indicate standard deviation of three technical replicates. Balony software generated images of each mutant normalized to the plate median colony size are illustrated along the x-axis. (C) Plot of fitness ratios for all *Δfpr3Δfpr4Δxxx* triple mutants relative to Δ*xxx* total haploid meiotic progeny controls. Green dots indicate synthetic sick/lethal genetic interactions, red dots indicate suppressor genetic interactions. Threshold cut-offs are indicated by red and green dashed horizontal lines. The location of significant hits coding for components of chromatin modifiers are labeled and accompanied with schematic illustrations of their complex components. Components coded for by paralog SGA hits are colored. Red text denotes essential complex components.

the four genes encoding components of the HIR complex (*HPC2*, *HIR1*, and *HIR3*) also displayed significantly improved fitness (Figure 23 B). Given that the SWI/SNF and ADA complexes are particularly important for the fitness of *Δfpr3* and *Δfpr4* yeast (Figure 18), shared suppressor interactions with known chromatin modifiers further support a chromatin defect underlying these phenotypes (Figure 23 C). Particularly notable is the fact that histone deacetylases are enriched among suppressors while histone acetyltransferases are enriched among synthetic sick/lethal interactors. One possibility is that Fpr3 and Fpr4 act cooperatively to generate an accessible chromatin environment and thus promote transcription from some genomic loci. In the absence of these NPL-FKBPs, this accessible environment is not generated resulting in the inhibition of transcription from Fpr3/Fpr4 regulated target genes. Double mutants of Fpr3/Fpr4 and factors which promote chromatin compaction such histone deacetylases may alleviate this transcriptionally repressive phenotype by promoting the transcription of Fpr3/Fpr4 targets, explaining why these HDACs display positive genetic interactions with *FPR3*/*FPR4*. Taken together, the presence of both aggravating and alleviating chromatin-related genetic interactions in in this Paralog-SGA screen is consistent with a chromatin-centric mode of action for Fpr3 and Fpr4.

Ontologies enriched among the 191 masked suppressor interactors of *FPR3* and *FPR4* are presented in appendix Table 8. Biological processes in this list with $p \leq 10^{-4}$ include: translation ($p=1.07 \times 10^{-11}$), rRNA export from the nucleus ($p=7.43 \times 10^{-6}$), and endonucleolytic cleavage to generate the mature 3'-end of SSU-rRNA ($p=8.90 \times 10^{-5}$) (Figure 24). Notable complex related ontologies include: the cytosolic large and small ribosomal subunits ($p=3.42 \times 10^{-3}$ and $p=6.18 \times 10^{-13}$ respectively), eukaryotic translation initiation factor 4F and eukaryotic translation elongation factor 1 (with $p=7.62 \times 10^{-3}$ for both), and the 26S proteasome ($p=2.37 \times 10^{-3}$) (Figure 24). The presence of ontologies significantly enriched among masked suppressors of *FPR3* and *FPR4* supports the model that these enzymes carry out some biological functions for which they are interchangeable. Particularly notable is the highly significant enrichment of genes coding for components of the large and small ribosomal subunits. However, the enrichment of other ribosomal protein coding genes among shared interactors of *FPR3* and *FPR4* and unique interactors of *FPR4* (Figure 22), makes a comparative interpretation of the relationship between these ontologies and the functions of Fpr3 and Fpr4 difficult.

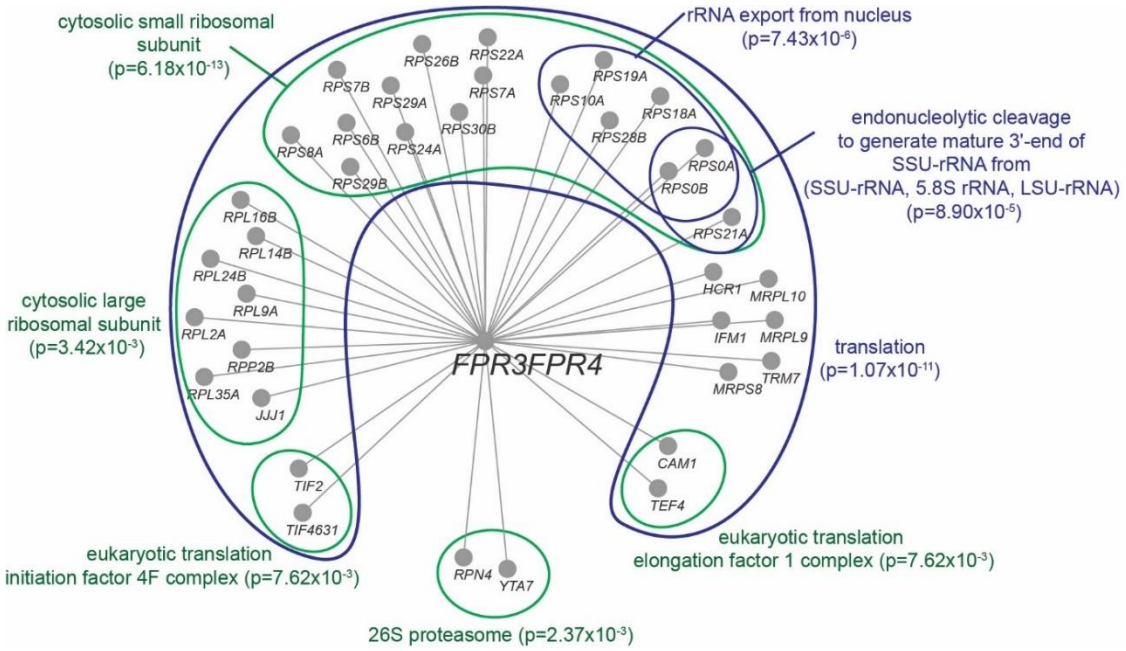

Figure 24. Suppressor mutants of Δ*fpr3*Δ*fpr4* yeast are enriched in ribosome biogenesis and translation related processes and complexes

Network diagram summarizing the masked suppressor genetic interactions of *FPR3* and *FPR4* as identified in Paralog-SGA screens. Genes displaying a positive interaction (grey circles) are clustered based on common biological processes (blue), and membership in annotated protein complexes (green). Interaction network was generated using the Cystoscope open source software platform[374]. Lines between genes indicate a positive genetic interaction.

2.3 Discussion

NPL-FKBPs are restricted to insects, plants, and fungi but are homologs of two classes of clinically relevant human proteins; the nucleoplasmin family histone chaperones (NPM1-3), and the nuclear FKBP prolyl-isomerases (FKBP25). There is thus an opportunity to use the power of yeast genetics to inform on the functions of these evolutionarily conserved protein domains. However, the high degree of similarity between Fpr3 and Fpr4 adds a layer of complexity to genetic approaches due to the potential for complete or partial redundancy between paralogs. Specifically, this presents a confounding factor that limits conventional SGA based functional analysis. To comprehensively assess their biological functions, I employed a modified paralog specific SGA screening workflow. This approach revealed that Fpr3 and Fpr4 have unique, cooperative, and redundant functions. The genetic interaction profiles associated with each enzyme support a unique centromeric chromatin related role for Fpr3 and a unique function in replicative cell aging for Fpr4. Also, shared genetic interactions with the ADA complex, SWI/SNF chromatin remodeler, and histone deacetylases highlight that the Fpr3/Fpr4 paralogs may operate cooperatively to regulate chromatin. Lastly, masked genetic interactions only

detectable in *Δfpr3Δfpr4* double mutants indicate that these enzymes also play a redundant role in the negative regulation of RNA.

The modified SGA approach at the basis of this work presents several advantages to conventional SGA methodologies in the study of paralogs. First, the multi-gene deletion mutant query improves screening efficiency with respect to both time and reagents. It also reduces variability because all three sets of meiotic progenies come from the same population of spores. Finally, the presence of *FPR4* on an episomal rescue plasmid reduces the likelihood of spontaneous suppressor mutations, that could arise during the multiple propagation steps required for the screen. These suppressors can interfere with the detection of genetic interactions by generating false negatives. Overall, the modified methodology of this screening approach represents a significant improvement to the study of paralog genetic interactions. Given that approximately 13% of yeast protein coding genes are duplicates[243], paralog-SGA may have wide applications to studies of other yeast genes.

Consistent with existing literature[224,294,299–301], *FPR3* genetic interactors support a unique function for Fpr3 in chromosome segregation dynamics associated with centromeres. The *FPR3* specific negative genetic interaction with the Swr1 chromatin remodeler is particularly interesting, given the fact that proline isomerization by Fpr3 is required for the degradation of the centromeric histone H3 variant Cse4[224] and that Swr1 has been implicated in the deposition of variant histone H2A.Z at centromeres[388–390]. Furthermore, like *FPR3*, genes encoding components of the Swr1 complex also have genetic interactions with kinetochore components[389]. Taken together, the interactions detected in these paralog-SGA screens may be evidence that Fpr3 and Swr1 work in a parallel pathway, ensuring the accurate generation of centromeric chromatin and consequently facilitating appropriate chromosome segregation dynamics with kinetochores during cell division (Figure 25 A). The fact that the proline isomerization activities of Fpr3 have been implicated in these centromeric processes[224], raises the exciting possibility that these negative genetic interactions may be used as a readout system in future paralog-SGA screens with catalytically dead mutants of Fpr3 to test the impact of proline isomerization on these Fpr3 unique functions.

The relationship between *FPR3* and the significant number of genes encoding mitochondrial proteins (including components of the inner membrane electron transport chain) is less clear, but may be related to Fpr3 interactions with free histones in the cytosol. In mammalian cells, physical interactions between histones and mitochondria have been implicated in destabilization of mitochondrial membrane integrity and the release of pro-apoptotic proteins from the mitochondrial intermembrane space[391,392]. Thus, cytosolic Fpr3 may play a role in sequestering

free histones to protect the mitochondrial membrane from degradation. The fact that mitochondrial ribosomal proteins have also been implicated in apoptosis[393] may explain why mitochondrial ribosome proteins also represent a significant proportion of negative genetic interactors of *FPR3*.

FPR4 genetic interactors support a unique function for Fpr4 in replicative cell aging. Genes encoding proteins crucial for chromatin mediated silencing and genomic stability at rDNA, such as the Fob1 replication fork block protein[320,321], are essential for viability in *Δfpr4* yeast but not in *Δfpr3*. This, taken together with the established physical association of Fpr4 with rDNA chromatin[284] and its ability to silence reporter expression[284] from this locus, is evidence that Fpr4 has a unique function in rDNA chromatin regulation (Figure 25 A). Collectively, the comparative biological functions associated with *FPR3* and *FPR4* genetic interaction profiles, provide additional systems-level evidence that these enzymes are not redundant. Furthermore they indicate that Fpr3 and Fpr4 may carry out their unique functions as homo-oligomers[109,239,282,294] (Figure 25 A).

I identified positive and negative genetic interactors as common hits in Fpr3 and Fpr4 single mutant screens. Notably, many of these genes are associated with chromatin. The implications of this observation are significant and not expected: shared genetic interactions with chromatin regulators indicate that Fpr3 and Fpr4 paralogs participate in chromatin related biological processes in which both proteins are equally important. This would be expected if Fpr3 and Fpr4 formed heteromeric complexes, and indeed our lab (Drew Bowie, unpublished results) and others[294] have observed that Fpr3 and Fpr4 co-immunoprecipitate. Key components of the SWI/SNF complex and the ADA histone acetyltransferase are shared synthetic sick/lethal interactors of Fpr3 and Fpr4, appearing as hits in both single mutant screens. Both the ADA complex and SWI/SNF have been implicated in generating open chromatin environments permissive to transcription at the promoters of a number of genes including *PHO5*[394] and *PHO8*[98]. Thus, the genetic interaction between these components and Fpr3 and Fpr4 may be explained by a model where Fpr3 and Fpr4 act together to chaperone nucleosomes, facilitating chromatin dynamics at their target loci in ways analogous to SWI/SNF and ADA (Figure 25 A). Whether this means that the chaperones operate together in a sequence of events, such as the removal and subsequent redeposition of nucleosomes during transcription, or in concert as a hetero-oligomeric complex, is not yet clear. As already stated, the fact that Fpr3 and Fpr4 co-purify [294] supports the latter model, but does not exclude the former. The presence of histone deacetylases and the HIR complex, which are known antagonizers of SWI/SNF and ADA, among suppressors of *FPR3* and *FPR4* lends additional support to this model.

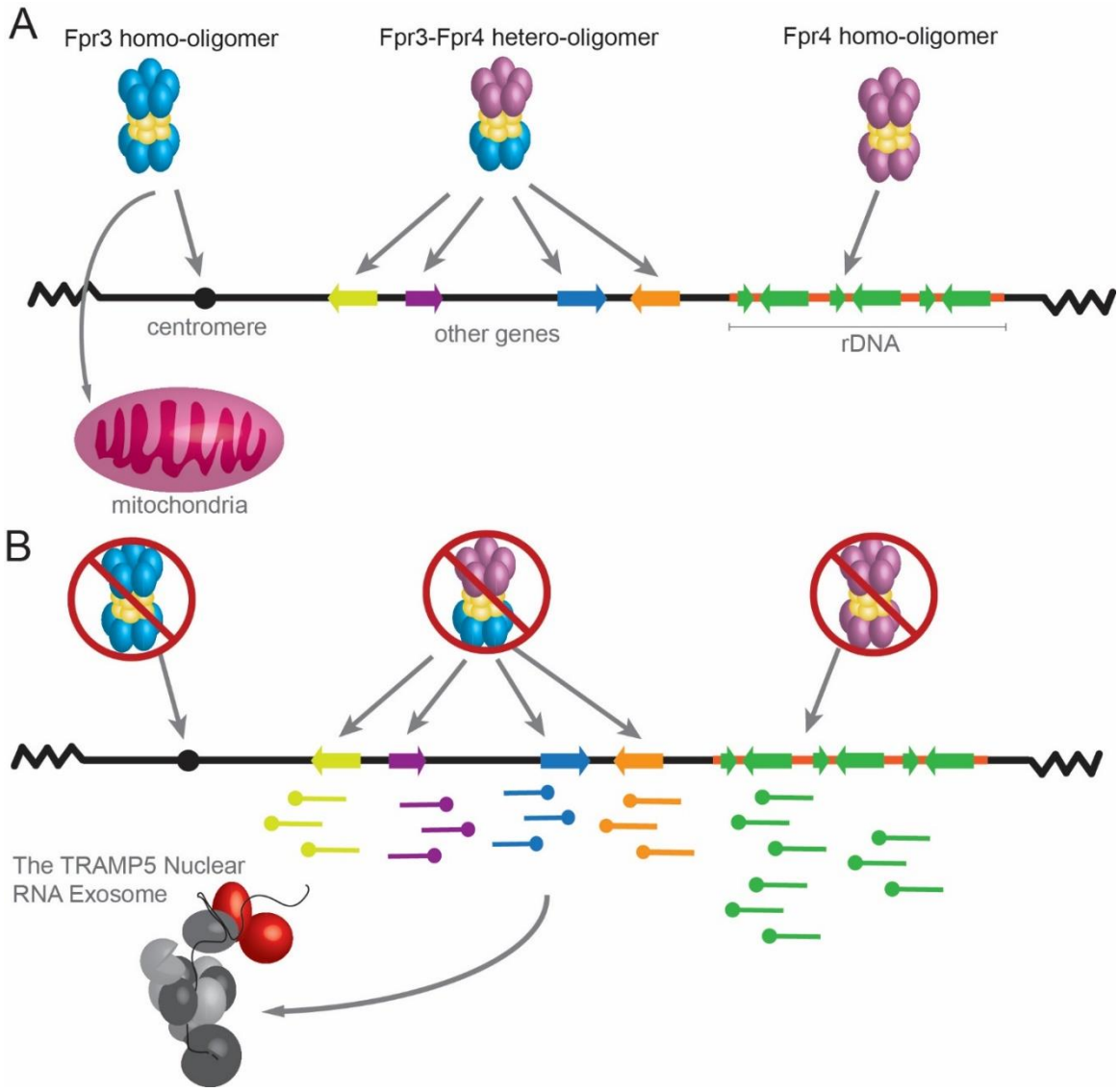

Figure 25. Model of Fpr3 and Fpr4 function.
(A) Fpr3 and Fpr4 function at discrete genomic loci as homo- and hetero- oligomers. (B) In the absence of Fpr3 and Fpr4, chromatin environments at Fpr3/Fpr4 target loci are not maintained in a state inhibitory to transcription. This results in the generation of spurious transcripts from these loci and renders the RNA exosome essential for clearing them from the cell.

My screens identified masked positive and negative genetic interactions of Fpr3 and Fpr4 which support the model that these enzymes carry out some functions redundantly. Particularly notable among them were masked interactions with components of the TRAMP5 complex and RNA exosome. The unique and cooperative genetic interactions of Fpr3 and Fpr4 suggest that these enzymes contribute to building chromatin at discrete genomic loci (including rDNA) (Figure 25 A). If Fpr3 and Fpr4 generate chromatin environments inhibitory to transcription at

these loci then cells lacking Fpr3, Fpr4, and exosome components may die or become extremely sick because they accumulate RNA species normally degraded by the exosome (Figure 25 B). This model may explain the redundant relationship of Fpr3 and Fpr4 in the negative regulation of RNAs. In support of this, known TRAMP5 targets include cryptic unstable transcripts generated from intragenic sites on the genome such as rDNA[344,352,377,379].

Taken together, the results presented in this chapter represent the first comprehensive functional analysis of Fpr3 and Fpr4 *in vivo* and provide at least a partial explanation for why these paralogs have been evolutionarily conserved over time. Furthermore, these findings represent the first genetic link between Fpr3 and Fpr4 and chromatin and implicate their function in the regulation of transcription at discrete genomic loci. Most importantly, it cannot be overstated that, like all systems-level screens and 'omics' approaches, the genetic screens described in this chapter represent a beginning, rather than an end of experimentation. They are designed and meant to serve as hypothesis generators of aggregate data which enables the formation and subsequent testing of pointed hypotheses. In this dissertation, I elected to pursue the most novel (and robust) finding i.e. the functional relationship between TRAMP5 and Fpr3/Fpr4. Given that this poly(A) polymerase complex stimulates transcript degradation, I hypothesized that it could be required for the degradation of Fpr3/Fpr4 target transcripts. Addressing this hypothesis necessitated an unbiased analysis of the impact of Fpr3/Fpr4 on the transcriptome genome-wide, which will be discussed in Chapter 3.

2.4 Materials and Methods

Strains and Plasmids

Yeast strain genotypes are described in detail in appendix Table 19. Strains in the MAT a non-essential yeast deletion collection (DMA) used for the paralog-SGA are all isogenic to BY4741 and were purchased from Thermofisher Dharmacon.

The plasmid rescued double genomic deletion *Δfpr3Δfpr4* SGA query strain (YNS 35) was created in a Y7092 genetic background as follows. The endogenous *FPR4* locus on a Y7092 WT strain was replaced with a nourseothricin resistance (*MX4-NATR*) PCR product deletion module[395,396]. The resulting single gene *Δfpr4* deletion mutant was subsequently transformed with prs316 FPR4: a single copy *URA3* marked shuttle vector, carrying an untagged full length copy of the *FPR4* open reading frame with endogenous promoter and terminator (originally described in [223]). The endogenous *FPR3* locus on this plasmid rescued *Δfpr4* deletion mutant was subsequently replaced with a *LEU2* PCR product deletion module.

Double and triple deletion mutants and corresponding mixed population total haploid meiotic progeny controls used in the validating spotting assays and growth curves were generated from the SGA cross (see below).

Paralog Synthetic Genetic Array (Paralog-SGA) Analysis

Paralog-SGA analysis was performed using a Singer Instruments ROTOR microbial arraying robot (https://www.singerinstruments.com/solution/rotor-hda/. Dec 2017) as previously described[365] with the following modifications. The MATa/α diploid zygotes resulting from the query-DMA cross were pinned onto diploid selective YPD + G418/clonNAT plates a total of two times for greater selection against residual haploids. Sporulation was carried out at room temperature for 14 days. Spores were pinned onto Mat a selective germination media for two rounds of selection as previously described[365].

The resulting MATa progeny were subsequently replica plated onto four kinds of selective media: 1) control media selective for the total haploid progeny population, 2) media selective for *Δfpr3Δxxx* haploid progeny, 3) media selective for *Δfpr4Δxxx* haploid progeny, and 4) media selective for *Δfpr3Δfpr4Δxxx* haploid progeny. Control media selective for the total haploid progeny population consisted of SD media lacking histidine, arginine, lysine and containing canavanine and thialysine both at a final concentration of 50mg/L, and G418 at a final concentration of 200mg/L. Media selective for *Δfpr3Δxxx* haploid progeny consisted of SD media lacking histidine, arginine, lysine, leucine, uracil (to maintain the pRS316-Fpr4 episomal plasmid, which harbors the *URA3* marker), and containing canavanine and thialysine both at a final concentration of 50mg/L, G418 and clonNAT both at a final concentration of 200mg/L. Media selective for *Δfpr4Δxxx* haploid progeny consisted of SD media lacking histidine, arginine, lysine, and containing canavanine and thialysine both at a final concentration of 50mg/L, G418 and clonNAT both at a final concentration of 200mg/L, and 5-fluoroorotic acid (to select against the pRS316-Fpr4 episomal plasmid, which harbors the *URA3* marker) at a final concentration of 1000mg/L. Media selective for *Δfpr3Δfpr4Δxxx* haploid progeny consisted of SD media lacking histidine, arginine, lysine, leucine, and containing canavanine and thialysine both at a final concentration of 50mg/L, G418 and clonNAT both at a final concentration of 200mg/L, and 5-fluoroorotic acid (to select against the pRS316-Fpr4 episomal plasmid, which harbors the *URA3* marker) at a final concentration of 1000mg/L. Plates were incubated at 30°C for 24 hours and were then expanded into triplicate and incubated for an additional 24 hours at 30°C.

Digital images of each plate were subsequently processed using the Balony image analysis software package (http://barrypyoung.github.io/balony/, Dec 2017) as previously described[373]. In

brief, pixel area occupied by each colony was measured to determine colony size. Progeny fitness was then scored as follows. The ratio of sizes for each double (*Δfpr3Δxxx*, *Δfpr4Δxxx*) and triple (*Δfpr3Δfpr4Δxxx*) mutant colony relative to its corresponding total haploid progeny control colony was determined. Ratio cutoff thresholds were estimated automatically by the software by extrapolating the central linear portion of the ratio distributions and finding the *y*-intercepts at either ends of the *x*-axis. Ratios below the cutoff value (*l*) correspond to synthetic sick/lethal mutants while ratios above the cutoff value (*u*) correspond to suppressor mutants. Genetic interactions were identified using the automatically estimated upper and lower cut-off thresholds and default Balony hit parameters (i.e. reproducibility in 3/3 sets and p-values < 0.05).

Paralog-SGA Data Processing

Unique, common, and masked synthetic sick/lethal interactors were identified as follows. First, duplicate genes from the list of hits from each dataset were removed. The three lists of hits were then compared to each other. The *FPR3* and *FPR4* screens were compared to identify unique and common interactors. Genes uniquely present in the *FPR3FPR4* double mutant screens were defined as masked interactors. Unique, common, and masked suppressor interactors were identified the same way.

The lists of unique, common, and masked synthetic sick/lethal and suppressor genetic interactors were subsequently analyzed using the web based FunSpec bioinformatics ontology analysis tool (http://funspec.med.utoronto.ca/, Dec 2017). The analysis was performed using a p-value cutoff score of 0.01, and without Bonferroni-correction. A full list of the ontologies uncovered and their corresponding p values is presented in appendix Tables 1-8. Networks of notable genetic interactions and ontologies were drawn using the Cytoscape software platform (http://www.cytoscape.org/, Dec 2017).

Spotting Assays

Spotting assays to validate the synthetic sickness phenotypes were carried out as follows. Colonies generated from the paralog-SGA assay corresponding to each double mutant of interest were isolated. Fresh single colony isolates of each strain were grown in liquid SD complete media to late log phase. Cells were subsequently collected, re-suspended in sterile deionized water, and normalized to an OD_{600}=1.4. The normalized cell suspensions were subjected to 10-fold serial dilutions and 5µL of each dilution was spotted onto media selective for *Δfpr3Δxxx* double mutants and, *Δfpr4Δxxx* double mutants. Media selective for *Δfpr3Δxxx* double mutants consisted of SD-media lacking histidine, arginine, lysine, leucine, and uracil and containing canavanine and

thialysine both at a final concentration of 50mg/L, and G418 and clonNAT both at a final concentration of 200mg/L. Media selective for *Δfpr4Δxxx* double mutants consisted of SD-media lacking histidine, arginine, and lysine and containing canavanine and thialysine both at a final concentration of 50mg/L, G418 and clonNAT both at a final concentration of 200mg/L, and 5-fluoroorotic acid at a final concentration of 1000mg/L. Plates were incubated at 30°C and growth was analyzed after 48 hours.

Growth Curves

Growth curves to validate the synthetic sickness phenotypes were carried out as follows. Colonies generated from the paralog-SGA assay corresponding to each triple mutant of interest and its respective control colony were isolated and validated for correct genotype by PCR. Confirmed strain isolates were then resuspended in fresh YPD media, normalized to an OD_{600} of 0.2 and distributed into triplicate wells of a 24 well cell culture plate. Plates were subsequently grown for 16h at 30ºC in a shaking plate reader. Readings of OD_{600} were taken every 30 minutes.

Chapter 3
Fpr3 and Fpr4 regulate transcription from multiple genomic loci

This chapter was adapted in part from the publication:

Savic, N., Shortill, S. P., Bilenky, M., Dobbs, J. M., Dilworth, D., Hirst, M., Nelson, C.J. Histone Chaperone Paralogs Have Redundant, Cooperative, and Divergent Functions in Yeast. *Genetics*. **213(4),** 1301-1316 (2019).

Contributions pertaining to data presented in this chapter: Experiments and data analysis were performed by NS under the supervision of CJN with the following exceptions: sequencing was carried out under the supervision of MH at the Michael Smith Genome Sciences Center. MB and DD preformed bioinformatic processing of the sequencing results.

3.1 Introduction

Many chromatin modifiers affect transcription by controlling the accessibility of DNA to RNA polymerases and transcription factors. Proteins related to *S. cerevisiae* Fpr3 and Fpr4 are no exception. Nucleoplasmin family proteins and nuclear FKBPs interact with transcription factors[131,227,234] and affect both RNA Pol I[116] and RNA Pol II[118] transcription. Less is known about the role of nucleoplasmin-like FKBPs in transcriptional regulation. Prior to the onset of this dissertation project, *S. cerevisiae* Fpr4 was known to directly repress the transcription of reporter genes both in an artificial recruitment assay[283] and integrated at ribosomal DNA (rDNA)[240,284]. Furthermore, a microarray gene expression analysis published in 2014 also revealed that Fpr3 and Fpr4 regulate the expression of a broad set of functionally diverse protein coding genes[283]. However, these experiments did not include an analysis of *Δfpr3Δfpr4* double mutants and were restricted to protein coding regions of the genome[283].

In Chapter 2 I presented genetic interaction data which support a model for separate, cooperative, and redundant functions of Fpr3 and Fpr4. These data further support the expected functional connection between these paralogs and transcriptional regulators, including other chromatin modifiers (the ADA HAT complex), nucleosome remodelers (the SWI/SNF complex) and RNA degradation machinery (the TRAMP5 RNA exosome). Given that Fpr4 physically associates with chromatin at rDNA and other genes[223,284], I hypothesized that Fpr3 and Fpr4 build chromatin at discrete genomic loci and thus regulate transcription from those locations. To test

this, and to obtain a more complete view of the comparative impact of Fpr3 and Fpr4 on transcription genome-wide, RNA from strategic deletion mutants was sequenced.

In this chapter I present transcriptomics data from these sequencing experiments. Consistent with their expected function as histone chaperone enzymes that modulate nucleosome dynamics, I find that these proteins positively regulate some genes and negatively regulate others. With respect to their functional differences, I show that, while a small number of RNAs may be separately regulated by Fpr3 or Fpr4, a more striking observation is the identification of genes sensitive to both proteins. This implies that at Fpr3 and Fpr4 cooperate at many genes. For example, both paralogs are required to repress transcription of ribosomal protein and phosphate metabolism genes. Furthermore, I find that several RNAs encoding additional ribosomal proteins are differentially expressed in *Δfpr3Δfpr4* double mutants, but not in either single mutants. This highlights that Fpr3 and Fpr4 are redundant in the regulation of these genes. Finally, I further probe the synthetic sickness of *Δfpr3Δfpr4Δtrf5* yeast revealed in Chapter 2 by sequencing the transcriptome of these and *Δfpr3Δtrf5* yeast. This strain is an appropriate control because it shows no fitness defects in my paralog-SGA screens (see Figure 20). This experiment revealed widespread transcriptional differences in *Δfpr3Δfpr4Δtrf5* yeast, including the accumulation of non-coding transcripts from rDNA. This signature of upregulated RNAs supports a model where the TRAMP5 RNA exosome masks the impact of Fpr4 on transcription by degrading aberrant RNAs.

Taken together, the transcriptomics data presented in this chapter support the model I proposed at the end of my first data chapter, i.e. that Fpr3 and Fpr4 have separate, cooperative, and redundant functions in chromatin regulation at discrete genomic loci including at protein coding genes and rDNA.

3.2 Results

3.2.1 Fpr3 and Fpr4 regulate the expression of separate and common genes

To determine the effect of Fpr3 and Fpr4 on transcription genome wide, we collaborated with the Hirst Lab at the BC Genome Sciences Centre to perform a singlicate strand-specific RNA-seq survey screen of the ribosomal RNA depleted (ribo-minus) fraction of RNAs from WT, *Δfpr3*, *Δfpr4*, and *Δfpr3Δfpr4* yeast. A *Δsir2* deletion mutant was included as a control, as the impact of Sir2 on gene expression has been well characterized[397,398]. Reads per kilobase million (RPKM) values were calculated for each gene and a differential expression (DE) analysis was performed

comparing expression levels in all mutants to WT controls (see materials and methods and appendix Figure 39). A false discovery rate (FDR) of 0.05 was used to identify genes that were significantly differentially expressed. At a cut-off threshold of 1.3-fold (similar to that used in the Park et al. 2014 microarray analysis[283]), the *Δsir2* control displayed 827 differentially expressed genes (Figure 26 A). Of these, 280 were upregulated while 547 were downregulated (Figure 26 A). The number and nature of differentially expressed genes in these *Δsir2* controls is consistent with previous reports of known Sir2 regulated genes and binding sites[397,398]. This validates the application of this sequencing approach to mutants of NPL-FKBPs.

In single gene deletion mutants of *Δfpr3* and *Δfpr4*, a total of 529 and 549 differentially expressed genes were uncovered respectively (Figure 26 A). In *Δfpr3* single gene deletion mutants, 195 genes were upregulated while 334 were downregulated, and in *Δfpr4* mutants 185 genes were upregulated while 364 were downregulated (Figure 26 A). Three general observations regarding this data are consistent with previous microarray analyses[283]. First, these DE transcripts originate from all 16 yeast chromosomes. Thus, Fpr3 and Fpr4 affect gene expression from multiple loci genome-wide. Second, the fact that approximately two thirds of DE genes were down-regulated indicates that these histone chaperones appear to promote gene expression more frequently than gene repression (Figure 26 A). Third, a comparison of these transcripts also revealed that roughly one third of Fpr3 regulated transcripts are also regulated by Fpr4, and vice versa (Figure 26 B). This confirms that on these genes, transcriptional regulation requires cooperation between both paralogs. Furthermore, although the effect of Fpr3 and Fpr4 on gene expression can be positive or negative, the impact of these histone chaperones on cooperatively regulated genes is always in the same direction.

In double *Δfpr3Δfpr4* mutants, a total of 683 differentially expressed genes were uncovered (Figure 26 A). Of these, 274 genes were upregulated while 409 were downregulated (Figure 26 A). A comparison of these transcripts to those uncovered in single *Δfpr3* or *Δfpr4* deletion mutants revealed 145 upregulated and 193 downregulated genes that were only differentially expressed in the *Δfpr3Δfpr4* double mutants (Figure 26 B). This indicates that Fpr3 and Fpr4 redundantly regulate some genes. Taken together, these data support the model proposed in Chapter 2; that Fpr3 and Fpr4 have unique, cooperative, and redundant functions.

To better understand the comparative effects of Fpr3 and Fpr4 on RNA steady state levels, I performed a gene ontology enrichment analysis on the DE gene lists represented by the sectors in Figure 26 B. I identified 120 upregulated genes which are uniquely regulated by Fpr3. At an arbitrary *p*-value cutoff of $\leq 10^{-5}$, ontologies present in this list were limited and included generic

terms such as pyridoxal phosphate binding (p=6.6x10^{-7}), catalytic activity (p=3.53x10^{-6}), and metabolic process (p=4.06x10^{-6}) (Figure 27 A and appendix Table 9). Likewise, the only ontology with $p \leq 10^{-5}$ enriched among the 217 genes uniquely downregulated by Fpr3, was the generic term signal transduction (p=3.37x10^{-7}) (Figure 27 B and appendix Table 10).

Notable ontology terms associated with the 110 upregulated genes which appear to be uniquely regulated by Fpr4 included trehalose biosynthetic processes (p=2.28x10^{-6}) and oxidation-reduction processes (p=7.38x10^{-6}) (Figure 27 A and appendix Table 11). The 247 genes downregulated by Fpr4 were enriched in RNA binding (p=2.19x10^{-7}), nucleic acid binding (p=6.18 x10^{-7}), and nucleotide binding (p=1.13 x10^{-6}) functions, and rRNA processing (p=9.03x10^{-11}) and ribosome biogenesis (p=4.39 x10^{-13}) processes (Figure 27 B and appendix Table 12). Taken together, these ontology analyses indicate that Fpr3 and Fpr4 have non-overlapping impacts on the transcriptome and that they uniquely regulate some functionally distinct genes.

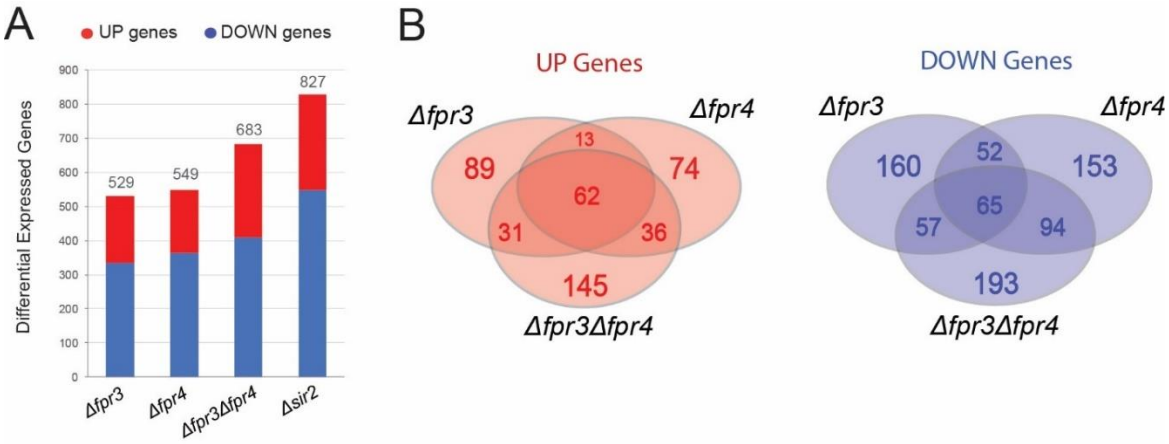

Figure 26. Fpr3 and Fpr4 have partially overlapping impacts on the transcriptome.
(A) Numbers of differentially expressed genes in *Δfpr3*, *Δfpr4*, *Δfpr3Δfpr4* and *Δsir2* mutants relative to wild type (WT). (B) Venn diagrams depicting the partial overlap in up- and downregulated genes in *Δfpr3*, *Δfpr4*, and *Δfpr3Δfpr4* mutants.

The 145 genes uniquely upregulated in *Δfpr3Δfpr4* double mutants were associated with ontology terms such as structural constituent of ribosome (p=9.83x10^{-6}) and cellular amino acid biosynthetic process (p=8.89x10^{-8}) (Figure 27 A and appendix Table 15). The only ontology term below the p-value cutoff of $\leq 10^{-5}$ enriched among the 193 genes uniquely downregulated in *Δfpr3Δfpr4* double mutants was (protein components of the) actin cortical patch (p=3.55x10^{-6}) (Figure 27 B and appendix Table 16). Collectively, these results support the model that Fpr3 and Fpr4 regulate the transcription of genes associated with these processes and complexes redundantly.

Figure 27. Fpr3 and Fpr4 regulate the expression of separate and common genes.
(A) Venn diagrams depicting notable ontologies related to molecular functions, biological processes, cellular components, and protein complexes associated with genes upregulated in *Δfpr3*, *Δfpr4*, and *Δfpr3Δfpr4* mutants. (B) Venn diagrams depicting notable ontologies related to molecular functions, biological processes, cellular components, and protein complexes associated with genes downregulated in *Δfpr3*, *Δfpr4*, and *Δfpr3Δfpr4* mutants.

I identified a total of 127 genes (62 up, 65 down) that were differentially expressed in all three RNA-seq libraries (*Δfpr3*, *Δfpr4* and *Δfpr3Δfpr4*) (Figure 26 B). The 65 genes downregulated in all three experiments included 5 genes encoding factors involved in iron siderophore transport (p=4.33x10^{-9}), and iron ion homeostasis (p=4.44x10^{-6}) (Figure 27 B and appendix Table 14).The 62 upregulated genes included 13 cytosolic ribosomal protein coding genes (p=2.10x10^{-7}), 4 factors involved in phosphate transport (p=1.94x 10^{-6}), 3 factors involved in phosphate metabolism (3.87x10^{-5}), and 4 factors involved in polyphosphate metabolism (p=4.20x 10^{-7}) (Figure 27 A and appendix Table 13). In fact, the most differentially expressed

genes in our survey (up to 60-fold upregulated), were phosphate metabolic genes such as *PHO5*, *PHO11*, and *PHO12* which encode acid phosphatases involved in phosphate hydrolysis, and *PHO89*, *PHO84*, and *PIC2* which encode phosphate transporters. Since previous studies had not identified *PHO* genes as Fpr3/Fpr4 regulated, I verified these RNA-seq observations using independent biological replicates and quantitative RT-PCR of two *PHO* genes as well as one down regulated siderophore transporter, *SIT1* (Figure 28). The identification of polyphosphate metabolism and ribosomal protein genes as Fpr3/Fpr4 targets is particularly noteworthy given a recent report which identified Fpr3 and Fpr4 as major direct targets of protein polyphosphorylation and established conserved links between the polyphosphorylation and ribosome biogenesis network in yeast and human cells[286]. In summary, these RNA-seq experiments demonstrate that Fpr3 and Fpr4 have non-overlapping impacts on the transcriptome and that both paralogs are required for repression of genes involved in phosphate uptake and polyphosphate metabolism, as well as ribosomal protein genes.

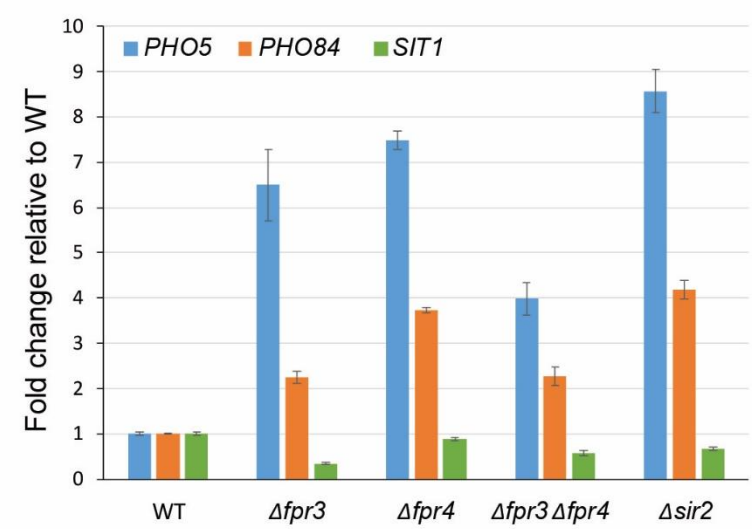

Figure 28. Fpr3 and Fpr4 downregulate the transcription of genes associated with phosphate metabolism and upregulate the transcription of a gene associated with a siderophore transporter.
Confirmation of select differentially expressed genes (*PHO5*, *PHO84*, and *SIT1*) by quantitative RT-qPCR of RNA isolated from independent biological replicates. Fold changes in gene expression are shown relative to WT. Error bars indicate standard deviation of three technical replicates.

3.2.2 The TRAMP5 RNA exosome masks the impact of Fpr4 on transcription

My paralog-SGA screens indicated that deletion of *TRF5*, a gene which encodes the defining component of the TRAMP5 complex, induces severe sickness in *Δfpr3Δfpr4* double mutant yeast (see Figure 20). Given that this poly(A) polymerase complex stimulates the degradation of

aberrant RNAs[344,356], I hypothesized that it could be required for the degradation of transcripts negatively regulated by Fpr3/Fpr4. I decided to test this hypothesis with respect to transcripts regulated by Fpr4, by sequencing the strand-specific ribo-minus transcriptomes of two strains from the paralog-SGA screen: *Δtrf5* haploids with a functional Fpr4 (*Δfpr3Δtrf5),* and isogenic haploids that lack both paralogs (*Δfpr3Δfpr4Δtrf5).* This provides a sensitized approach to reveal Fpr4-regulated RNAs because functional compensation by Fpr3 is not possible and potential degradation of upregulated RNAs by TRAMP5 is eliminated.

A comparison between the transcriptomes of *Δfpr3Δtrf5* and *Δfpr3Δfpr4Δtrf5* yeast uncovered a total of 1321 differentially expressed genes; 967 of which were upregulated and 354 downregulated in the *Δfpr3Δfpr4Δtrf5* triple mutants (Figure 29 A). The fact that nearly ¾ of the DE genes were upregulated in these *Δtrf5* deficient cells supports the hypothesis that Fpr4 negatively regulates genes which are also substrates for the TRAMP5 complex. An ontology enrichment analysis of these upregulated genes is provided in appendix Table 17. This analysis indicates that genes encoding ribosomal proteins (p=3.21x10^{-12}) and genes associated with rRNA processing (p=1.14x10^{-8}) are highly enriched as Fpr4 targets (Figure 29 B and appendix Table 17). Also enriched are genes encoding constituents of the fungal-type cell wall (p=1.87x10^{-4}) and the electron transport chain (p=6.12x10^{-8}) (Figure 29 B and appendix Table 17). Taken together, these results partially explain the imbalance of upregulated vs downregulated genes detected in *Δfpr4* transcriptomes (Figure 26 A). That is, many mRNAs that are negatively regulated by Fpr4 are also degraded by the TRAMP5 RNA exosome, which leads to an underestimation of negatively regulated genes in *Δfpr4* and *Δfpr3Δfpr4* yeast.

Significantly enriched ontologies present in the list of 354 downregulated genes included generic terms such as ATP binding (p<10^{-14}) and nucleotide binding (p=2.77x10^{-13}) functions, and general metabolic process (p=7.78x10^{-8}) and translation (p=1.53x10^{-9}) processes (appendix Table 18). These transcripts may represent secondary indirect effects of Fpr4 on the transcriptome.

3.2.3 Evidence for Fpr4 action at the 5’ end of the transcription unit

Further interrogation of RNA-sequencing data revealed additional evidence for Fpr4 in the regulation of transcription. Of the 1321 differentially expressed genes in *Δfpr3Δfpr4Δtrf5* yeast (Figure 29 A), I noticed that approximately 40% displayed an accumulation of reads at the 5’ end of the annotated transcript. Subsequent bioinformatic analysis of the total transcriptomes of *Δfpr3Δfpr4Δtrf5* and *Δfpr3Δtrf5* mutants revealed that this 5’-biased transcript asymmetry was

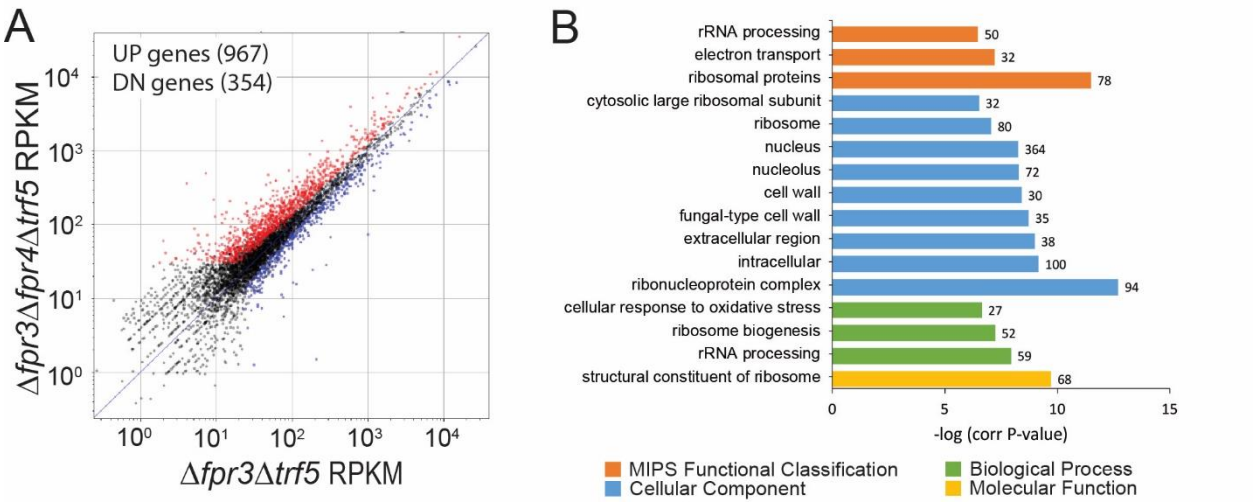

Figure 29. The TRAMP5 exosome masks the impact of Fpr4 on transcription.
(A) Scatter plot comparing the RNA-seq transcriptome analysis of *Δfpr3Δ fpr4Δtrf5* triple deletion mutants to *Δfpr3Δtrf5* double deletion mutants reveals an increase in Fpr4-repressed RNAs (red dots). Expression values are shown as log10 read per kilobase of transcript per million mapped reads (RPKM). Red dots indicate genes with a log2 fold change of >1.3 while blue dots indicate a fold change of <-1.3 (B) Gene ontology enrichment analysis of the 967 upregulated transcripts in *Δfpr3Δfpr4Δtrf5* triple deletion mutants. Enriched genes were classified by molecular function, biological process, cellular component, and MIPS functional database classification by FunSpec (http://funspec.med.utoronto.ca/).

widespread, and detectable in genes regardless of their net change in transcription (Figure 30 A). I present RNA-seq reads on two example genes illustrating this asymmetry signature in Figure 30 B. *SSF1* encodes a 66S pre-ribosome constituent and is required for large ribosomal subunit maturation, while *UTP9* encodes a component required for proper endonucleolytic cleavage of 35S rRNA. The paired-end tag coverage associated with both of these genes, but not a negative control gene (*ACT1*) (Figure 30 C) displays this characteristic 5'asymmetry in *Δfpr3Δfpr4Δtrf5* yeast. I independently validated these observations using biological replicates and quantitative RT-qPCR with 5' and 3' amplicons of *UTP9* and *SSF1*, which were normalized to the unchanged *GPD1* gene (Figure 30 D). Collectively, this transcriptome signature demonstrates three novel findings. First, that Fpr4 negatively regulates transcription from many genes even though total reads per gene may not change. Second, because this signature of accumulated 5' reads on genes is only readily detectable in the absence of Trf5, the TRAMP5 RNA exosome can mask these subtle transcriptional defects (Figure 26 A). Third, this signature indicates Fpr4 action is critical at a stage after initiation, likely during transcriptional elongation. These results alone do not rule out the possible explanation that Fpr4 (and Fpr3) potentially impact the stability of RNA. However, given their known roles as histone chaperones implicated in nucleosome dynamics [221,285,399], a more likely model that explains this bias is that it results from altered passage of RNA

polymerase through genes. In the absence of Fpr4 transcription from target genes can initiate but not proceed to completion resulting in the accumulation of incomplete 5' RNAs. These transcripts are consequently recognized and degraded by the TRAMP5 RNA exosome.

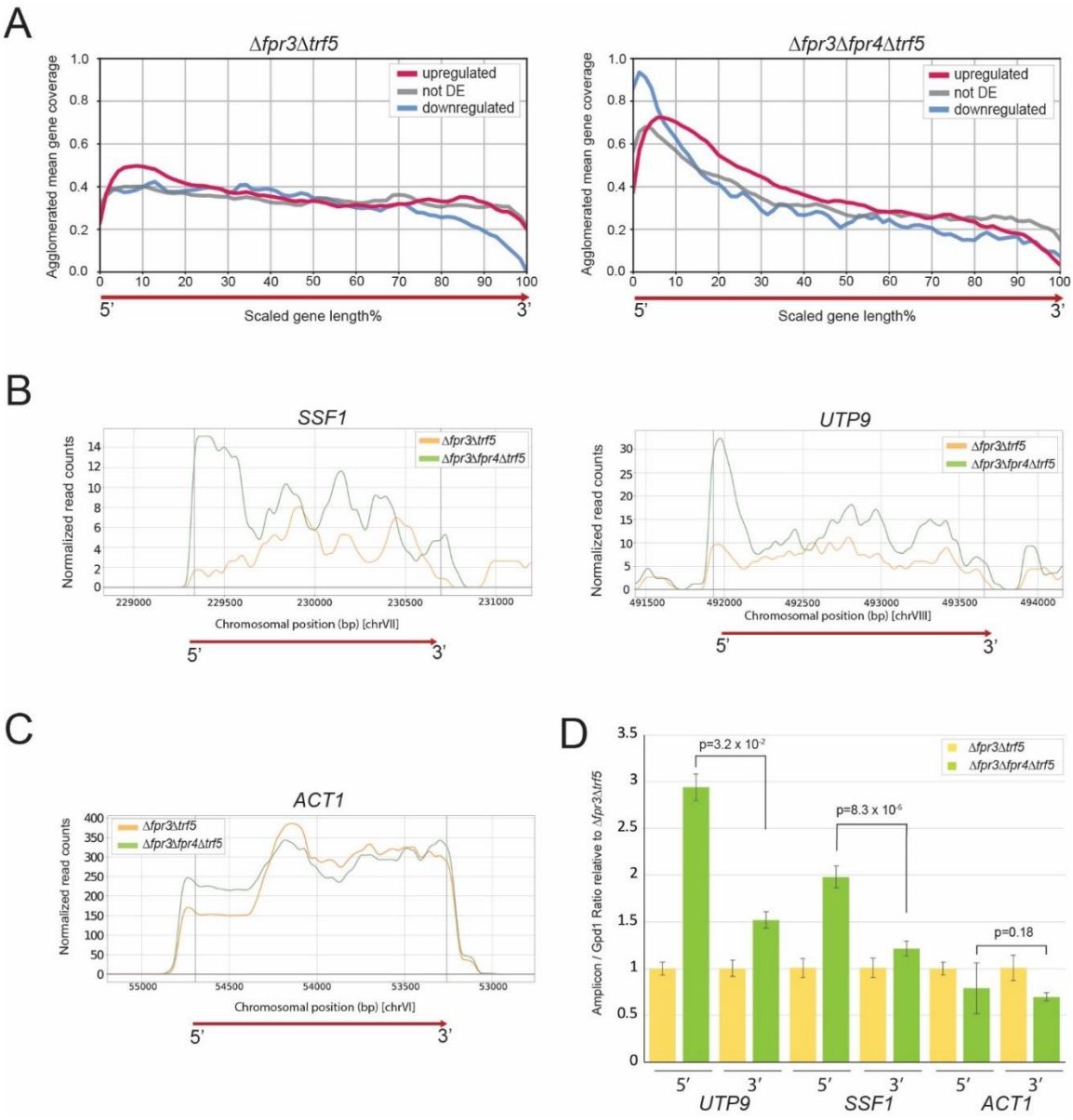

Figure 30. A signature of incomplete elongation is present in Δ*fpr4* yeast
(A) Plots of RNA-seq read density as a function of position on a scaled average gene. Upregulated, downregulated, and unchanged transcripts generated from *Δfpr3Δtrf5* double mutants (left) and *Δfpr3Δfpr4Δtrf5* triple mutants (right) are shown. (B) RNA-seq read density plots on two genes showing a signature of incomplete elongation: *SSF1* (left) and *UTP9* (right). (C) RNA-seq read density plot on *ACT1*, a gene without a signature of incomplete elongation. (D) Quantitative RT-PCR validation of RNA read densities on *UTP9*, *SSF1*, and *ACT1*. 5' and 3' amplicons were normalized to the unchanged *GPD1* gene. RNAs were extracted from independent biological replicates (from those subjected to RNA-seq). Error bars indicate standard deviation of three technical replicates.

3.2.4 Fpr3 and Fpr4 inhibit transcription from the non-transcribed spacers of ribosomal DNA

Given that Fpr3 and Fpr4 are enriched in the nucleolus[279–281,302], and that Fpr4 represses the expression of a reporter integrated at rDNA[284], I wondered whether cells lacking these paralogs displayed transcriptional defects at this locus. Despite being performed on strand-specific ribo-minus RNA, we were readily able to detect reads generated from the rDNA in our RNA-seq analysis (likely due to incomplete rRNA depletion during sample processing). The observation that reads generated from the rRNA coding sequences were unchanged in *Δfpr3* and *Δfpr4* single mutants and *Δfpr3Δfpr4* double mutants, implies that RNA Pol I transcription of 5S and RNA Pol III transcription of 35S pre-rRNA does not change in cells lacking Fpr3 and Fpr4. At the intergenic spacer regions flanking these rRNA coding sequences (the NTS loci), however, I detected a modest 2-3 fold increase in levels of transcripts generated from both strands in *Δfpr3* and *Δfpr4* single mutants and *Δfpr3Δfpr4* double mutants (not visible in Figure 31 A). Using the increased specificity of Northern analysis, I independently confirmed the observation that transcripts generated from both NTS1 and NTS2 accumulate in single mutants of *Δfpr3* and *Δfpr4* in a different strain background (Figure 31 B). Collectively, this indicates that both Fpr3 and Fpr4 impact silencing at rDNA intragenic spacers.

Given that TRAMP5 buffers the loss of Fpr4 (Figure 26 A), I asked if Trf5 might be degrading *NTS* RNAs in *Δfpr4* yeast. Consistent with this idea, transcripts from *NTS1* and *NTS2* were readily detected in *Δfpr3Δfpr4Δtrf5*, but not *Δfpr3Δtrf5* strains (Figure 31 C). Notably, these RNAs are templated from both strands. Taken together, the localized transcriptional defects uncovered at the *NTS* regions of rDNA support a model where Fpr3 and Fpr4 contribute to the establishment of a transcriptionally silent *NTS* chromatin environment. The absence of this chromatin structure permits pervasive transcription from both strands of *NTS1* and *NTS2*. Furthermore, as with 5’ asymmetric transcripts, the presence of a functional RNA exosome masks these subtle transcriptional defects because these RNAs are presumably targeted and degraded by TRAMP5.

3.2.5 Fpr3 and Fpr4 silence a Pol II transcribed reporter within the *NTS1* rDNA spacer

RNA-seq and Northern blot data revealed that transcripts generated from both rDNA *NTS* spacers accumulate in cells deficient for Fpr3 and Fpr4 (Figure 31). To further validate the effects of these paralogs on transcription at this locus, I used a classical reporter assay for transcriptional

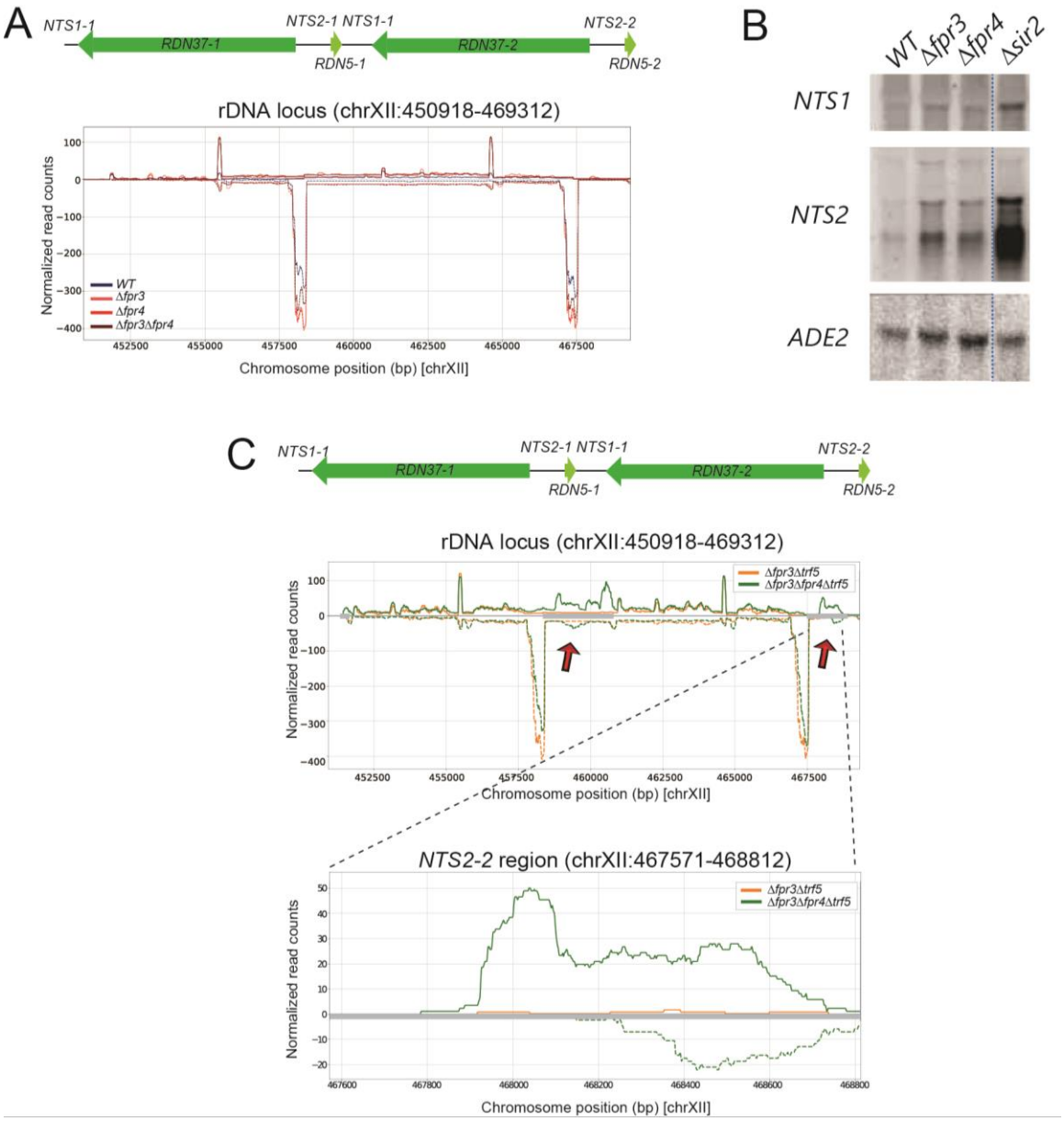

Figure 31. Fpr3 and Fpr4 silence the non-transcribed spacers (NTS) of rDNA.
(A) Plots of RNA-seq read density across the rDNA locus on chromosome XII in WT, *Δfpr3*, *Δfpr4*, and *Δfpr3Δfpr4* mutants. A modest increase of reads mapping to *NTS2-1*, *NTS1-1* and *NTS2-2* indicates that these paralogs impact silencing at this locus. (B) Northern analysis of RNAs generated from *NTS1*, *NTS2*, and the *ADE2* control gene in single mutants of Δ*fpr3*, Δ*fpr4*, and a positive control Δ*sir2*. Dashed lines indicate where images from the same membrane were spliced. The probes were 800bp fragments of DNA from each sequence and each lane contains 10µg of RNA. (C) Plots of RNA-seq read density across the rDNA locus on chromosome XII (top) and across *NTS2-2* (bottom) in *Δfpr3Δtrf5* and *Δfpr3Δfpr4Δtrf5* yeast. The reads mapping to *NTS2-1*, *NTS1-1* (center) and *NTS2-2* (right) indicate that the TRAMP5 exosome masks the transcriptional silencing of Fpr4 at the *NTS*s.

silencing[400]. Yeast genes embedded within and adjacent to constitutive heterochromatin loci such as the rDNA, telomere boundaries, or either of the two silent mating cassettes normally have

silenced expression. Although the impact of Fpr4 on the silencing of an rDNA integrated reporter had previously been observed[284], the contribution of Fpr3 and the functional relationship between Fpr3 and Fpr4 in this process had not been similarly investigated. Using a *URA3* reporter gene under the control of a minimal TRP1 promoter as a reporter, I investigated the impact of Fpr3 and Fpr4 on silencing from these three constitutive heterochromatin loci. I monitored the repression of this reporter in *Δfpr3*, *Δfpr4*, and *Δfpr3Δfpr4* double mutant yeast. A *Δsir2* deletion mutant served as a positive control, as Sir2 is known to silence *NTS*[401]. I found that Fpr3 and Fpr4 are each required for silencing the expression of this reporter and that the silencing effect of the two proteins was non-additive (Figure 32 A). This silencing affect was specific to rDNA heterochromatin, as deletion of Fpr3 or Fpr4 did not compromise silencing of the reporter at the telomere boundary and within the HMRα silent mating type cassette (Figure 32 B and C). Taken together, these results support the model that Fpr3 and Fpr4 are involved in silencing at rDNA and that they may function together in the context of this exogenous RNA Pol II driven reporter.

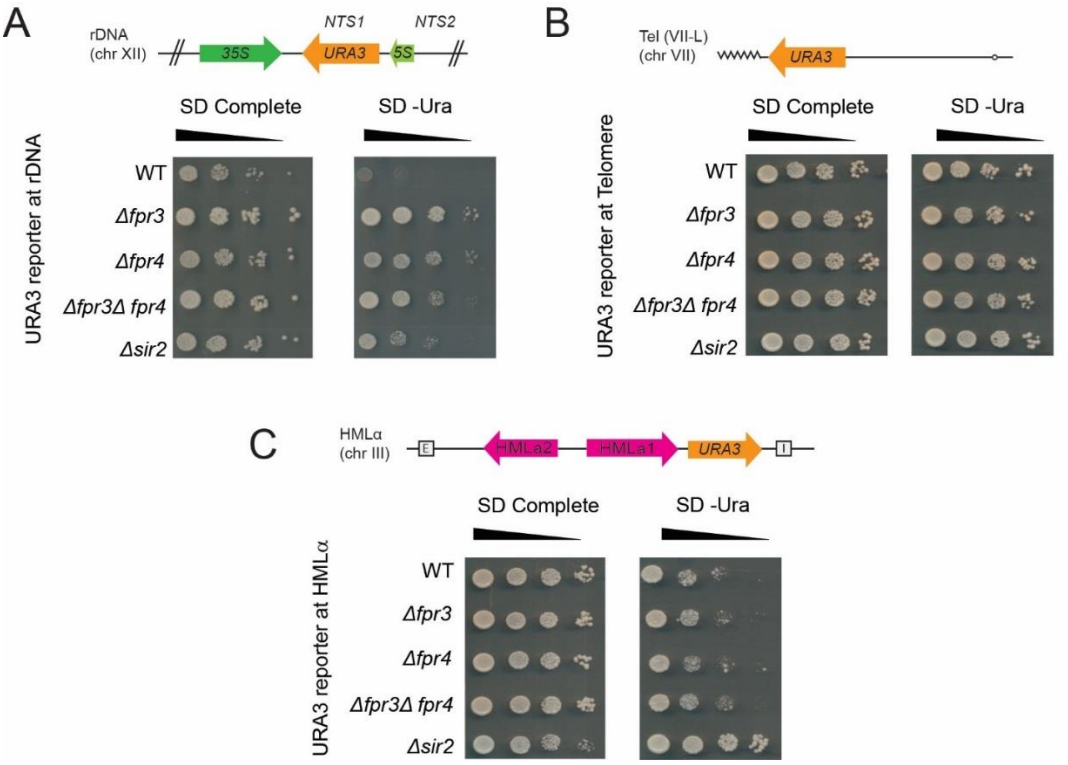

Figure 32. Fpr3 and Fpr4 are specific to reporter silencing at rDNA heterochromatin
Ten-fold serial dilution spotting assays of single and double gene deletion mutants in strain backgrounds carrying a *URA3* reporter integrated within: (A) an *NTS1* spacer of rDNA; (B) the telomere boundary on the left arm of chromosome 7; (C) within the *HMLα* locus. Cells were grown on either synthetic defined (SD) complete media or on SD media lacking uracil for 2 days at 30°C.

3.3 Discussion

Chromatin modifiers affect transcription by controlling DNA template accessibility. To assess the impact of Fpr3 and Fpr4 on this process we sequenced ribo-minus RNA from a series of strategic deletion mutants. Together with additional supporting experiments, data generated from this analysis revealed that Fpr3 and Fpr4 regulate transcription from multiple genomic locations both positively and negatively. They have unique and common targets, and impact ribosome biogenesis and phosphate metabolism genes. Furthermore, this data indicates that the *NTS* loci of rDNA are an additional shared target of both proteins. Collectively, the data presented in this chapter implicate Fpr3 and Fpr4 in establishing chromatin at diverse genomic loci.

Consistent with previous microarray results[283], differential gene expression in *Δfpr3* and *Δfpr4* mutants indicates that these enzymes affect the transcription of multiple genes genome-wide. Some DE transcripts may be the direct consequence of a failure to establish correct chromatin environments at Fpr3 and Fpr4 target loci, while others may be indirectly upregulated or downregulated. A chromatin immunoprecipitation (ChIP) based approach may be used to resolve the direct vs indirect targets of Fpr3/Fpr4 in future studies. While chromatin immunoprecipitation studies have been preformed on Fpr4 and suggest that this chaperone is enriched at both the transcribed and spacer loci of rDNA[402], genome wide mapping via ChIP has been limited by difficulties with crosslinking Fpr4 to chromatin using formaldehyde. These crosslinking difficulties do not appear to be unique to Fpr4, as other chromatin remodelers such as Asf1 also crosslink poorly[403]. The prospective Fpr3 and Fpr4 target genes identified in this study, may be prioritized in future ChIP analyses using different crosslinking agents in a targeted approach to uncover which loci represent direct vs indirect targets of Fpr3/Fpr4. Collectively, the identification of genes sensitive to each paralog individually, cooperatively, and redundantly supports the multimodal functional model presented in Chapter 2 (Figure 25), where these NPL-FKBPs may function as both homo- or hetero-oligomers to carry out unique, cooperative, and redundant biological functions. The fact that Fpr3 and Fpr4 co-immunoprecipitate[294] with each other provides additional support for this model.

A significant number of genes encoding protein components of the cytosolic ribosome were identified as sensitive to both paralogs. In *S. cerevisiae* many ribosomal protein coding genes share a common promoter architecture and are driven by common regulators[404]. By recognizing either common DNA sequences or transcription factors, and building chromatin at these ribosomal protein gene promoters, Fpr3/Fpr4 may function to downregulate ribosomal protein gene transcription. The significant enrichment of genes encoding ribosomal proteins among

alleviating suppressor genetic interactors of *FPR3*/*FPR4* (Figure 22 and Figure 24) lends further support to this model as it suggests that in the absence of *FPR3/FPR4* the presence of ribosomal protein coding genes becomes detrimental to viability. Alternatively, ribosomal protein coding genes may be upregulated in *Δfpr3/Δfpr4* mutants as an indirect consequence of some other primary effect. The 5' signature of incomplete elongation associated with many of these ribosomal protein coding genes in *Δfpr4* yeast, argues against this latter model as it implies that at least Fpr4 is associated with defects in nucleosomal positioning at gene promoters. Future experiments testing the accessibility of these ribosomal protein coding gene promoters to digestion by micrococcal nuclease will provide further insights into the impacts of Fpr3/Fpr4 on nucleosomal positioning at these target promoters. Collectively, these data implicate both Fpr3 and Fpr4 in ribosome biogenesis, and at least some elements of this role may be conserved in the human NPM family protein FKBP25[229,233].

The differential gene expression data presented in this chapter also indicates that Fpr3 and Fpr4 are necessary for the repression of several phosphate and polyphosphate metabolism and storage (*PHO*) genes. This is especially intriguing, given that Fpr3 and Fpr4 were recently found to be heavily polyphosphorylated together with other proteins in an evolutionarily conserved network of ribosome biogenesis factors[286,405]. Although the impact of Fpr3 and Fpr4 polyphosphorylation on their function remains to be determined, the identification of the well-studied *PHO5* gene as a common Fpr3 and Fpr4 target provides an ideal readout system for analyzing the impact of this modification on their function in future studies. This polyphosphorylation also appears to be conserved in the human acidic histone chaperone nucleolin[286].

Deletion of the Trf5 poly(A) polymerase enables the enhanced detection of additional Fpr4 regulated genes, including transcripts which are a signature of incomplete elongation. This suggests that Fpr4 plays a role in promoting transcriptional elongation. The additional observation that Fpr4 affected reads appear to span across the first 1-3 nucleosomes of genes is particularly interesting given that Fpr4 can bind nucleosomes through basic surface features[221], and is important for transcriptional induction kinetics[223]. It suggests that nucleosomes immediately downstream of the transcriptional start site are targets of Fpr4. One possibility is that Fpr4 deposits histones at gene promoters to inhibit transcriptional initiation (Figure 33 A). Another is that it evicts histones from sequences downstream of the transcriptional start site to remove nucleosome blocks to the polymerase (Figure 33 B). The cryo-EM structures of *Xenopus* nucleoplasmin pentamers directly engaging histone octamers[110], and additional *in vitro* studies which indicate that Fpr4 binds both free histones and nucleosomes[221] provide further support for

these models. The suite of genes showing this 5' incomplete elongation signature would be ideal candidates for analyzing the impact of Fpr4 on nucleosomal positioning and chromatin architecture in future micrococcal nuclease digestion assays. Because micrococcal nuclease preferentially digests naked DNA in the linker regions between nucleosomes, it can be used to assess the nucleosome density at genes showing this 5' incomplete elongation signature (such as *UTP9* and *SSF1*) and control genes such as *ACT1*. If Fpr4 deposits histones at these promoters then chromatin isolated from *Δfpr4* yeast would be expected to exhibit increased accessibility to micrococcal nuclease digestion at these loci, indicating the absence of nucleosomes. If Fpr4 removes histones downstream of the transcription start site, then *Δfpr4* yeast would be expected to exhibit decreased micrococcal nuclease digestion at these loci, indicating the presence of nucleosomes.

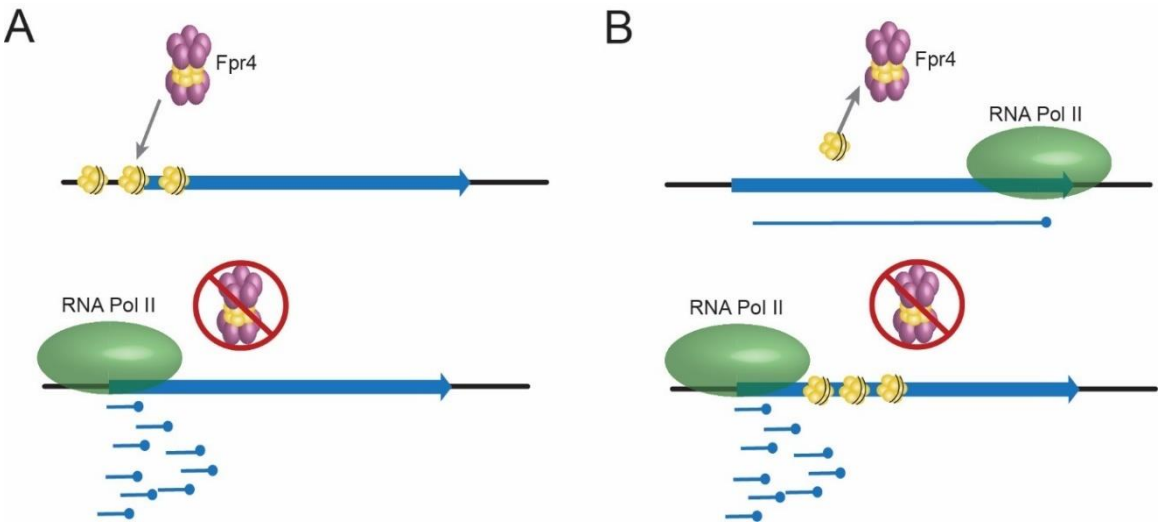

Figure 33. Models for Fpr4 regulation of elongation
(A) Fpr4 may regulate transcription by installing nucleosomes within promoters to inhibit transcriptional initiation (top). In the absence of Fpr4, this chromatin environment at the promoter is not generated allowing for spurious transcription from the 5' end of the gene (bottom). (B) Fpr4 may regulate transcription by removing nucleosomes immediately after the transcriptional start site (top). In the absence of Fpr4, the presence of these nucleosomes blocks or stalls polymerase progression and results in the generation of incomplete 5' transcripts (bottom).

In addition to impacting the transcription of ribosomal protein coding genes, Fpr3 and Fpr4 also impact transcription from the non-transcribed spacers of rDNA. This is consistent with their nucleolar enrichment[279–281,302], data indicating that Fpr4 inhibits transcription of exogenous reporters at rDNA in yeast[402], and orthologues operating similarly in plants[240]. The observation that Fpr3/Fpr4 regulate ribosomal protein coding genes, ribosomal RNA, and polyphosphate genes recently implicated in ribosome biogenesis, supports the idea that these NPL-FKBPs may

be functioning as master regulators of ribosome biogenesis by simultaneously coordinating the transcription of both ribosomal protein, ribosomal RNA, and polyphosphate factors involved in the ribosome biogenesis regulation. This role in ribosome biogenesis also appears to be conserved in the more distantly related human nuclear FKBP, FKBP25[233].

3.4 Materials and Methods

Strains

Yeast strain genotypes are described in detail in appendix Table 19. Single gene deletion mutants of *Δfpr3*, *Δfpr4*, and *Δsir2* used for the RNA sequencing and validating quantitative RT-PCR are all isogenic to BY4741 and were either purchased from open biosystems, or taken from the yeast deletion collection (purchased from Thermofisher Dharmacon). The isogenic double deletion *Δfpr3Δfpr4* mutant was constructed from the open biosystems *Δfpr3* single gene deletion mutant by replacing the endogenous *FPR4* locus with a nourseothricin resistance (*MX4-NATR*) PCR product deletion module [395,396].

The *FPR4(Δfpr3Δtrf5)* and *Δfpr3Δfpr4Δtrf5* isogenic strains used for the RNA sequencing and validating quantitative RT-PCR were generated from the SGA cross (see section 2.4 Materials and Methods).

The *Δfpr3* and *Δfpr4* deletion mutant strains used in the rDNA reporter spotting assays and Northern analysis were generated from a cross of the MATα UCC1188[406] with a MATa BY4741 deletion mutant (see appendix Table 19 for details). The UCC1188 background *Δfpr3Δfpr4* double deletion mutant, UCC1188 background *Δsir2* deletion mutant, and all deletion mutants in the Tel(VII-L) and HMLα reporter backgrounds were generated by lithium acetate transformation of UCC1188, UCC7266, or UCC1369[406] with PCR product deletion modules.

RNA-Seq Library Preparation and Sequencing

Single colony isolates of each strain were grown to mid-log phase in 50mL of liquid yeast extract- peptone- dextrose (YPD) media. Samples were then pelleted and washed once with sterile water before being flash frozen in liquid nitrogen and stored for 16 hours at -80°C. Samples were thawed on ice, and RNA was extracted using a phenol-freeze based approach as previously described[407]. The extracted RNA was subsequently treated with RNase- free DNase I (Thermo Fisher Scientific).

RNA samples were processed and sequenced at the BC Cancer agency Michael Smith Genome Sciences Centre following standard operating protocols. Briefly, total RNA samples were ribo-depleted using the Ribo-Zero Gold rRNA Removal Kit (Yeast) (Illumina) and analyzed

on an Agilent 2100 Bioanalyzer using Agilent 6000 RNA Nano Kit (Agilent Technologies, Santa Clara, California). cDNA was generated using the Superscript II Double-Stranded cDNA Synthesis kit (ThermoFisher) which enabled strand specificity due to the incorporation of dUTP into the second cDNA strand rather than dTTP. 100bp paired-end libraries were prepared using the Paired-End Sample Prep Kit (Illumina, San Diego, California). Sequencing was performed on an Illumina MySeq platform with paired-end reads of 100bp.

Processing of Sequencing Data

Sequenced paired-end reads were aligned to the sacCer3 reference genome (https://www.ncbi.nlm.nih.gov/assembly/GCF_000146045.2/, Dec 2014) using the Burrows-Wheeler aligner (BWA)[408] (version 0.6.1-r104-tpx). Out of 5110 *S. cerevisiae* genes annotated in Ensembl v90 only 267 were spliced with most of the spliced genes (251) having one intron. Therefore, a genomic alignment of RNA-seq reads was considered as a good approximation for the yeast transcriptome analysis. For every library a total of approximately 1.5 million to 2 million reads were sequenced, of which approximately 75-95% of reads were aligned.

To quantify gene expression, reads that aligned to multiple locations (and therefore can't be placed unambiguously) were filtered by applying a BWA mapping quality threshold of 5. Fragments that were duplicated were further collapsed (only counting a single copy of a read pair if a number of pairs with the same coordinates was sequenced). Chastity failed reads were also removed and only reads that were properly paired were considered. Post-processing was performed using the 'pysam' application for python (https://github.com/pysam-developers/pysam, Sept 2019). The alignment statistics were calculated using the 'sambamba' tool v 0.5.5 5 [409].

cDNA fragment length distributions and genome-wide distributions of read coverage were considered in order to ensure that these characteristics were similar for the pairs of data sets in the differential gene expression (DE) analysis. Genome wide pair-ended fragment coverage profiles for both strands were generated as well as read counts for every gene for further DE analysis.

The reads-per-kilobase-per-million (RPKM) values were calculated for every gene, and DE analysis was performed using the DEfine algorithm (M. Bilenky et al., unpublished). First, the chi2 p-value was estimated for every gene under the null hypothesis that the gene is not differentially expressed between two data sets. The Benjamini-Hochberg FDR-control procedure was applied (FDR=0.05) to find a *p*-value threshold. To further reduce noise, only genes with the fold-change (FC) between RPKM values FC>1.3, and required minimal number of aligned reads >5 per gene were considered. Only reads aligned to the proper strand were considered in the DE analysis.

In addition to the standard DE analysis, where gene expression quantification was done by counting reads falling into the gene boundaries, a model independent approach was considered by calculating read counts in every 175bp long bin genome wide (for both strands). A DE analysis between bins (with the same approach used for genes, see above) was performed. After defining the DE bins, their locations were overlapped with gene coordinates to determine DE genes. This second approach also provided a list of potential DE expressed intergenic regions.

Quantitative real time PCR (qRT-PCR) validation of DE transcripts

Total RNA was prepared from single colony isolates of each strain grown to mid log phase in 50ml of liquid yeast extract- peptone- dextrose (YPD) media using a phenol freeze based approach as previously described [407]. The extracted RNA was subsequently treated with RNase-free DNase I (Thermo Fisher Scientific) and cDNA was prepared using a High- capacity cDNA reverse transcription kit (Applied Biosystems). Quantitative real time PCR was performed using the Maxima SYBR Green qPCR Master Mix (Thermo Scientific) and the forward and reverse primers listed in appendix Table 20. In the qRT-PCR experiments presented in Figure 28 experimental gene Ct values were normalized to the mean Ct values of two housekeeping gene normalizers; *TCM1* and *GPD1*. In the qRT-PCR experiments presented in Figure 30 D experimental gene Ct values were normalized to the Ct values of *GPD1* only.

Ontology analysis of DE genes

Ontologies associated with differentially expressed genes or genetic interactions were identified using the web based FunSpec bioinformatics tool (http://funspec.med.utoronto.ca/, Dec 2018). The analysis was performed on genes displaying a fold change of 1.3 and up, using a *p*-value cut-off score of 0.001, and with Bonferroni-correction.

Averaged gene read maps

Universal gene coverage profiles were generated as follows. First cDNA fragment coverage profiles genome wide for both strands were created using all aligned read-pairs. Next, profiles for individual genes were selected, scaled to 100 units, and normalized by the total gene coverage. Subsequently all scaled and normalized gene coverage profiles were agglomerated together. When doing this, the profiles for genes on the negative strand were inverted (in other words the agglomeration was always on profiles from the 5’ to 3’ of a gene).

Spotting assays

The URA3 reporter expression spotting assays were performed in three biological replicates as follows. Freshly grown single colony isolates of each strain were grown in liquid YPD media to mid-log phase. Cells were subsequently collected, re-suspended in sterile water, and normalized to an OD_{600}=1 (approximately $3x10^7$ cells/mL). The normalized cell suspensions were subjected to 10-fold serial dilutions and 4µL of each dilution was spotted onto synthetic defined (SD) complete media and SD media without uracil. Plates were incubated at 30°C and growth was analyzed after 48 hours.

Northern Blots

Single colony isolates of each strain were grown to mid log phase in 50ml of liquid yeast extract- peptone- dextrose (YPD) media. Samples were then pelleted and washed once with sterile water before being flash frozen in liquid nitrogen and stored for 16 hours at -80°C. Samples were thawed on ice, and RNA was extracted using a phenol freeze based approach as previously described[407]. The extracted RNA was subsequently treated with RNase- free DNase I (Thermo Fisher Scientific).

Gel electrophoresis was performed as described in[410]. In brief, aliquots containing 10µg of total RNA were run on a 1% agarose gel containing 0.6M formaldehyde and 40mM morpholinepropanesulfonic acid (MOPS) acetate buffer. The gel was washed three times in distilled water to remove formaldehyde and was subsequently transferred to a positively charged nylon membrane (Roche). Membranes were hybridized with alpha [^{32}P]-dCTP labelled double-stranded oligonucleotide probes specific to *NTS1*, *NTS2*, and *ADE2*. Probes were generated from random primed (800bp) fragments of DNA as previously described[411] (primer sequences used to generate probes are listed in appendix Table 20). Membranes were visualized using a Storm 820 PhosphorImager and its associated ImageQuant Software (GE LifeSciences).

Chapter 4
Fpr4 contributes to genomic stability at ribosomal DNA

This chapter was adapted in part from the publication:

Savic, N., Shortill, S. P., Bilenky, M., Dobbs, J. M., Dilworth, D., Hirst, M., Nelson, C.J. Histone Chaperone Paralogs Have Redundant, Cooperative, and Divergent Functions in Yeast. *Genetics*. **213(4),** 1301-1316 (2019).

Contributions pertaining to data presented in this chapter: Experiments and data analysis were performed by NS under the supervision of CJN. Sequencing was carried out under the supervision of MH at the Michael Smith Genome Sciences Center. MB and DD preformed bioinformatic processing of the sequencing results. JD generated yeast strains under the supervision of NS

4.1 Introduction

Repetitive DNA, such as that found at the ribosomal DNA (rDNA) tandem repeats, is highly sensitive to recombination and excision events which disrupt genomic integrity and contribute to replicative cell aging. To minimize these deleterious events, non-transcribed rDNA spacers (*NTS*) and approximately 50% of rDNA repeats are maintained in a heterochromatin-like chromatin environment that is refractive to recombination and transcriptionally silent[309,412]. The rDNA is a classic example of epigenetic gene regulation because the chromatin state (active or silenced) of a given rDNA gene switches stochastically[317,318]. Consequently, enzymes that build or modify rDNA chromatin, such as the Sir2 histone deacetylase, are required for rDNA silencing[323,413] and stability at this locus[312,414,415]. At the onset of this dissertation Fpr3 and Fpr4 were known to be enriched at rDNA[279–281,302]. Their impact on rDNA stability, however, had never been explored.

In Chapter 3 I presented data which revealed that Fpr3 and Fpr4 are required to silence transcription of a reporter gene inserted at the *NTS1* locus of rDNA. Given that Fpr3 and Fpr4 have chromatin building[283,284] and modifying functions[223], I hypothesized that these enzymes silenced transcription from *NTS* regions through a mechanism that involved chromatin structure. Thus, yeast lacking these enzymes should also exhibit genomic instability at rDNA. To test this hypothesis, I employed a series of rDNA reporter-based assays with strategic mutants of Fpr3 and Fpr4.

In this chapter I present preliminary data which reveals that Fpr4 largely contributes to genomic stability at rDNA. I show that mutants of *Δfpr4* exhibit increased frequencies of rDNA reporter loss upon propagation over several generations. I present additional observations that suggest that *Δfpr4* mutants are associated with permanent genomic rearrangements at rDNA. Finally, I show that a novel transcript associated with these rearrangements is a useful readout for the mechanistic dissection of how Fpr4 impacts rDNA chromatin. Taken together the data presented in this chapter implicate Fpr4 in contributing to genomic stability at rDNA.

4.2 Results

4.2.1 Fpr4 is required for stability of the rDNA locus

To determine the impact of Fpr3 and Fpr4 on genomic stability at rDNA, I introduced *Δfpr3*, *Δfpr4*, *Δfpr3Δfpr4* and *Δsir2* deletions into a strain with a reporter gene (*URA3*) integrated within *NTS1*^{400,406}. The Ura$^+$ status of each strain was first confirmed by growth in liquid media lacking uracil. Next, strains were propagated in liquid non-selective media (YPD, containing uracil) for two days to permit either stochastic switching of *URA3* to the silent heterochromatinized state or reporter loss (both phenotypically Ura$^-$) (Figure 34 A). Subsequently, Ura$^-$ cells were isolated on solid 5'FOA selective media and approximately 96 colonies were selected at random from these plates using a colony picking robot. The Ura$^-$ status of cells could arise two ways: either from epigenetic silencing of the reporter at *NTS1*, or from permanent reporter gene loss via recombination and genomic excision. To discriminate between these two events, I replica plated the isolates onto media lacking uracil, where growth would indicate that the Ura$^-$ phenotype was a consequence of reversible epigenetic silencing of the reporter. Isolates which failed to grow on media lacking uracil would thus indicate that the Ura$^-$ phenotype was due to a permanent reporter loss event (Figure 34 B). This approach allowed me to quantify the effect of Fpr3 and Fpr4 on the rates of rDNA reporter loss.

These propagation assays revealed that, as expected in wild type (WT) yeast, epigenetic switching at rDNA occurs more frequently than permanent gene loss. In this experiment, 76.6% of the WT Ura$^-$ isolates retained the reporter, based on their ability to switch back to a Ura$^+$ state and grow in the absence of uracil at the end of the propagation assay. This indicates that epigenetic reporter silencing facilitated growth on 5'FOA (Figure 35 A and B). Reciprocally, 23.3% of the Ura$^-$ isolates were unable to switch back to a Ura$^+$ state, implying permanent loss of the *URA3* gene from rDNA. This genotype was confirmed by PCR of the genomic DNA from select Ura$^-$ and Ura$^+$ WT isolates (Figure 35 C). By contrast, nearly all (98.5%) of *Δsir2* colonies

isolated on 5-FOA represented permanent loss of the reporter (Figure 35 A and B). This is expected because Sir2 is required to establish silent chromatin at *NTS1*[323,413]. This control validates the ability of this assay to discriminate between reporter silencing and loss.

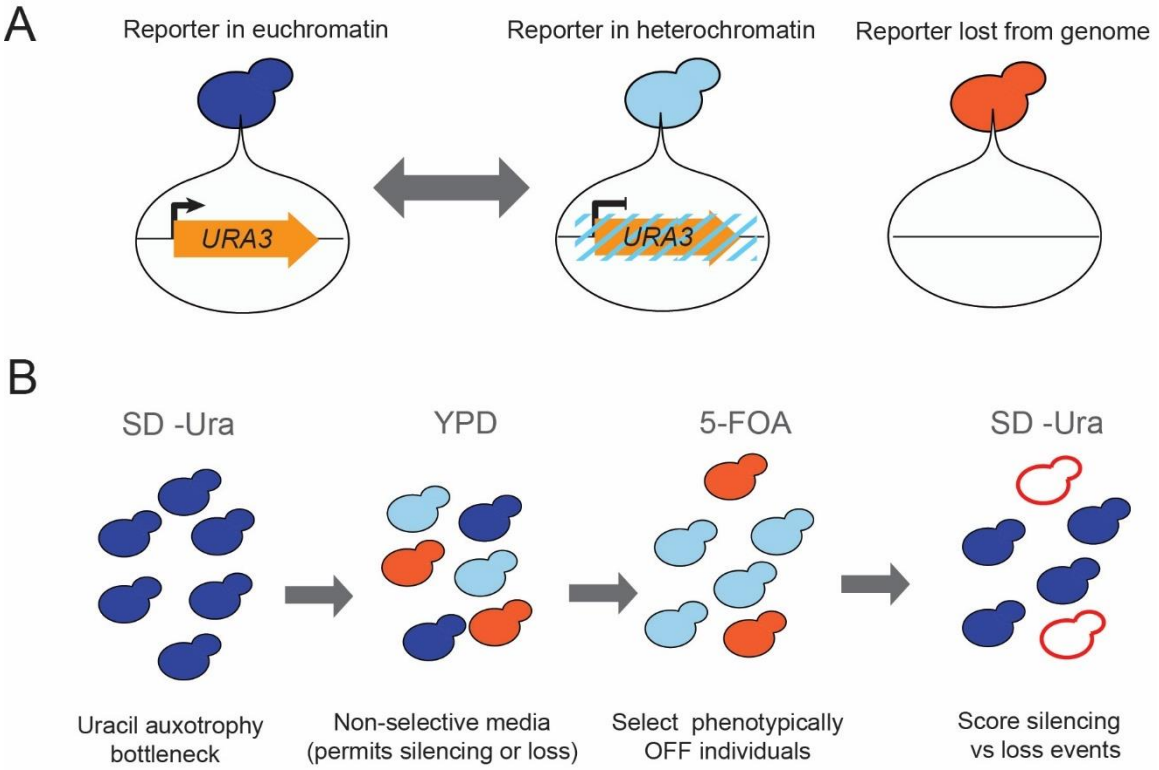

Figure 34. rDNA reporter loss assay workflow.
Schematic of propagation experiment carried out to assess the rate of *rDNA(NTS1)::URA3* reporter loss. (A) In a given population of cells, under non-selective conditions, the *rDNA(NTS1)::URA3* reporter may be in an accessible euchromatin environment and therefore expressed (dark blue cells), in an inaccessible heterochromatin-like environment and therefore silenced (light blue cells), or it may have been permanently lost from the genome via recombination between repeats (orange cells). The reporter may stochastically switch between the active euchromatin state and silenced heterochromatin-like state. (B) Individuals that lose the reporter due to instability can be distinguished from cells with a stochastically silenced reporter with the indicated workflow. The Ura^+ status of each cell is first confirmed via growth on synthetic defined (SD) media lacking uracil. Cells are then propagated under non-selective conditions to establish a mixed population with respect to the chromatin environment at the *URA3* reporter. Next, Ura^- members of this population are selected on 5'FOA media. These individuals are subsequently screened for *URA3* reporter silencing vs permanent reporter loss via growth or absence of growth on SD media lacking uracil.

In this assay *Δfpr3* single mutant yeast were phenotypically indistinguishable from WT yeast: I observed that 78.0% of Ura^- isolates retained the *URA3* reporter (Figure 35 A and B). This suggests that Fpr3 is not required for genomic stability at rDNA. However, *Δfpr4* single and *Δfpr3Δ fpr4* double deletion yeast behaved similarly to *Δsir2* strains: only 18.3% of *Δfpr4* and 27.6% of *Δfpr3Δfpr4* 5-FOA resistant isolates retained the *URA3* reporter gene (Figure 35 A and

B). Reporter loss from the genome was validated in Ura$^-$ isolates by genomic PCR (Figure 35 C). Thus, in yeast lacking Fpr4, reporter loss was more common than epigenetic silencing. This observation supports a model where Fpr4 is critical to maintaining genome stability at rDNA.

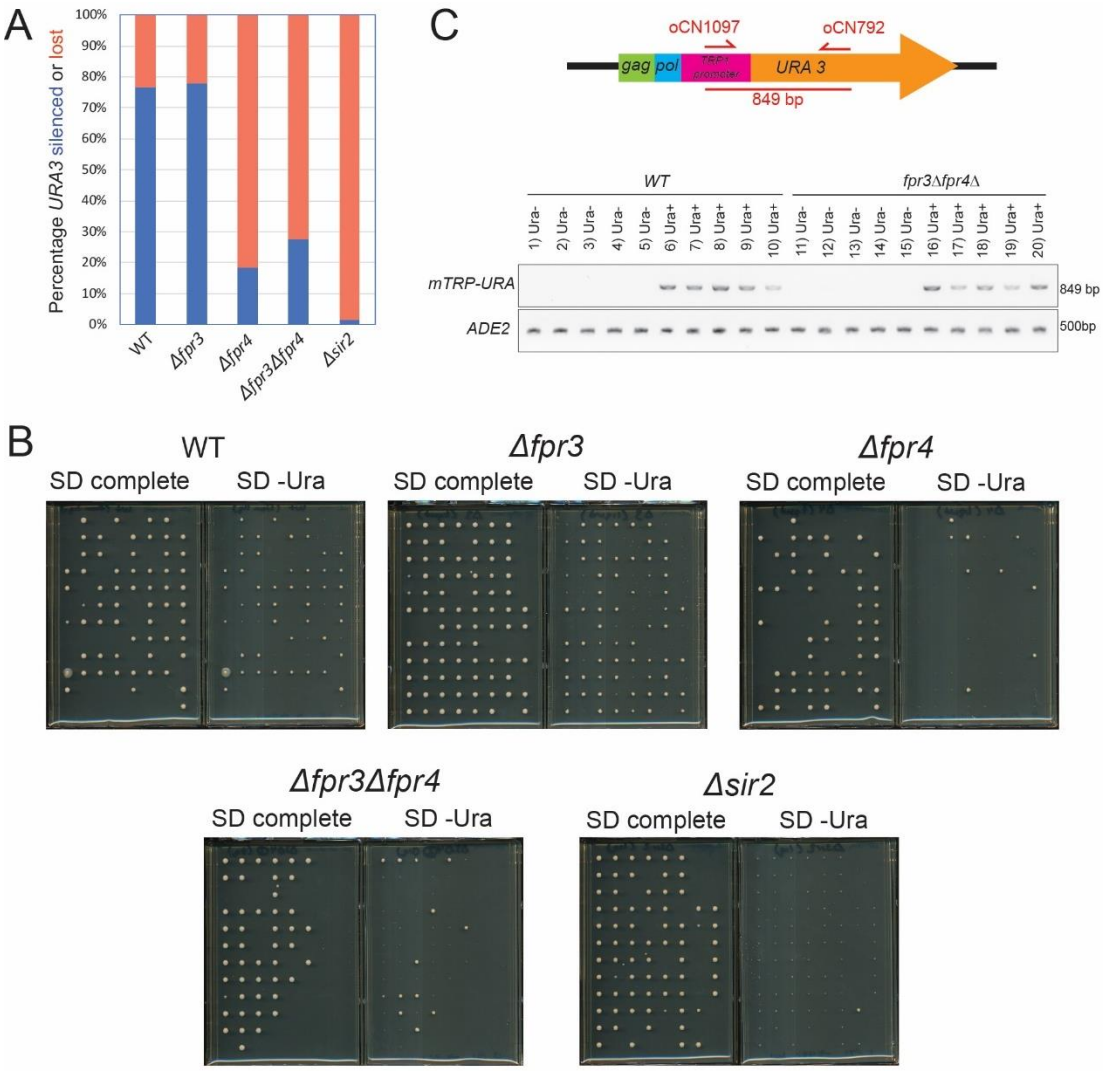

Figure 35. Fpr4 is required for genomic stability at rDNA.
(A) Percentage of total WT, *Δfpr3*, *Δfpr4*, *Δfpr3Δfpr4* and *Δsir2* colonies recovered after strain propagation that have retained or lost the ability to grow on SD media lacking uracil. Cells that have retained the ability (blue sections) indicate the *URA3* reporter gene had previously been silenced, cells that have lost the ability (orange sections) indicate the reporter has been permanently lost from the genome. (B) Images of the ~96 individual colonies recovered after strain propagation on control synthetic defined complete media (SD complete) and experimental SD media lacking uracil (SD-Ura). Colonies growing on the experimental media represent the fraction of the population in which the reporter was epigenetically silenced. Those that fail to grow indicate permanent loss of the reporter. (C) Diagram of the validation primer binding sites along the *rDNA(NTS1)::URA3* reporter. The forward primer oCN1097 binds within the minimal TRP1 promoter sequence upstream of the *URA3* transcription start site. The reverse primer oCN792 binds within the *URA3* open reading frame. The resulting PCR product is 849bp long (top). Images of the ethidium bromide stained PCR confirmation gels (bottom) indicating the presence or absence of the *URA3* reporter within the genomes in select Ura$^+$ and Ura$^-$ WT and *Δfpr3Δfpr4* individual colony isolates.

4.2.2 Fpr4 is required for the transcriptional fidelity of a reporter gene integrated in the *NTS* of rDNA

To further interrogate the effects of Fpr4 on transcription of the *NTS1* integrated *URA3* reporter, Northern blot analysis was performed on RNA extracted from reporter strains harboring *Δfpr4* deletions. In WT and *Δsir2* control strains, I detected the presence of the normal 0.8 kb *URA3* transcript (Figure 36 A). In *Δfpr4* yeasts; however, I detected the presence of an unusual aberrant *URA3* reporter transcript approximately 3.5 kb in length and a complete absence of the normal 0.8kb *URA3* transcript (Figure 36 A). Because these *Δfpr4* deletion mutants, were phenotypically Ura^+ (data not shown), the aberrant *URA3* transcript must be functional and generated from the coding strand.

The longer size of this transcript means that transcription of *URA3* is either initiating upstream of the normal start site, terminating downstream of the normal stop site, or both. In an effort to begin defining the boundaries of this longer transcript, I interrogated RNA-seq data from this, and a WT control (FPR4 expressing) strain. The *URA3* reporter gene is driven by a minimal *TRP1* promoter (*mTRP*) and was originally integrated within an rDNA *NTS1* spacer on a yeast transposable genetic element called a TY1 element[406,416] (Figure 36 B). Yeast TY1 elements contain several characteristic features: including two sets of long terminal repeats (LTRs) at each end and the *GAG* and *POL* genes[417]. They are found in hundreds of copies on the yeast genome[417]. To look for evidence of *URA3* transcripts that initiated upstream of the normal site, we aligned RNA-seq reads to a template contig of the rDNA *URA3* reporter. This revealed an increased number of reads corresponding to the junction between the *mTRP-URA3* reporter in the *Δfpr4* yeast (Figure 36 C). As shown in the figure, reads corresponding to the *mTRP* promoter were increased by 2 or 3-fold in *Δfpr4* yeast compared to WT yeast. This observation was confirmed by qPCR (Figure 36 D). Therefore, at least some of the aberrant transcript detected in *Δfpr4* deletion mutants contains RNA transcribed from the *mTRP* promoter. Additional interrogation of this RNA-seq read alignment revealed reads spanning the pol-mTRP junction. Thus, readthrough events must also be contributing to the larger *URA3* mRNA species detected in *Δfpr4* yeast

4.2.3 Aberrant transcription of the *NTS1 URA3* reporter can be used to dissect the Fpr4 mechanism of action

At least three functional features of the Fpr4 protein have been characterized in *in vitro* assays: the N-terminal NPL domain facilitates chromatin assembly[285,399], the acidic stretches within this domain mediate interactions with free histones[221], and basic patches within the C-terminal PPI domain interact with nucleosomal DNA[221]. However, the importance of each of

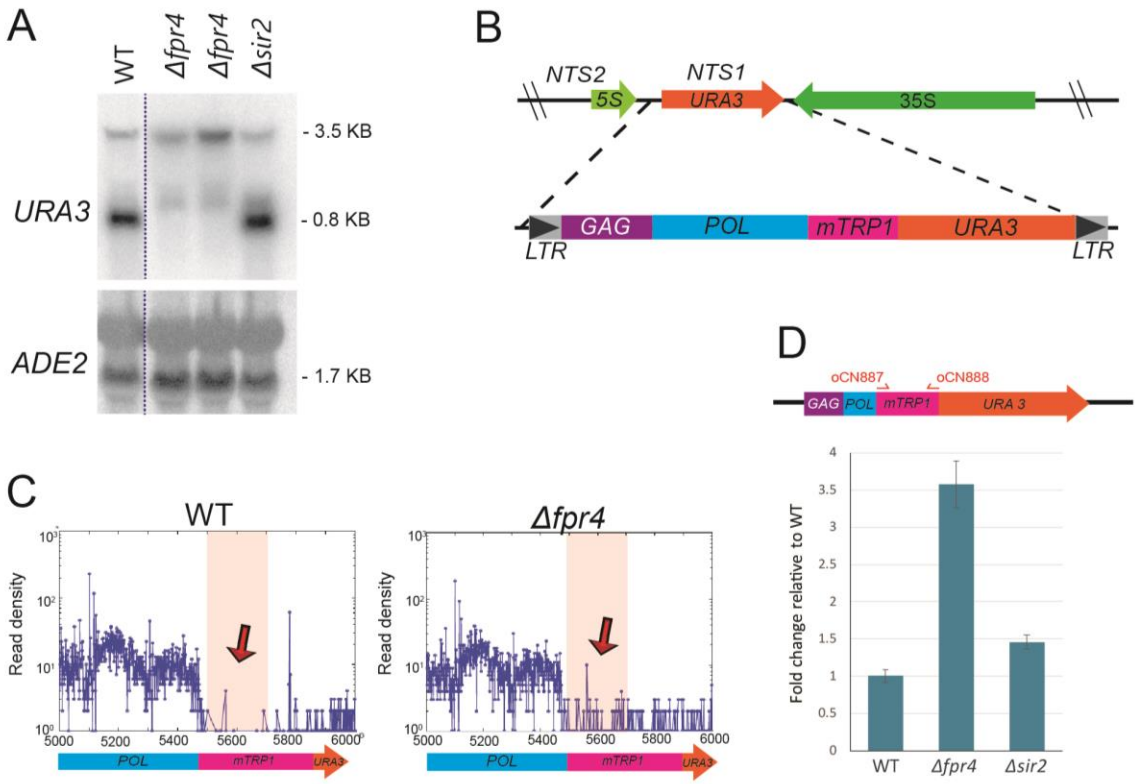

Figure 36. Fpr4 is required for transcriptional fidelity of a URA3 reporter integrated at *NTS1*
(A) Northern analysis of RNAs from *URA3* and the *ADE2* control gene in WT, *Δsir2*, and *Δfpr4* deletion mutants. Dashed lines indicate where images from the same membrane were spliced. The probes were 800bp fragments of DNA from each sequence and each lane contains 10µg of RNA. (B) Schematic of the minimal *mTRP* promoter driven *URA3* reporter integrated within rDNA *NTS1*. The reporter is flanked by TY1 transposable element features, including long terminal repeats (*LTR*s) and two open reading frames (*GAG* and *POL*). Features are not to scale. (C) Plots of read density across the *Pol-URA3* junction in WT and *Δfpr4* mutants. An increase of reads mapped to the *mTRP* promoter in *Δfpr4* mutants is indicated by the red arrows. Because the yeast genome encodes hundreds *POL* containing TY1 elements, reads corresponding to *POL* on the plot represent an amalgamation of *POL* transcripts from multiple genomic locations. (D) Diagram of the primer binding sites used for quantitative RT-PCR validation (top). Both forward (oCN 887) and reverse (oCN 888) primer bind within the *mTRP* promoter. Quantitative RT-PCR confirmation of increased transcription from the *mTRP* promoter in *Δfpr4* deletion mutants (bottom). Amplicons were normalized to the unchanged *GPD1* gene and fold changes in gene expression are shown relative to WT. Error bars indicate standard deviation of three technical replicates.

these features has never been tested *in vivo*. The discovery of a novel *URA3* mRNA in *Δfpr4* deletion mutants presented me with an opportunity to begin dissecting the importance of Fpr4's features. To this end, I asked if this RNA could be used as a readout to probe the importance of a given feature. I began by testing whether full length Fpr4 harboured on a plasmid could reduce the levels of the aberrant *mTRP-URA3* transcript using a diagnostic RT-PCR as a readout. I found that *Δfpr4* deletion mutants rescued with both untagged Fpr4 and C-terminal FLAG tagged Fpr4 on a vector exhibited a two-fold decrease in the levels of the transcript as detected by qPCR (Figure 37 A). While the magnitude of this restoration is only twofold, these results suggest that

this transcript might be a simple readout to probe the Fpr4 mechanism of action via rescue with strategic domain and point mutants of Fpr4.

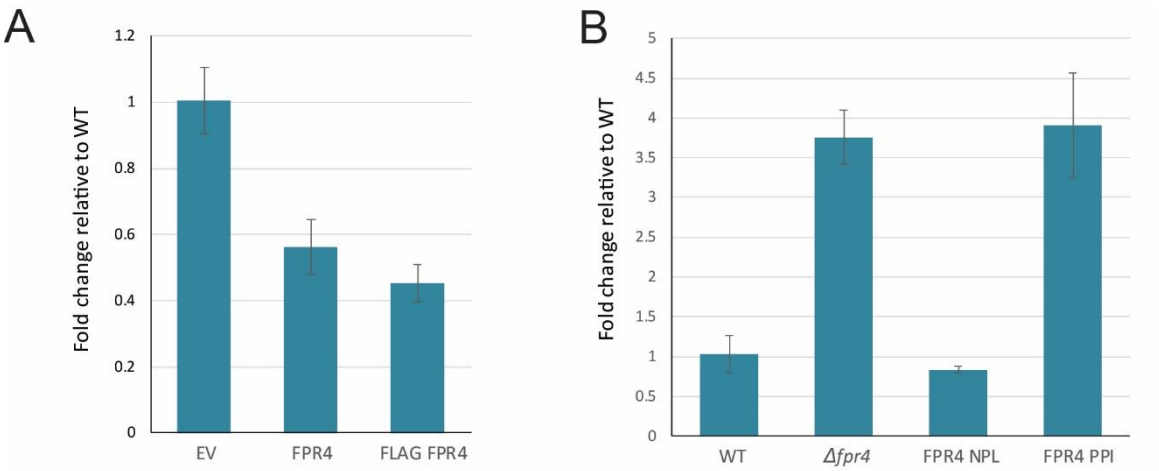

Figure 37. The aberrant *NTS1 URA3* reporter transcript can serve as a readout system for probing the mechanism of function of Fpr4.
(A) Quantitative RT-qPCR of the *mTRP* promoter in *rDNA(NTS1)::URA3 Δfpr4* mutants rescued with empty vector (EV), untagged FPR4 on a vector, and 3X C-terminal Flag tagged FPR4 on a vector. Amplicons were normalized to the unchanged *GPD1* gene and fold changes in gene expression are shown relative to WT. Error bars indicate standard deviation of three technical replicates. (B) Quantitative RT-qPCR of the *mTRP* promoter in *rDNA(NTS1)::URA3* background WT cells, *Δfpr4* deletion mutants, mutants possessing the FPR4 NPL domain only, and mutants possessing the FPR4 PPI domain only. Amplicons were normalized to the unchanged *GPD1* gene and fold changes in gene expression are shown relative to WT. Error bars indicate standard deviation of three technical replicates.

Next, I tested whether domain mutants of Fpr4 present endogenously on the genome (rather than on a vector) could also reduce the expression levels of this reporter transcript. I found that the Fpr4 NPL domain (amino acids 1-280) was sufficient to reduce expression of this transcript to WT levels (Figure 37 B). The Fpr4 PPI domain (amino acids 281-392) however, resulted in no reduction. These data suggest that the Fpr4 histone chaperone domain is necessary for Fpr4 regulation of transcription *in vivo*. One possibility is that this domain builds chromatin at the *mTRP* promoter resulting in an environment refractory to transcription.

4.3 Discussion

Enzymes that build and modify chromatin at rDNA affect genomic stability at this locus. To assess the impact of Fpr3 and Fpr4 on genomic stability at rDNA I performed a series of experiments based on a reporter gene integrated within the *NTS1* locus. I found that Fpr4 prevents the permanent loss of this reporter from the genome during multi-generational propagation. I also uncovered an unusual phenotype which may be the consequence of instability at this locus in

Δfpr4 deletion mutants generated by cross. Finally, I discovered that this phenotype could be used as a readout system to probe the mechanism of action of Fpr4 and presented preliminary evidence which implicates the NPL domain in its role in transcriptional regulation. Collectively the data presented in this chapter implicate Fpr4 in genomic stability at rDNA.

In Chapter 3 I presented observations which suggested that Fpr3 and Fpr4 function to build chromatin at the *NTS* of rDNA, protecting these loci from spurious transcription. The preliminary data presented in this chapter implicates Fpr4 (but not Fpr3) in additionally regulating the genomic stability at this locus. In support of this, I find that genes encoding proteins associated with replicative cell aging (such as *FOB1* which encodes for the rDNA replication fork block) have synthetic sick or lethal genetic interactions with *FPR4* uniquely. I propose a model where both Fpr3 and Fpr4 build chromatin at the *NTS* loci of rDNA but where Fpr4 alone also builds chromatin at heterochromatinized *RDN37* and *RDN5* coding regions. Because these coding regions are larger in size than the non-transcribed spacers (~7000bp vs ~2000bp respectively), recombination events which result in the excision of ERCs and genomic instability are more likely to occur at these Fpr4 only regulated loci than at the Fpr3/Fpr4 regulated *NTS*. This model would explain why phenotypes associated with genomic instability and cell aging occur primarily *Δfpr4* deletion mutants while transcription from *NTS* is perturbed in both *Δfpr3* and *Δfpr4* cells. Precisely how these chaperones regulate chromatin at these loci and how this chromatin differs from that at other genomic regions remains to be determined.

Additional data presented in this chapter further implicate Fpr4 in regulating stability at this locus and provide a novel readout system for further assessing its mechanism of action. Cross-derived *Δfpr4* deletion mutants are defective in normal transcription initiation of the *URA3* rDNA reporter. One possibility is that during the mating process required to generate these mutants, propagation in the absence of Fpr4 resulted in genomic instability and subsequent rearrangements at the *URA3* reporter locus. These rearrangements disrupted the normal transcription start site and generated a cryptic start site further upstream resulting in the functional but initiation aberrant *URA3* transcript. Rescue with plasmid borne Fpr4 does not eliminate this initiation aberrant transcription, indicating that it is the result of a permanent genomic change rather than an epigenetic alteration of the chromatin environment. Despite this, rescue with Fpr4 does reduce the levels of this transcript by two-fold. This phenotypic signature may make an effective readout system for probing the mechanism of action of Fpr4 *in vivo* via rescue with strategic domain and point mutants. A preliminary experiment using this readout system indicates that the Fpr4 histone chaperone domain is necessary for Fpr4 regulation of transcription from rDNA *in vivo* and opens

the door to future experiments which will dissect the roles of additional features of this domain in more detail.

4.4 Materials and Methods

Strains and Plasmids

Yeast strain genotypes are described in detail in appendix Table 19. Single gene deletion mutants of *Δfpr3*, *Δfpr4*, and *Δsir2* used for the propagation assays and genomic PCR validations are all isogenic to UCC1188 were constructed by replacing the endogenous WT locus with a Geneticin (G418) resistance PCR product deletion module[395,396]. The *Δfpr3Δfpr4* double deletion mutant is also isogenic to UCC1188 and was constructed from the *Δfpr4* single gene deletion mutant by replacing the endogenous *FPR3* locus with a nourseothricin resistance (*MX4-NATR*) PCR product deletion module[395,396].

Deletion mutants of *Δfpr4* used for the Northern analysis, RNA sequencing, and the validating qRT-PCR were generated from a cross of the MAT α UCC1188[406] with a MATa *Δfpr4* single gene deletion mutant in a BY4741 background purchased from open biosystems. Deletion mutants of *Δsir2* used for the Northern analysis, and the validating qRT-PCR were generated by lithium acetate transformation of UCC1188[406] with a Geneticin (G418) resistance PCR product deletion module[395,396].

Plasmid rescue mutants in Figure 37 A were constructed as follows. First the Geneticin (G418) resistance PCR product deletion module marker[395,396] in a cross-derived UCC1188 *Δfpr4* mutant (used in Figure 36) was replaced with a nourseothricin resistance (*MX4-NATR*) marker by transformation with linearized p4339[365]. The *TRP1* allele was then subsequently disrupted with a Geneticin (G418) resistance marker[395,396]. The resulting TRP^- mutants were transformed with prs414 (a single copy *TRP1* marked shuttle vector originally described in[418]), prs414 FPR4 (prs414 carrying an untagged full length copy of the *FPR4* open reading frame with endogenous promoter and terminator), and prs414 FLAG FPR4 (prs414 carrying an N-terminal 3X FLAG tagged full length copy of the *FPR4* open reading frame with endogenous promoter and terminator).

The FPR4 NPM domain mutant in Figure 37 B encodes a truncated FPR4 NPM domain (a.a. 1 – a.a. 280 followed by a C-terminal 3X FLAG tag) and was constructed by transformation of UCC1188 with a PCR product deletion module designed to incorporate a C-terminal 3X FLAG tag after amino acid 280 at the endogenous *FPR4* locus. The FPR4 PPI domain mutant encodes a truncated FPR4 PPI domain (a.a. 281 – a.a. 392 followed by a C-terminal 3X FLAG tag) and was constructed by transformation of a cross derived UCC1188 *Δfpr4* deletion mutant (used in Figure

36) with a PCR product deletion module containing FPR4 a.a. 281-392 followed by a C-terminal 3X FLAG tag.

Propagation assays

The Ura^+ status of each reporter containing strain was first confirmed by growth on SD media lacking uracil. Saturated overnights were then prepared from single colony isolates of each confirmed strain in liquid YPD media. Cultures were prepared from the overnights in 50ml YPD media and grown at 30ºC to mid log phase. Cells were subsequently collected, washed once, resuspended in sterile deionized water, and normalized to an OD_{600}=0.5. Normalized cell suspensions were subsequently diluted 10-fold and 250µl of each dilution was plated on 25ml SD 5-FoA plates. Plates were incubated at 30ºC for 16 hours. A total of 96 well-isolated colonies were randomly picked from each 5-FoA plate using the Genetix QPix-2 colony picking robot and deposited onto non-selective solid YPD plates. Plates were incubated for 5 days at 30ºC. All 96 colonies on each YPD plate were then replica plated onto SD complete control media and SD media lacking uracil and incubated for 5 days at 30ºC before being imaged.

Genomic PCR validation

Genomic DNA was prepared from each strain as follows. Single colony isolates of each mutant were resuspended in 100µl of yeast lysis buffer (200mM LiOAc 1% SDS). Mixture was incubated at 70°C while shaking for 15 minutes. After incubation 300µL of cold 95% ethanol were added to each sample. Samples were pelleted and the supernatant was decanted. Pellets were subsequently resuspended in 100µl of 1X TE buffer.

Genomic PCR was performed using Q5 High-Fidelity DNA polymerase (New England Biolabs) according to kit instructions. 2µl of each genomic DNA preparation were used for each 50µl PCR reaction and primer sequences are listed in appendix Table 20. PCR product was electrophoresed on a 1% agarose gel.

Northern blots

Single colony isolates of each strain were grown to mid log phase in 50ml of liquid yeast extract- peptone- dextrose (YPD) media. Samples were then pelleted and washed once with sterile water before being flash frozen in liquid nitrogen and stored for 16 hours at -80°C. Samples were thawed on ice, and RNA was extracted using a phenol freeze based approach as previously described[407]. The extracted RNA was subsequently treated with RNase- free DNase I (Thermo Fisher Scientific).

Gel electrophoresis was performed as described in[410]. In brief, aliquots containing 10µg of total RNA were run on a 1% agarose gel containing 0.6M formaldehyde and 40mM

morpholinepropanesulfonic acid (MOPS) acetate buffer. The gel was washed three times in distilled water to remove formaldehyde and was subsequently transferred to a positively charged nylon membrane (Roche). Membranes were hybridized with alpha [^{32}P]-dCTP labelled double-stranded oligonucleotide probes specific to *URA3* and *ADE2*. Probes were generated from random primed (800bp) fragments of DNA as previously described[411] (primer sequences used to generate probes are listed in appendix Table 20). Membranes were visualized using a Storm 820 PhosphorImager and its associated ImageQuant Software (GE LifeSciences).

RNA-Seq Library Preparation and Sequencing

Single colony isolates of each strain were grown to mid-log phase in 50ml of liquid yeast extract- peptone- dextrose (YPD) media. Samples were then pelleted and washed once with sterile water before being flash frozen in liquid nitrogen and stored for 16 hours at -80°C. Samples were thawed on ice, and RNA was extracted using a phenol freeze based approach as previously described[407]. The extracted RNA was subsequently treated with RNase- free DNase I (Thermo Fisher Scientific).

RNA samples were processed and sequenced at the BC Cancer agency Michael Smith Genome Sciences Centre following standard operating protocols. RNA seq libraries were prepared as described in[419]. Briefly, RNA samples were analyzed on an Agilent Bioanalyzer as per manufacturer's instructions and poly(A)+ RNA was purified from 2–10 μg of total RNA using the MACS mRNA isolation kit (Miltenyi Biotec, Bergisch Gladbach, Germany). The Superscript II Double-Stranded cDNA Synthesis kit (Invitrogen) and 200 ng random hexamers (Invitrogen) were used to synthesize double-stranded cDNA from the purified poly(A)+ RNA. The double-stranded cDNA was subsequently purified using 2 volumes of Ampure XP beads and fragmented using Covaris E series shearing (20% duty cycle, Intensity 5, 55 s). Samples were treated with RNA spike-in controls and used for paired-end sequencing library preparation (Illumina). Libraries were sequenced on an Illumina MySeq platform with paired-end reads of 60bp.Paired-end tag (PET) fragment distribution was found to be ~200bp. Sequenced paired-end reads were aligned ‘de-novo’ to a custom reference construct template of the rDNA Ty1-mTRP1-*URA3* reporter using the BWA aligner [408] (version 0.6.1-r104-tpx). Approximately ~2% of the reads were aligned to the construct in each of 2 libraries. Read density profiles plot the number of reads vs position on Ty1-mTRP1-*URA3* and indicate the number and position of the most left aligned read from every read pair.

Quantitative real time PCR (qRT-PCR) of the mTRP transcripts

Total RNA was prepared from single colony isolates of each strain grown to mid log phase in 50ml of liquid yeast extract- peptone- dextrose (YPD) media using a phenol freeze based approach as previously described[407]. The extracted RNA was subsequently treated with RNase-free DNase I (Thermo Fisher Scientific) and cDNA was prepared using a High- capacity cDNA reverse transcription kit (Applied Biosystems). Quantitative real time PCR was performed using the Maxima SYBR Green qPCR Master Mix (Thermo Scientific) and the forward and reverse primers listed in Table 20. Experimental gene Ct values were normalized to Ct values of the unchanged *GPD1* housekeeping gene.

Chapter 5
Discussion and Future Directions

5.1 Summary of research objectives

Chromatin modifying enzymes such as histone chaperones and histone post-translational modifiers play an important role in nearly every DNA related process. However, the biological functions of *S. cerevisiae* NPL-FKBPs (particularly with respect to chromatin) are poorly resolved. In this dissertation I used several systems-level approaches to characterize the comparative biology of Fpr3 and Fpr4. The data presented in the preceding three chapters represent a significant advancement in our understanding of the processes that these enzymes carry out *in vivo*.

In Chapter 2 of my dissertation I presented data from a comprehensive systems level comparative genetic interaction study designed to identify the shared, separate, and redundant roles of Fpr3 and Fpr4. This work has revealed that these enzymes are not completely functionally equivalent to each other and have diverged in complex ways over the course of evolution. It has also uncovered an unexpected cooperative role for these enzymes in chromatin biology.

Further interrogation of the transcriptomes of *Δfpr3* and *Δfpr4* mutant yeast in Chapter 3 indicated that these enzymes affect the transcription of genes from both diverse protein coding loci across the genome and from rDNA (consistent with their localization both in the nucleolus and enrichment in the nucleus). Furthermore, the data provided in this chapter provides transcriptomic evidence that Fpr3 and Fpr4 cooperate to regulate genes involved in polyphosphate metabolism and ribosome biogenesis, and indicate that Fpr4 plays an important role at the 5' for ends of protein coding genes and the non-transcribed spacers of ribosomal DNA.

Finally, in Chapter 4 I revealed that Fpr4 contributes to genomic stability at the recombination sensitive rDNA, which provides additional indirect evidence that it may function to build a chromatin environment that is refractive to recombination at this locus. I also unexpectedly discovered a novel simple readout system for further assessing its mechanism of

action *in vivo* and provided additional evidence for the importance of the histone chaperone domain in its function.

5.2 Future Directions

5.2.1 Identifying the Fpr3 and Fpr4 mechanism of action

In vitro studies have implicated the NPL domain[285,399], acidic patches[221], and PPI domain[221] of Fpr4 in various biochemical functions; however, very little is known about how these functions impact the mechanism of action of Fpr4 *in vivo*. The research presented in my dissertation introduces several attractive readout systems which may be used to further interrogate the mechanism of action of these proteins *in vivo* through rescue with strategic mutants. The simplest readout assay, presented in Chapter 4 involves changes in the transcription levels of the aberrant rDNA *URA3* reporter gene. Screening *Δ*fpr4 deletion mutants in this reporter background rescued with various vector borne Fpr4 domain and point mutants using RT-qPCR for reduced levels of this transcript would be a quick and easy way to identify features of the protein (and therefore biochemical functions) associated with its mechanism of action *in vivo*. Other readout assays for interrogating this mechanism of action include using RT-qPCR to measure the expression of differentially expressed genes such as *PHO5* and *PHO84* in yeast rescued with domain and point deletion mutants of Fpr3 and Fpr4. The advantage of this second rescue system is that nucleosome positioning at the promoters of these phosphate metabolism regulators is well characterized[420] and could be used to further interrogate the role of Fpr3 and Fpr4 mutants on promoter chromatin topologies using micrococcal nuclease digestion analysis.

5.2.2 Understanding the impact of Fpr3 and Fpr4 on chromatin topologies *in vivo*

Transcriptomics data presented in Chapter 3 indicate that Fpr3 and Fpr4 affect the expression of a number of genes genome-wide, however whether Fpr3/Fpr4 regulate these genes through direct interactions with nucleosomes at their promoters/ within their coding regions or indirectly as a consequence of some secondary effect remains to be determined. Also unknown is how Fpr3/Fpr4 impact the chromatin topologies at their direct target loci. The differentially expressed transcripts in *Δfpr3/Δfpr4* could be used as focused targets in future chromatin immunoprecipitation assays with alternative crosslinkers to test wild type and domain and point mutant NPL-FKBP binding to differentially expressed loci. The fact that Fpr4 can bind nucleosomes *in vitro*[221] and the 5’ signature of incomplete elongation in *Δfpr4* yeast supports the

model that at least some differentially expressed transcripts in *Δfpr3/Δfpr4* mutants are the direct consequence of defective nucleosomal positioning at these loci. At rDNA the chromosomal instability phenotype in *Δfpr4* yeast together with the defects in transcription at *NTS* loci are consistent with a direct effect on chromatin. Once the direct targets of Fpr3/Fpr4 have been identified, subsequent micrococcal nuclease digestion analysis in yeast rescued with domain and point deletion mutants of Fpr3 and Fpr4 may be used to analyze which of the features of these enzymes are necessary for their activities *in vivo* and how these activities impact their effect on chromatin.

5.2.3 Understanding the function of Fpr3 and Fpr4 polyphosphorylation

The identification of phosphate transport and polyphosphate metabolism genes as significantly upregulated in *Δfpr3* and *Δfpr4* deletion mutants is particularly intriguing given that these paralogs were recently found to be heavily polyphosphorylated together with other ribosome biogenesis factors[286]. The addition of this negatively charged post transactional modification to the already highly acidic histone chaperones would result in drastic changes to the overall protein charge and may play an important role in regulating their functions. Thus, the biological effect of Fpr3 and Fpr4 polyphosphorylation warrants further investigation. Given that the potential location(s) of the polyphosphorylation motifs in both of these enzymes are known[286], strategically designed domain and point mutants of these paralogs could be applied to the readout systems pioneered in this dissertation (see above) to interrogate the effect of this post-translational modification on the biological function and mechanism of action of these proteins.

5.2.4 Understanding the roles and functions of related proteins in mammals

My research has focused on understanding the biological functions of nucleoplasmin-like FKBP proteins in budding yeast. Because core features of these yeast paralogs are conserved in clinically relevant human proteins, the investigations presented in this dissertation performed in yeast may provide a basis for future studies of related mammalian proteins. The nucleoplasmin-like domains of yeast NPL-FKBPs share structural similarities to human NPM1 and NPM3, which are mutated in several bold and bone cancers. Thus, understanding the biological roles of this histone chaperone domain in yeast, may provide novel information to generate hypotheses about the functions of human NPM1 and NPM3 and how perturbations in these proteins drive

disease etiology. Likewise, the FKBP domains of yeast NPL-FKBPs are structurally similar to human nuclear FKBP25. Because the catalytic functions of these proteins are impaired by commonly used immunosuppressants, understanding the roles of this domain in yeast will provide a basis for understanding the roles and functional impact of immunosuppressant inhibition of its orthologue in humans.

Bibliography

1. Malik, H. S. & Henikoff, S. Phylogenomics of the nucleosome. *Nat. Struct. Biol.* **10**, 882–891 (2003).
2. Olins, A. L. & Olins, D. E. Spheroid chromatin units (v bodies). *Science* **183**, 330–2 (1974).
3. Kornberg, R. D. Chromatin structure: a repeating unit of histones and DNA. *Science* **184**, 868–71 (1974).
4. Richmond, T. J., Finch, J. T., Rushton, B., Rhodes, D. & Klug, A. Structure of the nucleosome core particle at 7 A resolution. *Nature* **311**, 532–7 (1984).
5. Luger, K., Mäder, A. W., Richmond, R. K., Sargent, D. F. & Richmond, T. J. Crystal structure of the nucleosome core particle at 2.8 A resolution. *Nature* **389**, 251–60 (1997).
6. Kornberg, R. D. & Thomas, J. O. Chromatin structure; oligomers of the histones. *Science* **184**, 865–8 (1974).
7. Collepardo-Guevara, R. & Schlick, T. Chromatin fiber polymorphism triggered by variations of DNA linker lengths. *Proc. Natl. Acad. Sci.* **111**, 8061–8066 (2014).
8. Wong, H., Victor, J.-M. & Mozziconacci, J. An All-Atom Model of the Chromatin Fiber Containing Linker Histones Reveals a Versatile Structure Tuned by the Nucleosomal Repeat Length. *PLoS One* **2**, e877 (2007).
9. Dixon, J. R. *et al.* Topological domains in mammalian genomes identified by analysis of chromatin interactions. *Nature* **485**, 376–380 (2012).
10. Rao, S. S. P. *et al.* A 3D map of the human genome at kilobase resolution reveals principles of chromatin looping. *Cell* **159**, 1665–1680 (2014).
11. Serizay, J. & Ahringer, J. Genome organization at different scales: nature, formation and function. *Curr. Opin. Cell Biol.* **52**, 145–153 (2018).
12. Cremer, T. *et al.* Rabl's model of the interphase chromosome arrangement tested in Chinise hamster cells by premature chromosome condensation and laser-UV-microbeam experiments. *Hum. Genet.* **60**, 46–56 (1982).
13. Fenley, A. T., Adams, D. A. & Onufriev, A. V. Charge state of the globular histone core controls stability of the nucleosome. *Biophys. J.* **99**, 1577–1585 (2010).
14. Zhou, K., Gaullier, G. & Luger, K. Nucleosome structure and dynamics are coming of age. *Nat. Struct. Mol. Biol.* **26**, 3–13 (2019).
15. Lai, W. K. M. & Pugh, B. F. Understanding nucleosome dynamics and their links to gene expression and DNA replication. *Nat. Rev. Mol. Cell Biol.* **18**, 548–562 (2017).
16. Li, G. & Widom, J. Nucleosomes facilitate their own invasion. *Nat. Struct. Mol. Biol.* **11**, 763–769 (2004).
17. Li, G., Levitus, M., Bustamante, C. & Widom, J. Rapid spontaneous accessibility of nucleosomal DNA. *Nat. Struct. Mol. Biol.* **12**, 46–53 (2005).
18. Eslami-Mossallam, B., Schram, R. D., Tompitak, M., Van Noort, J. & Schiessel, H. Multiplexing genetic and nucleosome positioning codes: A computational approach. *PLoS One* **11**, 1–14 (2016).
19. Kaplan, N. *et al.* The DNA-encoded nucleosome organization of a eukaryotic genome. *Nature* **458**, 362–366 (2009).

20. Lindseyt, G. G., Orgeig, S., Thompson, P., Davies, N. & Maeder, D. L. Extended C-terminal tail of wheat histone H2A interacts with DNA of the 'linker' region. *J. Mol. Biol.* **218**, 805–813 (1991).
21. Manohar, M. *et al.* Acetylation of histone H3 at the nucleosome dyad alters DNA-histone binding. *J. Biol. Chem.* **284**, 23312–23321 (2009).
22. Ottesen, J. J. *et al.* Histone fold modifications control nucleosome unwrapping and disassembly. *Proc. Natl. Acad. Sci.* **108**, 12711–12716 (2011).
23. Moore, L. D., Le, T. & Fan, G. DNA methylation and its basic function. *Neuropsychopharmacology* **38**, 23–38 (2013).
24. Hagerman, P. J. Pyrimidine 5-Methyl Groups Influence the Magnitude of DNA Curvature. *Biochemistry* **29**, 1980–1983 (1990).
25. Jimenez-Useche, I. *et al.* DNA methylation regulated nucleosome dynamics. *Sci. Rep.* **3**, 1–5 (2013).
26. Jimenez-Useche, I. & Yuan, C. The effect of DNA CpG methylation on the dynamic conformation of a nucleosome. *Biophys. J.* **103**, 2502–2512 (2012).
27. Jones, P. L. *et al.* Methylated DNA and MeCP2 recruit histone deacetylase to repress transcription. *Nat. Genet.* **19**, 187–91 (1998).
28. Srivastava, R., Singh, U. M. & Dubey, N. K. Histone Modifications by different histone modifiers. *J. Biol. Sci. Med.* **2**, 45–54 (2016).
29. Bannister, A. J. & Kouzarides, T. Regulation of chromatin by histone modifications. *Cell Res.* **21**, 381–95 (2011).
30. Pardal, A. J., Fernandes-Duarte, F. & Bowman, A. J. The histone chaperoning pathway: from ribosome to nucleosome. *Essays Biochem.* **63**, 29–43 (2019).
31. Burgess, R. J. & Zhang, Z. Histone chaperones in nucleosome assembly and human disease. *Nat Struct Mol Biol.* **20**, 14–22 (2014).
32. Paul, S. & Bartholomew, B. Regulation of ATP-dependent chromatin remodelers: accelerators/brakes, anchors and sensors. *Biochem. Soc. Trans.* **46**, 1423–1430 (2018).
33. Tyagi, M., Imam, N., Verma, K. & Patel, A. K. Chromatin remodelers: We are the drivers!! *Nucleus* **7**, 388–404 (2016).
34. Mersfelder, E. L. & Parthun, M. R. The tale beyond the tail: histone core domain modifications and the regulation of chromatin structure. *Nucleic Acids Res.* **34**, 2653–62 (2006).
35. Allfrey, V. G., Faulkner, R. & Mirsky, A. E. Acetylation and methylation of histones and their possible role in the regulation of RNA synthesis. *Proc. Natl. Acad. Sci. U. S. A.* **51**, 786–94 (1964).
36. Ord, M. & Stocken, L. Phosphate and thiol groups in histone f3 from rat liver and thymus nuclei. *Biochem. J.* **102**, 631–636 (1967).
37. Goldknopf, I. L. *et al.* Isolation and characterization of protein A24, a 'histone-like' non-histone chromosomal protein. *J. Biol. Chem.* **250**, 7182–7 (1975).
38. Shiio, Y. & Eisenman, R. N. Histone sumoylation is associated with transcriptional repression. *Proc. Natl. Acad. Sci.* **100**, 13225–13230 (2003).
39. Sakabe, K., Wang, Z. & Hart, G. W. β-N-acetylglucosamine (O-GlcNAc) is part of the histone code. *Proc. Natl. Acad. Sci.* **107**, 19915–19920 (2010).
40. Zou, C. *et al.* Acyl-CoA:lysophosphatidylcholine acyltransferase I (Lpcat1) catalyzes histone protein O-palmitoylation to regulate mRNA synthesis. *J. Biol.*

Chem. **286**, 28019–25 (2011).
41. Ye, J. *et al.* Histone H4 lysine 91 acetylation a core domain modification associated with chromatin assembly. *Mol. Cell* **18**, 123–30 (2005).
42. Neumann, H. *et al.* A method for genetically installing site-specific acetylation in recombinant histones defines the effects of H3 K56 acetylation. *Mol. Cell* **36**, 153–63 (2009).
43. Dhall, A. *et al.* Sumoylated human histone H4 prevents chromatin compaction by inhibiting long-range internucleosomal interactions. *J. Biol. Chem.* **289**, 33827–33837 (2014).
44. Wysocka, J. *et al.* A PHD finger of NURF couples histone H3 lysine 4 trimethylation with chromatin remodelling. *Nature* **442**, 86–90 (2006).
45. Hong, L., Schroth, G. P., Matthews, H. R., Yau, P. & Bradbury, E. M. Studies of the DNA binding properties of histone H4 amino terminus. Thermal denaturation studies reveal that acetylation markedly reduces the binding constant of the H4 'tail' to DNA. *J. Biol. Chem.* **268**, 305–314 (1993).
46. Kuo, M. H. *et al.* Transcription-linked acetylation by Gcn5p of histones H3 and H4 at specific lysines. *Nature* **383**, 269–72 (1996).
47. Imai, S., Armstrong, C. M., Kaeberlein, M. & Guarente, L. Transcriptional silencing and longevity protein Sir2 is an NAD-dependent histone deacetylase. *Nature* **403**, 795–800 (2000).
48. Wang, Y. *et al.* Human PAD4 regulates histone arginine methylation levels via demethylimination. *Science (80-.).* **306**, 279–283 (2004).
49. Cuthbert, G. L. *et al.* Histone deimination antagonizes arginine methylation. *Cell* **118**, 545–553 (2004).
50. Smith, B. C. & Denu, J. M. Chemical mechanisms of histone lysine and arginine modifications. *Biochim. Biophys. Acta - Gene Regul. Mech.* **1789**, 45–57 (2009).
51. Norton, V. G., Imai, B. S., Yau, P. & Bradbury, E. M. Histone acetylation reduces nucleosome core particle linking number change. *Cell* **57**, 449–457 (1989).
52. Nguyen, C. T. *et al.* Distinct localization of histone H3 acetylation and H3-K4 methylation to the transcription start sites in the human genome. *Proc. Natl. Acad. Sci.* **101**, 7357–7362 (2004).
53. Liu, C. L. *et al.* Single-nucleosome mapping of histone modifications in S. cerevisiae. *PLoS Biol.* **3**, e328 (2005).
54. Roh, T., Ngau, W. C., Cui, K., Landsman, D. & Zhao, K. High-resolution genome-wide mapping of histone modifications. *Nat. Biotechnol.* **22**, 1013–6 (2004).
55. Sealy, L. & Chalkley, R. DNA associated with hyperacetylated histone is preferentially digested by DNase I. *Nucleic Acids Res.* **5**, 1863–1876 (1978).
56. Vettese-Dadey, M. *et al.* Acetylation of histone H4 plays a primary role in enhancing transcription factor binding to nucleosomal DNA in vitro. *EMBO J.* **15**, 2508–2518 (1996).
57. Lee, D. Y., Hayes, J. J., Pruss, D. & Wolffe, A. P. A positive role for histone acetylation in transcription factor access to nucleosomal DNA. *Cell* **72**, 73–84 (1993).
58. Allis, C. D. *et al.* New nomenclature for chromatin-modifying enzymes. *Cell* **131**, 633–6 (2007).
59. Marmorstein, R. & Zhou, M.-M. Writers and readers of histone acetylation:

structure, mechanism, and inhibition. *Cold Spring Harb. Perspect. Biol.* **6**, 18762 (2014).
60. Eberharter, A. *et al.* The ADA complex is a distinct histone acetyltransferase complex in Saccharomyces cerevisiae. *Mol. Cell. Biol.* **19**, 6621–31 (1999).
61. Grant, P. A. *et al.* Yeast Gcn5 functions in two multisubunit complexes to acetylate nucleosomal histones: characterization of an Ada complex and the SAGA (Spt/Ada) complex. *Genes Dev.* **11**, 1640–50 (1997).
62. Lee, K. K. *et al.* Combinatorial depletion analysis to assemble the network architecture of the SAGA and ADA chromatin remodeling complexes. *Mol. Syst. Biol.* **7**, 1–12 (2011).
63. Syntichaki, P. & Thireos, G. The Gcn5·Ada complex potentiates the histone acetyltransferase activity of Gcn5. *J. Biol. Chem.* **273**, 24414–24419 (1998).
64. Kuo, M. H., Vom Baur, E., Struhl, K. & Allis, C. D. Gcn4 activator targets Gcn5 histone acetyltransferase to specific promoters independently of transcription. *Mol. Cell* **6**, 1309–1320 (2000).
65. Robert, F. *et al.* Global position and recruitment of HATs and HDACs in the yeast genome. *Mol. Cell* **16**, 199–209 (2004).
66. Rosaleny, L. E., Ruiz-García, A. B., García-Martínez, J., Pérez-Ortín, J. E. & Tordera, V. The Sas3p and Gcn5p histone acetyltransferases are recruited to similar genes. *Genome Biol.* **8**, 1–12 (2007).
67. Lee, T. I. *et al.* Redundant roles for the TFIID and SAGA complexes in global transcription. *Nature* **405**, 701–704 (2000).
68. Holstege, F. C. P. *et al.* Dissecting the regulatory circuitry of a eukaryotic genome. *Cell* **95**, 717–728 (1998).
69. Wu, J., Suka, N., Carlson, M. & Grunstein, M. TUP1 utilizes histone H3/H2B-specific HDA1 deacetylase to repress gene activity in yeast. *Mol. Cell* **7**, 117–126 (2001).
70. Robyr, D. *et al.* Microarray deacetylation maps determine genome-wide functions for yeast histone deacetylases. *Cell* **109**, 437–446 (2002).
71. Wang, A., Kurdistani, S. K. & Grunstein, M. Requirement of Hos2 histone deacetylase for gene activity in yeast. *Science* **298**, 1412–4 (2002).
72. Carmen, A. A. *et al.* Yeast HOS3 forms a novel trichostatin A-insensitive homodimer with intrinsic histone deacetylase activity. *Proc. Natl. Acad. Sci. U. S. A.* **96**, 12356–61 (1999).
73. Santos-Rosa, H. *et al.* Active genes are tri-methylated at K4 of histone H3. *Nature* **419**, 407–11 (2002).
74. Krogan, N. J. *et al.* COMPASS, a histone H3 (Lysine 4) methyltransferase required for telomeric silencing of gene expression. *J. Biol. Chem.* **277**, 10753–5 (2002).
75. Briggs, S. D. *et al.* Histone H3 lysine 4 methylation is mediated by Set1 and required for cell growth and rDNA silencing in Saccharomyces cerevisiae. *Genes Dev.* **15**, 3286–3295 (2001).
76. Miller, T. *et al.* COMPASS: a complex of proteins associated with a trithorax-related SET domain protein. *Proc. Natl. Acad. Sci. U. S. A.* **98**, 12902–7 (2001).
77. Krogan, N. J. *et al.* The Paf1 complex is required for histone H3 methylation by COMPASS and Dot1p: linking transcriptional elongation to histone methylation.

Mol. Cell **11**, 721–9 (2003).
78. Schneider, J. *et al.* Molecular regulation of histone H3 trimethylation by COMPASS and the regulation of gene expression. *Mol. Cell* **19**, 849–856 (2005).
79. Wood, A. *et al.* Ctk complex-mediated regulation of histone methylation by COMPASS. *Mol. Cell. Biol.* **27**, 709–720 (2007).
80. Soares, L. M. *et al.* Determinants of Histone H3K4 Methylation Patterns. *Mol. Cell* **68**, 773-785.e6 (2017).
81. Ramakrishnan, S. *et al.* Counteracting H3K4 methylation modulators Set1 and Jhd2 co-regulate chromatin dynamics and gene transcription. *Nat. Commun.* **7**, (2016).
82. Weiner, A. *et al.* Systematic dissection of roles for chromatin regulators in a yeast stress response. *PLoS Biol.* **10**, 17 (2012).
83. Hyun, K., Jeon, J., Park, K. & Kim, J. Writing, erasing and reading histone lysine methylations. *Exp. Mol. Med.* **49**, (2017).
84. Clapier, C. R., Iwasa, J., Cairns, B. R. & Peterson, C. L. Mechanisms of action and regulation of ATP-dependent chromatin-remodelling complexes. *Nat. Rev. Mol. Cell Biol.* **18**, 407–422 (2017).
85. Corona, D. F. V., Clapier, C. R., Becker, P. B. & Tamkun, J. W. Modulation of ISWI function by site-specific histone acetylation. *EMBO Rep.* **3**, 242–247 (2002).
86. Yang, X., Zaurin, R., Beato, M. & Peterson, C. L. Swi3p controls SWI/SNF assembly and ATP-dependent H2A-H2B displacement. *Nat. Struct. Mol. Biol.* **14**, 540–547 (2007).
87. Dechassa, M. L. *et al.* Architecture of the SWI/SNF-Nucleosome Complex. *Mol. Cell. Biol.* **28**, 6010–6021 (2008).
88. Zhang, Z. *et al.* Architecture of SWI/SNF chromatin remodeling complex. *Protein Cell* **9**, 1045–1049 (2018).
89. Awad, S. & Hassan, A. H. The Swi2/Snf2 bromodomain is important for the full binding and remodeling activity of the SWI/SNF complex on H3- and H4-acetylated nucleosomes. *Ann. N. Y. Acad. Sci.* **1138**, 366–75 (2008).
90. Zofall, M., Persinger, J., Kassabov, S. R. & Bartholomew, B. Chromatin remodeling by ISW2 and SWI/SNF requires DNA translocation inside the nucleosome. *Nat. Struct. Mol. Biol.* **13**, 339–346 (2006).
91. Kassabov, S. R., Zhang, B., Persinger, J. & Bartholomew, B. SWI/SNF unwraps, slides, and rewraps the nucleosome. *Mol. Cell* **11**, 391–403 (2003).
92. Dechassa, M. L. *et al.* SWI/SNF has intrinsic nucleosome disassembly activity that is dependent on adjacent nucleosomes. *Mol. Cell* **38**, 590–602 (2010).
93. Sudarsanam, P., Iyer, V. R., Brown, P. O. & Winston, F. Whole-genome expression analysis of Snf/Swi mutants of Saccharomyces cerevisiae. *Proc. Natl. Acad. Sci. U. S. A.* **97**, 3364–3369 (2000).
94. Roberts, S. M. & Winston, F. Essential functional interactions of SAGA, a Saccharomyces cerevisiae complex of Spt, Ada, and Gcn5 proteins, with the Snf/Swi and Srb/mediator complexes. *Genetics* **147**, 451–65 (1997).
95. Ryan, M. P., Jones, R. & Morse, R. H. SWI-SNF complex participation in transcriptional activation at a step subsequent to activator binding. *Mol. Cell. Biol.* **18**, 1774–82 (1998).
96. Wu, L. & Winston, F. Evidence that Snf-Swi controls chromatin structure over

both the TATA and UAS regions of the SUC2 promoter in Saccharomyces cerevisiae. *Nucleic Acids Res.* **25**, 4230–4234 (1997).
97. Rawal, Y. *et al.* SWI/SNF and RSC cooperate to reposition and evict promoter nucleosomes at highly expressed genes in yeast. *Genes Dev.* **32**, 695–710 (2018).
98. Zavari, M., Hörz, W., Schmid, A., Münsterkötter, M. & Gregory, P. D. Chromatin remodelling at the PHO8 promoter requires SWI–SNF and SAGA at a step subsequent to activator binding. *EMBO J.* **18**, 6407–6414 (2002).
99. Campos, E. I. *et al.* The program for processing newly synthesized histones H3.1 and H4. *Nat. Struct. Mol. Biol.* **17**, 1343–51 (2010).
100. Mosammaparast, N. A role for nucleosome assembly protein 1 in the nuclear transport of histones H2A and H2B. *EMBO J.* **21**, 6527–6538 (2002).
101. Cook, A. J. L., Gurard-Levin, Z. A., Vassias, I. & Almouzni, G. A Specific Function for the Histone Chaperone NASP to Fine-Tune a Reservoir of Soluble H3-H4 in the Histone Supply Chain. *Mol. Cell* **44**, 918–927 (2011).
102. Laskey, R. A., Honda, B. M., Mills, A. D. & Finch, J. T. Nucleosomes are assembled by an acidic protein which binds histones and transfers them to DNA. *Nature* **275**, 416–420 (1978).
103. Eirín-López, J. M., Frehlick, L. J. & Ausió, J. Long-term evolution and functional diversification in the members of the nucleophosmin/nucleoplasmin family of nuclear chaperones. *Genetics* **173**, 1835–50 (2006).
104. Cheung, C. T. *et al.* Double maternal-effect: Duplicated nucleoplasmin 2 genes, npm2a and npm2b, with essential but distinct functions are shared by fish and tetrapods. *BMC Evol. Biol.* **18**, 1–16 (2018).
105. Warren, W. C. *et al.* A New Chicken Genome Assembly Provides Insight into Avian Genome Structure. *G3 (Bethesda).* **7**, 109–117 (2017).
106. Payne, E. M. *et al.* Expression of the cytoplasmic NPM1 mutant (NPMc+) causes the expansion of hematopoietic cells in zebrafish. *Blood* **115**, 3329–3340 (2010).
107. Pontén, F. *et al.* A global view of protein expression in human cells, tissues, and organs. *Mol. Syst. Biol.* **5**, 1–9 (2009).
108. Uhlén, M. *et al.* Tissue-based map of the human proteome. *Science (80-.).* **347**, (2015).
109. Dutta, S. *et al.* The crystal structure of nucleoplasmin-core: Implications for histone binding and nucleosome assembly. *Mol. Cell* **8**, 841–853 (2001).
110. Franco, A. *et al.* Structural insights into the ability of nucleoplasmin to assemble and chaperone histone octamers for DNA deposition. *Sci. Rep.* **9**, 9487 (2019).
111. Frehlick, L. J., Eirín-López, J. M. & Ausió, J. New insights into the nucleophosmin/nucleoplasmin family of nuclear chaperones. *Bioessays* **29**, 49–59 (2007).
112. Namboodiri, V. M. H., Dutta, S., Akey, I. V., Head, J. F. & Akey, C. W. The crystal structure of Drosophila NLP-core provides insight into pentamer formation and histone binding. *Structure* **11**, 175–186 (2003).
113. Namboodiri, V. M. H., Akey, I. V, Schmidt-Zachmann, M. S., Head, J. F. & Akey, C. W. The structure and function of Xenopus NO38-core, a histone chaperone in the nucleolus. *Structure* **12**, 2149–60 (2004).
114. Lee, H. H. *et al.* Crystal structure of human nucleophosmin-core reveals plasticity of the pentamer-pentamer interface. *Proteins* **69**, 672–8 (2007).

115. Platonova, O., Akey, I. V, Head, J. F. & Akey, C. W. Crystal structure and function of human nucleoplasmin (Npm2): a histone chaperone in oocytes and embryos. *Biochemistry* **50**, 8078–89 (2011).
116. Murano, K., Okuwaki, M., Hisaoka, M. & Nagata, K. Transcription regulation of the rRNA gene by a multifunctional nucleolar protein, B23/nucleophosmin, through its histone chaperone activity. *Mol. Cell. Biol.* **28**, 3114–26 (2008).
117. Amin, M. A., Matsunaga, S., Uchiyama, S. & Fukui, K. Nucleophosmin is required for chromosome congression, proper mitotic spindle formation, and kinetochore-microtubule attachment in HeLa cells. *FEBS Lett.* **582**, 3839–3844 (2008).
118. Gurumurthy, M. *et al.* Nucleophosmin Interacts with HEXIM1 and Regulates RNA Polymerase II Transcription. *J. Mol. Biol.* **378**, 302–317 (2008).
119. Angelov, D. *et al.* Nucleolin is a histone chaperone with FACT-like activity and assists remodeling of nucleosomes. *EMBO J.* **25**, 1669–1679 (2006).
120. Kleinschmidt, J. A., Fortkamp, E., Krohne, G., Zentgraf, H. & Franke, W. W. Co-existence of two different types of soluble histone complexes in nuclei of Xenopus laevis oocytes. *J. Biol. Chem.* **260**, 1166–1176 (1985).
121. Li, Y. P., Busch, R. K., Valdez, B. C. & Busch, H. C23 interacts with B23, a putative nucleolar-localization-signal-binding protein. *Eur. J. Biochem.* **237**, 153–158 (1996).
122. Ginisty, H., Amalric, F. & Bouvet, P. Nucleolin functions in the first step of ribosomal RNA processing. *EMBO J.* **17**, 1476–1486 (1998).
123. Huang, N., Negi, S., Szebeni, A. & Olson, M. O. J. Protein NPM3 interacts with the multifunctional nucleolar protein B23/nucleophosmin and inhibits ribosome biogenesis. *J. Biol. Chem.* **280**, 5496–5502 (2005).
124. Lindström, M. S. & Zhang, Y. Ribosomal Protein S9 Is a Novel B23/NPM-binding Protein Required for Normal Cell Proliferation. *J. Biol. Chem.* **283**, 15568–15576 (2008).
125. Rocak, S. & Linder, P. Dead-box proteins: The driving forces behind RNA metabolism. *Nat. Rev. Mol. Cell Biol.* **5**, 232–241 (2004).
126. Yu, Y. *et al.* Nucleophosmin Is Essential for Ribosomal Protein L5 Nuclear Export. *Mol. Cell. Biol.* **26**, 3798–3809 (2006).
127. Savkur, R. S. & Olson, M. O. Preferential cleavage in pre-ribosomal RNA byprotein B23 endoribonuclease. *Nucleic Acids Res.* **26**, 4508–15 (1998).
128. Herrera, J. E., Savkur, R. & Olson, M. O. J. The ribonuclease activity of nucleolar protein B23. *Nucleic Acids Res.* **23**, 3974–3980 (1995).
129. Foltz, D. R. *et al.* The human CENP-A centromeric nucleosome-associated complex. *Nat. Cell Biol.* **8**, 458–469 (2006).
130. Zatsepina, O. V *et al.* The nucleolar phosphoprotein B23 redistributes in part to the spindle poles during mitosis. *J. Cell Sci.* **112**, 455–466 (1999).
131. Li, Z., Boone, D. & Hann, S. R. Nucleophosmin interacts directly with c-Myc and controls c-Myc-induced hyperproliferation and transformation. *Proc. Natl. Acad. Sci.* **105**, 18794–18799 (2008).
132. Zou, Y. *et al.* Nucleophosmin/B23 negatively regulates GCN5-dependent histone acetylation and transactivation. *J. Biol. Chem.* **283**, 5728–5737 (2008).
133. Federici, L. *et al.* Nucleophosmin C-terminal leukemia-associated domain interacts

with G-rich quadruplex forming DNA. *J. Biol. Chem.* **285**, 37138–37149 (2010).
134. Xu, Y. *et al.* The role of a single-stranded nucleotide loop in transcriptional regulation of the human sod2 gene. *J. Biol. Chem.* **282**, 15981–94 (2007).
135. Dhar, S. K., Lynn, B. C., Daosukho, C. & St Clair, D. K. Identification of nucleophosmin as an NF-kappaB co-activator for the induction of the human SOD2 gene. *J. Biol. Chem.* **279**, 28209–19 (2004).
136. Holmberg Olausson, K., Nistér, M. & Lindström, M. S. Loss of nucleolar histone chaperone NPM1 triggers rearrangement of heterochromatin and synergizes with a deficiency in DNA methyltransferase DNMT3A to drive ribosomal DNA transcription. *J. Biol. Chem.* **289**, 34601–34619 (2014).
137. Mills, A. D., Laskey, R. A., Black, P. & De Robertis, E. M. An acidic protein which assembles nucleosomes in vitro is the most abundant protein in Xenopus oocyte nuclei. *J. Mol. Biol.* **139**, 561–568 (1980).
138. Philpott, A., Leno, G. H. & Laskey, R. A. Sperm decondensation in Xenopus egg cytoplasm is mediated by nucleoplasmin. *Cell* **65**, 569–578 (1991).
139. Philpott, A. & Leno, G. H. Nucleoplasmin remodels sperm chromatin in Xenopus egg extracts. *Cell* **69**, 759–767 (1992).
140. Onikubo, T. *et al.* Developmentally regulated post-translational modification of nucleoplasmin controls histone sequestration and deposition. *Cell Rep.* **10**, 1735–1748 (2015).
141. Burns, K. H. *et al.* Roles of NPM2 in chromatin and nucleolar organization in oocytes and embryos. *Science* **300**, 633–6 (2003).
142. Emelyanov, A. V *et al.* Drosophila TAP/p32 is a core histone chaperone that cooperates with NAP-1, NLP, and nucleophosmin in sperm chromatin remodeling during fertilization. *Genes Dev.* **28**, 2027–40 (2014).
143. Ito, T., Tyler, J. K., Bulger, M., Kobayashi, R. & Kadonaga, J. T. ATP-facilitated chromatin assembly with a nucleoplasmin-like protein from Drosophila melanogaster. *J. Biol. Chem.* **271**, 25041–25048 (1996).
144. Falini, B. *et al.* Cytoplasmic nucleophosmin in acute myelogenous leukemia with a normal karyotype. *N. Engl. J. Med.* **352**, 254–66 (2005).
145. Verhaak, R. G. W. *et al.* Mutations in nucleophosmin (NPM1) in acute myeloid leukemia (AML): Association with other gene abnormalities and previously established gene expression signatures and their favorable prognostic significance. *Blood* **106**, 3747–3754 (2005).
146. Thiede, C. *et al.* Prevalence and prognostic impact of NPM1 mutations in 1485 adult patients with acute myeloid leukemia (AML). *Blood* **107**, 4011–20 (2006).
147. Den Besten, W., Kuo, M. L., Williams, R. T. & Sherr, C. J. Myeloid leukemia-associated nucleophosmin mutants perturb p53-dependent and independent activities of the Arf tumor suppressor protein. *Cell Cycle* **4**, 1591–1596 (2005).
148. Bertwistle, D., Sugimoto, M. & Sherr, C. J. Physical and functional interactions of the Arf tumor suppressor protein with nucleophosmin/B23. *Mol. Cell. Biol.* **24**, 985–96 (2004).
149. Falini, B. *et al.* Translocations and mutations involving the nucleophosmin (NPM1) gene in lymphomas and leukemias. *Haematologica* **92**, 519–32 (2007).
150. Werner, M. T., Zhao, C., Zhang, Q. & Wasik, M. A. Nucleophosmin-Anaplastic lymphoma kinase: The ultimate oncogene and therapeutic target. *Blood* **129**, 823–

831 (2017).
151. Morris, S. W. *et al.* Fusion of a kinase gene, ALK, to a nucleolar protein gene, NPM, in non-Hodgkin's lymphoma. *Science* **263**, 1281–4 (1994).
152. Fujimoto, J. *et al.* Characterization of the transforming activity of p80, a hyperphosphorylated protein in a Ki-1 lymphoma cell line with chromosomal translocation t(2;5). *Proc. Natl. Acad. Sci. U. S. A.* **93**, 4181–6 (1996).
153. Redner, R. L., Rush, E. A., Faas, S., Rudert, W. A. & Corey, S. J. The t(5;17) variant of acute promyelocytic leukemia expresses a nucleophosmin-retinoic acid receptor fusion. *Blood* **87**, 882–6 (1996).
154. Hallor, K. H. *et al.* Two genetic pathways, t(1;10) and amplification of 3p11-12, in myxoinflammatory fibroblastic sarcoma, haemosiderotic fibrolipomatous tumour, and morphologically similar lesions. *J. Pathol.* **217**, 716–27 (2009).
155. Pauling, L., Corey, R. B. & Branson, H. R. The structure of proteins: Two hydrogen-bonded helical configurations of the polypeptide chain. *Proc. Natl. Acad. Sci.* **37**, 205–211 (1951).
156. Ramachandran, G. N. & Sasisekharan, V. Conformation of polypeptides and proteins. *Adv. Protein Chem.* **23**, 283–438 (1968).
157. Stewart, D. E., Sarkar, a & Wampler, J. E. Occurrence and role of cis peptide bonds in protein structures. *J. Mol. Biol.* **214**, 253–60 (1990).
158. Zimmerman, S. S. & Scheraga, H. A. Stability of Cis, Trans, and Nonplanar Peptide Groups. *Macromolecules* **9**, 408–416 (1976).
159. Pal, D. & Chakrabarti, P. Cis peptide bonds in proteins: residues involved, their conformations, interactions and locations. *J. Mol. Biol.* **294**, 271–88 (1999).
160. MacArthur, M. W. & Thornton, J. M. Influence of proline residues on protein conformation. *J. Mol. Biol.* **218**, 397–412 (1991).
161. Steinberg, I. Z., Harrington, W. F., Berger, A., Sela, M. & Katchalski, E. The Configurational Changes of Poly-L-proline in Solution. *J. Am. Chem. Soc.* **82**, 5263–5279 (1960).
162. Grathwohl, C. & Wüthrich, K. Nmr studies of the rates of proline cis - trans isomerization in oligopeptides. *Biopolymers* **20**, 2623–2633 (1981).
163. Brandts, J. F., Brennan, M. & Lin, L. Unfolding and refolding occur much faster for a proline-free protein than for most proline-containing proteins. *Proc. Natl. Acad. Sci. U. S. A.* **74**, 4178–4181 (1977).
164. Levitt, M. Effect of proline residues on protein folding. *J. Mol. Biol.* **145**, 251–63 (1981).
165. Lang, K., Schmid, F. X. & Fischer, G. Catalysis of protein folding by prolyl isomerase. *Nature* **329**, 268–270 (1987).
166. Göthel, S. F. & Marahiel, M. A. Peptidyl-prolyl cis-trams isomerases, a superfamily of ubiquitous folding catalysts. *Cell. Mol. Life Sci.* **55**, 423–436 (1999).
167. Galat, A. Peptidylproline cis-trans-isomerases: immunophilins. *Eur. J. Biochem.* **216**, 689–707 (1993).
168. Arevalo-Rodriguez, M., Wu, X., Hanes, S. D. & Heitman, J. Prolyl Isomerases In Yeast. *J. Infect. Dis.* **209**, 2420–2446 (2004).
169. Wang, P. & Heitman, J. The cyclophilins. *Genome Biol.* **6**, (2005).
170. Tong, M. & Jiang, Y. FK506-Binding Proteins and Their Diverse Functions. *Curr.*

Mol. Pharmacol. **9**, 48–65 (2015).
171. Somarelli, J. A., Lee, S. Y., Skolnick, J. & Herrera, R. J. Structure-based classification of 45 FK506-binding proteins. *Proteins Struct. Funct. Genet.* **72**, 197–208 (2008).
172. Handschumacher, R. E., Harding, M. W., Rice, J., Drugge, R. J. & Speicher, D. W. Cyclophilin: a specific cytosolic binding protein for cyclosporin A. *Science* **226**, 544–7 (1984).
173. Harding, M. W., Galat, A., Uehling, D. E. & Schreiber, S. L. A receptor for the immunosuppressant FK506 is a cis-trans peptidyl-prolyl isomerase. *Nature* **341**, 758–60 (1989).
174. Siekierka, J. J., Hung, S. H. Y., Poe, M., C., L. S. & H, S. N. A cytosolic binding protein for the immunosuppressant FK506 has peptidyl-prolyl isomerase activity but is distinct from cyclophilin. *Nature* **341**, 755–757 (1989).
175. Rahfeld, J. U. *et al.* Confirmation of the existence of a third family among peptidyl-prolyl cis/trans isomerases Amino acid sequence and recombinant production of parvulin. *FEBS Lett.* **352**, 180–184 (1994).
176. Rahfeld, J. U., Schierhorn, A., Mann, K. & Fischer, G. A novel peptidyl-prolyl cisltrans isomerase from Escherichia coli. *FEBS Lett.* **343**, 65–69 (1994).
177. Pemberton, T. J. & Kay, J. E. Identification and Comparative Analysis of the Peptidyl-Prolyl cis/trans Isomerase Repertoires of H. sapiens, D. melanogaster, C. elegans, S. cerevisiae and Sz. pombe. *Comp. Funct. Genomics* **6**, 277–300 (2005).
178. Pemberton, T. J. Identification and comparative analysis of sixteen fungal peptidyl-prolyl cis/trans isomerase repertoires. *BMC Genomics* **7**, 244 (2006).
179. Gollan, P. J., Bhave, M. & Aro, E.-M. The FKBP families of higher plants: Exploring the structures and functions of protein interaction specialists. *FEBS Lett.* **586**, 3539–47 (2012).
180. Ke, H., Mayrose, D. & Cao, W. Crystal structure of cyclophilin A complexed with substrate Ala-Pro suggests a solvent-assisted mechanism of cis-trans isomerization. *Proc. Natl. Acad. Sci. U. S. A.* **90**, 3324–3328 (1993).
181. Kallen, J. *et al.* Structure of human cyclophilin and its binding site for cyclosporin A determined by X-ray crystallography and NMR spectroscopy. *Nature* **353**, 276–9 (1991).
182. Dornan, J., Taylor, P. & Walkinshaw, M. D. Structures of immunophilins and their ligand complexes. *Curr. Top. Med. Chem.* **3**, 1392–409 (2003).
183. Gemmecker, G. *et al.* Solution structure of Escherichia coli Par10: The prototypic member of the Parvulin family of peptidyl-prolyl cis/trans isomerases. *Protein Sci.* **13**, 2378–2387 (2004).
184. Wilson, K. P. *et al.* Comparative X-ray structures of the major binding protein for the immunosuppressant FK506 (tacrolimus) in unliganded form and in complex with FK506 and rapamycin. *Acta Crystallogr. D. Biol. Crystallogr.* **51**, 511–21 (1995).
185. Van Duyne, G. D., Standaert, R. F., Karplus, P. A., Schreiber, S. L. & Clardy, J. Atomic structure of FKBP-FK506, an immunophilin-immunosuppressant complex. *Science* **252**, 839–42 (1991).
186. Szep, S., Park, S., Boder, E. T., Van Duyne, G. D. & Saven, J. G. Structural coupling between FKBP12 and buried water. *Proteins* **74**, 603–11 (2009).

187. Singh, K., Winter, M., Zouhar, M. & Ryšánek, P. Cyclophilins: Less studied proteins with critical roles in pathogenesis. *Phytopathology* **108**, 6–14 (2018).
188. Kumari, S., Roy, S., Singh, P., Singla-Pareek, S. L. & Pareek, A. Cyclophilins: Proteins in search of function. *Plant Signal. Behav.* **8**, 25–32 (2013).
189. Matena, A., Rehic, E., Hönig, D., Kamba, B. & Bayer, P. Structure and function of the human parvulins Pin1 and Par14/17. *Biol. Chem.* **399**, 101–125 (2018).
190. Cheng, C. W. & Tse, E. PIN1 in cell cycle control and cancer. *Front. Pharmacol.* **9**, 1–10 (2018).
191. Dunyak, B. M. & Gestwicki, J. E. Peptidyl-Proline Isomerases (PPIases): Targets for Natural Products and Natural Product-Inspired Compounds. *J. Med. Chem.* **59**, 9622–9644 (2016).
192. Van Duyne, G. D., Standaert, R. F., Karplus, P. A., Schreiber, S. L. & Clardy, J. Atomic structures of the human immunophilin FKBP-12 complexes with FK506 and rapamycin. *J. Mol. Biol.* **229**, 105–24 (1993).
193. Xu, G. G., Zhang, Y., Mercedes-Camacho, A. Y. & Etzkorn, F. A. A reduced-amide inhibitor of Pin1 binds in a conformation resembling a twisted-amide transition state. *Biochemistry* **50**, 9545–50 (2011).
194. Ladani, S. T., Souffrant, M. G., Barman, A. & Hamelberg, D. Computational perspective and evaluation of plausible catalytic mechanisms of peptidyl-prolyl cis-trans isomerases. *Biochim. Biophys. Acta* **1850**, 1994–2004 (2015).
195. Fischer, S., Michnick, S. & Karplus, M. A mechanism for rotamase catalysis by the FK506 binding protein (FKBP). *Biochemistry* **32**, 13830–7 (1993).
196. Orozco, M., Tirado-Rives, J. & Jorgensen, W. L. Mechanism for the Rotamase Activity of FK506 Binding Protein from Molecular Dynamics Simulations. *Biochemistry* **32**, 12864–12874 (1993).
197. Kallen, J. & Walkinshaw, M. D. The X-ray structure of a tetrapeptide bound to the active site of human cyclophilin A. *FEBS Lett.* **300**, 286–90 (1992).
198. Quistgaard, E. M. *et al.* Molecular insights into substrate recognition and catalytic mechanism of the chaperone and FKBP peptidyl-prolyl isomerase SlyD. *BMC Biol.* **14**, 1–25 (2016).
199. Fraser, J. S. *et al.* Hidden alternative structures of proline isomerase essential for catalysis. *Nature* **462**, 669–73 (2009).
200. Bayer, E. *et al.* Structural analysis of the mitotic regulator hPin1 in solution: insights into domain architecture and substrate binding. *J. Biol. Chem.* **278**, 26183–93 (2003).
201. Fulton, K. F., Jackson, S. E. & Buckle, A. M. Energetic and structural analysis of the role of tryptophan 59 in FKBP12. *Biochemistry* **42**, 2364–2372 (2003).
202. Tonthat, N. K. *et al.* Structures of Pathogenic Fungal FKBP12s Reveal Possible Self-Catalysis Function. *MBio* **7**, 1–11 (2016).
203. Kino, T. *et al.* FK-506, a novel immunosuppressant isolated from a Streptomyces. II. Immunosuppressive effect of FK-506 in vitro. *J. Antibiot. (Tokyo).* **40**, 1256–65 (1987).
204. Kino, T. *et al.* FK-506, a novel immunosuppressant isolated from a Streptomyces. I. Fermentation, isolation, and physico-chemical and biological characteristics. *J. Antibiot. (Tokyo).* **40**, 1249–55 (1987).
205. Borel, J. F., Feurer, C., Gubler, H. U. & Stähelin, H. Biological effects of

cyclosporin A: a new antilymphocytic agent. *Agents Actions* **6**, 468–75 (1976).
206. Liu, J. *et al.* Calcineurin is a common target of cyclophilin-cyclosporin A and FKBP-FK506 complexes. *Cell* **66**, 807–815 (1991).
207. Clipstone NA & Crabtree GR. Identification of calcineurin as a key signalling enzyme in T lymphocyte activation. *Nature* **356**, 695–697 (1992).
208. Tocci, M. J. *et al.* The immunosuppressant FK506 selectively inhibits expression of early T cell activation genes. *J. Immunol.* **143**, 718–726 (1989).
209. Luo, C. *et al.* Recombinant NFAT1 (NFATp) is regulated by calcineurin in T cells and mediates transcription of several cytokine genes. *Mol. Cell. Biol.* **16**, 3955–3966 (1996).
210. Hogan, P. G. Calcium-NFAT transcriptional signalling in T cell activation and T cell exhaustion. *Cell Calcium* **63**, 66–69 (2017).
211. Bierer, B. E. *et al.* Two distinct signal transmission pathways in T lymphocytes are inhibited by complexes formed between an immunophilin and either FK506 or rapamycin. *Proc. Natl. Acad. Sci. U. S. A.* **87**, 9231–5 (1990).
212. Chiu, M. I., Katz, H. & Berlin, V. RAPT1, a mammalian homolog of yeast Tor, interacts with the FKBP12/rapamycin complex. *Proc. Natl. Acad. Sci. U. S. A.* **91**, 12574–8 (1994).
213. Brown, E. J. *et al.* A mammalian protein targeted by G1-arresting rapamycin-receptor complex. *Nature* **369**, 756–758 (1994).
214. Weichhart, T., Hengstschläger, M. & Linke, M. Regulation of innate immune cell function by mTOR. *Nat. Rev. Immunol.* **15**, 599–614 (2015).
215. Schlünzen, F. *et al.* The binding mode of the trigger factor on the ribosome: Implications for protein folding and SRP interaction. *Structure* **13**, 1685–1694 (2005).
216. Bose, S., Weikl, T., Bügl, H. & Buchner, J. Chaperone function of Hsp90-associated proteins. *Science* **274**, 1715–7 (1996).
217. Wang, Z. *et al.* Pro isomerization in MLL1 PHD3-Bromo cassette connects H3K4me readout to CyP33 and HDAC-mediated repression. *Cell* **141**, 1183–1194 (2010).
218. Ruiz-Estevez, M. *et al.* Promotion of Myoblast Differentiation by Fkbp5 via Cdk4 Isomerization. *Cell Rep.* **25**, 2537-2551.e8 (2018).
219. Ernst, P., Mabon, M., Davidson, A. J., Zon, L. I. & Korsmeyer, S. J. An Mll-dependent Hox program drives hematopoietic progenitor expansion. *Curr. Biol.* **14**, 2063–9 (2004).
220. Park, S. *et al.* The PHD3 domain of MLL Acts as a CYP33-regulated switch between MLL-mediated activation and repression. *Biochemistry* **49**, 6576–6586 (2010).
221. Leung, A. *et al.* Basic surface features of nuclear FKBPs facilitate chromatin binding. *Sci. Rep.* **7**, 3795 (2017).
222. Monneau, Y. R., Soufari, H., Nelson, C. J. & Mackereth, C. D. Structure and activity of the peptidyl-prolyl isomerase domain from the histone chaperone Fpr4 toward histone H3 proline isomerization. *J. Biol. Chem.* **288**, 25826–25837 (2013).
223. Nelson, C. J., Santos-Rosa, H. & Kouzarides, T. Proline isomerization of histone H3 regulates lysine methylation and gene expression. *Cell* **126**, 905–16 (2006).
224. Ohkuni, K., Abdulle, R. & Kitagawa, K. Degradation of Centromeric Histone H3

Variant Cse4 Requires the Fpr3 Peptidyl-prolyl Cis–Trans Isomerase. *Genetics* **196**, 1041–1045 (2014).
225. Tan, H. L. *et al.* Prolyl isomerization of the CENP-A N-Terminus regulates centromeric integrity in fission yeast. *Nucleic Acids Res.* **46**, 1167–1179 (2018).
226. Liu, F. *et al.* Molecular evolution of the vertebrate FK506 binding protein 25. *Int. J. Genomics* **2014**, 402603 (2014).
227. Prakash, A., Shin, J., Rajan, S. & Yoon, H. S. Structural basis of nucleic acid recognition by FK506-binding protein 25 (FKBP25), a nuclear immunophilin. *Nucleic Acids Res.* **44**, 2909–2925 (2016).
228. Helander, S. *et al.* Basic Tilted Helix Bundle - a new protein fold in human FKBP25/FKBP3 and HectD1. *Biochem. Biophys. Res. Commun.* **447**, 26–31 (2014).
229. Dilworth, D. *et al.* The basic tilted helical bundle domain of the prolyl isomerase FKBP25 is a novel double-stranded RNA binding module. *Nucleic Acids Res.* **45**, 1–16 (2017).
230. Rivière, S., Ménez, A. & Galat, A. On the localization of FKBP25 in T-lymphocytes. *FEBS Lett.* **315**, 247–51 (1993).
231. Prakash, A., Shin, J., Rajan, S. & Yoon, H. S. Structural basis of nucleic acid recognition by FK506-binding protein 25 (FKBP25), a nuclear immunophilin. *Nucleic Acids Res.* **44**, 2909–2925 (2016).
232. Foulger, L. E. *et al.* Efficient purification of chromatin architectural proteins: Histones, HMGB proteins and FKBP3 (FKBP25) immunophilin. *RSC Adv.* **2**, 10598–10604 (2012).
233. Gudavicius, G. *et al.* The prolyl isomerase, FKBP25, interacts with RNA-engaged nucleolin and the pre-60S ribosomal subunit. *RNA* **20**, 1014–1022 (2014).
234. Yang, W. M., Yao, Y. L. & Seto, E. The Fk506-binding protein 25 functionally associates with histone deacetylases and with transcription factor YY1. *EMBO J.* **20**, 4814–4825 (2001).
235. Jin, Y. J. & Burakoff, S. J. The 25-kDa FK506-binding protein is localized in the nucleus and associates with casein kinase II and nucleolin. *Proc. Natl. Acad. Sci. U. S. A.* **90**, 7769–7773 (1993).
236. Dilworth, D. *et al.* The prolyl isomerase FKBP25 regulates microtubule polymerization impacting cell cycle progression and genomic stability. *Nucleic Acids Res.* **46**, 2459–2478 (2018).
237. He, Z. Immunophilins and Parvulins. Superfamily of Peptidyl Prolyl Isomerases in Arabidopsis. *PLANT Physiol.* **134**, 1248–1267 (2004).
238. Ghartey-Kwansah, G. *et al.* Comparative analysis of FKBP family protein: evaluation, structure, and function in mammals and Drosophila melanogaster. *BMC Dev. Biol.* **18**, 7 (2018).
239. Edlich-Muth, C. *et al.* The pentameric nucleoplasmin fold is present in Drosophila FKBP39 and a large number of chromatin-related proteins. *J. Mol. Biol.* **427**, 1949–1963 (2015).
240. Li, H. & Luan, S. AtFKBP53 is a histone chaperone required for repression of ribosomal RNA gene expression in Arabidopsis. *Cell Res.* **20**, 357–66 (2010).
241. Dujon, B. *et al.* Genome evolution in yeasts. *Nature* **430**, 35–44 (2004).
242. Marcet-Houben, M. & Gabaldón, T. Beyond the whole-genome duplication:

Phylogenetic evidence for an ancient interspecies hybridization in the baker's yeast lineage. *PLoS Biol.* **13**, 1–26 (2015).
243. Wolfe, K. H. & Shields, D. C. Molecular evidence for an ancient duplication of the entire yeast genome. *Nature* **387**, 708–713 (1997).
244. Kellis, M., Birren, B. W. & Lander, E. S. Proof and evolutionary analysis of ancient genome duplication in the yeast Saccharomyces cerevisiae. *Nature* **428**, 617–624 (2004).
245. Gordon, J. L., Byrne, K. P. & Wolfe, K. H. Additions, losses, and rearrangements on the evolutionary route from a reconstructed ancestor to the modern Saccharomyces cerevisiae genome. *PLoS Genet.* **5**, e1000485 (2009).
246. Cliften, P. F., Fulton, R. S., Wilson, R. K. & Johnston, M. After the duplication: Gene loss and adaptation in saccharomyces genomes. *Genetics* **172**, 863–872 (2006).
247. Byrne, K. P. & Wolfe, K. H. The Yeast Gene Order Browser: Combining curated homology and syntenic context reveals gene fate in polyploid species. *Genome Res.* **15**, 1456–1461 (2005).
248. Dolinski, K., Muir, S., Cardenas, M. & Heitman, J. All cyclophilins and FK506 binding proteins are, individually and collectively, dispensable for viability in Saccharomyces cerevisiae. *Proc. Natl. Acad. Sci. U. S. A.* **94**, 13093–13098 (1997).
249. Costanzo, M. *et al.* The genetic landscape of a cell. *Science* **327**, 425–31 (2010).
250. Tautz, D. Redundancies, development and the flow of information. *Bioessays* **14**, 263–6 (1992).
251. Thomas, J. H. Thinking about genetic redundancy. *Trends Genet.* **9**, 395–399 (1993).
252. Gatherer, D. Gene Knockouts and Murine Development. *Dev. Growth Differ.* **35**, 365–370 (1993).
253. Kimura, M. & King, J. L. Fixation of a deleterious allele at one of two 'duplicate' loci by mutation pressure and random drift. *Proc. Natl. Acad. Sci. U. S. A.* **76**, 2858–61 (1979).
254. Li, W. H. Rate of gene silencing at duplicate loci. A theoretical study and interpretation of data from tetraploid fishes. *Genetics* **95**, 237–258 (1980).
255. Walsh, J. B. How often do duplicated genes evolve new functions? *Genetics* **139**, 421–8 (1995).
256. Ihmels, J., Collins, S. R., Schuldiner, M., Krogan, N. J. & Weissman, J. S. Backup without redundancy: genetic interactions reveal the cost of duplicate gene loss. *Mol. Syst. Biol.* **3**, 86 (2007).
257. Devis, D., Firth, S. M., Liang, Z. & Byrne, M. E. Dosage sensitivity of RPL9 and concerted evolution of ribosomal protein genes in plants. *Front. Plant Sci.* **6**, 1–12 (2015).
258. Musso, G. *et al.* The extensive and condition-dependent nature of epistasis among whole-genome duplicates in yeast. *Genome Res.* **18**, 1092–1099 (2008).
259. Gu, Z. *et al.* Role of duplicate genes in genetic robustness against null mutations. *Nature* **421**, 63–66 (2003).
260. Darlington, C. D. & Moffett, A. A. Primary and secondary chromosome balance in Pyrus. *J. Genet.* **22**, 129–151 (1930).
261. Bridges, C. B. The Bar 'Gene' a Duplication. *Science* **83**, 210–1 (1936).

262. Kataoka, T. *et al.* Genetic analysis of yeast RAS1 and RAS2 genes. *Cell* **37**, 437–45 (1984).
263. Basson, M. E., Thorsness, M. & Rine, J. Saccharomyces cerevisiae contains two functional genes encoding 3-hydroxy-3-methylglutaryl-coenzyme A reductase. *Proc. Natl. Acad. Sci. U. S. A.* **83**, 5563–5567 (1986).
264. Joyner, A. L., Herrup, K., Auerbach, B. A., Davis, C. A. & Rossant, J. Subtle cerebellar phenotype in mice homozygous for a targeted deletion of the En-2 homeobox. *Science* **251**, 1239–43 (1991).
265. Hoffmann, F. M. Drosophila abl and genetic redundancy in signal transduction. *Trends Genet.* **7**, 351–5 (1991).
266. Higashijima, S. I., Michiue, T., Emori, Y. & Saigo, K. Subtype determination of Drosophila embryonic external sensory organs by redundant homeo box genes BarH1 and BarH2. *Genes Dev.* **6**, 1005–1018 (1992).
267. Haldane, J. B. S. *The Causes of Evolution*. (Longmans, Green and Co, 1932).
268. Haldane, J. B. S. The Part Played by Recurrent Mutation in Evolution. *Am. Nat.* **67**, 5–19 (1933).
269. Katju, V. & Lynch, M. On the formation of novel genes by duplication in the caenorhabditis elegans genome. *Mol. Biol. Evol.* **23**, 1056–1067 (2006).
270. Innan, H. & Kondrashov, F. The evolution of gene duplications: Classifying and distinguishing between models. *Nat. Rev. Genet.* **11**, 97–108 (2010).
271. Setphens, S. G. Possible significance of duplication in evolution. in *Advances in genetics* **4**, 247–65 (1951).
272. Nei, M. Gene Duplication and Nucleotide Substitution in Evolution. *Nature* **221**, 40–42 (1969).
273. Ohno, S. Part 3: Why Gene Duplication? in *Evolution by Gene Duplication* 59–88 (Springer-Verlag, 1970).
274. Hughes, A. L. The evolution of functionally novel proteins after gene duplication. *Proc. R. Soc. London. Ser. B Biol. Sci.* **256**, 119–124 (1994).
275. Force, A. *et al.* Preservation of duplicate genes by complementary, degenerative mutations. *Genetics* **151**, 1531–45 (1999).
276. Penn, D. J., Damjanovich, K. & Potts, W. K. MHC heterozygosity confers a selective advantage against multiple-strain infections. *Proc. Natl. Acad. Sci. U. S. A.* **99**, 11260–4 (2002).
277. Lynch, M. & Katju, V. The altered evolutionary trajectories of gene duplicates. *Trends Genet.* **20**, 544–549 (2004).
278. Francino, M. P. An adaptive radiation model for the origin of new gene functions. *Nat. Genet.* **37**, 573–577 (2005).
279. Manning-Krieg, U. C. *et al.* Purification of FKBP-70, a novel immunophilin from Saccharomyces cerevisiae, and cloning of its structural gene, FPR3. *FEBS Lett.* **352**, 98–103 (1994).
280. Shan, X., Xue, Z. & Mélèse, T. Yeast NPI46 encodes a novel prolyl cis-trans isomerase that is located in the nucleolus. *J. Cell Biol.* **126**, 853–862 (1994).
281. Benton, B. M., Zang, J. H. & Thorner, J. A novel FK506- and rapamycin-binding protein (FPR3 gene product) in the yeast Saccharomyces cerevisiae is a proline rotamase localized to the nucleolus. *J. Cell Biol.* **127**, 623–639 (1994).
282. Koztowska, M. *et al.* Nucleoplasmin-like domain of FKBP39 from Drosophila

melanogaster forms a tetramer with partly disordered tentacle-like C-terminal segments. *Sci. Rep.* **7**, 1–14 (2017).
283. Park, S.-K., Xiao, H. & Lei, M. Nuclear FKBPs, Fpr3 and Fpr4 affect genome-wide genes transcription. *Mol. Genet. Genomics* **289**, 125–36 (2014).
284. Kuzuhara, T. & Horikoshi, M. A nuclear FK506-binding protein is a histone chaperone regulating rDNA silencing. *Nat. Struct. Mol. Biol.* **11**, 275–283 (2004).
285. Xiao, H., Jackson, V. & Lei, M. The FK506-binding protein, Fpr4, is an acidic histone chaperone. *FEBS Lett.* **580**, 4357–64 (2006).
286. Bentley-DeSousa, A. *et al.* A Screen for Candidate Targets of Lysine Polyphosphorylation Uncovers a Conserved Network Implicated in Ribosome Biogenesis. *Cell Rep.* **22**, 3427–3439 (2018).
287. Chi, A. *et al.* Analysis of phosphorylation sites on proteins from Saccharomyces cerevisiae by electron transfer dissociation (ETD) mass spectrometry. *Proc. Natl. Acad. Sci.* **104**, 2193–2198 (2007).
288. Wilson, L. K., Dhillon, N., Martin, G. S., Thorner, J. & Martin, G. S. Casein Kinase II Catalyzes Tyrosine Phosphorylation of the Yeast Nucleolar. *J. Biol. Chem.* **272**, 12961–12967 (1997).
289. Marin, O. *et al.* Tyrosine versus serine/threonine phosphorylation by protein kinase casein kinase-2. A study with peptide substrates derived from immunophilin Fpr3. *J. Biol. Chem.* **274**, 29260–5 (1999).
290. Bandhakavi, S., McCann, R. O., Hanna, D. E. & Glover, C. V. C. Genetic interactions among ZDS1,2, CDC37, and protein kinase CK2 in Saccharomyces cerevisiae. *FEBS Lett.* **554**, 295–300 (2003).
291. Wilson, L. K., Benton, B. M., Zhou, S., Thorner, J. & Martin, G. S. The yeast immunophilin Fpr3 is a physiological substrate of the tyrosine-specific phosphoprotein phosphatase Ptp1. *J. Biol. Chem.* **270**, 25185–25193 (1995).
292. Marchetta, M. *et al.* Expression of the Stp1 LMW-PTP and inhibition of protein CK2 display a cooperative effect on immunophilin Fpr3 tyrosine phosphorylation and Saccharomyces cerevisiae growth. *Cell. Mol. Life Sci.* **61**, 1176–1184 (2004).
293. Magherini, F. *et al.* The in vivo tyrosine phosphorylation level of yeast immunophilin Fpr3 is influenced by the LMW-PTP Ltp1. *Biochem. Biophys. Res. Commun.* **321**, 424–31 (2004).
294. Krogan, N. J. *et al.* Global landscape of protein complexes in the yeast Saccharomyces cerevisiae. *Nature* **440**, 637–43 (2006).
295. Sydorskyy, Y. *et al.* Nop53p is a novel nucleolar 60 S ribosomal subunit biogenesis protein. *Biochem. J* **388**, 819–826 (2005).
296. Davey, M., Hannam, C., Wong, C. & Brandl, C. J. The yeast peptidyl proline isomerases FPR3 and FPR4, in high copy numbers, suppress defects resulting from the absence of the E3 ubiquitin ligase TOM1. *Mol. Gen. Genet. MGG* **263**, 520–526 (2000).
297. Utsugi, T. *et al.* Yeast tom1 mutant exhibits pleiotropic defects in nuclear division, maintenance of nuclear structure and nucleocytoplasmic transport at high temperatures. *Gene* **234**, 285–295 (1999).
298. Saleh, a *et al.* TOM1p, a yeast hect-domain protein which mediates transcriptional regulation through the ADA/SAGA coactivator complexes. *J. Mol. Biol.* **282**, 933–46 (1998).

299. Ghosh, A. & Cannon, J. F. Analysis of Protein Phosphatase-1 and Aurora Protein Kinase Suppressors Reveals New Aspects of Regulatory Protein Function in Saccharomyces cerevisiae. *PLoS One* **8**, (2013).
300. Hochwagen, A., Tham, W.-H. H., Brar, G. A. & Amon, A. The FK506 binding protein Fpr3 counteracts protein phosphatase 1 to maintain meiotic recombination checkpoint activity. *Cell* **122**, 861–873 (2005).
301. Macqueen, A. J. & Roeder, G. S. Fpr3 and Zip3 ensure that initiation of meiotic recombination precedes chromosome synapsis in budding yeast. *Curr. Biol.* **19**, 1519–26 (2009).
302. Huh, W.-K. *et al.* Global analysis of protein localization in budding yeast. *Nature* **425**, 686–91 (2003).
303. Bersaglieri, C. & Santoro, R. Genome Organization in and around the Nucleolus. *Cells* **8**, 579 (2019).
304. Johnston, M. *et al.* The nucleotide sequence of Saccharomyces cerevisiae chromosome XII. *Nature* **387**, 87–90 (1997).
305. Olson, M. O. J. *The Nucleolus*. (Springer New York, 2004).
306. Reeder, R. H., Guevara, P. & Roan, J. G. Saccharomyces cerevisiae RNA polymerase I terminates transcription at the Reb1 terminator in vivo. *Mol. Cell. Biol.* **19**, 7369–76 (1999).
307. Linskens, M. H. K. & Huberman, J. A. Organization of replication of ribosomal DNA in Saccharomyces cerevisiae. *Mol. Cell. Biol.* **8**, 4927–35 (1988).
308. Choe, S. Y., Schultz, M. C. & Reeder, R. H. In vitro definition of the yeast RNA polymerase I promoter. *Nucleic Acids Res.* **20**, 279–85 (1992).
309. Warner, J. R. The economics of ribosome biosynthesis in yeast. *Trends Biochem. Sci.* **24**, 437–40 (1999).
310. Kressler, D., Hurt, E. & Bassler, J. Driving ribosome assembly. *Biochim. Biophys. Acta* **1803**, 673–83 (2010).
311. Nyström, T. & Liu, B. The mystery of aging and rejuvenation - a budding topic. *Curr. Opin. Microbiol.* **18**, 61–7 (2014).
312. Sinclair, D. a & Guarente, L. Extrachromosomal rDNA circles--a cause of aging in yeast. *Cell* **91**, 1033–42 (1997).
313. Murray, A. W. & Szostak, J. W. Pedigree analysis of plasmid segregation in yeast. *Cell* **34**, 961–970 (1983).
314. Shcheprova, Z., Baldi, S., Frei, S. B., Gonnet, G. & Barral, Y. A mechanism for asymmetric segregation of age during yeast budding. *Nature* **454**, 728–34 (2008).
315. Kwan, E. X. *et al.* A natural polymorphism in rDNA replication origins links origin activation with calorie restriction and lifespan. *PLoS Genet.* **9**, e1003329 (2013).
316. Dammann, R., Lucchini, R., Koller, T. & Sogo, J. M. Transcription in the yeast rRNA gene locus: distribution of the active gene copies and chromatin structure of their flanking regulatory sequences. *Mol. Cell. Biol.* **15**, 5294–303 (1995).
317. Goodfellow, S. J. & Zomerdijk, J. C. B. M. Basic mechanisms in RNA polymerase I transcription of the ribosomal RNA genes. *Subcell. Biochem.* **61**, 211–36 (2013).
318. Murayama, A., Ohmori, K. & Fujimura, A. Epigenetic control of rDNA loci in response to intracellular energy status. *Chemtracts* **21**, 210–212 (2008).
319. Srivastava, R., Srivastava, R. & Ahn, S. H. The Epigenetic Pathways to Ribosomal

DNA Silencing. *Microbiol. Mol. Biol. Rev.* **80**, 545–563 (2016).
320. Huang, J. & Moazed, D. Association of the RENT complex with nontranscribed and coding regions of rDNA and a regional requirement for the replication fork block protein Fob1 in rDNA silencing. *Genes Dev.* **17**, 2162–76 (2003).
321. Straight, A. F. *et al.* Net1, a Sir2-associated nucleolar protein required for rDNA silencing and nucleolar integrity. *Cell* **97**, 245–56 (1999).
322. Buck, S. W., Sandmeier, J. J. & Smith, J. S. RNA polymerase I propagates unidirectional spreading of rDNA silent chromatin. *Cell* **111**, 1003–1014 (2002).
323. Ha, C. W., Kim, K., Chang, Y. J., Kim, B. & Huh, W. K. The β-1,3-glucanosyltransferase Gas1 regulates Sir2-mediated rDNA stability in Saccharomyces cerevisiae. *Nucleic Acids Res.* **42**, 8486–8499 (2014).
324. Johzuka, K. & Horiuchi, T. The cis Element and Factors Required for Condensin Recruitment to Chromosomes. *Mol. Cell* **34**, 26–35 (2009).
325. Mekhail, K., Seebacher, J., Gygi, S. P. & Moazed, D. Role for perinuclear chromosome tethering in maintenance of genome stability. *Nature* **456**, 667–70 (2008).
326. Ben-Shem, A. *et al.* The structure of the eukaryotic ribosome at 3.0 Å resolution. *Science* **334**, 1524–9 (2011).
327. Woolford, J. L. & Baserga, S. J. Ribosome biogenesis in the yeast Saccharomyces cerevisiae. *Genetics* **195**, 643–681 (2013).
328. Horigome, C., Ikeda, R., Okada, T., Takenami, K. & Mizuta, K. Genetic interaction between ribosome biogenesis and inositol polyphosphate metabolism in saccharomyces cerevisiae. *Biosci. Biotechnol. Biochem.* **73**, 443–446 (2009).
329. Bohnsack, K. E. & Bohnsack, M. T. Uncovering the assembly pathway of human ribosomes and its emerging links to disease. *EMBO J.* **38**, e100278 (2019).
330. Keys, D. A. *et al.* Multiprotein transcription factor UAF interacts with the upstream element of the yeast RNA polymerase I promoter and forms a stable preinitiation complex. *Genes Dev.* **10**, 887–903 (1996).
331. Lin, C. W. *et al.* A novel 66-kilodalton protein complexes with Rrn6, Rrn7, and TATA-binding protein to promote polymerase I transcription initiation in Saccharomyces cerevisiae. *Mol. Cell. Biol.* **16**, 6436–6443 (1996).
332. Keys, D. A. *et al.* RRN6 and RRN7 encode subunits of a multiprotein complex essential for the initiation of rDNA transcription by RNA polymerase I in Saccharomyces cerevisiae. *Genes Dev.* **8**, 2349–2362 (1994).
333. Yamamoto, R. T., Nogi, Y., Dodd, J. A. & Nomura, M. RRN3 gene of Saccharomyces cerevisiae encodes an essential RNA polymerase I transcription factor which interacts with the polymerase independently of DNA template. *EMBO J.* **15**, 3964–3973 (1996).
334. Kufel, J., Dichtl, B. & Tollervey, D. Yeast Rnt1p is required for cleavage of the pre-ribosomal RNA in the 3' ETS but not the 5' ETS. *RNA* **5**, 909–17 (1999).
335. Udem, S. A. & Warner, J. R. Ribosomal RNA synthesis in Saccharomyces cerevisiae. *J. Mol. Biol.* **65**, 227–42 (1972).
336. Schmitt, M. E. & Clayton, D. A. Nuclear RNase MRP is required for correct processing of pre-5.8S rRNA in Saccharomyces cerevisiae. *Mol. Cell. Biol.* **13**, 7935–41 (1993).
337. Lygerou, Z., Allmang, C., Tollervey, D. & Séraphin, B. Accurate processing of a

eukaryotic precursor ribosomal RNA by ribonuclease MRP in vitro. *Science* **272**, 268–70 (1996).
338. Geerlings, T. H., Vos, J. C. & Raué, H. A. The final step in the formation of 25S rRNA in Saccharomyces cerevisiae is performed by 5'-->3' exonucleases. *RNA* **6**, 1698–703 (2000).
339. Henry, Y. *et al.* The 5' end of yeast 5.8S rRNA is generated by exonucleases from an upstream cleavage site. *EMBO J.* **13**, 2452–63 (1994).
340. Mitchell, P., Petfalski, E. & Tollervey, D. The 3' end of yeast 5.8S rRNA is generated by an exonuclease processing mechanism. *Genes Dev.* **10**, 502–13 (1996).
341. Kassavetis, G. A., Braun, B. R., Nguyen, L. H. & Peter Geiduschek, E. S. cerevisiae TFIIIB is the transcription initiation factor proper of RNA polymerase III, while TFIIIA and TFIIIC are assembly factors. *Cell* **60**, 235–245 (1990).
342. van Hoof, A. Three conserved members of the RNase D family have unique and overlapping functions in the processing of 5S, 5.8S, U4, U5, RNase MRP and RNase P RNAs in yeast. *EMBO J.* **19**, 1357–1365 (2000).
343. Allmang, C. Degradation of ribosomal RNA precursors by the exosome. *Nucleic Acids Res.* **28**, 1684–1691 (2000).
344. LaCava, J. *et al.* RNA degradation by the exosome is promoted by a nuclear polyadenylation complex. *Cell* **121**, 713–24 (2005).
345. Makino, D. L. & Conti, E. Structure determination of an 11-subunit exosome in complex with RNA by molecular replacement. *Acta Crystallogr. Sect. D Biol. Crystallogr.* **69**, 2226–2235 (2013).
346. Wasmuth, E. V., Januszyk, K. & Lima, C. D. Structure of an Rrp6–RNA exosome complex bound to poly(A) RNA. *Nature* **511**, 435–439 (2014).
347. Briggs, M. W., Burkard, K. T. D. & Butler, J. S. Rrp6p, the yeast homologue of the human PM-Scl 100-kDa autoantigen, is essential for efficient 5.8 S rRNA 3' end formation. *J. Biol. Chem.* **273**, 13255–13263 (1998).
348. Mitchell, P., Petfalski, E., Shevchenko, A., Mann, M. & Tollervey, D. The exosome: A conserved eukaryotic RNA processing complex containing multiple 3'→5' exoribonucleases. *Cell* **91**, 457–466 (1997).
349. Li, Y., Burclaff, J. & Anderson, J. T. Mutations in Mtr4 structural domains reveal their important role in regulating tRNAiMet turnover in saccharomyces cerevisiae and Mtr4p enzymatic activities in vitro. *PLoS One* **11**, 1–20 (2016).
350. Vanácová, S. *et al.* A new yeast poly(A) polymerase complex involved in RNA quality control. *PLoS Biol.* **3**, e189 (2005).
351. Houseley, J., Kotovic, K., El Hage, A. & Tollervey, D. Trf4 targets ncRNAs from telomeric and rDNA spacer regions and functions in rDNA copy number control. *EMBO J.* **26**, 4996–5006 (2007).
352. Reis, C. C. & Campbell, J. L. Contribution of Trf4/5 and the nuclear exosome to genome stability through regulation of histone mRNA levels in Saccharomyces cerevisiae. *Genetics* **175**, 993–1010 (2007).
353. Reis, C. C. & Campbell, J. L. Contribution of Trf4/5 and the nuclear exosome to genome stability through regulation of histone mRNA levels in Saccharomyces cerevisiae. *Genetics* **175**, 993–1010 (2007).
354. Houseley, J. & Tollervey, D. Yeast Trf5p is a nuclear poly(A) polymerase. *EMBO*

Rep. **7**, 205–11 (2006).
355. Milligan, L. *et al.* A Yeast Exosome Cofactor, Mpp6, Functions in RNA Surveillance and in the Degradation of Noncoding RNA Transcripts. *Mol. Cell. Biol.* **28**, 5446–5457 (2008).
356. Karyn Schmidt and J. Scott Butler. Nuclear RNA Surveillance: Role of TRAMP in Controlling Exosome Specificity. *Wiley Interdiscip Rev* **4**, 217–231 (2013).
357. Butler, J. S. Nuclear RNA Surveillance: Role of TRAMP in Controlling Exosome Specificity. **4**, 217–231 (2014).
358. Houseley, J. & Tollervey, D. The Many Pathways of RNA Degradation. *Cell* **136**, 763–776 (2009).
359. Wery, M., Ruidant, S., Schillewaert, S., Leporé, N. & Lafontaine, D. L. J. The nuclear poly(A) polymerase and Exosome cofactor Trf5 is recruited cotranscriptionally to nucleolar surveillance. *Rna* **15**, 406–419 (2009).
360. Wolin, S. L., Sim, S. & Chen, X. Nuclear noncoding RNA surveillance: Is the end in sight? *Trends Genet.* **28**, 306–313 (2012).
361. Mani, R., St.Onge, R. P., Hartman, J. L., Giaever, G. & Roth, F. P. Defining genetic interaction. *Proc. Natl. Acad. Sci.* **105**, 3461–3466 (2008).
362. Boucher, B. & Jenna, S. Genetic interaction networks: better understand to better predict. *Front. Genet.* **4**, 290
363. Tong, A. H. Y. *et al.* Global mapping of the yeast genetic interaction network. *Science* **303**, 808–13 (2004).
364. Tong, A. H. Y. & Boone, C. High-Throughput Strain Construction and Systematic Synthetic Lethal Screening in Saccharomyces cerevisiae. in *Methods in Microbiology, Volume 36: Yeast Gene Analysis* (eds. Stansfield, I. & Stark, M.) 369–388 (Academic Press, 2007).
365. Tong, A. H. Y. & Boone, C. Synthetic genetic array analysis in Saccharomyces cerevisiae. *Methods Mol. Biol. (Totowa, N.J.)* **313**, 171–92 (2006).
366. Tong, A. *et al.* Global Mapping of the Yeast Genetic Interaction Network : Discovering Gene and Drug Function. *Genetics* 47–55 (2003).
367. Costanzo, M. *et al.* A global genetic interaction network maps a wiring diagram of cellular function. *Science* **353**, 505–11 (2016).
368. Collins, S. R. *et al.* Functional dissection of protein complexes involved in yeast chromosome biology using a genetic interaction map. *Nature* **446**, 806–810 (2007).
369. Stirling, P. C. *et al.* The complete spectrum of yeast chromosome instability genes identifies candidate cin cancer genes and functional roles for astra complex components. *PLoS Genet.* **7**, 9–13 (2011).
370. Milliman, E. J. *et al.* Recruitment of Rpd3 to the Telomere Depends on the Protein Arginine Methyltransferase Hmt1. *PLoS One* **7**, 1–11 (2012).
371. Usaj, M. *et al.* TheCellMap.org: A Web-Accessible Database for Visualizing and Mining the Global Yeast Genetic Interaction Network. *G3 (Bethesda).* **7**, 1539–1549 (2017).
372. Robinson, M. D., Grigull, J., Mohammad, N. & Hughes, T. R. FunSpec: a web-based cluster interpreter for yeast. *BMC Bioinformatics* **3**, 35 (2002).
373. Young, B. P. & Loewen, C. J. R. Balony: a software package for analysis of data generated by synthetic genetic array experiments. *BMC Bioinformatics* **14**, 354 (2013).

374. Shannon, P. *et al.* Cytoscape: a software environment for integrated models of biomolecular interaction networks. *Genome Res.* **13**, 2498–504 (2003).
375. Bitterman, K. J., Medvedik, O. & Sinclair, D. A. Longevity regulation in Saccharomyces cerevisiae: linking metabolism, genome stability, and heterochromatin. *Microbiol. Mol. Biol. Rev.* **67**, 376–99 (2003).
376. Collart, M. A. The Ccr4-Not complex is a key regulator of eukaryotic gene expression. *Wiley Interdiscip. Rev. RNA* **7**, 438–454 (2016).
377. San Paolo, S. *et al.* Distinct roles of non-canonical poly(A) polymerases in RNA metabolism. *PLoS Genet.* **5**, 13–17 (2009).
378. Houseley, J. & Tollervey, D. The nuclear RNA surveillance machinery: The link between ncRNAs and genome structure in budding yeast? *Biochim. Biophys. Acta - Gene Regul. Mech.* **1779**, 239–46 (2008).
379. Wery, M., Ruidant, S., Schillewaert, S., Leporé, N. & Lafontaine, D. L. J. The nuclear poly(A) polymerase and Exosome cofactor Trf5 is recruited cotranscriptionally to nucleolar surveillance. *RNA* **15**, 406–19 (2009).
380. Wang, Y. *et al.* Architecture and subunit arrangement of the complete Saccharomyces cerevisiae COMPASS complex. *Sci. Rep.* **8**, 1–10 (2018).
381. Dubouloz, F., Deloche, O., Wanke, V., Cameroni, E. & De Virgilio, C. The TOR and EGO protein complexes orchestrate microautophagy in yeast. *Mol. Cell* **19**, 15–26 (2005).
382. San-Segundo, P. A. & Roeder, G. S. Role for the silencing protein Dot1 in meiotic checkpoint control. *Mol. Biol. Cell* **11**, 3601–3615 (2000).
383. Nimmo, E. R., Pidoux, A. L., Perry, P. E. & Allshire, R. C. Defective meiosis in telomere-silencing mutants of Schizosaccharomyces pombe. *Nature* **392**, 825–828 (1998).
384. Singer, M. S. *et al.* Identification of high-copy disruptors of telomeric silencing in Saccharomyces cerevisiae. *Genetics* **150**, 613–632 (1998).
385. Alber, F. *et al.* The molecular architecture of the nuclear pore complex. *Nature* **450**, 695–701 (2007).
386. Rempel, I. L. *et al.* Age-dependent deterioration of nuclear pore assembly in mitotic cells decreases transport dynamics. *Elife* **8**, 1–26 (2019).
387. Ii, T., Fung, J., Mullen, J. R. & Brill, S. J. The yeast Slx5-Slx8 DNA integrity complex displays ubiquitin ligase activity. *Cell Cycle* **6**, 2800–2809 (2007).
388. Mizuguchi, G. *et al.* ATP-driven exchange of histone H2AZ variant catalyzed by SWR1 chromatin remodeling complex. *Science* **303**, 343–8 (2004).
389. Krogan, N. J. *et al.* Regulation of chromosome stability by the histone H2A variant Htz1, the Swr1 chromatin remodeling complex, and the histone acetyltransferase NuA4. *Proc. Natl. Acad. Sci. U. S. A.* **101**, 13513–8 (2004).
390. Hou, H. *et al.* Histone variant H2A.Z regulates centromere silencing and chromosome segregation in fission yeast. *J. Biol. Chem.* **285**, 1909–1918 (2010).
391. Cascone, A., Bruelle, C., Lindholm, D., Bernardi, P. & Eriksson, O. Destabilization of the outer and inner mitochondrial membranes by core and linker histones. *PLoS One* **7**, (2012).
392. Garg, M., Ramdas, N., Vijayalakshmi, M., Shivashankar, G. V. & Sarin, A. The C-terminal domain (CTD) in linker histones antagonizes anti-apoptotic proteins to modulate apoptotic outcomes at the mitochondrion. *Cell Death Dis.* **5**, e1058-10

(2014).
393. Cavdar Koc, E. *et al.* A new face on apoptosis: death-associated protein 3 and PDCD9 are mitochondrial ribosomal proteins. *FEBS Lett.* **492**, 166–70 (2001).
394. Gregory, P. D. *et al.* Absence of Gcn5 HAT activity defines a novel state in the opening of chromatin at the PHO5 promoter in yeast. *Mol. Cell* **1**, 495–505 (1998).
395. Goldstein, A. L. & McCusker, J. H. Three new dominant drug resistance cassettes for gene disruption in Saccharomyces cerevisiae. *Yeast* **15**, 1541–53 (1999).
396. Gietz, R. D. Yeast transformation by the LiAc/SS carrier DNA/PEG method. *Methods Mol. Biol.* **1163**, 33–44 (2014).
397. Ellahi, A., Thurtle, D. M. & Rine, J. The chromatin and transcriptional landscape of native saccharomyces cerevisiae telomeres and subtelomeric domains. *Genetics* **200**, 505–521 (2015).
398. Li, M., Valsakumar, V., Poorey, K., Bekiranov, S. & Smith, J. S. Genome-wide analysis of functional sirtuin chromatin targets in yeast. *Genome Biol.* **14**, (2013).
399. Kuzuhara, T. & Horikoshi, M. A nuclear FK506-binding protein is a histone chaperone regulating rDNA silencing. *Nat. Struct. Mol. Biol.* **11**, 275–283 (2004).
400. VanLeeuwen, F. & Gottschling, D. E. Assays for gene silencing in yeast. *Methods Enzymol.* **350**, 165–86 (2002).
401. Li, C., Mueller, J. E. & Bryk, M. Sir2 Represses Endogenous Polymerase II Transcription Units in the Ribosomal DNA Nontranscribed Spacer. *Mol. Biol. Cell* **17**, 3848–3859 (2006).
402. Kuzuhara, T. & Horikoshi, M. A nuclear FK506-binding protein is a histone chaperone regulating rDNA silencing. *Nat. Struct. Mol. Biol.* **11**, 275–83 (2004).
403. Adkins, M. W., Howar, S. R. & Tyler, J. K. Chromatin disassembly mediated by the histone chaperone Asf1 is essential for transcriptional activation of the yeast PHO5 and PHO8 genes. *Mol. Cell* **14**, 657–66 (2004).
404. Fermi, B., Bosio, M. C. & Dieci, G. Promoter architecture and transcriptional regulation of Abf1-dependent ribosomal protein genes in Saccharomyces cerevisiae. *Nucleic Acids Res.* **44**, 6113–6126 (2016).
405. Neef, D. W. & Kladde, M. P. Polyphosphate Loss Promotes SNF/SWI- and Gcn5-Dependent Mitotic Induction of PHO5. *Mol. Cell. Biol.* **23**, 3788–3797 (2003).
406. VanLeeuwen, F., Gafken, P. R. & Gottschling, D. E. Dot1p modulates silencing in yeast by methylation of the nucleosome core. *Cell* **109**, 745–756 (2002).
407. Schmitt, M. E., Brown, T. A. & Trumpower, B. L. A rapid and simple method for preparation of RNA from Saccharomyces cerevisiae. *Nucleic Acids Res.* **18**, 3091–3092 (1990).
408. Li, H. & Durbin, R. Fast and accurate short-read alignment with Burrows-Wheeler transform. *Bioinformatics* **26**, 589–595 (2010).
409. Tarasov, A., Vilella, A. J., Cuppen, E., Nijman, I. J. & Prins, P. Sambamba: fast processing of NGS alignment formats. *Bioinformatics* **31**, 2032–4 (2015).
410. Mai, B. & Breeden, L. L. Identification of target genes of a yeast transcriptional repressor. *Methods Mol. Biol.* **317**, 267–77 (2006).
411. Sambrook, J. & Russell, D. W. Random priming: radiolabeling of purified DNA fragments by extension of random oligonucleotides. *CSH Protoc.* **2006**, (2006).
412. Vogelauer, M. *et al.* In vivo Studies of the Non-transcribed Spacer Region of rDNA in Saccharomyces cerevisiae. *Food Technol. Biotechnol.* **38**, 315–321

(2000).
413. Cuperus, G., Shafaatian, R. & Shore, D. Locus specificity determinants in the multifunctional yeast silencing protein Sir2. *EMBO J.* **19**, 2641–51 (2000).
414. Gottlieb, S. & Esposito, R. E. A new role for a yeast transcriptional silencer gene, SIR2, in regulation of recombination in ribosomal DNA. *Cell* **56**, 771–6 (1989).
415. Kobayashi, T., Horiuchi, T., Tongaonkar, P., Vu, L. & Nomura, M. SIR2 regulates recombination between different rDNA repeats, but not recombination within individual rRNA genes in yeast. *Cell* **117**, 441–453 (2004).
416. Ryu, H.-Y. & Ahn, S. Yeast histone H3 lysine 4 demethylase Jhd2 regulates mitotic rDNA condensation. *BMC Biol.* **12**, 75 (2014).
417. Curcio, M. J., Lutz, S. & Lesage, P. The Ty1 LTR-Retrotransposon of Budding Yeast, Saccharomyces cerevisiae. *Microbiol. Spectr.* **3**, MDNA3-0053–2014 (2015).
418. Sikorski, R. S. & Hieter, P. A system of shuttle vectors and yeast host strains designed for efficient manipulation of DNA in Saccharomyces cerevisiae. *Genetics* **122**, 19–27 (1989).
419. Gascard, P. *et al.* Epigenetic and transcriptional determinants of the human breast. *Nat. Commun.* **6**, 6351 (2015).
420. Korber, P. & Barbaric, S. The yeast PHO5 promoter: From single locus to systems biology of a paradigm for gene regulation through chromatin. *Nucleic Acids Res.* **42**, 10888–10902 (2014).
421. Consortium, T. G. O. Creating the Gene Ontology Resource: Design and Implementation. *Genome Res.* **11**, 1425–1433 (2001).
422. Mewes, H. W. *et al.* MIPS: a database for genomes and protein sequences. *Nucleic Acids Res.* **28**, 37–40 (2000).
423. Brachmann, C. B. *et al.* Designer deletion strains derived from Saccharomyces cerevisiae S288C: A useful set of strains and plasmids for PCR-mediated gene disruption and other applications. *Yeast* **14**, 115–132 (1998).
424. Winzeler, E. A. *et al.* Functional characterization of the S. cerevisiae genome by gene deletion and parallel analysis. *Science* **285**, 901–906 (1999).

Appendix

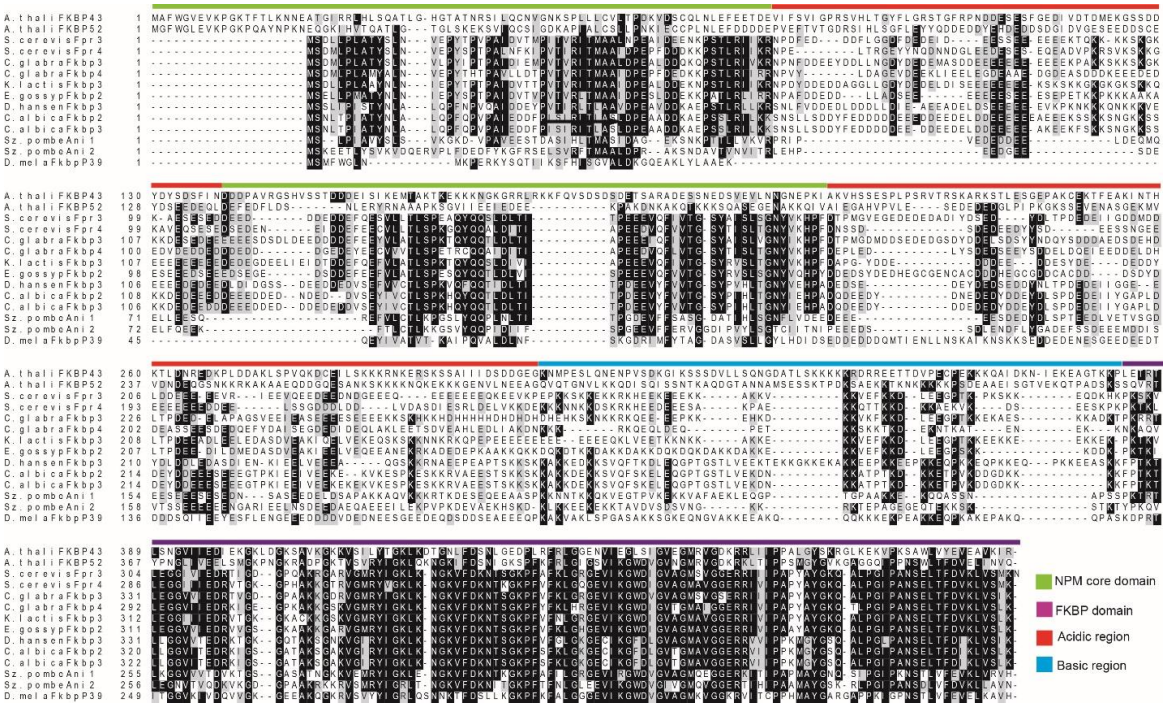

Figure 38. NPL-FKBPs share common features.
Structural alignment of NPL-FKBP protein sequences form *A. thaliana*, *D. melanogaster*, *S. cerevisiae*, *C. glabrata*, *K. lactis*, *E. gossypii*, *D. hansenii*, *C. albicans*, and *Sz. pombe*. Colored bars above alignment indicate protein domains and features.

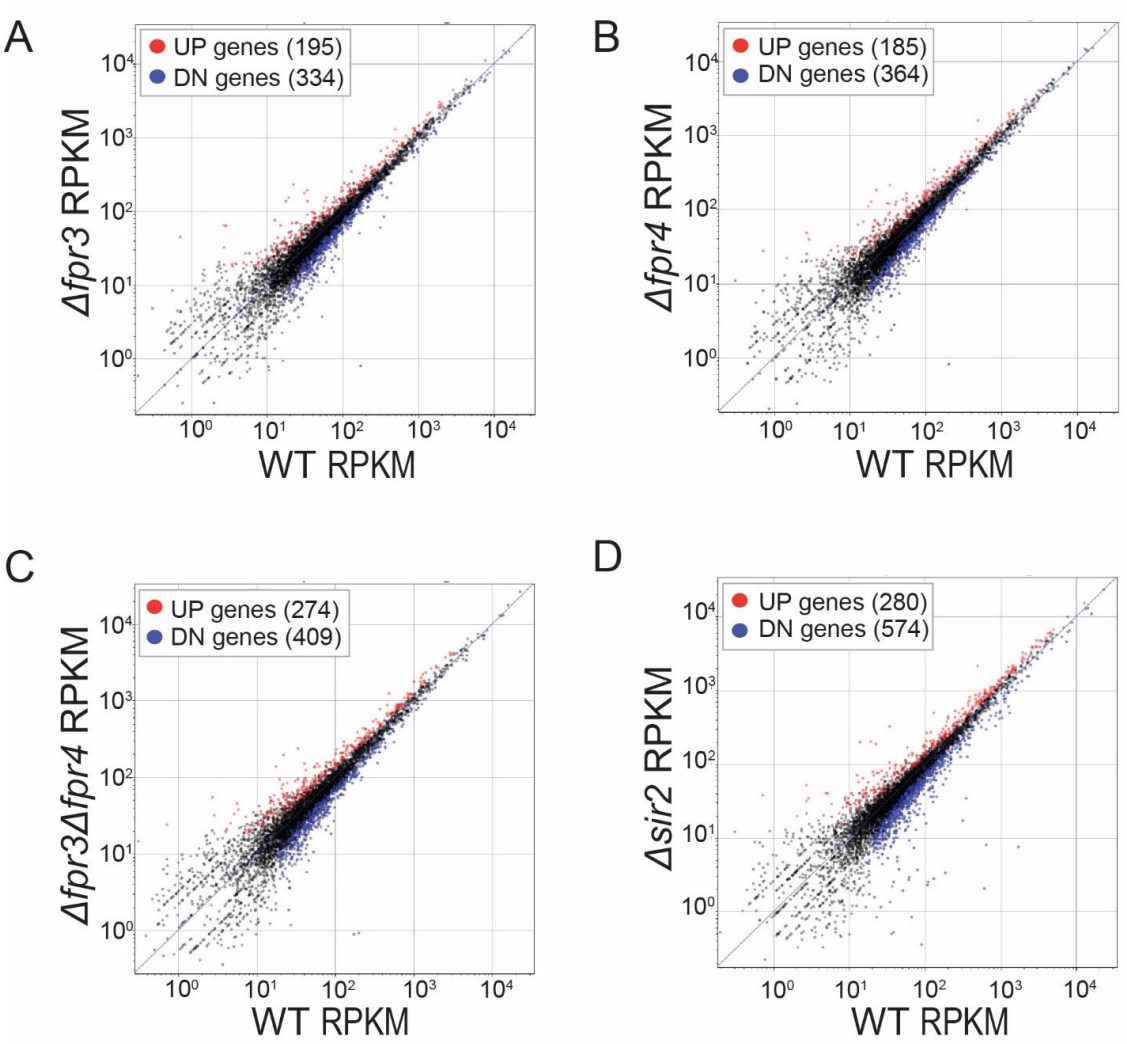

Figure 39. Differential gene expression analysis of single and double Δ*fpr3*/Δ*fpr4* mutants does not support a model of general redundancy.

Scatter plots indicating the correlation of gene expression between (A) WT and *Δfpr3*, (B) WT and *Δfpr4*, (C) WT and *Δfpr3Δfpr4* and (D) WT and *Δsir2* deletion mutants. Expression values are shown as log10 read per kilobase of transcript per million mapped reads (RPKM). Red dots indicate upregulated genes with a log2 fold change of >1.3 while blue dots indicate downregulated genes with a fold change of <-1.3.

Gene ontology analysis of synthetic sick and lethal genetic interactors

Ontologies enriched among the unique, cooperative, and masked synthetic sick and lethal genetic interactors of *FPR3* and *FPR4* are presented in the tables below (Table 1, Table 2, Table 3, and Table 4).

Lists of ontologies were generated by the FunSpec web-based cluster interpreter for yeast (http://funspec.med.utoronto.ca/)[372]. This program outputs a summary of ontologies significantly enriched in a given input list of yeast genes using ontology annotations from the Gene Ontology Consortium (GO) database[421] and from the Munich Information Center for Protein Sequences (MIPS) database[422].

Ontologies in this analysis were classified by molecular function, biological process, cellular component, MIPS functional classification, MIPS phenotypes, MIPS subcellular localization, and MIPS protein complexes. The *p*-values associated with each ontology were calculated automatically by FunSpec using hypergeometric distribution, they represent the probability that the intersection of a given list of genes with any ontology occurs by chance.

Only ontology categories with *p*-values≤0.01 are presented in the following lists. Bonferroni correction was not applied.

k: number of input genes in ontology category
f: total number of genes in ontology category

Table 1. List of ontologies enriched among the 456 synthetic sick and lethal genetic interactors unique to *FPR3*

Ontology	p- value	Genes in ontology category	k	f
GO Molecular Function (1646 categories)				
structural constituent of ribosome [GO:0003735]	<1e-14	RPL19B MRPL16 RPS8A MRP21 MRPL36 MRPL37 MRPL11 RSM24 MRPL7 MRPL35 MRPS28 MRP1 RPL12B RPL37B RPL12A RPL34A RPL9A MRPL25 MRPS35 RSM27 MRPL9 RPL27A RPS27B MRPL6 RSM25 MRPL49 RSM26 RSM22 MRPL38 MRPL13 MRPL20 MRPL15 MRPL4 RPS1A RPL6B RPL13B RPS16A MRPL33 MRP7 RPL16B RPL42A MRPL22 MRPL17 MRPL10 RPS19B MRPS12 MRPL23 PET123 RPS6A MRP51 MRPL40 RPL36B RPL43A	53	218
minus-end-directed microtubule motor activity [GO:0008569]	0.0003062	CIN8 CIK1 KAR3	3	3
structural molecule activity [GO:0005198]	0.0008769	SCS22 ASM4 CHL4 SCS2 CLC1 PDX1 RPN10 VPS25 NUP120 NUP133 NUP188 GAC1	12	63
serine-type peptidase activity [GO:0008236]	0.001123	PIM1 RRT12 PCP1 IMP2 IMP1	5	13
ubiquinol-cytochrome-c reductase activity [GO:0008121]	0.001969	RIP1 QCR10 QCR8 QCR2	4	9
microtubule motor activity [GO:0003777]	0.003108	CIN8 DYN1 CIK1 KAR3	4	10
inositol heptakisphosphate kinase activity [GO:0000829]	0.004553	KCS1 VIP1	2	2

Ontology	p- value	Genes in ontology category	k	f
peptidyltransferase activity [GO:0000048]	0.004553	MRPL16 MRP7	2	2
carboxyl- or carbamoyltransferase activity [GO:0016743]	0.004553	ARG3 URA2	2	2
inositol trisphosphate 3-kinase activity [GO:0008440]	0.004553	KCS1 ARG82	2	2
inositol 1,3,4,5,6-pentakisphosphate kinase activity [GO:0000827]	0.004553	KCS1 ARG82	2	2
inositol hexakisphosphate 5-kinase activity [GO:0000832]	0.004553	KCS1 VIP1	2	2
aminoacyl-tRNA ligase activity [GO:0004812]	0.00537	MSW1 AIM10 DIA4 MST1 NAM2 MSK1 MSE1 MSY1	8	41
ligase activity [GO:0016874]	0.00625	UBC4 MSW1 AIM10 YGR102C DIA4 AIM22 GSH1 URA2 MST1 LIP2 NAM2 UBC7 HFA1 MSK1 MSE1 GSH2 MSY1	17	130
protein binding [GO:0005515]	0.006344	IWR1 SAC3 TRM82 PEX3 AFG3 BUB1 SWI6 VPS20 YTA12 YOP1	10	60
microtubule binding [GO:0008017]	0.009128	FIN1 BIM1 ALF1 IRC15 NIP100	5	20
GO Biological Process (2062 categories)				
mitochondrial translation [GO:0032543]	<1e-14	MRPL16 MRP21 MRPL36 MRPL37 MRPL11 RSM24 MRPL7 MRPL35 MRPS28 MRP1 MRPL25 MRPS35 RSM27 MRPL6 RSM25 MRPL49 RSM26 RSM22 MRPL38 MRPL13 MRPL20 MEF1 MRPL15 NAM2 MRPL4 MTG1 MRPL33 MRP7 MSK1 MRPL22 MRPL17 MRPL10 MRPS12 MSE1 MRPL23 PET123 TUF1 MRP51 MRPL40	39	88
translation [GO:0006412]	3.23E-09	RPL19B MRPL16 RPS8A MRP21 MTF2 MRPL7 MSW1 MRPS28 RPL12B RPL37B RPL12A RPL34A AIM10 RPL9A YGR102C MRPL9 RPL27A DIA4 RPS27B MRPL6 RSM25 MRPL49 CTK1 RSM22 MRPL38 MST1 MEF1 NAM2 MRPL4 RPS1A RPL6B RPL13B RPS16A MRPL33 MRP7 RPL16B MSK1 RPL42A MRPL22 MRPL10 RPS19B MRPS12 MSE1 MRPL23 TUF1 AIM41 RPS6A MSY1 MRPL40 RPL36B RPL43A	51	318
mitotic sister chromatid cohesion [GO:0007064]	1.42E-05	DCC1 MRC1 BIM1 CTF8 CSM3 TOF1 ELG1 CTF4 KAR3	9	24
protein lipoylation [GO:0009249]	2.06E-05	GCV3 AIM22 LIP2 LIP5	4	4
ubiquitin-dependent protein catabolic process via the multivesicular body sorting pathway [GO:0043162]	2.45E-05	UBC4 STP22 VPS25 VPS36 VPS20 SNF8 VPS28	7	15
establishment of mitotic spindle orientation [GO:0000132]	5.98E-05	DYN1 LDB18 CIK1 JNM1 BNI1 NIP100	6	12
mitochondrial genome maintenance [GO:0000002]	9.20E-05	MDM10 EXO5 RIM1 MDJ1 RPO41 ILM1 GEP5 ABF2 MGM1 RRG8	10	36
positive regulation of transcription elongation, DNA-dependent [GO:0032786]	0.0003062	CTK2 CTK1 CTK3	3	3
maintenance of DNA repeat elements [GO:0043570] *	0.0003062	MRC1 CSM3 TOF1	3	3
tRNA aminoacylation for protein translation [GO:0006418]	0.0003916	MSW1 AIM10 ARC1 DIA4 MST1 NAM2 MSK1 MSE1 MSY1	9	35
fatty acid biosynthetic process [GO:0006633]	0.000428	ETR1 CEM1 HTD2 HFA1 SCS7 MCT1 PPT2	7	22

Ontology	p- value	Genes in ontology category	k	f
signal peptide processing [GO:0006465]	0.0006101	AFG3 PCP1 SPC2 YTA12	4	7
'de novo' pyrimidine base biosynthetic process [GO:0006207]	0.0006101	URA2 URA1 URA4 URA5	4	7
negative regulation of transcription from RNA polymerase II promoter by glucose [GO:0000433]	0.0006101	VPS25 VPS36 SNF8 GCR1	4	7
acetyl-CoA biosynthetic process from pyruvate [GO:0006086]	0.001163	PDB1 PDX1 LAT1	3	4
establishment of mitotic sister chromatid cohesion [GO:0034087]	0.001651	CHL4 MCM21 CTF3 CSM3 CTF19	5	14
aerobic respiration [GO:0009060]	0.002263	ETR1 PET100 RIP1 RPO41 RMD9 COX13 QCR10 QCR8 ISF1 MCT1 QCR2	11	61
phospholipid biosynthetic process [GO:0008654]	0.002751	SCS22 CHO1 SCS2 CHO2 GEP4 INO1 PSD1 PDR17	8	37
inositol phosphate biosynthetic process [GO:0032958]	0.002762	KCS1 ARG82 VIP1	3	5
mRNA export from nucleus in response to heat stress [GO:0031990]	0.003108	ASM4 NUP120 NUP133 NUP188	4	10
meiosis [GO:0007126]	0.003726	TRS85 CHL4 ZIP1 MCM21 SPR6 AMA1 SWI6 NKP2 CTF3 CSM3 CIK1 CNM67 RAD50 TOF1 GAC1 MSC6 CTF19 KAR3	18	134
ascospore formation [GO:0030437]	0.004355	SHP1 UME6 SPT3 SPR6 AMA1 SET2 IRC19 UBI4 SUR7 RIM9	10	57
mitochondrial translational elongation [GO:0070125]	0.004553	MEF1 TUF1	2	2
zinc ion transmembrane transport [GO:0071577]	0.004553	ZRT1 ZRT2	2	2
negative regulation of Rho protein signal transduction [GO:0035024]	0.004553	BEM2 BEM3	2	2
cysteine biosynthetic process via cystathionine [GO:0019343]	0.004553	CYS3 CYS4	2	2
mitochondrial DNA replication [GO:0006264]	0.004553	RIM1 MIP1	2	2
replication fork arrest [GO:0043111]	0.004553	CSM3 TOF1	2	2
pyrimidine nucleotide biosynthetic process [GO:0006221]	0.004626	URA2 URA1 URA4 URA5	4	11
histone exchange [GO:0043486]	0.004626	SWC5 VPS72 VPS71 YAF9	4	11
mitochondrial electron transport, ubiquinol to cytochrome c [GO:0006122]	0.004626	RIP1 QCR10 QCR8 QCR2	4	11
mRNA transport [GO:0051028]	0.004953	ASM4 SAC3 KAP123 MOG1 NUP120 NUP133 NUP188 PML39 CBC2 NEW1	10	58
positive regulation of translational fidelity [GO:0045903]	0.005248	CTK2 CTK1 CTK3	3	6
DNA replication checkpoint [GO:0000076]	0.005248	MRC1 CSM3 TOF1	3	6
replication fork protection [GO:0048478]	0.005248	MRC1 CSM3 TOF1	3	6
protein targeting to vacuole [GO:0006623]	0.00537	STP22 VPS25 DID2 VPS33 VPS36 VPS71 SNF8 VPS28	8	41
piecemeal microautophagy of nucleus [GO:0034727]	0.005615	SHP1 ATG14 TRS85 ATG18 ATG1 VPS33 ATG4	7	33

Ontology	p- value	Genes in ontology category	k	f
mRNA 3'-end processing [GO:0031124]	0.008995	SAC3 CTK2 CTK1 CTK3	4	13
late endosome to vacuole transport [GO:0045324]	0.009128	STP22 ATG18 DID2 VPS20 VPS4	5	20
GO Cellular Component (625 categories)				
mitochondrial large ribosomal subunit [GO:0005762]	<1e-14	MRPL16 MRPL36 MRPL37 MRPL11 MRPL7 MRPL35 MRPL25 MRPL9 MRPL6 MRPL49 MRPL38 MRPL13 MRPL20 MRPL15 MRPL4 MRPL33 MRP7 MRPL22 MRPL17 MRPL10 MRPL23 MRPL40	22	43
mitochondrion [GO:0005739]	<1e-14	MDM10 GCV3 PIM1 MRPL16 MRP21 ETR1 YMC2 MRPL36 EXO5 FZO1 PDB1 MRPL37 RIM1 MTF2 MSS2 MRPL11 TPS2 PET100 NUM1 RSM24 MSS116 CBS2 COQ4 MRPL7 MSW1 MRPL35 MRPS28 MRP1 RIP1 CIN8 AFG3 CHO1 CEM1 AIM9 AIM10 PET122 OXA1 BEM2 MDJ1 RPO41 PUS2 MRH4 FMP37 RMD9 COX13 DOC1 MRPL25 PCP1 YGR102C CYS4 MRPS35 PDX1 RSM27 MRPL9 MTM1 QCR10 DIA4 HTD2 GEP4 MRPL6 YHR162W AIM18 RSM25 GTT1 PET130 AIM22 IML2 MRPL49 URA2 QCR8 CBF1 AIM25 RSM26 NFU1 OAC1 RSM22 MRPL38 MST1 MRPL13 PAM17 MRPL20 MEF1 ALT1 GEP5 QRI5 LIP2 YLR253W MRPL15 SSQ1 NAM2 ECM19 COX8 MRPL4 FMP27 SUR7 ATP18 ALO1 IMP2 SOV1 ABF2 YTA12 MTG1 IMP1 HFA1 MTF1 MRPL33 MRP7 POR1 LAT1 MSK1 LEU4 PSD1 MRPL22 RAD50 MRPL17 MRPL10 ATP11 MRPS12 COQ10 MSE1 CAT5 ELG1 MRPL23 PET123 TUF1 LIP5 MRM1 GEP3 MGM1 AIM41 MCT1 FSF1 RRG7 MIP1 MSC6 MSY1 MRP51 PPT2 MRPL40 PGC1 MMT2 NEW1 ISA2 RRG8 QCR2	145	1072
ribonucleoprotein complex [GO:0030529]	2.58E-12	RPL19B MRPL16 RPS8A MRP21 MRPL36 MRPL37 MRPL11 RSM24 MRPL7 MRPL35 MRPS28 MRP1 LSM6 RPL12B RPL37B RPL12A RPL34A RPL9A MRPL25 MRPS35 RSM27 MRPL9 RPL27A RPS27B MRPL6 RSM25 MSL1 MRPL49 RSM26 RSM22 MRPL38 MRPL13 MRPL20 MRPL15 MRPL4 RPS1A RPL6B RPL13B RPS16A MRPL33 MRP7 RPL16B LSM7 RPL42A MRPL22 MRPL17 MRPL10 RPS19B MRPS12 MRPL23 PET123 RPS6A MRP51 MRPL40 RPL36B RPL43A	56	307
ribosome [GO:0005840]	3.91E-12	RPL19B MRPL16 RPS8A MRP21 MRPL36 MRPL37 MRPL11 RSM24 MRPL7 MRPL35 MRPS28 MRP1 RPL12B RPL37B YEL043W RPL12A RPL34A RPL9A MRPL25 MRPS35 RSM27 MRPL9 RPL27A RPS27B MRPL6 RSM25 YJL028W MRPL49 RSM26 RSM22 MRPL38 MRPL13 MRPL20 MRPL15 MRPL4 RPS1A RPL6B PML39 RPL13B RPS16A MRPL33 MRP7 RPL16B RPL42A MRPL22 MRPL17 MRPL10 RPS19B MRPS12 MRPL23 PET123 RPS6A MRP51 MRPL40 RPL36B RPL43A	56	310
mitochondrial matrix [GO:0005759]	1.29E-08	PIM1 ETR1 PDB1 MTF2 MSS2 MSS116 MSW1 MDJ1 RPO41 PDX1 DIA4 GEP4 PET130 NFU1 MST1 ALT1 SSQ1 NAM2 MTF1 LAT1 MSK1 ATP11 MSE1 TUF1 MSY1 ISA2	26	111

Ontology	p- value	Genes in ontology category	k	f
mitochondrial small ribosomal subunit [GO:0005763]	7.49E-07	MRP21 RSM24 MRPS28 MRP1 MRPS35 RSM27 RSM25 RSM26 RSM22 MRPS12 PET123 MRP51	12	33
astral microtubule [GO:0000235]	6.48E-06	FIN1 CIN8 DYN1 LDB18 JNM1 NIP100	6	9
intracellular [GO:0005622]	0.0001325	LTE1 RPL19B MRPL16 RPS8A MRP21 NRP1 MRPL11 MRPL7 PEP7 MRPS28 RPL37B RPL34A BEM2 GYP8 RPL9A KEM1 MRPL9 RNH70 RPL27A RPS27B MRPL6 HYR1 MRPL49 GSH1 MEF1 SFP1 VPS36 RPS1A RPL6B MTG1 RPL13B RPS16A MRPL33 MRP7 RPL42A MRPL22 RPS19B MRPS12 GSH2 TUF1 RPS6A BEM3 MRPL40 RPL36B RPL43A	45	381
mitochondrial inner membrane [GO:0005743]	0.0002289	YMC2 FZO1 MSS2 PET100 COQ4 AFG3 PET122 OXA1 RMD9 COX13 PCP1 MTM1 QCR10 GEP4 QCR8 OAC1 PAM17 QRI5 COX8 IMP2 YTA12 MTG1 IMP1 PSD1 COQ10 CAT5 MGM1 QCR2	28	204
mitochondrial inner boundary membrane [GO:0097002]	0.0003062	AFG3 YTA12 MGM1	3	3
ESCRT II complex [GO:0000814]	0.0003062	VPS25 VPS36 SNF8	3	3
carboxy-terminal domain protein kinase complex [GO:0032806]	0.0003062	CTK2 CTK1 CTK3	3	3
microtubule [GO:0005874]	0.0006731	CIN8 BIM1 KEM1 DYN1 CIK1 JNM1 ALF1 PAC1 IRC15 NIP100 KAR3	11	53
spindle pole body [GO:0005816]	0.0009183	FIN1 KRE28 BIM1 DBF2 DYN1 LDB18 NKP2 CIK1 JNM1 CNM67 NIP100 CLB2 KAR3	13	72
kinetochore [GO:0000776]	0.001138	CHL4 MCM21 KRE28 BIM1 SPT4 BUB1 CBF1 NKP2 CTF3 CTF19	10	48
mitochondrial pyruvate dehydrogenase complex [GO:0005967]	0.001163	PDB1 PDX1 LAT1	3	4
cell cortex [GO:0005938]	0.001547	NUM1 BEM2 DYN1 LDB18 SUR7 JNM1 BEM3 NIP100	8	34
cytoplasmic microtubule [GO:0005881]	0.001651	BIM1 DYN1 CIK1 PAC1 KAR3	5	14
dynactin complex [GO:0005869]	0.002762	LDB18 JNM1 NIP100	3	5
mitochondrial respiratory chain complex III [GO:0005750]	0.003108	RIP1 QCR10 QCR8 QCR2	4	10
large ribosomal subunit [GO:0015934]	0.003218	MRPL38 MRPL33 RPL16B MRPL22 MRPL10	5	16
condensed nuclear chromosome kinetochore [GO:0000778]	0.003284	FIN1 MCM21 KRE28 CIN8 BUB1 CTF3 BUB3 CTF19	8	38
m-AAA complex [GO:0005745]	0.004553	AFG3 YTA12	2	2
mitochondrial DNA-directed RNA polymerase complex [GO:0034245]	0.004553	RPO41 MTF1	2	2
cytosolic large ribosomal subunit [GO:0022625]	0.0058	RPL19B RPL12B RPL37B RPL12A RPL34A RPL9A RPL27A RPL6B RPL13B RPL16B RPL42A RPL36B RPL43A	13	88
extrinsic to mitochondrial inner membrane [GO:0031314]	0.00724	MSS2 CBS2 MDJ1 RMD9 MGM1	5	19
dynein complex [GO:0030286]	0.008727	DYN1 JNM1 NIP100	3	7

Ontology	p- value	Genes in ontology category	k	f
Swr1 complex [GO:0000812]	0.008995	SWC5 VPS72 VPS71 YAF9	4	13
MIPS Functional Classification (459 categories)				
mitochondrion [42.16]	<1e-14	MDM10 MRPL16 MRP21 MRPL36 FZO1 MRPL37 MRPL11 RSM24 MSS116 MRPL7 MRPL35 MRPS28 MRP1 RPO41 MRH4 MRPL25 PCP1 MRPS35 RSM27 MRPL9 MRPL6 RSM25 MRPL49 RSM26 RSM22 MRPL38 MRPL13 PAM17 MRPL20 MRPL15 MRPL4 ABF2 MTF1 MRPL33 MRP7 POR1 MRPL22 MGS1 MRPL17 MRPL10 ATP11 MRPS12 MRPL23 PET123 MGM1 MRP51 MRPL40	47	170
ribosomal proteins [12.01.01]	<1e-14	RPL19B MRPL16 RPS8A MRP21 MRPL36 MRPL37 MRPL11 RSM24 MRPL7 MRPL35 MRPS28 MRP1 RPL12B RPL37B RPL12A RPL34A RPL9A MRPL25 MRPS35 RSM27 MRPL9 RPL27A RPS27B MRPL6 RSM25 MRPL49 RSM26 RSM22 MRPL38 MRPL13 MRPL20 MRPL15 MRPL4 RPS1A RPL6B RPL13B RPS16A MRPL33 MRP7 RPL16B RPL42A MRPL22 MRPL17 MRPL10 RPS19B MRPS12 MRPL23 PET123 RPS6A MRP51 MRPL40 RPL36B RPL43A	53	246
aerobic respiration [02.13.03]	0.0001582	ETR1 PET100 RSM24 RIP1 COX13 MRPS35 QCR10 DIA4 QCR8 COX8 ISF1 POR1 MRPL22 MCT1 QCR2	15	77
vacuolar/lysosomal transport [20.09.13]	0.0005584	UBC4 STP22 PEP7 VPS72 GYP8 ATG18 ATG1 VMA7 CLC1 VPS25 LST4 DID2 VPS33 VPS36 VMA6 VPS71 VPS20 ATG4 VPS75 SNF8 VPS28 VPS4	22	153
aminoacyl-tRNA-synthetases [12.10]	0.0009229	MSW1 AIM10 ARC1 DIA4 MST1 NAM2 MSK1 MSE1 MSY1	9	39
cytoskeleton-dependent transport [20.09.14]	0.002086	CIN8 DYN1 CIK1 JNM1 ATG4 NIP100 KAR3	7	28
pyruvate dehydrogenase complex [02.08]	0.002762	PDB1 PDX1 LAT1	3	5
DNA synthesis and replication [10.01.03]	0.003116	MRC1 HTL1 RIM1 RPO41 RNR4 RNH70 CBF1 SWI6 SSQ1 CSM3 ABF2 ELG1 CTF4	13	82
protein binding [16.01]	0.004919	UBC4 UMP1 STP22 PET100 FIN1 NUM1 SAC3 TRM82 MCM21 SCS2 MDJ1 CDC26 YRB30 BUB1 PDX1 CPR7 LIA1 MOG1 CAP1 PAM17 ENT4 UBI4 SWI6 SSQ1 CTF3 SST2 SPC2 UBC7 SRV2 ALF1 ATG4 RAD50 BNI1 ATP11 CIN1 SNX3 CTF19 SSE1 NIP100 YOP1	40	391
M phase [10.03.01.01.11]	0.006443	SAC3 CIN8 CDC26 DOC1 DYN1 CIK1 JNM1 NIP100 KAR3	9	51
protein targeting, sorting and translocation [14.04]	0.007891	STP22 ASM4 SAC3 PEP7 PEX3 VPS72 KAP123 SCS2 ATG18 MOG1 VPS25 NUP120 LST4 DID2 NUP133 VPS33 VPS36 UBX2 VPS71 NUP188 IMP2 IMP1 YDJ1 ATG4 VPS75 COQ10 SNX3 SNF8 VPS28 VPS4	30	281
MIPS Phenotypes (142 categories)				
Slow-growth (slg) [12.15]	4.34E-09	MDM10 RPL19B SHP1 FZO1 BUD23 BUD31 SAC3 HMO1 UME6 MNN10 PEP7 BIM1 BEM2 ARC1 KEM1 ZRT1 SPT4 CLC1 RNR4 PRS3 RPL27A HTD2 MET18 MSL1 GTT1 CTK2 GSH1 CPR7 NUP120 CTK1 NUP133 RSC2 SSQ1 SFP1 CTK3 IES2 CNM67 MRPL17 GSH2 BUB3 SSE1 QCR2	42	237

Ontology	p- value	Genes in ontology category	k	f
Respiratory deficiency [42.25.20]	9.54E-09	PIM1 FZO1 MRPL11 PET100 MRPS28 MRP1 RIP1 AFG3 PET122 OXA1 MDJ1 COX13 RNR4 MRPL6 PET130 SSQ1 NAM2 MRPL4 ATP18 ABF2 YTA12 MTF1 MRP7 POR1 CAT5 PET123 LIP5 MRM1 MCT1 MIP1 MSY1 MRP51 PPT2 QCR2	34	173
Mitochondrial mutants [52.55]	4.08E-07	MDM10 PIM1 ETR1 FZO1 MRPS28 MRP1 RPO41 QCR10 QCR8 SSQ1 ATP18 PET123 MGM1	13	37
benomyl sensitivity [52.30.05.10]	4.03E-05	CHL4 BIM1 BEM2 KEM1 RNR4 CBF1 DYN1 ALF1 CIN1 CTF19	10	33
Divalent cations and heavy metals sensitivity [62.35.02]	0.005418	UBC4 BUD23 PEP7 AFT1 ZRT1 DBF2 GSH1 VMA6 UBC7 CUP9 VPS4	11	68
MIPS Subcellular Localization (48 categories)				
mitochondria [755]	<1e-14	MDM10 GCV3 PIM1 MRPL16 MRP21 ETR1 YMC2 MRPL36 ATG14 EXO5 FZO1 PDB1 MRPL37 RIM1 MTF2 MSS2 MRPL11 YDR008C TPS2 PET100 YDR149C NUM1 RSM24 MSS116 CBS2 COQ4 MRPL7 MSW1 MRPL35 MRPS28 MRP1 RIP1 CIN8 AFG3 CHO1 CEM1 AIM9 PET122 OXA1 BEM2 MDJ1 GYP8 RPO41 MRH4 FMP37 RMD9 COX13 DOC1 MRPL25 PCP1 YGR102C CYS4 MRPS35 PDX1 RSM27 MRPL9 MTM1 QCR10 DIA4 HTD2 GEP4 MRPL6 YHR162W AIM18 RSM25 GTT1 PET130 YJL055W IML2 MRPL49 URA2 QCR8 CBF1 AIM25 RSM26 NFU1 OAC1 RSM22 MRPL38 MST1 MRPL13 PAM17 MRPL20 MEF1 ALT1 GEP5 QRI5 LIP2 YLR253W MRPL15 SSQ1 NAM2 ECM19 COX8 MRPL4 FMP27 SUR7 ATP18 ALO1 IMP2 SOV1 ABF2 YTA12 MTG1 IMP1 HFA1 MTF1 MRPL33 MRP7 POR1 LAT1 MSK1 LEU4 PSD1 MRPL22 RAD50 MRPL17 MRPL10 ATP11 MRPS12 MSE1 CAT5 ELG1 MRPL23 PET123 TUF1 LIP5 MRM1 GEP3 MGM1 AIM41 MCT1 FSF1 RRG7 MIP1 MSC6 MSY1 MRP51 MRPL40 PGC1 MMT2 NEW1 ISA2 RRG8 QCR2	145	1042
mitochondrial matrix [755.07]	2.30E-08	GCV3 PIM1 MRPL16 MRP21 MRPL36 PDB1 MRPL37 RIM1 MRPL11 MSS116 RSM27 RSM25 MRPL49 RSM26 NFU1 LIP2 ABF2 MRPL22 MRP51 ISA2	20	71
mitochondrial inner membrane [755.05]	2.00E-05	YMC2 MSS2 CBS2 COQ4 RIP1 AFG3 PET122 OXA1 MDJ1 COX13 PCP1 MTM1 QCR10 QCR8 OAC1 PAM17 COX8 ATP18 IMP2 YTA12 IMP1 PSD1 COQ10 CAT5 QCR2	25	150
spindle pole body [730.05]	0.0003269	FIN1 MCM21 KRE28 CIN8 BUB1 DYN1 NKP2 CTF3 CIK1 JNM1 CNM67 CTF19 NIP100 CLB2 KAR3	15	82
tubulin cytoskeleton [730.03]	0.002751	CHL4 CIN8 BIM1 BUB1 DYN1 CIK1 JNM1 KAR3	8	37
MIPS Protein Complexes (1142 categories)				
mitochondrial ribosomal large subunit [500.60.10]	<1e-14	MRPL16 MRPL36 MRPL37 MRPL11 MRPL7 MRPL35 MRPL25 MRPL9 MRPL6 MRPL49 MRPL38 MRPL13 MRPL20 MRPL15 MRPL4 MRPL33 MRP7 MRPL22 MRPL17 MRPL10 MRPL23 MRPL40	22	44

Ontology	p- value	Genes in ontology category	k	f
Complex Number 108, probably protein synthesis turnover [550.1.108]	4.29E-08	MRPL16 MRPL36 MRPL7 MRPL35 BEM2 MRH4 MRPL25 MRPL9 MRPL6 MRPL13 MRPL20 MRPL4 MRP7 MRPL17 MRPL10 MRPL23 MRM1	17	54
mitochondrial ribosomal small subunit [500.60.20]	2.90E-06	MRP21 RSM24 MRPS28 MRP1 MRPS35 RSM27 RSM25 RSM26 RSM22 PET123 MRP51	11	31
Complex Number 104, probably protein synthesis turnover [550.1.104]	7.62E-06	MRP21 RSM24 MRPS28 MRP1 BEM2 RSM27 RSM25 RSM26 RSM22 PET123 GEP3 MRP51	12	40
TFIIK (CTD kinase) [510.110]	0.0003062	CTK2 CTK1 CTK3	3	3
Ctk1p complex [133.50]	0.0003062	CTK2 CTK1 CTK3	3	3
Complex Number 221, probably transcription/DNA maintenance/chromatin structure [550.1.221]	0.001155	CHL4 MCM21 CTF3 CTF19	4	8
Complex Number 215, probably transcription/DNA maintenance/chromatin structure [550.1.215]	0.001163	CTK2 CTK1 CTK3	3	4
Complex Number 9, probably cell cycle [550.1.9]	0.001651	SHP1 MRPS28 RAI1 DOA1 BNI1	5	14
Pyruvate dehydrogenase [390]	0.002762	PDB1 PDX1 LAT1	3	5
cytoplasmic ribosomal large subunit [500.40.10]	0.002789	RPL19B RPL12B RPL37B RPL12A RPL34A RPL9A RPL27A RPL6B RPL13B RPL16B RPL42A RPL36B RPL43A	13	81
Cytochrome bc1 complex (Ubiquinol-cytochrome c reductase complex, complex III) [420.30]	0.003108	RIP1 QCR10 QCR8 QCR2	4	10
Inner membrane protease [350.20]	0.004553	IMP2 IMP1	2	2
m-AAA protease complex [350.10.10]	0.004553	AFG3 YTA12	2	2

*in S. cerevisiae the three genes coding for components of the Mrc1/Csm3/Tof1 complex are listed under GO:0043570

Table 2. List of ontologies enriched among the 138 synthetic sick and lethal genetic interactors unique to *FPR4*

Ontology	p- value	Genes in ontology category	k	f
GO Molecular Function (1646 categories)				
S-adenosylmethionine-dependent methyltransferase activity [GO:0008757]	0.007848	YBR271W OMS1 CRG1	3	20
GO Biological Process (2062 categories)				
replicative cell aging [GO:0001302]	0.001206	FOB1 SNF1 LAG1 GUT2 DNL4	5	39
regulation of carbohydrate metabolic process [GO:0006109]	0.002531	REG1 SNF1	2	4
mitochondrion degradation [GO:0000422]	0.002891	SNX4 ATG17 ATG3 ATG29	4	29
piecemeal microautophagy of nucleus [GO:0034727]	0.00467	SNX4 ATG17 ATG3 ATG29	4	33
positive regulation of transcription, DNA-dependent	0.007848	SNF5 HAC1 SNF2	3	20

Ontology	p- value	Genes in ontology category	k	f
[GO:0045893]				
GO Cellular Component (625 categories)				
membrane [GO:0016020]	2.35E-05	DRS2 FUR4 MBA1 YBR196C-A YCP4 CPR4 SNQ2 MTC5 OMS1 HXT3 YDR348C ATP22 SNF1 QCR7 SHC1 TPN1 MDM34 LAG1 YHK8 IRE1 TOM71 YHR140W GVP36 YIL092W GUT2 SNX4 JEM1 YJL127C-B TRK1 YJL163C CPS1 YJL193W YJR054W APS2 ENT3 AIM27 PTR2 ARV1 PRM6 YMR010W TVP18 YNL058C RHO2 YCK2 ASI2 BOR1 PHO91 PEX15 YOL075C SHR5 FRE7 PEP12 CYT1 ALE1 COA2 OPY2 AQY1	57	1671
integral to membrane [GO:0016021]	0.0054	DRS2 FUR4 YBR196C-A CPR4 SNQ2 OMS1 HXT3 QCR7 TPN1 MDM34 LAG1 YHK8 IRE1 TOM71 YHR140W YIL092W YJL127C-B TRK1 YJL163C CPS1 YJL193W YJR054W AIM27 PTR2 ARV1 PRM6 YMR010W TVP18 YNL058C ASI2 BOR1 PHO91 PEX15 YOL075C FRE7 PEP12 CYT1 ALE1 OPY2 AQY1	40	1303
membrane raft [GO:0045121]	0.006773	FUR4 YCP4 TRK1	3	19
MIPS Functional Classification (459 categories)				
regulation of C-compound and carbohydrate metabolism [01.05.25]	0.004706	SNF5 REG1 SNF1 HAP2 RHO2 SHR5 SNF2 PHO85	8	126
MIPS Protein Complexes (1142 categories)				
NOT complex [510.190.40]	0.004161	NOT3 NOT5	2	5
Complex Number 540 [550.2.540]	0.008501	PET112 SNF1	2	7
Complex Number 198, probably transcription/DNA maintenance/chromatin structure [550.1.198]	0.009017	SNF5 YJL016W SNF2	3	21

Table 3. List of ontologies enriched among the 78 synthetic sick and lethal genetic interactors common to *FPR3* and *FPR4*.

Ontology	p- value	Genes in ontology category	k	f
GO Molecular Function (1646 categories)				
basic amino acid transmembrane transporter activity [GO:0015174]	0.001953	CAN1 ALP1	2	6
alpha-1,6-mannosyltransferase activity [GO:0000009]	0.003591	MNN11 HOC1	2	8
histone acetyltransferase activity [GO:0004402]	0.003647	NGG1 ADA2 GCN5	3	27
GO Biological Process (2062 categories)				
intralumenal vesicle formation [GO:0070676]	1.50E-05	DID4 VPS24 SNF7	3	5
ubiquitin-dependent protein catabolic process via the	2.12E-05	DOA4 DID4 VPS24 SNF7	4	15

Ontology	p- value	Genes in ontology category	k	f
multivesicular body sorting pathway [GO:0043162]				
septin checkpoint [GO:0000135]	0.0007933	ELM1 HSL1	2	4
late endosome to vacuole transport [GO:0045324]	0.001507	DID4 VPS24 SNF7	3	20
basic amino acid transport [GO:0015802]	0.002714	CAN1 ALP1	2	7
protein autophosphorylation [GO:0046777]	0.005685	ELM1 HSL1	2	10
mitochondrial proton-transporting ATP synthase complex assembly [GO:0033615]	0.005685	FMC1 ATP25	2	10
Group I intron splicing [GO:0000372]	0.005685	CBP2 SUV3	2	10
cell wall mannoprotein biosynthetic process [GO:0000032]	0.008214	LDB7 HOC1	2	12
GO Cellular Component (625 categories)				
ESCRT III complex [GO:0000815]	6.05E-06	DID4 VPS24 SNF7	3	4
Ada2/Gcn5/Ada3 transcription activator complex [GO:0005671]	1.50E-05	NGG1 ADA2 GCN5	3	5
mitochondrion [GO:0005739]	0.0007932	FUN12 LDB16 VPS54 DOA4 ATP5 SOM1 CAN1 LPD1 MRM2 COX18 MRP4 CBP2 YIA6 FMC1 SOD1 RPL40B UPS1 OGG1 ATP25 MDM32 TUM1 AEP3 SUV3 SMK1	24	1072
SLIK (SAGA-like) complex [GO:0046695]	0.0009218	NGG1 ADA2 GCN5	3	17
SAGA complex [GO:0000124]	0.001507	NGG1 ADA2 GCN5	3	20
endosome [GO:0005768]	0.001541	VPS54 DOA4 DID4 VPS24 SNF7 BRO1	6	108
alpha-1,6-mannosyltransferase complex [GO:0000136]	0.001953	MNN11 HOC1	2	6
mitochondrial inner membrane [GO:0005743]	0.002444	ATP5 SOM1 COX18 YIA6 UPS1 ATP25 MDM32 AEP3	8	204
mediator complex [GO:0016592]	0.003269	SOH1 SRB2 CSE2	3	26
endosome membrane [GO:0010008]	0.004231	VPS54 DID4 VPS24 SNF7	4	57
membrane [GO:0016020]	0.005501	LDB16 CDC10 FEN2 YET3 VPS54 DOA4 VPS64 ATP5 SOM1 CAN1 COX18 CHS7 NVJ1 YIA6 MNN11 HOC1 DID4 VPS24 SNF7 YPS1 UPS1 ATP25 YNL095C ALP1 ERG24 PFA4 YOR008C-A MDM32 AEP3 KRE6	30	1671
site of polarized growth [GO:0030427]	0.006897	MSB2 KRE6	2	11
MIPS Functional Classification (459 categories)				
vacuolar/lysosomal transport [20.09.13]	0.001934	VPS64 VPS3 DID4 VPS24 SNF7 ATG2 BRO1	7	153
MIPS Phenotypes (142 categories)				
3-Aminotriazole sensitivity [92.25.10]	0.001953	FEN2 GCN5	2	6
Heat-sensitivity (ts) [12.05]	0.003223	CDC10 FEN2 NGG1 ADA2 GCN5 SRB2 HIT1 SNF7 CSE2 BRO1	10	313

Ontology	p- value	Genes in ontology category	k	f
MIPS Subcellular Localization (48 categories)				
endosome [765]	0.0004934	DOA4 DID4 VPS24 SNF7 BRO1	5	57
vacuole [770]	0.001098	FEN2 VPS3 CAN1 MSB2 CHS7 DID4 SNF7 BRO1 KRE6	9	224
mitochondria [755]	0.006764	FUN12 LDB16 VPS54 DOA4 ATP5 SOM1 CAN1 LPD1 COX18 MRP4 CBP2 FMC1 SOD1 RPL40B UPS1 ATP25 MDM32 TUM1 AEP3 SUV3 SMK1	21	1042
MIPS Protein Complexes (1142 categories)				
ADA complex [510.190.10.10]	2.97E-05	NGG1 ADA2 GCN5	3	6
ADA complex [230.20.10]	2.97E-05	NGG1 ADA2 GCN5	3	6
Vps4p ATPase complex (Vps protein complex) [260.70]	0.0003997	VPS24 SNF7	2	3
SAGA complex [510.190.10.20.10]	0.0007656	NGG1 ADA2 GCN5	3	16
SAGA complex [230.20.20]	0.0007656	NGG1 ADA2 GCN5	3	16
Complex Number 209, probably transcription/DNA maintanance/chromatin structure [550.1.209]	0.001495	ADA2 GCN5 SRB2 CSE2	4	43
Complex Number 33 [550.2.33]	0.002714	CDC10 LPD1	2	7
Complex Number 207, probably transcription/DNA maintanance/chromatin structure [550.1.207]	0.00405	NGG1 ADA2 GCN5	3	28
Complex Number 112 [550.2.112]	0.004583	ADA2 GCN5	2	9
Complex Number 42, probably intermediate and energy metabolism [550.1.42]	0.009634	DOA4 LPD1	2	13

Table 4. List of ontologies enriched among the 75 masked synthetic sick and lethal genetic interactors of *FPR3* and *FPR4*.

Ontology	p- value	Genes in ontology category	k	f
GO Biological Process (2062 categories)				
mitochondrial membrane organization [GO:0007006]	0.0001239	CRD1 CYC2	2	2
nuclear polyadenylation-dependent snRNA catabolic process [GO:0071037]	0.001212	AIR1 TRF5	2	5
nuclear polyadenylation-dependent snoRNA catabolic process [GO:0071036]	0.001212	AIR1 TRF5	2	5
ncRNA polyadenylation [GO:0043629]	0.001212	AIR1 TRF5	2	5
fructose metabolic process [GO:0006000]	0.001805	HXK2 PFK27	2	6
cellular calcium ion homeostasis [GO:0006874]	0.004239	CSG2 GET1	2	9
mitochondrial proton-transporting ATP synthase complex assembly [GO:0033615]	0.005261	ATP12 ATP10	2	10

Ontology	p- value	Genes in ontology category	k	f
nuclear polyadenylation-dependent CUT catabolic process [GO:0071039]	0.005261	AIR1 TRF5	2	10
GO Cellular Component (625 categories)				
TRAMP complex [GO:0031499]	0.001805	AIR1 TRF5	2	6
MIPS Functional Classification (459 categories)				
assembly of protein complexes [14.10]	0.006631	TOM1 CUL3 ATP12 APL1 ATP10 ASI1 CYC2	7	199
MIPS Phenotypes (142 categories)				
other carbohydrate and lipid biosynthesis defects [72.99]	0.007401	CSG2 CRD1 FAA2	3	36
MIPS Subcellular Localization (48 categories)				
mitochondria [755]	0.004097	PSY4 CRD1 FAA2 YER140W YFR045W PIB2 NCS6 CUL3 GND1 ATP12 MCR1 LOS1 ATP10 ADH3 PGM3 CYC2 YOR114W MSB1 ISU1 ATP20 TOM5	21	1042
MIPS Protein Complexes (1142 categories)				
Complex Number 78, probably membrane biogenesis and traffic [550.1.78]	0.005261	APS3 APL1	2	10

Gene ontology analysis of suppressor genetic interactors

Ontologies enriched among the unique, cooperative, and masked suppressor genetic interactors of *FPR3* and *FPR4* are presented in the tables below (Table 5, Table 6, Table 7, and Table 8).

Lists of ontologies were generated by the FunSpec web-based cluster interpreter for yeast (http://funspec.med.utoronto.ca/)[372]. This program outputs a summary of ontologies significantly enriched in a given input list of yeast genes using ontology annotations from the Gene Ontology Consortium (GO) database[421] and from the Munich Information Center for Protein Sequences (MIPS) database[422].

Ontologies in this analysis were classified by molecular function, biological process, cellular component, MIPS functional classification, MIPS phenotypes, MIPS subcellular localization, and MIPS protein complexes. The *p*-values associated with each ontology were calculated automatically by FunSpec using hypergeometric distribution, they represent the probability that the intersection of a given list of genes with any ontology occurs by chance.

Only ontology categories with *p*-values≤0.01 are presented in the following lists. Bonferroni correction was not applied.

k: number of input genes in ontology category
f: total number of genes in ontology category

Table 5. Ontologies enriched among the 218 suppressor genetic interactors unique to *FPR3*

Ontology	p- value	Genes in ontology category	k	f
GO Molecular Function (1646 categories)				
methylated histone residue binding [GO:0035064]	0.0001147	JHD1 BYE1 SET3 SPP1	4	9
histone methyltransferase activity (H3-K4 specific) [GO:0042800]	0.001622	SWD1 BRE2 SPP1	3	8
GO Biological Process (2062 categories)				
chromatin silencing at telomere [GO:0006348]	0.0004758	SWD1 DPB3 ASF1 BRE2 IES3 ESC1 RTT106 SPP1	8	58
histone H3-K4 methylation [GO:0051568]	0.002375	SWD1 BRE2 SPP1	3	9
regulation of protein localization [GO:0032880]	0.005792	BUD14 SCH9 PHO85	3	12
aromatic amino acid family biosynthetic process [GO:0009073]	0.005792	ARO4 PHA2 ARO7	3	12
positive regulation of macroautophagy [GO:0016239]	0.005899	PCL1 PHO85	2	4
regulation of establishment or maintenance of cell polarity [GO:0032878]	0.005899	PCL1 PHO85	2	4

Ontology	p- value	Genes in ontology category	k	f
regulation of transcription, DNA-dependent [GO:0006355]	0.005985	SWD1 BUD14 ISW1 MET32 MIG3 JHD1 IES1 PUF4 NUT1 IRE1 IKI1 ASF1 BYE1 SET3 IES3 ARG80 ESC1 RTT106 DAL82 ESC8 MSN1 HIR2 STD1 ETT1 AZF1 SPP1 HDA3	27	507
negative regulation of transcription from RNA polymerase II promoter [GO:0000122]	0.009462	MIG3 BYE1 RTT106 LAP3 PHO85 HDA3	6	57
DNA replication-dependent nucleosome assembly [GO:0006335]	0.009624	ASF1 RTT106	2	5
regulation of fungal-type cell wall organization [GO:0060237]	0.009624	SSD1 MSG5	2	5
DNA replication-independent nucleosome assembly [GO:0006336]	0.009624	ASF1 HIR2	2	5
negative regulation of glycogen biosynthetic process [GO:0045719]	0.009624	PSK2 PHO85	2	5
GO Cellular Component (625 categories)				
fungal-type vacuole membrane [GO:0000329]	0.0003741	SSA1 SLM4 YBR241C VPS41 FAB1 MON1 TPO2 SCH9 MEH1 NYV1 PFA3 YVC1	12	118
Set1C/COMPASS complex [GO:0048188]	0.001622	SWD1 BRE2 SPP1	3	8
EGO complex [GO:0034448]	0.003013	SLM4 MEH1	2	3
anchored to membrane [GO:0031225]	0.003187	FLO1 ECM33 MKC7 YDR524C-B DSE2 GAS3 DFG5	7	61
vacuole [GO:0005773]	0.005726	SLM4 YBR241C VPS41 VAB2 FAB1 MON1 MEH1 NYV1 YPT7 PFA3 YVC1 RNY1	12	162
GSE complex [GO:0034449]	0.009624	SLM4 MEH1	2	5
MIPS Functional Classification (459 categories)				
posttranslational modification of amino acids (e.g. hydroxylation, methylation) [14.07.09]	0.001233	SWD1 PPM1 JHD1 BRE2 SPP1	5	26
cell wall [42.01]	0.001288	ECM1 GDH3 ECM33 PPH22 LRG1 SSD1 KRE2 ECM10 SKN1 ECM29 DSE2 ECM25 OSW2 GAS3 DFG5 MSN1	16	213
C-compound and carbohydrate metabolism [01.05]	0.002075	PMT2 BDH2 YAT1 YBL086C IFA38 KRE2 ATF2 GND2 IRE1 DSE2 BCH2 PSK2 ALG6 STD1 SPR1 PNG1	16	223
DNA conformation modification (e.g. chromatin) [10.01.09.05]	0.002782	SWD1 ISW1 DPB3 JHD1 IES1 SPO13 SET3 BRE2 IES3 YKU80 ESC1 ESC8 SPP1 HDA3	14	188
modification by phosphorylation, dephosphorylation, autophosphorylation [14.07.03]	0.006651	PPH22 CKB1 IRE1 SCH9 TPK1 SWE1 PRR1 SAP190 KNS1 PPZ1 MSG5 PSK2 PHO85	13	186
cell growth / morphogenesis [40.01]	0.00758	BUD14 BOI1 RVS161 PPH22 SSD1 BMH1 CKB1 NCS6 RSR1 FAR1 SWE1 DFG5 RNY1	13	189
MIPS Phenotypes (142 categories)				
Calcofluor white sensitivity [52.15.15.10]	0.007508	ECM1 GDH3 ECM33 KRE2 ECM10 ECM29 ECM25 MSN1	8	89

Ontology	p- value	Genes in ontology category	k	f
Rapamycin resistance [112.30.05]	0.009624	FPR1 RRD2	2	5
MIPS Protein Complexes (1142 categories)				
Complex Number 199, probably transcription/DNA maintenance/chromatin structure [550.1.199]	0.002375	SWD1 BRE2 SPP1	3	9
Complex Number 29 [550.2.29]	0.007354	SSD1 ECM10 SEC28	3	13
Gim complexes [177]	0.009624	GIM5 GIM3	2	5

Table 6. Ontologies enriched among the 232 suppressor genetic interactors unique to *FPR4*

Ontology	p- value	Genes in ontology category	k	f
GO Molecular Function (1646 categories)				
structural constituent of ribosome [GO:0003735]	8.08E-08	RPL23A RPS11B MRPL36 IMG2 RPP1A RPS11A RPL29 RPL24A MRPL25 RPL17B RPS14B RPS4A RPL14A RPL22A RPS17A RPS18B RPS16A RPL20A MRP7 RPL9B RPL42A RPP2A RPS6A RPL36B RPL43A	25	218
GO Biological Process (2062 categories)				
translation [GO:0006412]	9.69E-06	RPL23A RPS11B SLM5 IMG2 RPP1A SSB1 RPS11A AIM10 RPL29 RPL24A RPL17B RPS14B RPS4A RPL14A RPL22A NAM2 RPS17A RPS18B RPS16A RPL20A MRP7 RPL9B RPL42A RPP2A RPS6A RPL36B RPL43A	27	318
ribosomal small subunit assembly [GO:0000028]	6.99E-05	RPS11B RPS11A NSR1 RPS14B RPS17A	5	14
cysteine biosynthetic process via cystathionine [GO:0019343]	0.001166	CYS3 CYS4	2	2
ribosomal protein import into nucleus [GO:0006610]	0.002852	NUP84 SEH1 NUP120	3	9
snRNA export from nucleus [GO:0006408]	0.002852	NUP84 SEH1 NUP120	3	9
snRNP protein import into nucleus [GO:0006608]	0.002852	NUP84 SEH1 NUP120	3	9
vesicle fusion with vacuole [GO:0051469]	0.00342	VPS33 VAM3	2	3
tRNA export from nucleus [GO:0006409]	0.004203	NUP84 SEH1 NUP120 SOL1	4	20
mRNA-binding (hnRNP) protein import into nucleus [GO:0006609]	0.005325	NUP84 SEH1 NUP120	3	11
chromosome localization [GO:0050000]	0.006686	NUP84 NUP120	2	4
positive regulation of catalytic activity [GO:0043085]	0.006686	PTC6 PTC5	2	4
transsulfuration [GO:0019346]	0.006686	CYS3 CYS4	2	4
mitotic sister chromatid cohesion [GO:0007064]	0.008282	CTF8 TOP3 CSM3 KAR3	4	24
GO Cellular Component (625 categories)				

Ontology	p- value	Genes in ontology category	k	f
ribonucleoprotein complex [GO:0030529]	1.45E-07	RPL23A RPS11B MRPL36 IMG2 RPP1A RPS11A LSM6 RPL29 RPL24A MRPL25 MSL1 LSM1 RPL17B RPS14B TMA22 RPS4A RPL14A RPL22A RPS17A RPS18B RPS16A RPL20A MRP7 RPL9B LSM7 RPL42A RPP2A RPS6A RPL36B RPL43A	30	307
ribosome [GO:0005840]	6.05E-07	RPL23A RPS11B MRPL36 IMG2 RPP1A RPS11A TMA64 YDR186C RPL29 RPL24A MRPL25 MTC1 RPL17B RPS14B TMA22 RPS4A RPL14A RPL22A RPS17A RPS18B RPS16A RPL20A MRP7 RPL9B RPL42A RPP2A RPS6A RPL36B RPL43A	29	310
cytosolic large ribosomal subunit [GO:0022625]	7.72E-06	RPL23A RPP1A RPL29 RPL24A RPL17B RPL14A RPL22A RPL20A RPL9B RPL42A RPP2A RPL36B RPL43A	13	88
cytosolic small ribosomal subunit [GO:0022627]	0.001141	RPS11B RPS11A RPS14B RPS4A RPS17A RPS18B RPS16A RPS6A	8	62
intracellular [GO:0005622]	0.001209	RPS11B IMG2 RPP1A NRP1 RPS11A RPL29 RPL17B RPS14B RPS4A RPL14A APN1 RPL22A BUD20 ROM2 SFP1 RPS17A RPS18B RPS16A MRP7 RPL9B RPL42A RPP2A RPS6A RPL36B RPL43A	25	381
Nup107-160 complex [GO:0031080]	0.001251	NUP84 SEH1 NUP120	3	7
vacuolar lumen [GO:0005775]	0.00342	ATG15 SNA3	2	3
cytoplasm [GO:0005737]	0.004406	CYS3 DEP1 FUS3 RPL23A RTG3 RPS11B PEX34 SLM5 YDL063C RPP1A NRP1 SSB1 PHO13 TRP1 KCS1 RPS11A TPI1 HMO1 YDR186C CRF1 LSM6 GRX2 KRE28 AIM10 RIM15 RPL29 RPL24A AFT1 ARC1 CYS4 RNR4 PRS3 ARD1 VPS53 IML2 MTC1 LSM1 RPL17B RPS14B UBP12 TMA22 HIT1 URA8 RPS4A YJR154W RPL14A DID2 UBR2 AAT2 RPL22A YKE2 LIP2 NMA1 YLR345W NAM2 SFP1 BER1 ATG23 RPS17A RPS18B CTK3 MUB1 RPS16A RPL20A RPL9B YAF9 NCS2 SRV2 LSM7 RPL42A BNI1 SMM1 SOL1 RPP2A ARP8 SER1 VTS1 RPS6A RDS2 BEM4 NEW1 YAR1 RPL36B NTO1 RPL43A SPE3 MDM36 KAR3	88	2026
MIPS Functional Classification (459 categories)				
ribosomal proteins [12.01.01]	5.96E-08	RPL23A RPS11B MRPL36 IMG2 RPP1A RPS11A RPL29 RPL24A MRPL25 NSR1 RPL17B RPS14B RPS4A RPL14A RPL22A RPS17A RPS18B RPS16A RPL20A MRP7 RPL9B RPL42A RPP2A RPS6A RSA1 RPL36B RPL43A	27	246
cell cycle arrest [10.03.01.02]	0.005054	FUS3 FAR7 FAR11 RAD17	4	21
RNA binding [16.03.03]	0.005182	TMA64 RPL24A ARC1 NSR1 MSL1 LSM1 RPS14B TMA22 RPL14A NAM2 LSM7 NOP12 VTS1 RPL36B	14	189
biosynthesis of cysteine [01.01.09.03.01]	0.006686	CYS3 CYS4	2	4
MIPS Phenotypes (142 categories)				
Cold-sensitivity (cs) [12.10]	1.17E-05	RPS11B CDC50 SSB1 RPS11A SEH1 ARC1 NSR1 RNR4 MSL1 YKE2 ROM2 MCK1 BEM4 YAR1	14	105
Slow-growth (slg) [12.15]	5.40E-05	MDM10 DEP1 BUD31 HMO1 MNN10 SEH1 ARC1 VMA21 RNR4 PRS3	21	237

Ontology	p- value	Genes in ontology category	k	f
		MSL1 CPR7 NUP120 YKE2 TOP3 RSC2 SUR4 SFP1 CTK3 IES2 YAR1		
Cystein auxotrophy [42.20]	0.001166	DEP1 CYS4	2	2
other cell morphology mutants [52.99]	0.003086	DEP1 HHF1 MNN10 AFT1 SUR4 SRV2 BNI1	7	57
other vacuolar mutants [52.65.99]	0.006142	VAM6 VMA21 CYS4 CNB1 VPS33 VAM3	6	49
MIPS Protein Complexes (1142 categories)				
cytoplasmic ribosomal large subunit [500.40.10]	2.98E-06	RPL23A RPP1A RPL29 RPL24A RPL17B RPL14A RPL22A RPL20A RPL9B RPL42A RPP2A RPL36B RPL43A	13	81
cytoplasmic ribosomal small subunit [500.40.20]	0.0006458	RPS11B RPS11A RPS14B RPS4A RPS17A RPS18B RPS16A RPS6A	8	57
NUP84 complex [310.40]	0.0007331	NUP84 SEH1 NUP120	3	6
Complex Number 252 [550.2.252]	0.00342	PRS3 PTC5	2	3
Complex Number 372 [550.2.372]	0.006686	SUM1 SRV2	2	4
Complex Number 34, probably intermediate and energy metabolism [550.1.34]	0.008775	TPI1 ROM2 FAR11	3	13

Table 7. Ontologies enriched among the 119 suppressor genetic interactors common to *FPR3* and *FPR4*.

Ontology	p- value	Genes in ontology category	k	f
GO Molecular Function (1646 categories)				
histone deacetylase activity (H3-K9 specific) [GO:0032129]	5.28E-05	HOS2 HDA1 HOS3	3	5
histone deacetylase activity (H3-K16 specific) [GO:0034739]	5.28E-05	HOS2 HDA1 HOS3	3	5
histone deacetylase activity (H3-K14 specific) [GO:0031078]	5.28E-05	HOS2 HDA1 HOS3	3	5
NAD-dependent histone deacetylase activity (H4-K16 specific) [GO:0046970]	0.0001043	HOS2 HDA1 HOS3	3	6
NAD-dependent histone deacetylase activity (H3-K14 specific) [GO:0032041]	0.0001043	HOS2 HDA1 HOS3	3	6
NAD-dependent histone deacetylase activity (H3-K9 specific) [GO:0046969]	0.0001043	HOS2 HDA1 HOS3	3	6
adenine phosphoribosyltransferase activity [GO:0003999]	0.0003113	APT2 APT1	2	2
transcription regulator activity [GO:0030528]	0.0007218	HIR1 RPB9 RTG2 YOX1 RLF2	5	41
transferase activity, transferring glycosyl groups [GO:0016757]	0.002815	CSH1 PMT1 APT2 FKS1 APT1 SUR1	6	80
nucleosome binding [GO:0031491]	0.003644	HIR1 HPC2 HIR3	3	18

Ontology	p- value	Genes in ontology category	k	f
histone deacetylase activity [GO:0004407]	0.004271	HOS2 HDA1 HOS3	3	19
mannosyltransferase activity [GO:0000030]	0.006531	CSH1 PMT1 SUR1	3	22
histone methyltransferase activity (H3-K4 specific) [GO:0042800]	0.008129	SWD3 SDC1	2	8
GO Biological Process (2062 categories)				
DNA replication-independent nucleosome assembly [GO:0006336]	5.28E-05	HIR1 HPC2 HIR3	3	5
adenine salvage [GO:0006168]	0.0003113	APT2 APT1	2	2
transcription elongation from RNA polymerase II promoter [GO:0006368]	0.0003513	HIR1 HPC2 RTF1 HIR3 POP2 ELC1	6	54
regulation of transcription involved in G1/S phase of mitotic cell cycle [GO:0000083]	0.0005942	HPC2 HIR3 HOS3	3	10
glycosphingolipid biosynthetic process [GO:0006688]	0.0009232	CSH1 SUR1	2	3
histone monoubiquitination [GO:0010390]	0.0009232	BRE1 RTF1	2	3
nucleoside metabolic process [GO:0009116]	0.001362	APT2 APT1 PRS5	3	13
purine ribonucleoside salvage [GO:0006166]	0.001825	APT2 APT1	2	4
sphingolipid biosynthetic process [GO:0030148]	0.002112	TSC3 CSH1 SUR1	3	15
regulation of transcription, DNA-dependent [GO:0006355]	0.003306	HIR1 SMP1 HPC2 SGF29 NHP10 SLX5 SDC1 HOS2 RTF1 HIR3 BAS1 YOX1 HDA1 SKO1 GCR2 NRM1 POP2 HOS3	18	507
chromatin modification [GO:0016568]	0.003954	HIR1 HPC2 SGF29 BRE1 HOS2 HDA1 HOS3	7	114
transcription, DNA-dependent [GO:0006351]	0.006403	HIR1 SMP1 HPC2 SGF29 NHP10 SLX5 RPB9 HOS2 RTF1 HIR3 BAS1 YOX1 HDA1 SKO1 GCR2 NRM1 POP2 HOS3	18	540
GO Cellular Component (625 categories)				
HIR complex [GO:0000417]	2.14E-05	HIR1 HPC2 HIR3	3	4
cytosolic large ribosomal subunit [GO:0022625]	0.004528	RPL19A RPL35B RPL27B RPL37B RPL26A RPL20B	6	88
intracellular [GO:0005622]	0.007138	RPL19A BRE1 RPL35B SDC1 RPL27B RPL37B BEM2 YLF2 RPS21B RHO4 IRC25 RPL26A MSB4 SUR1	14	381
ubiquitin ligase complex [GO:0000151]	0.008129	SLX5 SLX8	2	8
Set1C/COMPASS complex [GO:0048188]	0.008129	SWD3 SDC1	2	8
MIPS Functional Classification (459 categories)				
centromere/kinetochore complex maturation [10.03.04.01]	0.001362	HIR1 HIR3 RLF2	3	13
G1/S transition of mitotic cell cycle [10.03.01.01.03]	0.003939	HPC2 PPH21 HIR3 SIC1	4	37
biosynthesis of methionine [01.01.06.05.01]	0.004457	MET6 MET2	2	6

Ontology	p- value	Genes in ontology category	k	f
DNA conformation modification (e.g. chromatin) [10.01.09.05]	0.005949	SWD3 YBR238C NHP10 BRE1 SDC1 HOS2 HDA1 HOS3 RLF2	9	188
vacuole or lysosome [42.25]	0.007363	CCZ1 VBA2 VAM7 TRX2	4	44
MIPS Phenotypes (142 categories)				
Divalent cations and heavy metals sensitivity [62.35.02]	0.006875	CCZ1 HSP150 GTR1 POP2 SUR1	5	68
MIPS Protein Complexes (1142 categories)				
Complex Number 227 [550.2.227]	0.001825	PIL1 TPK3	2	4
cytoplasmic ribosomal large subunit [500.40.10]	0.002997	RPL19A RPL35B RPL27B RPL37B RPL26A RPL20B	6	81

Table 8. Ontologies enriched among the 191 masked suppressor genetic interactors of *FPR3* and *FPR4*.

Ontology	p- value	Genes in ontology category	k	f
GO Molecular Function (1646 categories)				
structural constituent of ribosome [GO:0003735]	1.13E-11	RPS8A RPS6B RPS29B RPL35A RPP2B RPS18A RPS24A RPS26B RPL2A RPL9A RPL24B RPS0A MRPL9 RPL14B RPS22A RPS21A RPS0B RPS28B MRPL15 RPS29A MRPS8 RPL16B RPS7B MRPL10 RPS19A RPS7A RPS30B RPS10A	28	218
GO Biological Process (2062 categories)				
translation [GO:0006412]	1.07E-11	RPS8A TRM7 RPS6B RPS29B RPL35A RPP2B RPS18A RPS24A RPS26B RPL2A RPL9A RPL24B TIF4631 RPS0A MRPL9 RPL14B TIF2 RPS22A TEF4 RPS21A RPS0B HCR1 RPS28B RPS29A MRPS8 RPL16B RPS7B MRPL10 IFM1 RPS19A RPS7A RPS30B RPS10A CAM1	34	318
rRNA export from nucleus [GO:0006407]	7.43E-06	RPS18A RPS26B RPS0A RPS0B RPS28B RPS19A RPS10A	7	27
endonucleolytic cleavage to generate mature 3'-end of SSU-rRNA from (SSU-rRNA, 5.8S rRNA, LSU-rRNA) [GO:0000461]	8.90E-05	RPS0A RPS21A RPS0B	3	4
endonucleolytic cleavage in ITS1 to separate SSU-rRNA from 5.8S rRNA and LSU-rRNA from tricistronic rRNA transcript (SSU-rRNA, 5.8S rRNA, LSU-rRNA) [GO:0000447]	0.0008426	BUD23 RPS18A RPS0A RPS21A RPS0B BUD21	6	40
maturation of SSU-rRNA from tricistronic rRNA transcript (SSU-rRNA, 5.8S rRNA, LSU-rRNA) [GO:0000462]	0.001462	RPS8A RPS6B RPS24A FYV7 HCR1 TSR2 BUD21	7	60
rRNA processing [GO:0006364]	0.009496	RPS6B RPS0A LRP1 MRT4 RPS21A RPS0B FYV7 TSR2 RPS7B JJJ1 BUD21 RPS7A	12	195
GO Cellular Component (625 categories)				
cytosolic small ribosomal subunit [GO:0022627]	6.18E-13	RPS8A RPS6B RPS29B RPS18A RPS24A RPS26B RPS0A RPS22A RPS21A	17	62

Ontology	p- value	Genes in ontology category	k	f
GO Molecular Function (1646 categories)				
structural constituent of ribosome [GO:0003735]	1.13E-11	RPS8A RPS6B RPS29B RPL35A RPP2B RPS18A RPS24A RPS26B RPL2A RPL9A RPL24B RPS0A MRPL9 RPL14B RPS22A RPS21A RPS0B RPS28B MRPL15 RPS29A MRPS8 RPL16B RPS7B MRPL10 RPS19A RPS7A RPS30B RPS10A	28	218
		RPS0B RPS28B RPS29A RPS7B RPS19A RPS7A RPS30B RPS10A		
ribosome [GO:0005840]	1.20E-10	RPS8A RPS6B RPS29B RPL35A RPP2B RPS18A RPS24A RPS26B RPL2A RPL9A RPL24B TIF4631 RPS0A MRPL9 RPL14B TIF2 RPS22A TEF4 RPS21A RPS0B RPS28B MRPL15 RPS29A MRPS8 RPL16B RPS7B MRPL10 RPS19A RPS7A RPS30B RPS10A YPR096C	32	310
ribonucleoprotein complex [GO:0030529]	1.88E-09	RPS8A RPS6B RPS29B RPL35A RPP2B RPS18A RPS24A RPS26B RPL2A RPL9A RPL24B RPS0A MRPL9 RPL14B RPS22A RPS21A RPS0B RPS28B MRPL15 RPS29A MRPS8 RPL16B RPS7B MRPL10 RPS19A BUD21 RPS7A RPS30B RPS10A SNU66	30	307
intracellular [GO:0005622]	7.82E-08	RPS8A RPS6B RPN4 RPS29B RPL35A AIM7 PEP7 RPP2B RPS18A GEA2 RPS24A RPS26B RPL2A RPL9A RPS0A MRPL9 RPL14B RPS22A MRT4 RPS21A RPS0B ACE2 RPS28B RPS29A MRPS8 RPS7B JJJ1 IFM1 RPS19A RPS7A RPS30B	31	381
cytoplasm [GO:0005737]	0.0003208	SLA1 PIN4 SHP1 KTI11 RPS8A AKL1 TRM7 SMY2 RPS6B SDS24 STE50 BUD23 PUS9 RPS29B IWR1 RPL35A AIM7 RUB1 ATC1 PEP7 RPP2B RPS18A VPS72 FDC1 GEA2 RPS24A PTP3 RPS26B RPL2A YGL101W RPL9A YGR042W YGR122W RPL24B TIF4631 RPS0A RPL14B RIM4 GUT1 OSH3 TIF2 RPS22A RAV1 ADO1 DID4 MDM35 TEF4 KTI12 RPS21A RPS0B HCR1 RPS28B RPS29A PUN1 TSR2 PSP2 YMR074C YMR124W PPA2 RPL16B RPS7B NPR1 JJJ1 ZWF1 RTC4 HAL9 RPS19A VPS5 RPS7A RPS30B RPS10A YOR352W PDE2 HST2 SKS1 CAM1 GLR1 RTT10 YPL191C NAT3	80	2026
extrinsic to membrane [GO:0019898]	0.003114	AST1 SMY2 GEA2 RAV1	4	22
cytosolic large ribosomal subunit [GO:0022625]	0.003418	RPL35A RPP2B RPL2A RPL9A RPL24B RPL14B RPL16B JJJ1	8	88
eukaryotic translation initiation factor 4F complex [GO:0016281]	0.00762	TIF4631 TIF2	2	5
eukaryotic translation elongation factor 1 complex [GO:0005853]	0.00762	TEF4 CAM1	2	5
MIPS Functional Classification (459 categories)				
ribosomal proteins [12.01.01]	2.08E-10	RPS8A RPS6B RPS29B RPL35A RPP2B RPS18A RPS24A RPS26B RPL2A RPL9A RPL24B RPS0A MRPL9 RPL14B RPS22A RPS21A RPS0B RPS28B MRPL15 RPS29A MRPS8 RPL16B RPS7B MRPL10 RPS19A RPS7A RPS30B RPS10A	28	246

Ontology	p- value	Genes in ontology category	k	f
GO Molecular Function (1646 categories)				
structural constituent of ribosome [GO:0003735]	1.13E-11	RPS8A RPS6B RPS29B RPL35A RPP2B RPS18A RPS24A RPS26B RPL2A RPL9A RPL24B RPS0A MRPL9 RPL14B RPS22A RPS21A RPS0B RPS28B MRPL15 RPS29A MRPS8 RPL16B RPS7B MRPL10 RPS19A RPS7A RPS30B RPS10A	28	218
translation elongation [12.04.02]	0.002605	RPP2B MRPL9 TEF4 CAM1	4	21
MIPS Subcellular Localization (48 categories)				
cytoplasm [725]	0.0001352	PAU7 SLA1 PIN4 SHP1 AST1 KTI11 RPS8A AKL1 TRM7 SMY2 RPS6B SDS24 TDP1 SHG1 AGP1 STE50 MRC1 BUD23 RPN4 PUS9 RPS29B IWR1 RPL35A YDR056C AIM7 RUB1 ATC1 IPK1 YDR338C RPP2B RPS18A VPS72 FDC1 GEA2 ISC1 GLN3 RPS24A PTP3 SWI4 RPS26B RPL2A YGL072C YGL101W RPL9A YGR042W YGR122W RPL24B TIF4631 RPS0A YTA7 RPL14B RIM4 GUT1 RPI1 POT1 TIF2 YJL169W CPS1 RPS22A PHO90 MOG1 ADO1 DID4 MDM35 TEF4 KTI12 RPS21A COX17 RPS0B ACE2 MMR1 HCR1 RPS28B RPS29A PUN1 TSR2 PSP2 CGI121 YMR074C YMR124W RPL16B RPS7B YNL120C NPR1 SPS18 JJJ1 ZWF1 RTC4 HAL9 RPS19A SLG1 BUB3 VPS5 RPS7A RPS30B RPS10A YOR352W PDE2 HST2 SKS1 CAM1 GLR1 YPL150W RTT10 YPL191C VMA13 NAT3	107	2879
MIPS Protein Complexes (1142 categories)				
cytoplasmic ribosomal small subunit [500.40.20]	1.29E-13	RPS8A RPS6B RPS29B RPS18A RPS24A RPS26B RPS0A RPS22A RPS21A RPS0B RPS28B RPS29A RPS7B RPS19A RPS7A RPS30B RPS10A	17	57
Complex Number 431 [550.2.431]	0.0008065	SHP1 TDP1	2	2
Complex Number 85, Trm7 (2) [550.3.85]	0.0008065	TRM7 RTT10	2	2
Complex Number 432 [550.2.432]	0.002374	SHP1 TDP1	2	3
26S proteasome [360.10]	0.002374	RPN4 YTA7	2	3
Complex Number 152, probably RNA metabolism [550.1.152]	0.004659	RPP2B MRPL10	2	4
Complex Number 394 [550.2.394]	0.00762	TIF4631 TIF2	2	5
cytoplasmic ribosomal large subunit [500.40.10]	0.007984	RPL35A RPP2B RPL2A RPL9A RPL24B RPL14B RPL16B	7	81

Gene ontology analysis of differentially expressed genes

Ontologies enriched among differentially expressed genes unique to *Δfpr3* yeast, unique to *Δfpr4* yeast, common to both *Δfpr3* and *Δfpr4* yeast, and only present in *Δfpr3Δfpr4* double mutant yeast are presented in the tables below (Table 9, Table 10, Table 11, Table 12, Table 13, Table 14, Table 15, Table 16).

Lists of ontologies were generated by the FunSpec web-based cluster interpreter for yeast (http://funspec.med.utoronto.ca/)[372]. This program outputs a summary of ontologies significantly enriched in a given input list of yeast genes using ontology annotations from the Gene Ontology Consortium (GO) database[421] and from the Munich Information Center for Protein Sequences (MIPS) database[422].

Ontologies in this analysis were classified by molecular function, biological process, cellular component, MIPS functional classification, MIPS phenotypes, MIPS subcellular localization, and MIPS protein complexes. The *p*-values associated with each ontology were calculated automatically by FunSpec using hypergeometric distribution, they represent the probability that the intersection of a given list of genes with any ontology occurs by chance.

Only ontology categories with *p*-values≤0.01 are presented in the following lists. Bonferroni correction was not applied.

k: number of input genes in ontology category
f: total number of genes in ontology category

Table 9. Ontologies enriched among the 120 genes uniquely upregulated in *Δfpr3* yeast (89+31 from Figure 26 B)

Ontology	p- value	Genes in ontology category	k	f
GO Molecular Function (1646 categories)				
pyridoxal phosphate binding [GO:0030170]	6.60E-07	CYS3 THR4 ALT2 AGX1 ARO9 SHM2 CAR2 LCB1	8	43
catalytic activity [GO:0003824]	3.53E-06	CYS3 COR1 THR4 ALT2 ARO1 PRO3 PHM8 AGX1 BIO2 ARO9 ERG9 MDH1 FAS1 PDC1 SHM2 CAR2 ALO1 LCB1 ZWF1 ACC1 YPK9 GDH1 FAS2	23	455
transaminase activity [GO:0008483]	1.53E-05	GCV1 ALT2 AGX1 ARO9 CAR2	5	19
fatty-acyl-CoA synthase activity [GO:0004321]	0.00031	FAS1 FAS2	2	2
transferase activity [GO:0016740]	0.00037	VPS15 NOP1 POL3 GCV1 ALT2 ARO1 AGX1 ATG1 BIO2 THR1 ARO9 ERG9 FAS1 PDC1 SHM2 CAR2 LCB1 ADE4 BUD17 TPT1 NAT5 FAS2 MAK3	23	611
ubiquitin binding [GO:0043130]	0.00044	VPS15 TAF5 STP22 TUP1 ATG18	5	37
fatty acid synthase activity [GO:0004312]	0.00092	FAS1 FAS2	2	3

Ontology	p- value	Genes in ontology category	k	f
transferase activity, transferring nitrogenous groups [GO:0016769]	0.00106	ALT2 ARO9 LCB1	3	12
structural constituent of ribosome [GO:0003735]	0.00158	RPS6B RPP1A RPL41B RPL41A RPL9A RPS23A RPL27A RPL22A RPP0 MRPS8 RPL42A	11	218
binding [GO:0005488]	0.00238	PET9 VPS15 MSS2 ARO1 PRO3 GCN1 HGH1 MIR1 MDH1 ZWF1 GDH1 FAS2 TIF5	13	300
structural constituent of cell wall [GO:0005199]	0.00257	HSP150 YPS3 KRE1	3	16
ATPase activity [GO:0016887]	0.00358	ADP1 HSP150 CDC6 ATP2 MDN1 YPK9 ATP15	7	112
hydrolase activity, acting on acid anhydrides, catalyzing transmembrane movement of substances [GO:0016820]	0.00742	VMA10 ATP2 YPK9	3	23
transcription factor binding [GO:0008134]	0.00813	MDN1 CTI6	2	8
transferase activity, transferring alkyl or aryl (other than methyl) groups [GO:0016765]	0.00813	ARO1 ERG9	2	8
oxidoreductase activity [GO:0016491]	0.00853	ARO1 PRO3 YHB1 ERG9 MDH1 FAS1 AHP1 ALO1 ZWF1 GDH1 FAS2	11	272
GO Biological Process (2062 categories)				
metabolic process [GO:0008152]	4.06E-06	ILV6 THR4 ARO1 URH1 PRO3 PHM8 AGX1 BIO2 ERG9 MDH1 FAS1 PDC1 CAR2 ADE4 ZWF1 ACC1 DSE4 NAT5 YPK9 GDH1 FAS2 MAK3	22	425
biosynthetic process [GO:0009058]	6.39E-05	ALT2 ARO9 ERG9 ALO1 LCB1 FAS2	6	40
negative regulation of translational initiation [GO:0045947]	0.00092	PAT1 TIF5	2	3
translation [GO:0006412]	0.00139	PET112 RPS6B RPP1A RPL41B RPL41A RPL9A RPS23A RPL27A RPL22A RPP0 MRPS8 RPL42A CAM1 TIF5	14	318
threonine metabolic process [GO:0006566]	0.00183	THR4 THR1	2	4
ATP transport [GO:0015867]	0.00183	PET9 ANT1	2	4
glycine metabolic process [GO:0006544]	0.00183	GCV1 SHM2	2	4
oxidation-reduction process [GO:0055114]	0.00302	ARO1 PRO3 YHB1 ERG9 MDH1 FAS1 AHP1 HMX1 ALO1 ZWF1 GDH1 FAS2	12	272
transcription of nuclear rRNA large RNA polymerase I transcript [GO:0042790]	0.00308	RPA14 RRN5 RPA43	3	17
threonine biosynthetic process [GO:0009088]	0.00446	THR4 THR1	2	6
N-terminal protein amino acid acetylation [GO:0006474]	0.00446	NAT5 MAK3	2	6
late endosome to vacuole transport [GO:0045324]	0.00496	VPS15 STP22 ATG18	3	20
proton transport [GO:0015992]	0.00572	VMA10 ATP2 ATP15 ANT1	4	41
cellular response to methylmercury [GO:0071406]	0.00617	HRT3 UFO1	2	7

Ontology	p- value	Genes in ontology category	k	f
fatty acid biosynthetic process [GO:0006633]	0.00653	FAS1 ACC1 FAS2	3	22
translational elongation [GO:0006414]	0.00653	RPP1A RPP0 CAM1	3	22
cellular amino acid biosynthetic process [GO:0008652]	0.00763	CYS3 ILV6 THR4 ARO1 PRO3 THR1	6	98
generation of catalytic spliceosome for first transesterification step [GO:0000349]	0.00813	SPP381 SNU114	2	8
GO Cellular Component (625 categories)				
cytosolic large ribosomal subunit [GO:0022625]	2.24E-05	RPP1A RPL41B RPL41A ARX1 RPL9A RPL27A RPL22A RPP0 RPL42A	9	88
ribonucleoprotein complex [GO:0030529]	0.00031	SPP381 RPS6B NOP1 RPP1A RPL41B SAS10 RPL41A SNU13 RPL9A RPS23A RPL27A RPL22A RPP0 MRPS8 RPL42A	15	307
fatty acid synthase complex [GO:0005835]	0.00031	FAS1 FAS2	2	2
cytoplasm [GO:0005737]	0.00107	CYS3 RPS6B STP22 ADP1 THR4 PAT1 RPP1A RPL41B RPL41A GCV1 ARX1 ALT2 ARO1 URH1 PRO3 PHM8 RET2 RPL9A ATG1 RPS23A HGH1 YHB1 PUP2 RPL27A ARO9 RRD1 FAS1 PDC1 SHM2 RPL22A AHP1 SSP120 RPP0 CAR2 AMD1 UFO1 LCB1 ADE4 DBP2 DMA2 RPL42A ZWF1 ACC1 BUD17 NAT5 VTS1 GDH1 CAM1 CAR1 FAS2 MAK3 ANT1	52	2026
cytosol [GO:0005829]	0.00205	ATG18 ATG1 GCN1 YHB1 FAS1 PDC1 CAR2 VTS1 CAR1 FAS2	10	192
box C/D snoRNP complex [GO:0031428]	0.00301	NOP1 SNU13	2	5
proton-transporting ATP synthase complex, catalytic core F(1) [GO:0045261]	0.00446	ATP2 ATP15	2	6
Cdc73/Paf1 complex [GO:0016593]	0.00617	HPR1 LEO1	2	7
pre-autophagosomal structure membrane [GO:0034045]	0.00617	ATG18 ATG1	2	7
ribosome [GO:0005840]	0.0085	RPS6B NOP1 RPP1A RPL41B RPL41A RPL9A RPS23A RPL27A RPL22A RPP0 MRPS8 RPL42A	12	310
small-subunit processome [GO:0032040]	0.00929	RPS6B NOP1 SAS10 SNU13	4	47
MIPS Functional Classification (459 categories)				
ribosomal proteins [12.01.01]	0.0001	RPS6B RRP7 NOP1 RPP1A RPL41B RPL41A RPL9A RPS23A RPL27A RPL22A MDN1 RPP0 MRPS8 RPL42A	14	246
degradation of arginine [01.01.03.05.02]	0.00031	CAR2 CAR1	2	2
translational control [12.07]	0.00039	PAT1 GCN1 RPS23A TAP42 CAM1 TIF5	6	55
fatty acid metabolism [01.06.05]	0.00076	FAS1 ACC1 FAS2 ANT1	4	24
biosynthesis of threonine [01.01.06.04.01]	0.00092	THR4 THR1	2	3
degradation of glycine [01.01.09.01.02]	0.00446	GCV1 SHM2	2	6

Ontology	p- value	Genes in ontology category	k	f
metabolism of urea (urea cycle) [01.01.05.03]	0.00446	CAR2 CAR1	2	6
nucleotide/nucleoside/nucleobase transport [20.01.17]	0.00496	PET9 FCY21 ANT1	3	20
translation elongation [12.04.02]	0.00571	RPP1A RPP0 CAM1	3	21
metabolism of tryptophan [01.01.09.06]	0.00813	ARO1 ARO9	2	8
MIPS Subcellular Localization (48 categories)				
cytoplasm [725]	0.00013	CYS3 RPS6B STP22 ADP1 THR4 PAT1 RPP1A MSS2 RPL41B SAS10 RPL41A ARX1 ALT2 ARO1 URH1 PRO3 PHM8 AGX1 RET2 RPL9A ATG1 GCN1 PEX31 RPS23A HGH1 YHB1 PUP2 RPL27A THR1 ARO9 RRD1 PRY3 HSP150 CDC6 CYC1 FAS1 YRA2 YEH1 PDC1 SHM2 RPL22A HRT3 MDN1 AHP1 RPP0 CAR2 AMD1 UFO1 GAT2 LCB1 ADE4 DBP2 DMA2 RPL42A ZWF1 KRE1 ACC1 BUD17 TPT1 NAT5 YPK9 VTS1 GDH1 CAM1 SEC16 CAR1 CTI6 FAS2 TIF5 MAK3 ANT1	71	2879
mitochondria [755]	0.00379	PET9 COR1 PET112 VPS15 SPP381 ILV6 MSS2 GCV1 BAP3 MZM1 AGX1 GCN1 YHB1 BIO2 MSH1 CYC1 MIR1 ATP2 MDH1 FAS1 MDN1 YPS3 ALO1 ABF2 MRPS8 DBP2 ACC1 YPK9 FAS2 ATP15	30	1042
MIPS Protein Complexes (1142 categories)				
cytoplasmic ribosomal large subunit [500.40.10]	8.36E-05	RPP1A RPL41B RPL41A RPL9A RPL27A RPL22A RPP0 RPL42A	8	81
Fatty acid synthetase, cytoplasmic [170]	0.00031	FAS1 FAS2	2	2
Complex Number 51, probably intermediate and energy metabolism [550.1.51]	0.00092	CYS3 ADE4	2	3
Complex Number 27 [550.2.27]	0.00183	MDH1 CAR1	2	4
Complex Number 403 [550.2.403]	0.00183	NOP1 TPT1	2	4
Complex Number 196, probably transcription/DNA maintanance/chromatin structure [550.1.196]	0.00211	TAF5 GCN1 PDC1	3	15
Complex Number 132 [550.2.132]	0.00275	COR1 SAS10 SGM1 MDH1 CAR2	5	55
Complex Number 95 [550.2.95]	0.00308	PUP2 MDN1 CAR2	3	17
Complex Number 123, probably protein/RNA transport [550.1.123]	0.00496	GCN1 MIR1 LCB1	3	20
Complex Number 224 [550.2.224]	0.00617	AGX1 YHB1	2	7
Complex Number 338 [550.2.338]	0.00862	PET9 COR1 PRO3 RET2	4	46

Table 10. Ontologies enriched among the 217 genes uniquely downregulated in *Δfpr3* yeast (160+57 from Figure 26 B)

Ontology	p- value	Genes in ontology category	k	f
GO Molecular Function (1646 categories)				
glucosidase activity [GO:0015926]	3.11E-05	DSE2 SCW10 SUN4 KRE6	4	7
transferase activity [GO:0016740]	0.00015	FUS3 GPI18 YPK3 PGK1 MPS1 MSS4 POL5 FAB1 TYW3 SLT2 TRM5 SET1 GTT1 HOC1 MCD4 TOR2 RTT109 KNS1 GRC3 ADE16 PDC5 DPH5 COQ5 ILV2 PFK2 GAS3 SKY1 NRK1 NPR1 MCK1 MNT4 CMK2 SER1 PHO85 SUR1 EEB1	36	611
kinase activity [GO:0016301]	0.00025	FUS3 YPK3 PGK1 MPS1 MSS4 FAB1 SLT2 TOR2 KNS1 GRC3 PFK2 SKY1 NRK1 NPR1 MCK1 CMK2 PHO85	17	206
Rho GTPase activator activity [GO:0005100]	0.00027	RGD1 GIC2 RGD2 BEM3	4	11
hydrolase activity [GO:0016787]	0.00043	UBP13 MAP2 EXO5 ISW1 PPS1 ATG15 NTH1 DOA4 TPS2 IRC3 PPN1 SCW11 PAN2 MCM6 PCP1 FSH1 SRS2 CPS1 ADE16 CTS1 SEN1 IMP2 TPP1 DNF3 SCW10 RIB2 SIA1 ULS1 PTP2 PDE2 EEB1 HOS3 RBD2 PLC1	34	596
DNA binding [GO:0003677]	0.0008	OAF1 PDR3 EXO5 ISW1 SNT1 GIS1 ADR1 RSC3 IRC3 POL5 GLN3 ACA1 RAD51 RPH1 PHO4 DST1 MCM6 RSC1 STE12 SRS2 RFC2 PHD1 ABF1 SEN1 MOT3 ULS1 RPB10	27	449
phosphatidylinositol-3-phosphate binding [GO:0032266]	0.00094	BEM1 RGD1 FAB1 MVP1 BEM3	5	25
phosphatidylinositol phosphate kinase activity [GO:0016307]	0.00099	MSS4 FAB1	2	2
nucleotide binding [GO:0000166]	0.00105	FUS3 YPK3 NGR1 ISW1 PGK1 MPS1 SNQ2 MSS4 IRC3 POL5 GPA2 RAD51 PAB1 FAB1 RSM23 MCM6 MSM1 VMR1 SLT2 RHO3 SRS2 RFC2 TOR2 KNS1 GRC3 MDL1 SEN1 NAB6 DNF3 PFK2 SKY1 MSK1 NRK1 NPR1 MCK1 CMK2 ULS1 CPA1 PHO85 PUF2	40	778
protein serine/threonine kinase activity [GO:0004674]	0.00153	FUS3 YPK3 MPS1 SLT2 TOR2 KNS1 SKY1 NPR1 MCK1 CMK2 PHO85	11	122
ATP binding [GO:0005524]	0.00183	FUS3 YPK3 ISW1 PGK1 MPS1 SNQ2 MSS4 IRC3 RAD51 FAB1 RSM23 MCM6 MSM1 VMR1 SLT2 SRS2 RFC2 TOR2 KNS1 GRC3 MDL1 SEN1 DNF3 PFK2 SKY1 MSK1 NRK1 NPR1 MCK1 CMK2 ULS1 CPA1 PHO85	33	622
DNA-dependent ATPase activity [GO:0008094]	0.00189	RSC3 RAD51 RSC1 SEN1 ULS1	5	29
sequence-specific DNA binding [GO:0043565]	0.00202	OAF1 REI1 GIS1 ADR1 RSC3 GLN3 ACA1 RPH1 PHO4 STE12 PHD1 ABF1 AFT2	13	165
recombinase activity [GO:0000150]	0.0029	RAD51 RAD52	2	3
protein serine/threonine/tyrosine kinase activity [GO:0004712]	0.0029	MPS1 MCK1	2	3
histone demethylase activity (H3-K36 specific) [GO:0051864]	0.0029	GIS1 RPH1	2	3

Ontology	p- value	Genes in ontology category	k	f
phosphatidylinositol-4,5-bisphosphate binding [GO:0005546]	0.00314	RGD1 GIC2 ROM2	3	10
cation binding [GO:0043169]	0.00529	SCW11 CTS1 GAS3 SCW10	4	23
transcription activator activity [GO:0016563]	0.00567	OAF1 PDR3 GIS1 ABF1 MOT3	5	37
protein kinase activity [GO:0004672]	0.0062	FUS3 YPK3 MPS1 SLT2 KNS1 SKY1 NPR1 MCK1 CMK2 PHO85	10	126
serine-type peptidase activity [GO:0008236]	0.00698	PCP1 IMP2 RBD2	3	13
transcription repressor activity [GO:0016564]	0.00867	PDR3 ABF1 MOT3	3	14
protein phosphatase type 2A regulator activity [GO:0008601]	0.00928	CDC55 RTS1	2	5
aldehyde dehydrogenase (NAD) activity [GO:0004029]	0.00928	ALD4 ALD6	2	5
MAP kinase activity [GO:0004707]	0.00928	FUS3 SLT2	2	5
GO Biological Process (2062 categories)				
signal transduction [GO:0007165]	3.37E-07	RGD1 MTH1 GPA2 RGD2 CDC55 SLT2 TOR2 CMK2 RTS1 STD1 PDE2 BEM3 PLC1	13	73
cellular cell wall organization [GO:0007047]	9.84E-05	SBE2 HLR1 SCW11 SBE22 DSE2 MCD4 CTS1 GAS3 SCW10 SUN4 KRE6	11	89
negative regulation of transposition, RNA-mediated [GO:0010526]	0.00011	FUS3 RTT109 ELG1 MMS1	4	9
phosphorylation [GO:0016310]	0.00025	FUS3 YPK3 PGK1 MPS1 MSS4 FAB1 SLT2 TOR2 KNS1 GRC3 PFK2 SKY1 NRK1 NPR1 MCK1 CMK2 PHO85	17	206
regulation of transcription, DNA-dependent [GO:0006355]	0.00053	OAF1 SWD1 PDR3 SIF2 ISW1 SNT1 GIS1 SAS4 ADR1 RSC3 GLN3 ACA1 RPH1 PHO4 DST1 NUT1 RSC1 STE12 PHD1 ABF1 RTT109 RGR1 MOT3 MKS1 STD1 ULS1 HOS3 AFT2 ACM1 CCL1	30	507
intracellular signal transduction [GO:0035556]	0.00099	RGD2 GIS3 ROM2 PLC1	4	15
phosphatidylinositol phosphorylation [GO:0046854]	0.00154	MSS4 FAB1 TOR2	3	8
fungal-type cell wall organization [GO:0031505]	0.00224	LRE1 SBE2 HLR1 MPT5 SLT2 SBE22 CWP1 CWP2 MID2 PHO85 KRE6	11	128
response to acid [GO:0001101]	0.00225	RGD1 SLT2 MID2	3	9
positive regulation of stress-activated MAPK cascade [GO:0032874]	0.0029	SIF2 SNT1	2	3
acetate biosynthetic process [GO:0019413]	0.0029	ALD4 ALD6	2	3
meiotic joint molecule formation [GO:0000709]	0.0029	RAD51 RAD52	2	3
pseudohyphal growth [GO:0007124]	0.00377	GPA2 CDC55 STE12 DSE2 PHD1 BUD8 BEM3	7	64
positive regulation of transcription from RNA polymerase II	0.00409	PDR3 ISW1 GIS1 GLN3 PHO4 PHD1 ABF1 HOS3 HAL1	9	100

Ontology	p- value	Genes in ontology category	k	f
promoter [GO:0045944]				
cytokinesis, completion of separation [GO:0007109]	0.00422	SCW11 DSE2 CTS1	3	11
cell cycle [GO:0007049]	0.00488	FUS3 PPS1 CDC55 MCM6 DMA1 NET1 RFC2 TOR2 RAX2 CDC25 BUD8 CTF3 PDS5 SUN4 ELG1 LDB19 PHO85 ACM1 CCL1	19	316
transcription, DNA-dependent [GO:0006351]	0.00567	OAF1 PDR3 ISW1 GIS1 SAS4 ADR1 RSC3 GLN3 ACA1 RPH1 PHO4 DST1 NUT1 RSC1 STE12 PHD1 ABF1 RTT109 RGR1 MOT3 MKS1 STD1 ULS1 RPB10 HOS3 AFT2 ACM1 CCL1	28	540
histone demethylation [GO:0016577]	0.00568	GIS1 RPH1	2	4
transcription elongation, DNA-dependent [GO:0006354]	0.00568	ISW1 DST1	2	4
phosphatidylinositol metabolic process [GO:0046488]	0.00568	MSS4 FAB1	2	4
protein dephosphorylation [GO:0006470]	0.00636	PPS1 CDC55 PSY2 RTS1 PTP2	5	38
double-strand break repair via nonhomologous end joining [GO:0006303]	0.0072	RSC1 SRS2 RTT109 MCK1	4	25
response to drug [GO:0042493]	0.0072	PDR3 SNQ2 VMR1 SKY1	4	25
iron ion homeostasis [GO:0055072]	0.0083	FRE6 FRE8 FET3 ENB1	4	26
negative regulation of transcription from RNA polymerase II promoter [GO:0000122]	0.00865	PDR3 RPH1 ABF1 MOT3 MKS1 PHO85	6	57
nitrogen compound metabolic process [GO:0006807]	0.00867	GDH2 CPS1 CPA1	3	14
establishment of cell polarity [GO:0030010]	0.00881	BEM1 GIC2 ROM2 MSB1 BEM3	5	41
protein phosphorylation [GO:0006468]	0.00899	FUS3 YPK3 MPS1 SLT2 KNS1 SKY1 NPR1 MCK1 CMK2 PHO85	10	133
positive regulation of translation [GO:0045727]	0.00928	PBP1 MKT1	2	5
UFP-specific transcription factor mRNA processing involved in endoplasmic reticulum unfolded protein response [GO:0030969]	0.00928	SLT2 MID2	2	5
regulation of nitrogen utilization [GO:0006808]	0.00928	MKS1 NPR1	2	5
GO Cellular Component (625 categories)				
cell wall [GO:0005618]	0.00025	SCW11 DSE2 CWP1 CWP2 CTS1 GAS3 SCW10 SUN4 AGA1	9	68
fungal-type cell wall [GO:0009277]	0.00031	SCW11 DSE2 CWP1 CWP2 MCD4 CTS1 GAS3 SCW10 SUN4 AGA1	10	85
cellular bud tip [GO:0005934]	0.00053	BEM1 GIC2 CDC55 SLT2 RAX2 BUD8 ROM2 MSB1 BEM3	9	75
extracellular region [GO:0005576]	0.00076	SCW11 DSE2 CWP1 CWP2 PRY2 CTS1 GAS3 SCW10 SUN4 AGA1	10	95
microtubule organizing center [GO:0005815]	0.00099	SPC97 SPC98	2	2

Ontology	p- value	Genes in ontology category	k	f
cellular bud membrane [GO:0033101]	0.00225	TPO1 ENB1 NCE102	3	9
gamma-tubulin small complex, spindle pole body [GO:0000928]	0.0029	SPC97 SPC98	2	3
inner plaque of spindle pole body [GO:0005822]	0.00568	SPC97 SPC98	2	4
endosome membrane [GO:0010008]	0.00865	SYN8 FAB1 HSV2 VPS53 ENB1 MRL1	6	57
cytoplasm [GO:0005737]	0.00919	PDR3 FUS3 MAP2 YPK3 OPY1 ADH5 ARA1 BEM1 NGR1 RGD1 REI1 RNQ1 PGK1 YPD1 NTH1 DOA4 TPS2 GIC2 VPS74 HLR1 GEA2 GPA2 PAB1 RGD2 PHO4 PAN2 MPT5 MCM6 SEC15 MSM1 PBP1 HSV2 SLT2 FSH1 TRM5 SBE22 DMA1 SPC97 VPS53 SFH5 GIS3 PDC5 DPH5 CDC25 NAB6 MVP1 EIS1 INP2 PFK2 SKY1 SCW10 MSK1 MKS1 MKT1 APP1 SPC98 NRK1 NPR1 VID27 BRE5 CMK2 RIB2 RTS1 ELG1 SER1 PTP2 RCN2 CPA1 LDB19 PDE2 PHO85 ALD6 BEM3 HOS3 ACM1 HAL1 PUF2 MRL1 MDM36 NCE102	80	2026
Elg1 RFC-like complex [GO:0031391]	0.00928	RFC2 ELG1	2	5
outer plaque of spindle pole body [GO:0005824]	0.00928	SPC97 SPC98	2	5
protein phosphatase type 2A complex [GO:0000159]	0.00928	CDC55 RTS1	2	5
MIPS Functional Classification (459 categories)				
budding, cell polarity and filament formation [43.01.03.05]	1.36E-05	BEM1 MSS4 GIC2 SBE2 GPA2 CDC55 SEC15 SLT2 TRM5 STE12 SBE22 RHO3 AXL2 HOC1 PHD1 RGR1 RAX2 BUD8 ROM2 APP1 MSB1 SUR1 BEM3 RBD2 PLC1	25	312
regulator of G-protein signalling [18.02.05]	4.69E-05	FUS3 RGD2 CDC25 ROM2 BEM3	5	14
pheromone response, mating-type determination, sex-specific proteins [34.11.03.07]	8.59E-05	FUS3 OPY1 BEM1 GIC2 GPA2 RAD51 MPT5 STE12 RGR1 MID2 ROM2 RAD52 MCK1 AGA1 ULS1 PTP2 BEM3	17	189
osmosensing and response [34.11.03.13]	8.83E-05	RGD1 YPD1 DOA4 SLT2 STD1 PTP2 HAL1	7	35
cell wall [42.01]	0.00012	LRE1 SBE2 HLR1 MPT5 SLT2 SBE22 SET1 DSE2 HOC1 CWP1 CWP2 MID2 BUD8 ROM2 GAS3 MKS1 PLC1 KRE6	18	213
phosphate metabolism [01.04]	0.00013	FUS3 YPK3 ISW1 PPS1 PGK1 MPS1 YPD1 TPS2 MSS4 PPN1 FAB1 CDC55 VMR1 SLT2 TOR2 KNS1 MDL1 TPP1 PFK2 SKY1 NRK1 NPR1 MCK1 CMK2 RTS1 PTP2 PHO85	27	401
mating (fertilization) [41.01.01]	0.00028	OPY1 BEM1 PRM7 RAD51 STE12 MID2 SCW10 AGA1 ULS1	9	69
directional cell growth (morphogenesis) [40.01.03]	0.00041	BEM1 GIC2 RGD2 SLT2 ROM2 BEM3	6	32
DNA repair [10.01.05.01]	0.00046	GIS1 RAD51 RPH1 PAN2 SRS2 RFC2 RAD52 IMP2 TPP1 MKT1 MCK1 ULS1 CCL1 MMS1	14	159
cell growth / morphogenesis [40.01]	0.00086	GPA2 CDC55 SEC15 TRM5 RHO3 HOC1 TOR2 GRC3 MID2 BUD8 APP1 MSB1 RBD2 PLC1 KRE6	15	189

Ontology	p- value	Genes in ontology category	k	f
regulation of nitrogen metabolism [01.02.07.01]	0.00154	GLN3 MKS1 NPR1	3	8
modification by phosphorylation, dephosphorylation, autophosphorylation [14.07.03]	0.00211	FUS3 YPK3 PPS1 MPS1 CDC55 SLT2 KNS1 SKY1 NPR1 MCK1 CMK2 RTS1 PTP2 PHO85	14	186
small GTPase mediated signal transduction [30.01.05.05.01]	0.00214	GIC2 RGD2 RHO3 TOR2 CDC25 ROM2 BEM3	7	58
CELLULAR COMMUNICATION/SIGNAL TRANSDUCTION MECHANISM [30]	0.00256	MTH1 GLN3 STD1 MRL1	4	19
cytoskeleton/structural proteins [42.04]	0.00285	BEM1 GIC2 SEC15 TRM5 TOR2 BUD8 MSB1 BEM3 RBD2 ICY2	10	113
proteins necessary for transposon movement [38.07]	0.00314	RTT109 ELG1 MMS1	3	10
regulation of C-compound and carbohydrate metabolism [01.05.25]	0.0062	ADR1 MTH1 RGR1 CDC25 ROM2 PFK2 MKS1 PSY2 STD1 PHO85	10	126
alcohol fermentation [02.16.01]	0.00698	ADH5 PDC5 ALD4	3	13
DNA recombination [10.01.05.03]	0.00951	RTT109 ELG1 ULS1 MMS1	4	27
transcription activation [11.02.03.04.01]	0.00975	OAF1 SWD1 PDR3 GLN3 MOT3	5	42
MIPS Phenotypes (142 categories)				
other cell wall mutants [52.15.99]	0.00043	LRE1 MSS4 SLT2 SET1 CWP2 CDC25 BUD8 MKS1 KRE6	9	73
other cell cycle defects [22.99]	0.00215	BEM1 MPS1 DOA4 RSC3 RAD51 FAB1 STE12 SPC97 RFC2 ERG3 RGR1 ROM2 SPC98 RTS1 PLC1	15	207
Calcofluor white sensitivity [52.15.15.10]	0.00672	HOC1 CWP1 CWP2 BUD8 ROM2 MKS1 PLC1 KRE6	8	89
MIPS Subcellular Localization (48 categories)				
neck [705.03]	4.49E-05	BEM1 RGD1 MPS1 RGD2 SEC15 AXL2 CWP2 RAX2 BUD8 ROM2 MSB1 BEM3 HOS3	13	112
cell wall [710]	0.00034	SCW11 DSE2 CWP1 CWP2 CTS1 SCW10 SUN4	7	43
bud [705]	0.00071	BEM1 RGD1 GIC2 AXL2 TPO1 BUD8 ROM2 FET3 INP2	9	78
cell periphery [715]	0.00324	BEM1 SNQ2 GPA2 RGD2 SEC15 TNA1 AXL2 GTT1 CWP2 TPO1 RAX2 MID2 BUD8 HXT2 FET3	15	216
vacuole [770]	0.00456	CPR4 PPN1 AXL2 CPS1 MCD4 TOR2 PRY2 FRE6 CTS1 HXT2 SCW10 SUN4 VAM3 SUR1 KRE6	15	224
MIPS Protein Complexes (1142 categories)				
Complex Number 301 [550.2.301]	0.00154	RNQ1 RFC2 ELG1	3	8
Complex Number 199, probably transcription/DNA maintanance/chromatin structure [550.1.199]	0.00225	SWD1 DOA4 SET1	3	9
Complex Number 347 [550.2.347]	0.00225	SIF2 SNT1 AVT2	3	9

Ontology	p- value	Genes in ontology category	k	f
gamma-tubulin complex [480.10.05]	0.0029	SPC97 SPC98	2	3
Complex Number 299 [550.2.299]	0.00568	MAP2 RNQ1	2	4
Complex Number 194 [550.2.194]	0.00568	FUS3 SLT2	2	4
Complex Number 233 [550.2.233]	0.00698	CDC55 MKT1 RTS1	3	13
other DNA repair complexes [510.180.20]	0.00928	RAD51 RAD52	2	5

Table 11. Ontologies enriched among the 110 genes uniquely upregulated in *Δfpr4* yeast (74+36 from Figure 26 B)

Ontology	p- value	Genes in ontology category	k	f
GO Molecular Function (1646 categories)				
alpha,alpha-trehalose-phosphate synthase (UDP-forming) activity [GO:0003825]	4.26E-06	TPS1 TSL1 TPS3	3	3
oxidoreductase activity [GO:0016491]	7.38E-06	RFS1 MXR2 PST2 MET10 ERG26 ERG4 ERG11 GND1 SER33 HYR1 HOM6 PUT1 FRE1 IDH1 MDH2 IDH2	16	272
hexokinase activity [GO:0004396]	4.16E-05	GLK1 EMI2 HXK1	3	5
glucokinase activity [GO:0004340]	0.00027	GLK1 EMI2	2	2
isocitrate dehydrogenase (NAD+) activity [GO:0004449]	0.00027	IDH1 IDH2	2	2
catalytic activity [GO:0003824]	0.00037	TPS1 PHO13 GLC3 MET10 HXK1 ERG26 BGL2 GND1 SER33 HOM6 GSY2 TAL1 TSL1 TPS3 IDH1 NMA111 MDH2 IDH2	18	455
oxidoreductase activity, acting on the CH-OH group of donors, NAD or NADP as acceptor [GO:0016616]	0.00066	SER33 IDH1 MDH2 IDH2	4	25
trehalose-phosphatase activity [GO:0004805]	0.00079	TSL1 TPS3	2	3
phosphotransferase activity, alcohol group as acceptor [GO:0016773]	0.00117	GLK1 EMI2 HXK1 ADO1	4	29
transferase activity, transferring glycosyl groups [GO:0016757]	0.00188	TPS1 GLC3 GPI1 GSY2 APT1 ALG12	6	80
transferase activity [GO:0016740]	0.00188	PSK1 TPS1 GLK1 RTK1 STE7 RAD30 EMI2 GLC3 HXK1 GPI1 ADO1 YKT6 GSY2 TAL1 APT1 ALG12 PFA4 OST3 OST2 PIS1	20	611
enzyme regulator activity [GO:0030234]	0.00204	COX13 TSL1 TPS3	3	16
structural constituent of ribosome [GO:0003735]	0.00287	RPS14A RPP2B RPL7A RPL1B RPS0A RPS16A RPL9B RPS7A MRPL23 RPL1A	10	218
NAD binding [GO:0051287]	0.00594	SER33 IDH1 IDH2	3	23
dolichyl-diphosphooligosaccharide-protein glycotransferase activity [GO:0004579]	0.00885	OST3 OST2	2	9
magnesium ion binding [GO:0000287]	0.00938	ENO1 PGM2 IDH1 IDH2	4	51
GO Biological Process (2062 categories)				
trehalose biosynthetic process [GO:0005992]	2.28E-06	TPS1 TSL1 PGM2 TPS3	4	7
oxidation-reduction process [GO:0055114]	7.38E-06	RFS1 MXR2 PST2 MET10 ERG26 ERG4 ERG11 GND1 SER33 HYR1 HOM6 PUT1 FRE1 IDH1 MDH2 IDH2	16	272
glucose 6-phosphate metabolic process [GO:0051156]	1.68E-05	GLK1 EMI2 PGM2	3	4
glycogen biosynthetic process [GO:0005978]	3.03E-05	GLC3 GSY2 PGM2 GAC1	4	12
glutamate biosynthetic process [GO:0006537]	4.32E-05	PUT1 ACO1 IDH1 IDH2	4	13

Ontology	p- value	Genes in ontology category	k	f
carbohydrate metabolic process [GO:0005975]	0.00014	GLK1 EMI2 GLC3 HXK1 BGL2 TAL1 PGM2 MDH2	8	94
AMP biosynthetic process [GO:0006167]	0.00027	ADO1 APT1	2	2
cellular response to oxidative stress [GO:0034599]	0.00074	MXR2 AFG1 GND1 HYR1 MSN4 TRX1	6	67
glucose import [GO:0046323]	0.00079	GLK1 HXK1	2	3
glycolysis [GO:0006096]	0.00102	GLK1 EMI2 HXK1 ENO1	4	28
tricarboxylic acid cycle [GO:0006099]	0.00134	ACO1 IDH1 MDH2 IDH2	4	30
mannose metabolic process [GO:0006013]	0.00156	GLK1 HXK1	2	4
purine ribonucleoside salvage [GO:0006166]	0.00156	ADO1 APT1	2	4
isocitrate metabolic process [GO:0006102]	0.00257	IDH1 IDH2	2	5
mitotic cell cycle spindle assembly checkpoint [GO:0007094]	0.00523	PPH22 CEP3 GAC1	3	22
ergosterol biosynthetic process [GO:0006696]	0.00594	ERG26 ERG4 ERG11	3	23
glucose metabolic process [GO:0006006]	0.00594	GLK1 HXK1 PGM2	3	23
steroid biosynthetic process [GO:0006694]	0.00753	ERG26 ERG4 ERG11	3	25
electron transport chain [GO:0022900]	0.00815	MXR2 MET10 TRX1 FRE1	4	49
protein import into peroxisome matrix [GO:0016558]	0.00885	AFG1 MDH2	2	9
septin ring assembly [GO:0000921]	0.00885	SKP1 CEP3	2	9
metabolic process [GO:0008152]	0.00901	PHO13 MET10 HXK1 ERG26 BGL2 GND1 SER33 HOM6 GSY2 ACO1 TAL1 IDH1 MDH2 IDH2	14	425
GO Cellular Component (625 categories)				
alpha,alpha-trehalose-phosphate synthase complex (UDP-forming) [GO:0005946]	1.68E-05	TPS1 TSL1 TPS3	3	4
mitochondrial isocitrate dehydrogenase complex (NAD+) [GO:0005962]	0.00027	IDH1 IDH2	2	2
cytoplasm [GO:0005737]	0.00042	SSA1 PSK1 RFS1 TPS1 AMN1 ARC40 RPS14A STE7 PHO13 PST2 SKP1 RPP2B PSP1 EMI2 RBA50 GLC3 RGI1 RTR1 HXK1 RPL7A RPL1B CAF130 PRE9 RPS0A ENO1 GND1 SER33 MOB1 HYR1 ADO1 HOM6 TTI1 MSN4 KAE1 AIM29 TRX1 GSY2 ACO1 TAL1 APT1 TSL1 PGM2 RPS16A TPS3 RPL9B MDH2 RPS7A LSP1 RTT10 RPL1A	50	2026
CBF3 complex [GO:0031518]	0.00156	SKP1 CEP3	2	4
plasma membrane enriched fraction [GO:0001950]	0.00271	SSA1 GLK1 PST2 MRH1 ENO1 LSP1	6	86
mitochondrion [GO:0005739]	0.00323	GCV3 MXR2 PST2 MRH1 PSP1 AFG1 HXK1 COX13 MSP1 IMO32	29	1072

Ontology	p- value	Genes in ontology category	k	f
		PHB1 PRE9 ENO1 GND1 TTI1 YKT6 ISA1 COX12 PUT1 ACO1 IDH1 POR1 MDM12 IDH2 MRPL23 HEM15 LSP1 PEP4 PIS1		
endoplasmic reticulum [GO:0005783]	0.00752	YPC1 ERG26 ERG4 ERG11 BIG1 PER33 UBC7 HOR7 ALG12 PFA4 MDM12 OST3 YOP1 PIS1	14	416
oligosaccharyltransferase complex [GO:0008250]	0.00885	OST3 OST2	2	9
intracellular [GO:0005622]	0.00892	PRP6 RPS14A RPP2B RPL7A RPL1B RPS0A HYR1 MSN4 RPS16A RPL9B NOG2 RPS7A RPL1A	13	381
MIPS Functional Classification (459 categories)				
metabolism of energy reserves (e.g. glycogen, trehalose) [02.19]	3.09E-05	TPS1 GLC3 GSY2 TSL1 PGM2 TPS3 GAC1	7	56
sugar, glucoside, polyol and carboxylate catabolism [01.05.02.07]	4.72E-05	TPS1 ENO1 ACO1 TAL1 PGM2 TPS3 IDH1 IDH2	8	81
biosynthesis of glutamate [01.01.03.02.01]	8.04E-05	PUT1 ACO1 IDH1 IDH2	4	15
sugar, glucoside, polyol and carboxylate anabolism [01.05.02.04]	0.00023	TPS1 TAL1 TSL1 PGM2 TPS3	5	35
NAD/NADP binding [16.21.07]	0.00027	MET10 GND1 SER33 IDH1 IDH2	5	36
C-compound and carbohydrate metabolism [01.05]	0.00338	PSK1 GLK1 EMI2 HXK1 ENO1 BGL2 BIG1 GND1 ALG12 MDH2	10	223
glycolysis and gluconeogenesis [02.01]	0.0043	GLK1 ENO1 PGM2 MDH2	4	41
stress response [32.01]	0.00487	TPS1 RTK1 MRH1 MSN4 TSL1 UBC7 HOR7 TPS3	8	162
phosphate metabolism [01.04]	0.00547	SSA1 PSK1 GLK1 RTK1 STE7 PPH22 PHO13 AFG1 HXK1 MSP1 ADO1 CNB1 ORC5 GAC1	14	401
pentose-phosphate pathway [02.07]	0.00594	GND1 TAL1 PGM2	3	23
ribosomal proteins [12.01.01]	0.00673	RPS14A RPP2B RPL7A RPL1B RPS0A RPS16A RPL9B RPS7A MRPL23 RPL1A	10	246
enzymatic activity regulation / enzyme regulator [18.02.01]	0.00875	COX13 MOB1 CNB1 TSL1 GAC1	5	78
MIPS Subcellular Localization (48 categories)				
mitochondrial outer membrane [755.01]	0.00396	MSP1 POR1 MDM12	3	20
cytoplasm [725]	0.00451	SSA1 PSK1 PRP6 TPS1 AMN1 GLK1 RPS14A STE7 PPH22 PHO13 PST2 SKP1 RPP2B RAD30 PSP1 EMI2 RBA50 GLC3 RGI1 RTR1 MET10 HXK1 RPL7A RPL1B IMO32 CAF130 PRE9 RPS0A ENO1 BIG1 GND1 SER33 MOB1 HYR1 ADO1 HOM6 TTI1 MSN4 CNB1 KAE1 AIM29 COX12 TRX1 FRE1 GSY2 ACO1 TAL1 RAD33 APT1 TSL1 PGM2 RPS16A TPS3 POR1 RPL9B MDH2 RPS7A GAC1 LSP1 RTT10 RPL1A	61	2879

Ontology	p- value	Genes in ontology category	k	f
ER [735]	0.00597	PST2 ERG26 ERG4 PRE9 GPI1 BGL2 ERG11 BIG1 PER33 FRE1 UBC7 HOR7 ALG12 OST3 OST2 YOP1 PIS1	17	537
MIPS Protein Complexes (1142 categories)				
Isocitrate dehydrogenase [250]	0.00027	IDH1 IDH2	2	2
Complex Number 504 [550.2.504]	0.00031	TPS1 PST2 APT1 IDH1 POR1	5	37
Complex Number 244 [550.2.244]	0.00095	PRP6 TPS1 ADO1 PGM2 LSP1	5	47
CBF3 protein complex [270.10.10]	0.00156	SKP1 CEP3	2	4
Complex Number 168 [550.2.168]	0.00156	TAL1 POR1	2	4
Complex Number 29, probably intermediate and energy metabolism [550.1.29]	0.00204	TPS1 TSL1 TPS3	3	16
Complex Number 308 [550.2.308]	0.00245	TPS1 PRE9 TSL1	3	17
Complex Number 64 [550.2.64]	0.00528	CNB1 IDH1	2	7
Complex Number 442 [550.2.442]	0.00528	MSN4 POR1	2	7
Complex Number 508 [550.2.508]	0.00528	SKP1 IDH1	2	7
Complex Number 435 [550.2.435]	0.00603	PPH22 PST2 GND1 POR1	4	45
Complex Number 454 [550.2.454]	0.00696	SKP1 PGM2	2	8
Complex Number 78 [550.2.78]	0.00696	MOB1 IDH2	2	8
Complex Number 142 [550.2.142]	0.00696	ADO1 POR1	2	8
Oligosaccharyltransferase [520.20]	0.00885	OST3 OST2	2	9
Complex Number 525 [550.2.525]	0.00885	PGM2 LSP1	2	9
Complex Number 232 [550.2.232]	0.00885	PPH22 HEM15	2	9

Table 12. Ontologies enriched among the 247 genes uniquely downregulated in *Δfpr4* yeast (153+94 from Figure 26 B)

Ontology	p- value	Genes in ontology category	k	f
GO Molecular Function (1646 categories)				
RNA binding [GO:0003723]	2.19E-07	NCL1 HEK2 GBP2 SRO9 KRR1 LHP1 TRM3 NOP6 CFT1 NPL3 NUG1 LSM4 ECM32 RNA15 TIF4631 RNH70 RPF1 PRP8 DBP8 SCP160 DRS1 DPS1 ECM16 RRP5 RLP7 NOP15 WHI3 NOP12 NOP8 BFR1 DED1 NOP4 MRD1	33	337
nucleic acid binding [GO:0003676]	6.18E-07	GBP2 SPB1 LHP1 NOP6 CFT1 NPL3 BRR2 RNA15 RNH70 DBP8 STH1 MTR4 DRS1 DPS1 STP3 DUS3 ECM16 NOP15 WHI3 GIS2 NOP12 NOP8 RAT1 DED1 RAD1 NOP4 MOT1 MRD1	28	270
nucleotide binding [GO:0000166]	1.13E-06	RBG1 PIM1 MCX1 GBP2 APA1 RBK1 LHP1 NOP6 RVB1 NPL3 PKH1 NUG1 BRR2 ECM32 SMC1 SMC2 RNA15 PKP2 ADE3 MYO1 YCK1 DBP8 STH1 MTR4 CCT7 RPB4 SWE1 SSC1 TOR1 STE6 DRS1 DPS1 MDN1 RCK2 STT4 PIF1 MYO5 ECM16 NOP15 KRE33 YCK2 WHI3 NOP12 NOP8 VPS21 GLN4 DED1 RFC1 NOP4 MOT1 BMS1 NEW1 RVB2 MRD1 VPS4	55	778
DNA secondary structure binding [GO:0000217]	5.05E-05	SPT2 SMC1 SMC2	3	3
ATP binding [GO:0005524]	8.02E-05	PIM1 MCX1 APA1 RBK1 RVB1 PKH1 BRR2 ECM32 SMC1 SMC2 PKP2 ADE3 MYO1 RPF1 YCK1 DBP8 STH1 MTR4 CCT7 SWE1 SSC1 TOR1 STE6 DRS1 DPS1 MDN1 RCK2 STT4 PIF1 MYO5 ECM16 KRE33 YCK2 BRX1 GLN4 DED1 RFC1 MOT1 BMS1 NEW1 RVB2 VPS4	42	622
helicase activity [GO:0004386]	0.0003613	RVB1 BRR2 ECM32 DBP8 STH1 MTR4 DRS1 PIF1 ECM16 DED1 MOT1 RVB2	12	102
ATPase activity [GO:0016887]	0.0008508	RVB1 SMC1 SMC2 DBP8 STH1 SSC1 STE6 MDN1 MOT1 NEW1 RVB2 VPS4	12	112
DNA binding [GO:0003677]	0.002248	PIM1 HHF1 GBP2 RPO21 RPC53 SPT2 ECM32 RPO41 RSC8 SUA5 ZUO1 CRP1 CTF8 STH1 ASG1 CSE4 SWI6 ECM22 PIF1 SIS1 HHT2 HIR2 RPB2 RFC1 MBF1 TFC8 RAD1 MOT1 DPB2	29	449
DNA helicase activity [GO:0003678]	0.002366	RVB1 ECM32 PIF1 RVB2	4	16
peptidyl-prolyl cis-trans isomerase activity [GO:0003755]	0.003004	FPR2 CPR7 FPR4 CWC27	4	17
rRNA primary transcript binding [GO:0042134]	0.004013	RPF1 BRX1	2	3
tRNA (guanine) methyltransferase activity [GO:0016423]	0.004013	TRM3 TRM10	2	3
AT DNA binding [GO:0003680]	0.004013	SMC1 SMC2	2	3
nucleoside-triphosphatase activity [GO:0017111]	0.006822	PIM1 MCX1 RVB1 STE6 MDN1 RFC1 NEW1 RVB2 VPS4	9	92
mRNA binding [GO:0003729]	0.007017	HEK2 NPL3 UBP3 LOC1 RNA15 GIS2 STI1	7	61

Ontology	p- value	Genes in ontology category	k	f
DNA-directed RNA polymerase activity [GO:0003899]	0.007785	RPO21 RPC53 RPO41 RPB4 RPB2	5	34
tRNA dihydrouridine synthase activity [GO:0017150]	0.00783	DUS3 DUS4	2	4
RNA-directed RNA polymerase activity [GO:0003968]	0.008657	RPO21 RPB4 RPB2	3	12
GO Biological Process (2062 categories)				
ribosome biogenesis [GO:0042254]	4.39E-13	SPB1 KRR1 NOP6 MAK21 UTP4 NPL3 NUG1 UTP7 LOC1 SDA1 RNH70 RPF1 DBP8 TOR1 MRT4 DRS1 RSA3 ECM16 RRP5 RLP7 RPS7B NOP15 KRI1 NOP12 BRX1 NOP8 NOB1 NOC2 NOP4 BMS1	30	170
rRNA processing [GO:0006364]	9.03E-11	SPB1 KRR1 NOP6 UTP4 NPL3 NUG1 UTP7 LSM4 RNH70 ZUO1 RPF1 DBP8 MTR4 MRT4 DRS1 MDN1 PWP1 ECM16 RRP5 RPS7B NOP15 KRI1 NOP12 RAT1 NOP4 MOT1 BMS1 RVB2 MRD1	29	195
ribosomal large subunit biogenesis [GO:0042273]	4.86E-05	LOC1 TIF4631 SDA1 MRT4 RLP7 NOP15 NOP8 JIP5	8	37
ribosomal large subunit assembly [GO:0000027]	0.0004185	MAK21 RPF1 MRT4 DRS1 MDN1 RSA3 BRX1	7	38
endonucleolytic cleavage in ITS1 to separate SSU-rRNA from 5.8S rRNA and LSU-rRNA from tricistronic rRNA transcript (SSU-rRNA, 5.8S rRNA, LSU-rRNA) [GO:0000447]	0.0005803	KRR1 UTP7 LOC1 DBP8 RRP5 KRI1 MRD1	7	40
protein folding [GO:0006457]	0.0007935	FPR2 BUD27 ZUO1 CCT7 CPR7 SSC1 FPR4 SIS1 STI1 MGE1 CWC27	11	96
intracellular mRNA localization [GO:0008298]	0.00138	HEK2 LOC1 SCP160 SHE4	4	14
ribosomal small subunit biogenesis [GO:0042274]	0.001608	KRR1 NOP6 KRE33 NOB1 NEW1	5	24
regulation of transcription from RNA polymerase II promoter [GO:0006357]	0.002216	RVB1 SSN2 PGD1 SUT1 SPT5 GAL11 HIR2 MOT1 ELP4 RVB2	10	93
protein refolding [GO:0042026]	0.002366	MCX1 CPR7 SSC1 MGE1	4	16
tRNA processing [GO:0008033]	0.002674	NCL1 LHP1 TRM3 LSM4 SUA5 RNH70 DUS3 DUS4 TRM10	9	80
fungal-type cell wall organization [GO:0031505]	0.002707	TIP1 ECM33 HKR1 CRH1 SIM1 MHP1 CIS3 KRE9 TOR1 ARG7 MYO5 WSC2	12	128
endonucleolytic cleavage in 5'-ETS of tricistronic rRNA transcript (SSU-rRNA, 5.8S rRNA, LSU-rRNA) [GO:0000480]	0.002789	UTP7 LOC1 DBP8 RRP5 MRD1	5	27
protein peptidyl-prolyl isomerization [GO:0000413]	0.003004	FPR2 CPR7 FPR4 CWC27	4	17
cell cycle [GO:0007049]	0.003129	AME1 RGP1 CDC37 VPS64 SMC1 SMC2 MAD1 SDA1 CTF8 STH1 SWE1 TOR1 SAP190 HOF1 SIS1 APC1 WHI3 PCL1 WHI2 RFC1 CLN2 DPB2	22	316
nucleosome assembly [GO:0006334]	0.003752	HHF1 CSE4 FPR4 HHT2	4	18
retrograde transport, endosome to Golgi [GO:0042147]	0.003752	RGP1 SNX41 BTN2 VPS17	4	18

Ontology	p- value	Genes in ontology category	k	f
maturation of LSU-rRNA from tricistronic rRNA transcript (SSU-rRNA, 5.8S rRNA, LSU-rRNA) [GO:0000463]	0.003752	SPB1 RPF1 RLP7 NOP12	4	18
endonucleolytic cleavage to generate mature 5'-end of SSU-rRNA from (SSU-rRNA, 5.8S rRNA, LSU-rRNA) [GO:0000472]	0.003862	UTP7 LOC1 DBP8 RRP5 MRD1	5	29
response to glucose stimulus [GO:0009749]	0.004013	YCK1 YCK2	2	3
ribosome assembly [GO:0042255]	0.004013	NOC2 BMS1	2	3
cytokinesis, actomyosin contractile ring assembly [GO:0000915]	0.004013	MYO1 NOP15	2	3
regulation of cyclin-dependent protein kinase activity [GO:0000079]	0.005604	PCL10 SWE1 PCL1 CLN2	4	20
intracellular protein transport [GO:0006886]	0.005912	RET2 BTN2 SED5 VTI1 TOM70 VPS27 SSO1 APM1 SEC23	9	90
actin cytoskeleton organization [GO:0030036]	0.007785	SDA1 SFK1 WSC2 SHE4 PIN3	5	34
sexual sporulation resulting in formation of a cellular spore [GO:0043935]	0.00783	HHF1 HHT2	2	4
GO Cellular Component (625 categories)				
nucleolus [GO:0005730]	<1e-14	NCL1 SPB1 KRR1 LHP1 NOP6 MAK21 UTP4 NPL3 NUG1 UTP7 LSM4 LOC1 SDA1 ZUO1 RPF1 SPO12 DBP8 RRT14 MTR4 MRT4 DRS1 PWP1 RSA3 PIF1 ECM16 RRP5 RLP7 RPS7B NOP15 KRE33 KRI1 NOP12 BRX1 NOP8 NOB1 NOC2 NOP4 BMS1 MRD1 JIP5	40	253
nucleus [GO:0005634]	9.47E-11	NCL1 HEK2 HHF1 AME1 HSM3 GBP2 APA1 SPB1 KRR1 RBK1 LHP1 RPO21 RPC53 NOP6 MAK21 NGG1 RVB1 CFT1 UTP4 SPC110 ADE8 NPL3 SSN2 KRE28 NUG1 CHZ1 UTP7 LSM4 SPT2 BRR2 SMC1 IES1 LOC1 SMC2 RSC8 PGD1 RNA15 MAD1 SUT1 SUA5 NUP57 ADE3 SDA1 RNH70 SNF6 RPF1 CRP1 SPO12 PRP8 DBP8 CTF8 STH1 RRT14 ASG1 MTR4 SCP160 RPB4 SWE1 SSC1 TOR1 MRT4 CSE4 MLP1 DRS1 DPS1 STU2 MDN1 SWI6 PWP1 RSA3 ECM22 STP3 DUS3 FPR4 SPT5 VPS71 PIF1 ECM16 RRP5 RLP7 SIS1 HHT2 BOP3 RPS7B NOP15 KRE33 APC1 PCL1 KRI1 NOP12 GAL11 PSH1 BRX1 TRM10 NOP8 HIR2 RAT1 NOB1 SLD7 RUP1 RPB2 NOC2 RFC1 MBF1 PRO2 TFC8 RAD1 NOP4 CWC27 MOT1 ELP4 BMS1 NEW1 RVB2 CLN2 FCY1 MRD1 PIN3 JIP5 DPB2	120	1965
preribosome, large subunit precursor [GO:0030687]	3.36E-06	SPB1 NUG1 LOC1 RPF1 MRT4 DRS1 RSA3 RLP7 NOP15 BRX1	10	44
polysome [GO:0005844]	4.18E-05	RBG1 SRO9 ECM32 ZUO1 SCP160 BFR1 NEW1	7	27
90S preribosome [GO:0030686]	0.000365	KRR1 NOP6 UTP4 UTP7 DBP8 ECM16 RRP5 KRE33 BMS1 MRD1	10	74
Noc1p-Noc2p complex [GO:0030690]	0.001371	MAK21 NOC2	2	2

Ontology	p- value	Genes in ontology category	k	f
late endosome [GO:0005770]	0.003004	SEC7 SNX41 BTN2 VPS21	4	17
endosome membrane [GO:0010008]	0.00482	SNX41 TOR1 VTA1 EAR1 VPS27 VPS21 VPS4	7	57
cytoplasmic vesicle [GO:0031410]	0.005305	SEC31 RET2 VRG4 MTC1 APM1 SEC23	6	44
nuclear nucleosome [GO:0000788]	0.006673	HHF1 CSE4 HHT2	3	11
nucleosome [GO:0000786]	0.006673	HHF1 CSE4 HHT2	3	11
small-subunit processome [GO:0032040]	0.007358	KRR1 UTP4 UTP7 ECM16 RRP5 RPS7B	6	47
polysomal ribosome [GO:0042788]	0.00783	RBG1 GIS2	2	4
mitochondrial matrix [GO:0005759]	0.00791	PIM1 MCX1 HEM1 RPO41 PKP2 BAT1 SSC1 ARG7 ATP11 MGE1	10	111
Ino80 complex [GO:0031011]	0.008657	RVB1 IES1 RVB2	3	12
DNA-directed RNA polymerase II, core complex [GO:0005665]	0.008657	RPO21 RPB4 RPB2	3	12
MIPS Functional Classification (459 categories)				
rRNA processing [11.04.01]	5.04E-08	SPB1 KRR1 NOP6 UTP4 NPL3 NUG1 UTP7 LSM4 RPF1 DBP8 MTR4 MRT4 DRS1 MDN1 ECM16 RRP5 RLP7 NOP8 RAT1 NOP4 BMS1 RVB2 MRD1	23	169
ribosome biogenesis [12.01]	4.47E-07	KRR1 NUG1 LOC1 SDA1 TOR1 MRT4 ECM16 RLP7 NOP15 GIS2 KRI1 NOC2 BMS1	13	64
RNA binding [16.03.03]	2.02E-05	HEK2 GBP2 SRO9 LHP1 CFT1 UTP4 NPL3 UTP7 LOC1 RNA15 RPF1 SCP160 RRP5 RLP7 WHI3 NOP12 BRX1 BFR1 NOP4 MRD1	20	189
ATP binding [16.19.03]	2.36E-05	PIM1 MCX1 RBK1 RVB1 BRR2 SMC1 SMC2 DBP8 STH1 MTR4 SSC1 STE6 DRS1 MDN1 VBA1 APC1 MOT1 NEW1 RVB2 VPS4	20	191
general transcription activities [11.02.03.01]	9.15E-05	RPO21 NGG1 RVB1 SSN2 RPO41 PGD1 SUT1 RPB4 SWI6 ECM22 URE2 GAL11 HIR2 RPB2 MBF1 TFC8	16	146
unfolded protein response (e.g. ER quality control) [32.01.07]	0.0002033	MCX1 CDC37 ZUO1 CCT7 CPR7 SIS1 ATP11 STI1 NOB1 MGE1	10	69
microtubule cytoskeleton [42.04.05]	0.0002871	ATS1 NUM1 CDC37 SPC110 SIM1 MHP1 STU2 CRN1	8	47
actin cytoskeleton [42.04.03]	0.0007935	SDA1 ACF4 SFK1 STT4 ARC18 CRN1 SIW14 WSC2 SHE4 WHI2 PIN3	11	96
cellular export and secretion [20.09.16]	0.0009123	SEC9 ERP5 STE6 FPS1 STT4 SSO1 SYT1	7	43
mitotic cell cycle [10.03.01.01]	0.001015	AME1 SPO12 BFR1 CLN2	4	13
cytokinesis (cell division) /septum formation and hydrolysis [10.03.03]	0.001147	SKT5 CHS3 MYO1 YCK1 HOF1 NOP15 YCK2 BNI4 BFR1	9	71
intra Golgi transport [20.09.07.05]	0.00117	SEC7 COG2 SED5 VTI1 VPS27 VPS4	6	33
cell growth / morphogenesis [40.01]	0.001669	SKT5 RGP1 SUA5 MYO1 YCK1 KRE9 SWE1 CPR7 ACF4 CRN1 HOF1	16	189

Ontology	p- value	Genes in ontology category	k	f
		YCK2 BNI4 STI1 SSO1 CLN2		
budding, cell polarity and filament formation [43.01.03.05]	0.002675	SKT5 CHS3 HKR1 BUD27 SEC9 MYO1 YCK1 CIS3 KRE9 SWE1 ACF4 SAP190 CHS5 CRN1 HOF1 MYO5 YCK2 WHI3 BNI4 BFR1 SSO1 CLN2	22	312
tRNA modification [11.06.02]	0.004725	NCL1 TRM3 ADE3 DUS3 DUS4 TRM10	6	43
protein binding [16.01]	0.00514	MCX1 NUM1 CDC37 RET2 COG2 ZUO1 CCT7 CPR7 TOR1 STU2 SWI6 CRN1 HOF1 SIS1 APC1 BNI4 ATP11 VPS27 STI1 SHE4 NOB1 RUP1 MGE1 APM1 ATG13	25	391
cell wall [42.01]	0.005513	SKT5 CHS3 TIP1 ECM33 HKR1 PKH1 TIR1 ECM32 MHP1 CIS3 KRE9 SWI6 ARG7 MYO5 ECM16 WSC2	16	213
DNA binding [16.03.01]	0.005674	HHF1 GBP2 RPO21 RPC53 SPT2 SMC1 RPO41 SMC2 CRP1 RPB4 CSE4 HHT2 RPB2	13	158
endocytosis [20.09.18.09.01]	0.005842	PKH1 YCK1 MYO5 SIW14 YCK2 WHI2 VPS21	7	59
phosphate metabolism [01.04]	0.007061	APA1 RBK1 RVB1 PKH1 SMC1 SMC2 PKP2 YCK1 STH1 SWE1 SSC1 TOR1 STE6 SAP190 PSR1 MDN1 RCK2 STT4 SIW14 YCK2 MOT1 PPQ1 NEW1 RVB2 VPS4	25	401
protein folding and stabilization [14.01]	0.007316	CDC37 FPR2 ZUO1 CCT7 CPR7 SSC1 FPR4 STI1 MGE1	9	93
transcriptional control [11.02.03.04]	0.007918	HHF1 SPB1 NGG1 RVB1 SSN2 UBP3 SPT2 RSC8 PGD1 SUT1 SNF6 STH1 ASG1 CPR7 RCN1 SWI6 ECM22 SPT5 HHT2 GIS2 GAL11 HIR2 MBF1 MOT1 ELP4 RVB2	26	426
enzymatic activity regulation / enzyme regulator [18.02.01]	0.007979	VAM6 PCL10 SWE1 SSC1 RCN1 SIW14 PCL1 CLN2	8	78
protein targeting, sorting and translocation [14.04]	0.008021	BSD2 VPS64 SNX41 NPL3 NUP57 ERP5 SSC1 MLP1 STT4 VPS71 VTI1 TOM70 VPS27 VPS21 VPS17 MGE1 APM1 VPS4 ATG13	19	281
MIPS Phenotypes (142 categories)				
Secretory mutants [52.45]	7.00E-05	SEC31 SEC7 RET2 SEC9 COG2 VTI1 VPS21 VPS17 VPS4 SEC23	10	61
other cell wall mutants [52.15.99]	0.001402	SKT5 ECM33 HKR1 ECM32 YCK1 FPS1 CHS5 ECM16 BNI4	9	73
Silencing mutants [82.15.50]	0.002342	HHF1 SPB1 NPL3 UBP3 HHT2	5	26
Mutator phenotypes [82.25]	0.004013	HSM3 RFC1	2	3
Calcofluor white resistance [52.15.15.05]	0.004616	SKT5 CHS3 CHS5 ARG7	4	19
Killer toxin hypersensitivity [52.15.35.20]	0.004989	ATS1 ECM33 MHP1	3	10
Papulacandin B sensitivity [52.15.30.10]	0.007983	ECM32 YCK1 ECM16 YCK2	4	22
other cell cycle defects [22.99]	0.009781	NUM1 CDC37 SPC110 SMC1 SMC2 MYO1 PRP8 BAT1 SIM1 HOF1 APC1 WHI2 BFR1 RFC1 CLN2	15	207

Ontology	p- value	Genes in ontology category	k	f
MIPS Subcellular Localization (48 categories)				
nucleolus [750.05]	2.05E-09	KRR1 NOP6 MAK21 UTP4 NUG1 UTP7 LOC1 DBP8 RRT14 MTR4 MRT4 DRS1 PWP1 RSA3 FPR4 ECM16 RRP5 NOP15 KRE33 KRI1 NOP12 BRX1 TRM10 NOP8 NOC2 NOP4 BMS1 JIP5	28	208
nucleus [750]	3.79E-08	NCL1 SKT5 HHF1 TOS1 HIS7 GBP2 APA1 SPB1 KRR1 RBK1 LHP1 RPO21 RPC53 NOP6 MAK21 CDC37 NGG1 RVB1 CFT1 UTP4 SAC7 ADE8 NPL3 SSN2 NUG1 CHZ1 UTP7 LSM4 SPT2 BRR2 ECM32 SMC1 IES1 LOC1 SMC2 RSC8 PGD1 RNA15 MAD1 SUT1 NUP57 ADE3 SDA1 ZUO1 SNF6 YCK1 SPO12 PRP8 DBP8 STH1 RRT14 ASG1 MHP1 MTR4 SCP160 RPB4 SWE1 MRT4 CSE4 MLP1 DRS1 STU2 MDN1 SWI6 PWP1 ECM22 STP3 DUS3 FPR4 SPT5 VPS71 PIF1 ECM16 RRP5 RLP7 SIS1 HHT2 BOP3 NST1 NOP15 YCK2 APC1 GIS2 KRI1 GAL11 PSH1 BRX1 TRM10 NOP8 HIR2 RAT1 NOB1 SLD7 VPS21 RUP1 RPB2 DED1 NOC2 RFC1 MBF1 PRO2 TFC8 RAD1 NOP4 CWC27 MOT1 BMS1 NEW1 CLN2 FCY1 PIN3 JIP5 DPB2	113	1976
chromosome structure [750.09]	0.000246	HEK2 HHF1 GBP2 SPT2 RSC8 ZUO1 STH1 HHT2	8	46
transport vesicles [745]	0.0009123	SEC31 SEC7 RET2 VTI1 VPS21 APM1 SEC23	7	43
inter-golgi transport vesicles [745.05]	0.004013	SEC7 VTI1	2	3
endosome [765]	0.00482	SNX41 BLI1 VTA1 EAR1 VPS27 VPS17 VPS4	7	57
cytoskeleton [730]	0.006133	SPC110 SAC7 SDA1 MYO1 MHP1 ARC18 CRN1 HOF1 MYO5 BNI4	10	107
MIPS Protein Complexes (1142 categories)				
Complex Number 149, probably RNA metabolism [550.1.149]	4.19E-12	SPB1 LHP1 MAK21 SEC7 NUG1 LOC1 SDA1 RPF1 MRT4 DRS1 MDN1 RSA3 FPR4 RLP7 NOP15 KRE33 NOP12 BRX1 NOC2 NOP4 BMS1	21	88
Complex Number 140, probably RNA metabolism [550.1.140]	4.16E-11	SRO9 KRR1 LHP1 NOP6 MAK21 NUG1 TIF4631 DRS1 MDN1 RLP7 KRE33 NOP12 BRX1 NOC2 NOP4	15	46
Complex Number 446 [550.2.446]	4.12E-08	GBP2 KRR1 NOP6 NPL3 NUG1 TIF4631 DRS1 PWP1 RRP5 KRE33 KRI1 NOP12 NOC2	13	53
Complex Number 6 [550.2.6]	4.56E-06	KRR1 PWP1 KRE33 KRI1 BRX1 NOP4 APM1	7	20
Complex Number 74 [550.2.74]	7.53E-06	HHF1 GBP2 CDC37 NPL3 KRE33	5	9
Complex Number 204 [550.2.204]	9.27E-06	TIF4631 DRS1 RRP5 KRI1 NOC2 NOP4	6	15
Complex Number 200 [550.2.200]	3.19E-05	HHF1 LOC1 PWP1 KRE33 KRI1 NOP12 SEC23	7	26
Complex Number 517 [550.2.517]	3.19E-05	NPL3 TIF4631 KRE33 KRI1 NOP12 NOC2 NOP4	7	26
Complex Number 56 [550.2.56]	7.61E-05	HHF1 NUG1 TIF4631 PWP1 RRP5 KRE33 KRI1 NOP12 NOP4	9	50

Ontology	p- value	Genes in ontology category	k	f
Complex Number 40, Pwp1/Brx1/Nop12 (3) [550.3.40]	0.0001964	PWP1 NOP12 BRX1	3	4
Complex Number 142, probably RNA metabolism [550.1.142]	0.0002399	RBG1 HEK2 SRO9 LHP1 SUT1 TIF4631	6	25
Complex Number 144, probably RNA metabolism [550.1.144]	0.0002474	KRR1 NOP6 UTP4 UTP7 DBP8 ECM16 KRE33 BRX1 NOB1 NOC2 BMS1	11	84
Complex Number 17, Pab1 (1) [550.3.17]	0.0003255	TIF4631 MTR4 RRP5 NOC2	4	10
Complex Number 125, probably protein/RNA transport [550.1.125]	0.0003261	SRO9 KRR1 NOP6 UTP4 UTP7 DBP8 ECM16 KRE33 NOP12 BMS1	10	73
Complex Number 441 [550.2.441]	0.0004775	NUG1 NOP12 NOB1	3	5
Complex Number 94 [550.2.94]	0.0004942	NUG1 MRT4 FPR4 RLP7 NOP15 BRX1 NOC2	7	39
Complex Number 520 [550.2.520]	0.0004942	NUG1 MRT4 FPR4 RLP7 NOP15 BRX1 NOC2	7	39
Complex Number 201 [550.2.201]	0.0007235	HHF1 NUG1 LOC1 NOP12	4	12
Complex Number 150 [550.2.150]	0.001058	RVB1 UTP7 TIF4631 KRE33 BRX1	5	22
Complex Number 325 [550.2.325]	0.001371	RVB1 RVB2	2	2
Complex Number 436 [550.2.436]	0.001371	YCK1 YCK2	2	2
Complex Number 247 [550.2.247]	0.001371	PSR1 WHI2	2	2
Complex Number 339 [550.2.339]	0.001371	SEC31 CRN1	2	2
Complex Number 137 [550.2.137]	0.00138	HHF1 KRI1 HIR2 NOP4	4	14
Complex Number 12, Sit4 (6) [550.3.12]	0.001581	SAP190 RCK2 RAT1	3	7
rRNA splicing [440.30.20]	0.001608	UTP4 NPL3 UTP7 DRS1 RAT1	5	24
Complex Number 229, probably transcription/DNA maintanance/chromatin structure [550.1.229]	0.00246	SMC1 PWP1 FPR4	3	8
Complex Number 24, RNA Polymerase II (12) [550.3.24]	0.003004	RPO21 RPB4 SPT5 RPB2	4	17
Complex Number 200, probably transcription/DNA maintanance/chromatin structure [550.1.200]	0.003294	RSC8 SUT1 STH1 MOT1 RVB2	5	28
Complex Number 155, probably RNA metabolism [550.1.155]	0.003752	LHP1 NPL3 SUT1 TIF4631	4	18
Complex Number 13, U4/U6.U5 tri-snRNP (2) [550.3.13]	0.004013	BRR2 PRP8	2	3
Complex Number 210, probably transcription/DNA maintanance/chromatin structure [550.1.210]	0.004616	RPO21 RPB4 SPT5 RPB2	4	19
Complex Number 480 [550.2.480]	0.004989	RRP5 KRE33 NOC2	3	10
Complex Number 7, Dbp7/Rrp5 (4) [550.3.7]	0.004989	MAK21 RRP5 NOC2	3	10

Ontology	p- value	Genes in ontology category	k	f
Complex Number 344 [550.2.344]	0.004989	NPL3 SPT2 TIF4631	3	10
Complex Number 106, probably protein synthesis turnover [550.1.106]	0.006673	TIF4631 ZUO1 SCP160	3	11
Complex Number 82 [550.2.82]	0.007785	SPB1 KRE33 KRI1 NOP12 BMS1	5	34
Complex Number 11, Noc (3) [550.3.11]	0.00783	MAK21 NOC2	2	4
Casein kinase I [120.10]	0.00783	YCK1 YCK2	2	4
Complex Number 253 [550.2.253]	0.00783	HHF1 RRP5	2	4
Complex Number 518 [550.2.518]	0.00783	PIM1 MDN1	2	4
Complex Number 473 [550.2.473]	0.00783	NPL3 KRE33	2	4
Complex Number 375 [550.2.375]	0.007983	UTP7 SPT2 TIF4631 NOP12	4	22
Complex Number 16, Ded1 (1) [550.3.16]	0.008657	TIF4631 MTR4 DED1	3	12
Complex Number 8, probably cell cycle [550.1.8]	0.008657	SMC1 NOP12 RVB2	3	12
Complex Number 109, probably protein synthesis turnover [550.1.109]	0.008814	KRR1 UTP7 ECM16 KRE33 NOB1	5	35
Complex Number 139, probably RNA metabolism [550.1.139]	0.008814	SRO9 NPL3 SUT1 TIF4631 SCP160	5	35
Complex Number 214, probably transcription/DNA maintanance/chromatin structure [550.1.214]	0.009931	RPO21 NGG1 MYO1 RPB2 MOT1 RVB2	6	50

Table 13. Ontologies enriched among the 62 genes upregulated in both *Δfpr3* and *Δfpr4* yeast

Ontology	p- value	Genes in ontology category	k	f
GO Molecular Function (1646 categories)				
structural constituent of ribosome [GO:0003735]	5.07E-08	RPL23A RPS13 RPS17B RPL23B RPL30 RPL26B RPS4A RPL14A RPS21A RPL38 RPL21B RPS9A RPS23B	13	218
inorganic phosphate transmembrane transporter activity [GO:0005315]	7.04E-06	PHO89 PIC2 PHO84	3	5
acid phosphatase activity [GO:0003993]	5.77E-05	PHO11 PHO5 PHO12	3	9
phosphatase activity [GO:0016791]	0.0001235	PHO11 PHO5 PHO8 PHO12	4	29
GDP binding [GO:0019003]	0.0002422	TEF2 TEF1	2	3
spermine transmembrane transporter activity [GO:0000297]	0.0004815	TPO2 TPO3	2	4
ion channel activity [GO:0005216]	0.002195	YRO2 HSP30	2	8
antiporter activity [GO:0015297]	0.005939	TPO2 TPO3	2	13
fructose transmembrane transporter activity [GO:0005353]	0.007902	HXT3 HXT4	2	15
mannose transmembrane transporter activity [GO:0015578]	0.007902	HXT3 HXT4	2	15
translation elongation factor activity [GO:0003746]	0.008978	TEF2 TEF1	2	16
nucleotide phosphatase activity [GO:0019204]	0.009087	PHO8	1	1
acireductone synthase activity [GO:0043874]	0.009087	UTR4	1	1
ATP phosphoribosyltransferase activity [GO:0003879]	0.009087	HIS1	1	1
stearoyl-CoA 9-desaturase activity [GO:0004768]	0.009087	OLE1	1	1
oxidoreductase activity, acting on paired donors, with oxidation of a pair of donors resulting in the reduction of molecular oxygen to two molecules of water [GO:0016717]	0.009087	OLE1	1	1
cyclosporin A binding [GO:0016018]	0.009087	CPR1	1	1
polyphosphate kinase activity [GO:0008976]	0.009087	VTC4	1	1
dihydroorotate oxidase activity [GO:0004158]	0.009087	URA1	1	1
dihydroorotate dehydrogenase activity [GO:0004152]	0.009087	URA1	1	1
ATP-dependent protein binding [GO:0043008]	0.009087	UBI4	1	1
3'(2'),5'-bisphosphate nucleotidase activity [GO:0008441]	0.009087	MET22	1	1
glycogen phosphorylase activity [GO:0008184]	0.009087	GPH1	1	1
phosphorylase activity [GO:0004645]	0.009087	GPH1	1	1

Ontology	p- value	Genes in ontology category	k	f
sodium:inorganic phosphate symporter activity [GO:0015319]	0.009087	PHO89	1	1
GO Biological Process (2062 categories)				
translation [GO:0006412]	9.27E-08	RPL23A TEF2 RPS13 RPS17B RPL23B RPL30 RPL26B RPS4A RPL14A RPS21A RPL38 RPL21B RPS9A TEF1 RPS23B	15	318
polyphosphate metabolic process [GO:0006797]	4.20E-07	VTC1 VTC4 PHO84 VTC3	4	8
phosphate transport [GO:0006817]	1.24E-06	PHO89 PIC2 PHO86 PHO84	4	10
phosphate metabolic process [GO:0006796]	3.87E-05	PHO11 PHO5 PHO81	3	8
microautophagy [GO:0016237]	8.18E-05	VTC1 VTC4 VTC3	3	10
vacuole fusion, non-autophagic [GO:0042144]	0.0001235	VTC1 TRX2 VTC4 VTC3	4	29
dephosphorylation [GO:0016311]	0.0001832	PHO11 PHO5 PHO8 PHO12	4	32
vacuolar transport [GO:0007034]	0.0003673	VTC1 VTC4 VTC3	3	16
spermine transport [GO:0000296]	0.0004815	TPO2 TPO3	2	4
sulfate assimilation [GO:0000103]	0.004237	TRX2 MET22	2	11
transmembrane transport [GO:0055085]	0.005721	PHO89 HXT3 PIC2 TPO2 HXT4 PHO84 ECM3 TPO3	8	303
fungal-type cell wall organization [GO:0031505]	0.005896	PRS4 PST1 MKC7 HPF1 ECM3	5	128
hexose transport [GO:0008645]	0.006888	HXT3 HXT4	2	14
negative regulation of nuclear mRNA splicing, via spliceosome [GO:0048025]	0.009087	RPL30	1	1
unsaturated fatty acid biosynthetic process [GO:0006636]	0.009087	OLE1	1	1
positive regulation of transcription from RNA polymerase II promoter involved in unfolded protein response [GO:0006990]	0.009087	HAC1	1	1
response to temperature stimulus [GO:0009266]	0.009087	SPL2	1	1
regulation of phosphate transport [GO:0010966]	0.009087	PHO86	1	1
cell wall assembly [GO:0070726]	0.009087	YGP1	1	1
hyperosmotic salinity response [GO:0042538]	0.009087	MET22	1	1
nicotinamide nucleotide metabolic process [GO:0046496]	0.009087	PHO8	1	1
GO Cellular Component (625 categories)				
ribosome [GO:0005840]	6.61E-08	RPL23A TEF2 RPS13 RPS17B RPL23B RPL30 RPL26B RPS4A RPL14A RPS21A RPL38 RPL21B RPS9A TEF1 RPS23B	15	310
ribonucleoprotein complex [GO:0030529]	4.10E-07	RPL23A RPS13 SNU56 RPS17B RPL23B RPL30 RPL26B RPS4A	14	307

Ontology	p- value	Genes in ontology category	k	f
		RPL14A RPS21A RPL38 RPL21B RPS9A RPS23B		
vacuolar transporter chaperone complex [GO:0033254]	2.84E-06	VTC1 VTC4 VTC3	3	4
intracellular [GO:0005622]	5.41E-06	STP4 RPS13 RPS17B HIS1 RPL30 MIG2 RPL26B RPS4A RPL14A RPS21A RPL38 RPL21B RPS9A RPS23B	14	381
cytosolic large ribosomal subunit [GO:0022625]	1.28E-05	RPL23A RPL23B RPL30 RPL26B RPL14A RPL38 RPL21B	7	88
cytosolic small ribosomal subunit [GO:0022627]	1.81E-05	RPS13 RPS17B RPS4A RPS21A RPS9A RPS23B	6	62
intrinsic to vacuolar membrane [GO:0031310]	8.12E-05	VTC1 VTC4	2	2
extracellular region [GO:0005576]	0.0002026	PHO11 PHO5 PST1 SPI1 YGP1 HPF1	6	95
eukaryotic translation elongation factor 1 complex [GO:0005853]	0.0007979	TEF2 TEF1	2	5
fungal-type cell wall [GO:0009277]	0.0009838	PHO5 PST1 MKC7 SPI1 HPF1	5	85
anchored to membrane [GO:0031225]	0.002185	PST1 MKC7 SPI1 HPF1	4	61
cytoplasm [GO:0005737]	0.002998	PRS4 RPL23A TEF2 STP4 RPS13 CPR1 RPS17B PHO8 UTR4 HIS1 HMF1 RPL23B RPL30 RPL26B TRX2 PHO81 SPL2 RPS4A RPL14A PRR1 URA1 RPS21A UBI4 RPL38 RGS2 RPS9A TEF1 RPS23B GPH1	29	2026
small ribosomal subunit [GO:0015935]	0.006888	RPS9A RPS23B	2	14
MIPS Functional Classification (459 categories)				
ribosomal proteins [12.01.01]	2.10E-07	RPL23A RPS13 RPS17B RPL23B RPL30 RPL26B RPS4A RPL14A RPS21A RPL38 RPL21B RPS9A RPS23B	13	246
phosphate transport [20.01.01.07.07]	1.94E-06	PHO89 PIC2 PHO86 PHO84	4	11
homeostasis of phosphate [34.01.03.03]	5.77E-05	PHO89 PHO86 PHO84	3	9
vacuole or lysosome [42.25]	0.0006376	VTC1 TRX2 VTC4 VTC3	4	44
stress response [32.01]	0.003331	YRO2 HSP30 CPR1 HMF1 UBI4 YGP1	6	162
amine / polyamine transport [20.01.11]	0.006888	TPO2 TPO3	2	14
biosynthesis of histidine [01.01.09.07.01]	0.007902	PRS4 HIS1	2	15
sodium driven symporter [20.03.02.02.02]	0.009087	PHO89	1	1
MIPS Phenotypes (142 categories)				
other stress response defects [62.99]	0.002806	HSP30 UBI4	2	9
MIPS Subcellular Localization (48 categories)				
vacuole [770]	0.0001658	PHO11 PHO5 MKC7 HXT3 PHO8 PIC2 SPI1 PHO12 VTC3	9	224

Ontology	p- value	Genes in ontology category	k	f
vacuolar membrane [770.01]	0.0002402	PHO8 VTC1 TPO2 VTC4 VTC3 TPO3	6	98
plasma membrane [720]	0.00129	HSP30 PST1 MKC7 HXT3 VTC1 HXT4 PHO84	7	184
extracellular [701]	0.001294	PHO11 PHO5 PHO12 YGP1	4	53
cytoplasm [725]	0.003543	PRS4 RPL23A TEF2 STP4 RPS13 CPR1 RPS17B PHO8 UTR4 HMF1 RPL23B SPI1 HAC1 RPL30 OLE1 MIG2 RPL26B TRX2 PHO81 SPL2 VTC4 RPS4A RPL14A PRR1 URA1 RPS21A UBI4 RPL38 YGP1 MET22 HPF1 RGS2 RPL21B RPS9A TEF1 RPS23B GPH1	37	2879
MIPS Protein Complexes (1142 categories)				
cytoplasmic ribosomal large subunit [500.40.10]	7.36E-06	RPL23A RPL23B RPL30 RPL26B RPL14A RPL38 RPL21B	7	81
cytoplasmic ribosomal small subunit [500.40.20]	1.11E-05	RPS13 RPS17B RPS4A RPS21A RPS9A RPS23B	6	57
eEF1 [500.20.10]	0.00119	TEF2 TEF1	2	6
Complex Number 329 [550.2.329]	0.001656	UBI4 PHO84	2	7
Complex Number 413 [550.2.413]	0.002806	HMF1 UBI4	2	9
Complex Number 119 [550.2.119]	0.005939	CPR1 UBI4	2	13

Table 14. Ontologies enriched among the 65 genes downregulated in both *Δfpr3* and *Δfpr4* yeast

Ontology	p- value	Genes in ontology category	k	f
GO Molecular Function (1646 categories)				
siderophore transmembrane transporter activity [GO:0015343]	9.54E-05	ARN1 ARN2	2	2
protein serine/threonine kinase activity [GO:0004674]	0.001193	PKC1 KSS1 KSP1 KIC1 HAL5 HSL1	6	122
protein kinase activity [GO:0004672]	0.00141	PKC1 KSS1 KSP1 KIC1 HAL5 HSL1	6	126
Rab GTPase activator activity [GO:0005097]	0.004956	GYP7 GYL1	2	11
GTPase activator activity [GO:0005096]	0.009625	GYP7 LRG1 GLO3	3	45
syntaxin binding [GO:0019905]	0.009844	SLY1	1	1
peroxisome matrix targeting signal-1 binding [GO:0005052]	0.009844	PEX5	1	1
siderophore uptake transmembrane transporter activity [GO:0015344]	0.009844	SIT1	1	1
carnitine transporter activity [GO:0015226]	0.009844	AGP2	1	1
myosin I binding [GO:0017024]	0.009844	BBC1	1	1
tripeptide transporter activity [GO:0042937]	0.009844	PTR2	1	1
protein kinase C activity [GO:0004697]	0.009844	PKC1	1	1
GO Biological Process (2062 categories)				
siderophore transport [GO:0015891]	4.33E-09	SIT1 ARN1 ARN2 FIT2 FIT3	5	8
iron ion homeostasis [GO:0055072]	4.44E-06	SIT1 ARN1 ARN2 FIT2 FIT3	5	26
transport [GO:0006810]	0.00178	AGP2 SLY1 PEX5 PDR15 SIT1 GLO3 ARN1 ARN2 GGA2 SEC28 PTR2 NUP2 YMD8 NUP1 PDR5 FIT2 FIT3	17	815
protein phosphorylation [GO:0006468]	0.001861	PKC1 KSS1 KSP1 KIC1 HAL5 HSL1	6	133
vesicle-mediated transport [GO:0016192]	0.002413	RCR1 GYP7 SLY1 PIB2 GGA2 SEC28	6	140
retrograde vesicle-mediated transport, Golgi to ER [GO:0006890]	0.002502	SLY1 GLO3 SEC28	3	28
transcription-dependent tethering of RNA polymerase II gene DNA at nuclear periphery [GO:0000972]	0.002572	NUP2 NUP1	2	8
response to osmotic stress [GO:0006970]	0.002771	AGP2 MSB2 SKN7	3	29
ion transport [GO:0006811]	0.003886	SIT1 ARN1 ARN2 FIT2 FIT3	5	107
signal transduction involved in filamentous growth [GO:0001402]	0.004081	MSB2 KSS1	2	10
positive regulation of Rab GTPase activity [GO:0032851]	0.004956	GYP7 GYL1	2	11

Ontology	p- value	Genes in ontology category	k	f
positive regulation of GTPase activity [GO:0043547]	0.006464	GYP7 LRG1 GLO3	3	39
regulation of Rab GTPase activity [GO:0032313]	0.00694	GYP7 GYL1	2	13
ER to Golgi vesicle-mediated transport [GO:0006888]	0.007731	SLY1 GLO3 SEC28 GYL1	4	80
fungal-type cell wall organization [GO:0031505]	0.00826	SLA1 PKC1 RCR1 KIC1 SRL1	5	128
intracellular signal transduction [GO:0035556]	0.009225	PKC1 IML1	2	15
regulation of transcription, DNA-dependent [GO:0006355]	0.009826	CCR4 TEC1 UPC2 SUM1 SPT6 SKN7 RSC4 SOK2 CAF120 AZF1 HHO1	11	507
COPI coating of Golgi vesicle [GO:0048205]	0.009844	GLO3	1	1
siderophore metabolic process [GO:0009237]	0.009844	ARN2	1	1
vesicle coating [GO:0006901]	0.009844	SEC28	1	1
tripeptide transport [GO:0042939]	0.009844	PTR2	1	1
phosphatidylcholine catabolic process [GO:0034638]	0.009844	NTE1	1	1
meiotic sister chromatid separation [GO:0051757]	0.009844	SGO1	1	1
positive regulation of maintenance of meiotic sister chromatid cohesion [GO:0034096]	0.009844	SGO1	1	1
response to carbohydrate stimulus [GO:0009743]	0.009844	AZF1	1	1
maturation of 5S rRNA [GO:0000481]	0.009844	SNU66	1	1
negative regulation of chromatin silencing [GO:0031936]	0.009844	HHO1	1	1
carnitine transport [GO:0015879]	0.009844	AGP2	1	1
GO Cellular Component (625 categories)				
cytoplasmic membrane-bounded vesicle [GO:0016023]	7.33E-05	SIT1 ARN1 ARN2	3	9
membrane [GO:0016020]	0.001275	SLA1 RCR1 CSG2 AGP2 MTC5 SLY1 UPC2 PEX5 PDR15 SIT1 PIB2 MNT2 ARN1 ARN2 SEC28 AIM19 FAR1 IML1 PTR2 PSR2 NUP2 YMD8 NTE1 CHS1 NUP1 PDR5 FIT2 FIT3	28	1671
extrinsic to fungal-type vacuolar membrane [GO:0097042]	0.001395	MTC5 IML1	2	6
integral to plasma membrane [GO:0005887]	0.00159	AGP2 MSB2 PTR2	3	24
endosome membrane [GO:0010008]	0.002285	SLA1 SIT1 ARN1 ARN2	4	57
Seh1-associated complex [GO:0035859]	0.002572	MTC5 IML1	2	8
COPI vesicle coat [GO:0030126]	0.002572	GLO3 SEC28	2	8
endosome [GO:0005768]	0.004044	SLA1 SIT1 ARN1 ARN2 SEC28	5	108

Ontology	p- value	Genes in ontology category	k	f
COPI coated vesicle membrane [GO:0030663]	0.004081	SEC28 YMD8	2	10
site of polarized growth [GO:0030427]	0.004956	PKC1 MSB2	2	11
COPI-coated vesicle [GO:0030137]	0.00591	GLO3 YMD8	2	12
cell surface [GO:0009986]	0.009844	SRL1	1	1
MIPS Functional Classification (459 categories)				
siderophore-iron transport [20.01.01.01.01.01]	0.000188	SIT1 ARN1 ARN2	3	12
drug/toxin transport [20.01.27]	0.0005432	SIT1 ARN1 ARN2 PDR5	4	39
budding, cell polarity and filament formation [43.01.03.05]	0.0008478	SLA1 PKC1 TEC1 MSB2 KSS1 FAR1 BUD4 HSL1 SOK2 CHS1	10	312
detoxification [32.07]	0.001077	SIT1 ARN1 ARN2 PDR5 SRL1	5	80
ion transport [20.01.01]	0.001941	FIT2 FIT3	2	7
modification by phosphorylation, dephosphorylation, autophosphorylation [14.07.03]	0.002201	PKC1 KSS1 RTS3 KSP1 HAL5 HSL1 PSR2	7	186
GTPase activator (GAP) [18.02.01.01.01]	0.003684	GYP7 LRG1 GLO3	3	32
ER to Golgi transport [20.09.07.03]	0.004822	SLY1 GLO3 SEC28 GYL1	4	70
mitotic cell cycle and cell cycle control [10.03.01]	0.004929	PKC1 GLO3 RPN12 CLG1 KIC1 SKN7 CLN1	7	215
transcriptional control [11.02.03.04]	0.008193	CCR4 TEC1 ASF2 UPC2 GLO3 SPT6 SKN7 SOK2 CAF120 HHO1	10	426
MIPS Phenotypes (142 categories)				
Staurosporine sensitivity [92.60]	0.001941	CCR4 PKC1	2	7
G1 arrest [22.05]	0.002502	PKC1 RPN12 SPT6	3	28
Divalent cations and heavy metals sensitivity [62.35.02]	0.004346	CCR4 CSG2 UPC2 RPN12	4	68
Nitrogen utilization [42.30]	0.009844	AGP2	1	1
MIPS Subcellular Localization (48 categories)				
neck [705.03]	0.0007624	PKC1 LRG1 BUD4 HSL1 GYL1 CAF120	6	112
golgi-ER transport vesicles [745.03]	0.002759	SLY1 GLO3 SEC28 YMD8	4	60
bud [705]	0.007075	PKC1 GYL1 CAF120 SRL1	4	78
plasma membrane [720]	0.009127	SIT1 MSB2 PTR2 GYL1 CHS1 PDR5	6	184
MIPS Protein Complexes (1142 categories)				
Complex Number 151 [550.2.151]	0.004081	KSP1 CHS1	2	10

Ontology	p- value	Genes in ontology category	k	f
Complex Number 156 [550.2.156]	0.00694	SLA1 RPN12	2	13
Nuclear pore complex (NPC) [310]	0.00694	NUP2 NUP1	2	13
Complex Number 79, probably membrane biogenesis and traffic [550.1.79]	0.009225	GLO3 SEC28	2	15
Complex Number 169 [550.2.169]	0.009225	IMD2 HHO1	2	15

Table 15. Ontologies enriched among the 145 genes only upregulated in *Δfpr3Δfpr4* yeast (from Figure 26 B)

Ontology	p- value	Genes in ontology category	k	f
GO Molecular Function (1646 categories)				
structural constituent of ribosome [GO:0003735]	9.83E-06	RPS9B MRPL35 RPS18A RPL37B RPS27B MRPL6 RPL40A RPL39 RPL40B RPS31 RPS18B RPS1B RPS10B RPS3 RPL25 RPS6A	16	218
rRNA binding [GO:0019843]	1.25E-05	RPS9B RPS18A RPL37B MRPL6 EMG1 RPS18B RPL25	7	39
transferase activity [GO:0016740]	0.00011	HMT1 ARO4 RIB5 SAT4 ARO3 RKM2 VHS1 WBP1 MNN1 HOM3 MET6 TOS3 PRS3 IRE1 HIS5 ELO1 AAT2 EMG1 OST6 LEU4 RIO2 LEU9 TUM1 POS5 ALG5 SAM4 SPE3	27	611
catalytic activity [GO:0003824]	0.0004	TYR1 ARO4 GDH2 ARO3 DLD3 SEC53 SCW11 IRE1 HIS5 CPA2 AAT2 CTS1 GCV2 GAD1 LEU4 RIO2 LEU9 PDE2 ULA1 SPE3 AXL1	21	455
3-deoxy-7-phosphoheptulonate synthase activity [GO:0003849]	0.00043	ARO4 ARO3	2	2
2-isopropylmalate synthase activity [GO:0003852]	0.00043	LEU4 LEU9	2	2
protein tag [GO:0031386]	0.00067	RPL40A RPL40B RPS31	3	9
receptor activity [GO:0004872]	0.00331	COS7 STE2 IZH2	3	15
glucosidase activity [GO:0015926]	0.00838	SKN1 DSE2	2	7
transferase activity, transferring acyl groups, acyl groups converted into alkyl on transfer [GO:0046912]	0.00838	LEU4 LEU9	2	7
GO Biological Process (2062 categories)				
cellular amino acid biosynthetic process [GO:0008652]	8.89E-08	TYR1 ARO4 ARO3 GCN4 HOM3 MET6 LEU1 HIS5 CPA2 LEU4 ARG1 LEU9 SAM4	13	98
cytokinesis, completion of separation [GO:0007109]	5.23E-05	DSE1 SCW11 DSE2 CTS1	4	11
leucine biosynthetic process [GO:0009098]	8.48E-05	LEU1 LEU4 LEU9	3	5
carboxylic acid metabolic process [GO:0019752]	0.00045	GAD1 LEU4 LEU9	3	8
ribosome biogenesis [GO:0042254]	0.00076	RPS9B CIC1 RPL40A RPL40B RPS31 EMG1 RIO2 RPS6A NAN1 NIP7 RRP9	11	170
maturation of SSU-rRNA from tricistronic rRNA transcript (SSU-rRNA, 5.8S rRNA, LSU-rRNA) [GO:0000462]	0.00143	RPS9B RPS27B RPS1B RIO2 RPS6A NAN1	6	60
aromatic amino acid family biosynthetic process [GO:0009073]	0.00168	TYR1 ARO4 ARO3	3	12
branched chain family amino acid biosynthetic process [GO:0009082]	0.00215	LEU1 LEU4 LEU9	3	13
rRNA export from nucleus [GO:0006407]	0.00215	RPS18A RPS18B RPS10B RPS3	4	27
translation [GO:0006412]	0.00233	RPS9B RPS18A RPL37B RPS27B MRPL6 RPL40A RPL39 RPL40B	15	318

Ontology	p- value	Genes in ontology category	k	f
		RPS31 RPS18B RPS1B RPS10B RPS3 RPL25 RPS6A		
cellular cell wall organization [GO:0007047]	0.00238	DSE1 SCW11 SKN1 DSE2 SKG1 CTS1 WSC3	7	89
protein N-linked glycosylation via asparagine [GO:0018279]	0.0025	WBP1 OST6	2	4
carbon catabolite activation of transcription from RNA polymerase II promoter [GO:0000436]	0.0041	HAP4 HAP5	2	5
regulation of cellular respiration [GO:0043457]	0.0041	HAP4 HAP5	2	5
fungal-type cell wall organization [GO:0031505]	0.00495	CDC10 MTL1 SKN1 PRS3 IRE1 SKG1 RHO2 WSC3	8	128
axial cellular bud site selection [GO:0007120]	0.00568	CDC10 ERV14 AXL1	3	18
metabolic process [GO:0008152]	0.00659	TYR1 ARO4 GDH2 ARO3 HOM3 SEC53 LEU1 SCW11 IRE1 HIS5 CPA2 CTS1 LEU4 LEU9 PDE2 ULA1 POS5	17	425
biosynthetic process [GO:0009058]	0.00909	ARO4 ARO3 HIS5 AAT2	4	40
GO Cellular Component (625 categories)				
cytosolic small ribosomal subunit [GO:0022627]	4.37E-06	RPS9B RPS18A RPS27B RPS31 RPS18B RPS1B RPS10B RPS3 RPS6A	9	62
ribonucleoprotein complex [GO:0030529]	1.63E-05	RPS9B MRPL35 RPS18A RPL37B RPS27B MRPL6 RPL40A RPL39 RPL40B RPS31 EMG1 RPS18B RPS1B RPS10B RPS3 RPL25 RPS6A NAN1 RRP9	19	307
ribosome [GO:0005840]	0.00064	RPS9B MRPL35 RPS18A RPL37B RPS27B MRPL6 RPL40A RPL39 RPL40B RPS31 RPS18B RPS1B RPS10B RPS3 RPL25 RPS6A	16	310
90S preribosome [GO:0030686]	0.0008	RPS9B EMG1 RPS1B RPS3 RPS6A NAN1 RRP9	7	74
intracellular [GO:0005622]	0.00083	RPS9B RPS18A RPL37B RME1 RPS27B MRPL6 HIS5 RPL40A RPL39 UFD4 RPL40B RPS31 RPS18B RPS1B RHO2 RPS3 RPL25 RPS6A	18	381
cytoplasm [GO:0005737]	0.00133	HMT1 TYR1 RPS9B ARO4 RVS161 ARO3 EBS1 VHS1 NSE3 RPS18A RPL37B GRX2 DLD3 KRE29 HOM3 MET6 SEC4 SEC53 TOS3 ACB1 RNR4 PRS3 RPS27B RRP4 NAS2 DFG10 DPH1 RPL40A PRE3 RPL39 CPA2 TTI2 UFD4 RPL40B AAT2 RPS31 EMG1 HRI1 NMD4 GLO1 RPS18B RPS1B RPS10B GAD1 PRC1 ELP6 LEU4 RPS3 RIO2 RPL25 TUM1 PDE2 RPS6A ATG5 NIP7 PCL8 SAM4 NTO1 SPE3	59	2026
CCAAT-binding factor complex [GO:0016602]	0.0025	HAP4 HAP5	2	4
small-subunit processome [GO:0032040]	0.00272	RPS9B EMG1 RPS6A NAN1 RRP9	5	47
cytosolic large ribosomal subunit [GO:0022625]	0.00964	RPL37B RPL40A RPL39 RPL40B RPL25 NIP7	6	88
MIPS Functional Classification (459 categories)				
ribosomal proteins [12.01.01]	1.14E-05	RPS9B MRPL35 RPS18A RPL37B RPS27B MRPL6 RPL40A RPL39 RPL40B RPS31 RPS18B RPS1B RPS10B RPS3 RPL25 RPS6A NIP7	17	246

Ontology	p- value	Genes in ontology category	k	f
biosynthesis of tyrosine [01.01.09.05.01]	0.00043	TYR1 HIS5	2	2
biosynthesis of leucine [01.01.11.04.01]	0.00045	LEU1 LEU4 LEU9	3	8
aromate anabolism [01.05.11.04]	0.00127	ARO4 ARO3	2	3
metabolism of the cysteine - aromatic group [01.01.09]	0.00127	ARO4 ARO3	2	3
biosynthesis of phenylalanine [01.01.09.04.01]	0.00127	TYR1 HIS5	2	3
metabolism of glutamate [01.01.03.02]	0.0041	GDH2 AAT2	2	5
peptidoglycan anabolism [01.05.03.02.04]	0.0048	WBP1 OST6 ALG5	3	17
MIPS Phenotypes (142 categories)				
Inappropriate sporulation [32.15]	0.00607	RVS161 RME1	2	6
MIPS Subcellular Localization (48 categories)				
vacuole [770]	0.00072	PMP2 MNN1 FCY2 STE2 ERV14 VMA5 EMP70 NYV1 CTS1 PRC1 AQR1 ATG5 DIP5	13	224
cytoplasm [725]	0.00315	HMT1 VID24 TYR1 RPS9B ARO4 RIB5 RVS161 PMP1 GDH2 ARO3 RKM2 VHS1 NSE3 RPS18A RPL37B GRX2 GCN4 DLD3 KRE29 HOM3 MET6 SEC4 SEC53 COG7 LEU1 TOS3 ACB1 RME1 RNR4 PRS3 RPS27B CIC1 MED6 RRP4 DSE2 NAS2 DPH1 HIS5 RPL40A PET130 NCA3 RPL39 CPA2 TTI2 UFD4 HAP4 RPL40B SKG1 AAT2 RPS31 EMG1 HRI1 NMD4 GLO1 RPS18B RPS1B RIM9 RPS10B GAD1 PRC1 ELP6 RHO2 LEU4 RPS3 RIO2 ARG1 RPL25 TUM1 HAP5 PDE2 RPS6A NIP7 PCL8 SAM4 NTO1 SPE3	76	2879
golgi [740]	0.00429	MNN1 TMN3 SEC4 COG7 ERV14 SKN1 RHO2 ATX2	8	125
MIPS Protein Complexes (1142 categories)				
cytoplasmic ribosomal small subunit [500.40.20]	2.12E-06	RPS9B RPS18A RPS27B RPS31 RPS18B RPS1B RPS10B RPS3 RPS6A	9	57
H+-ATPase, plasma mebrane [210]	0.0025	PMP1 PMP2	2	4
CCAAT-binding factor complex [510.160]	0.0025	HAP4 HAP5	2	4
Complex Number 35 [550.2.35]	0.00331	CDC10 MET6 SEC53	3	15

Table 16. Ontologies enriched among the 193 genes only downregulated in *Δfpr3Δfpr4* yeast (from Figure 26 B)

Ontology	p- value	Genes in ontology category	k	f
GO Molecular Function (1646 categories)				
histone binding [GO:0042393]	0.00111	CDC28 NAP1 POB3 VPS75	4	17
calcium-dependent protein serine/threonine phosphatase activity [GO:0004723]	0.002349	CNA1 CMP2	2	3
cation transmembrane transporter activity [GO:0008324]	0.003118	KHA1 TRK1 FSF1	3	11
ATPase activity [GO:0016887]	0.004315	CHD1 INO80 YOR1 KAR2 DYN1 HSP60 DDR48 YTA6 MDL2	9	112
actin binding [GO:0003779]	0.004549	ABP1 RVS167 PAN1 ARP3 SLA2	5	39
ATP binding [GO:0005524]	0.00472	AKL1 CDC28 KIN1 EKI1 GCN2 CHD1 DNF1 PRP43 INO80 YOR1 THR1 KAR2 TAH11 ARP3 URA8 DYN1 HSP60 LCB5 VPS33 UTP14 CTF18 ARK1 TOP2 CLA4 SSK2 YTA6 FRK1 HSP82 MDL2	29	622
chromatin binding [GO:0003682]	0.005674	HDA2 CHD1 IRR1 TOS4 SIR3 POB3	6	58
nucleotide binding [GO:0000166]	0.006113	AKL1 CDC28 NRP1 KIN1 EKI1 GCN2 GCD11 CHD1 DNF1 PRP43 INO80 YOR1 THR1 KAR2 ARP3 URA8 VPS1 DYN1 HSP60 LCB5 CDC3 TEM1 UTP14 CTF18 PUB1 ARK1 TOP2 RHO5 CLA4 SSK2 YTA6 FRK1 HSP82 MDL2	34	778
GO Biological Process (2062 categories)				
actin cortical patch assembly [GO:0000147]	2.81E-05	ABP1 ENT1 ARC15 PAN1 ARK1	5	14
cell division [GO:0051301]	0.0002946	CDC28 PCL2 SSD1 YCG1 CLB1 DAM1 IRR1 NNF1 VPS1 CDC3 TEM1 BUB2 SIN3 RAX1 NUD1	15	190
actin cytoskeleton organization [GO:0030036]	0.0003306	AKL1 BEM2 GEA1 VPS1 SSK2 SLG1	6	34
endocytosis [GO:0006897]	0.000476	EDE1 ENT1 RVS167 DNF1 PAN1 VPS1 VPS33 SLA2 SCD5	9	82
ER-associated misfolded protein catabolic process [GO:0071712]	0.0007979	PMT2 PMT1	2	2
positive regulation of telomere maintenance via telomerase [GO:0032212]	0.0007979	SBA1 HSP82	2	2
cell cycle [GO:0007049]	0.001461	CDC28 PCL2 SSD1 YCG1 CDC14 CLB1 DAM1 YNG2 IRR1 NNF1 VPS1 CDC3 TEM1 BUB2 CTF18 SIN3 SLG1 RAX1 NUD1	19	316
regulation of exit from mitosis [GO:0007096]	0.002114	CDC14 TEM1 BUB2 CLA4	4	20
ER-associated protein catabolic process [GO:0030433]	0.002172	SHP1 HUL5 KAR2 LCL2 SCJ1 DSK2	6	48
lipid tube assembly [GO:0060988]	0.002349	RVS167 VPS1	2	3
cytokinesis [GO:0000910]	0.004057	SEC3 PAN1 CDC3 ARK1 CLA4	5	38
regulation of DNA-dependent DNA replication initiation	0.004072	SET2 TAH11 SIN3	3	12

Ontology	p- value	Genes in ontology category	k	f
[GO:0030174]				
mitosis [GO:0007067]	0.004087	CDC28 SSD1 YCG1 CLB1 DAM1 IRR1 NNF1 TEM1 BUB2 NUD1	10	132
regulation of endocytosis [GO:0030100]	0.00461	AKL1 ARK1	2	4
phosphatidylethanolamine biosynthetic process [GO:0006646]	0.00461	EKI1 ECT1	2	4
reactive oxygen species metabolic process [GO:0072593]	0.00461	SOD2 TDH2	2	4
protein folding [GO:0006457]	0.005635	CNS1 PIH1 SBA1 HSP60 GSF2 ERO1 SCJ1 HSP82	8	96
protein localization [GO:0008104]	0.006461	ABP1 PUF4 LAA1	3	14
actin filament organization [GO:0007015]	0.006944	ENT1 ARP3 ARK1 SLA2 SCD5	5	43
regulation of actin filament polymerization [GO:0030833]	0.007541	ARC15 ARP3	2	5
positive regulation of histone acetylation [GO:0035066]	0.007541	SET2 VPS75	2	5
protein exit from endoplasmic reticulum [GO:0032527]	0.007541	PMT2 PMT1	2	5
transcription, DNA-dependent [GO:0006351]	0.009465	SAS3 SPT7 RSC6 PHO2 SWI5 HDA2 UTP5 DOT6 CHD1 PUF4 INO80 SRB5 YAP3 DOT5 SET2 IXR1 SIR3 POB3 ARP5 TOP2 RPC31 SIN3 CTR9 SFL1 SWT1	25	540
Rho protein signal transduction [GO:0007266]	0.009536	RHO5 CLA4 SLG1	3	16
GO Cellular Component (625 categories)				
actin cortical patch [GO:0030479]	3.55E-06	EDE1 ABP1 ENT1 RVS167 ARC15 PAN1 ARP3 ARK1 SLA2 SCD5	10	57
cytoplasm [GO:0005737]	1.16E-05	EDE1 SHP1 AKL1 CNS1 CDC28 PCS60 ABP1 PCL2 ENT1 NRP1 RBS1 KIN1 SWI5 EKI1 STB3 SSD1 YCG1 MSN5 RVS167 GAL83 DOT6 BEM2 BCK2 CDC14 PUF4 HEM2 SDS23 HUL5 SAE2 ECT1 CLB1 DAM1 CBF2 YAP3 RPL8A RPN1 PIH1 AAP1 KEL1 SET5 ARC15 PAN1 RPS14B TDH2 GEA1 TAH11 ARP3 URA8 SBA1 PGM1 LOT5 VPS1 NAP1 DYN1 PXL1 MHT1 TOS4 HSP60 IMH1 KAP95 CNA1 ECM30 GSF2 CMP2 BUB2 DDR48 GFD1 PUB1 ARK1 RPL9B RHO5 SLA2 EMW1 SOL1 TRM112 CUE5 SWT1 GPB1 NUD1 VPS28 FRK1 RPL7B HSP82 TIP41 PRE2	85	2026
nucleus [GO:0005634]	1.24E-05	NTG1 SAS3 SHP1 SPT7 CDC28 MRC1 RSC6 PRP11 PHO2 PCL2 SWI5 STB3 HDA2 YCG1 MSN5 UTP5 GAL83 DOT6 CHD1 BCK2 CDC14 HEM2 SDS23 SEH1 PRP43 HUL5 INO80 SAE2 ECT1 SRB5 CLB1 DAM1 CBF2 YAP3 RPN1 PIH1 AAP1 YNG2 RTT107 SET5 DOT5 IRR1 NUP159 PAN1 SET2 RPS14B POL32 TAH11 NNF1 IXR1 DEF1 MPE1 SBA1 LOT5 NAP1 TOS4 KAP95 SIR3 POB3 UTP14 CTF18 GFD1 DSK2 PUB1 ARP5 TOP2 RPC31 RHO5 UBP10 VPS75 CLA4 EMW1 SOL1 TRM112 SIN3 CTR9 CDC21 SFL1 SWT1 SCD5 NUD1	83	1965

Ontology	p- value	Genes in ontology category	k	f
		TIP41 PRE2		
cellular bud neck [GO:0005935]	2.94E-05	EDE1 AKL1 CDC28 PCL2 SSD1 SEC3 TOS2 KEL1 NAP1 PXL1 CDC3 SSK2 SLG1 RAX1	14	137
mating projection tip [GO:0043332]	3.65E-05	EDE1 ABP1 ENT1 RVS167 SEC3 BEM2 KEL1 PAN1 PXL1 ARK1 SLA2 SLG1	12	105
cellular bud tip [GO:0005934]	4.37E-05	EDE1 PCL2 SEC3 BEM2 TOS2 KEL1 PXL1 SLA2 SSK2 RAX1	10	75
cytoskeleton [GO:0005856]	0.0001322	ABP1 RVS167 DAM1 CBF2 ARC15 PAN1 ARP3 VPS1 DYN1 BUB2 ARK1 SLA2 NUD1	13	138
dolichyl-phosphate-mannose-protein mannosyltransferase complex [GO:0031502]	0.0007979	PMT2 PMT1	2	2
chromosome [GO:0005694]	0.001082	YCG1 DAM1 CBF2 DOT5 IRR1 SET2 NNF1 DEF1 POB3 TOP2 UBP10	11	130
actin cap [GO:0030478]	0.002316	GSC2 CLA4 SLG1	3	10
calcineurin complex [GO:0005955]	0.002349	CNA1 CMP2	2	3
cell cortex [GO:0005938]	0.002464	ABP1 BEM2 DYN1 SLA2 YTA6	5	34
spindle pole body [GO:0005816]	0.004067	CDC28 CDC14 CBF2 DYN1 TEM1 BUB2 NUD1	7	72
MIPS Functional Classification (459 categories)				
budding, cell polarity and filament formation [43.01.03.05]	6.57E-06	SHP1 CDC28 ABP1 ENT1 SSD1 RVS167 SEC3 GAL83 DOT6 BEM2 TOS2 KEL1 ARC15 PAN1 NAP1 PXL1 CDC3 BUB2 ARK1 SLA2 CLA4 SLG1 DFG16 RAX1	24	312
actin cytoskeleton [42.04.03]	1.46E-05	AKL1 ABP1 ENT1 BEM2 ARC15 PAN1 ARP3 ARK1 SLA2 SSK2 SLG1 SCD5	12	96
protein binding [16.01]	9.68E-05	CNS1 ABP1 ENT1 MSN5 RVS167 SEC3 HUL5 KOG1 IRR1 ARC15 PAN1 KAR2 ARP3 SBA1 NAP1 PXL1 SRP40 APS1 SIR3 TEM1 SCJ1 DSK2 SLA2 SLG1 SCD5	25	391
endocytosis [20.09.18.09.01]	0.0002293	EDE1 AKL1 ENT1 RVS167 PAN1 ARK1 SLA2 SCD5	8	59
DNA conformation modification (e.g. chromatin) [10.01.09.05]	0.0002625	SAS3 SPT7 MRC1 RSC6 HDA2 DOT6 CHD1 INO80 YNG2 HOS4 NAP1 SIR3 POB3 TOP2 SIN3	15	188
protein targeting, sorting and translocation [14.04]	0.0003499	PEX3 MSN5 SEC20 PUF4 SEH1 TAM41 KAR2 VPS1 HSP60 IMH1 KAP95 VPS33 SCJ1 GOT1 ARP5 VPS75 TRE2 SCD5 VPS28	19	281
transcriptional control [11.02.03.04]	0.000876	SAS3 SPT7 RSC6 PHO2 STB3 HDA2 GAL83 DOT6 CHD1 PTR3 INO80 SRB5 YAP3 RTT107 DOT5 HOS4 SET2 IXR1 TOS4 CNA1 SIR3 CMP2 UBP10 SIN3	24	426
phosphate metabolism [01.04]	0.0008844	AKL1 CDC28 KIN1 EKI1 GCN2 GAL83 CHD1 CDC14 INO80 ECT1 THR1 KAR2 LCB5 CNA1 CMP2 DDR48 ARK1 CLA4 SSK2 YTA6 FRK1 HSP82 MDL2	23	401

Ontology	p- value	Genes in ontology category	k	f
pheromone response, mating-type determination, sex-specific proteins [34.11.03.07]	0.002626	SAS3 SWI5 MSN5 KEL1 PRY1 SBA1 CDC3 CNA1 SIR3 CMP2 SLA2 SIN3 HSP82	13	189
mitotic cell cycle and cell cycle control [10.03.01]	0.003013	SHP1 RSC6 PCL2 SSD1 BEM2 CDC14 SDS23 KAR2 CDC3 DSK2 VPS75 CTR9 NUD1 PRE2	14	215
protein folding and stabilization [14.01]	0.00465	CNS1 PIH1 KAR2 SBA1 HSP60 ERO1 SCJ1 HSP82	8	93
modification by phosphorylation, dephosphorylation, autophosphorylation [14.07.03]	0.006339	AKL1 CDC28 KIN1 GCN2 GAL83 CDC14 CNA1 CMP2 ARK1 CLA4 SSK2 FRK1	12	186
cell growth / morphogenesis [40.01]	0.007179	CDC28 ABP1 SSD1 RVS167 TOS2 CDC3 CNA1 CMP2 BUB2 RHO5 SLA2 CLA4	12	189
ATP binding [16.19.03]	0.007786	CHD1 PRP43 HUL5 INO80 YOR1 KAR2 VPS33 DDR48 TOP2 YTA6 HSP82 MDL2	12	191
MIPS Phenotypes (142 categories)				
Actin cytoskeleton mutants [52.30.10]	5.09E-05	RVS167 BEM2 PAN1 ARP3 CDC3 ARK1 SLA2 CLA4	8	48
Heat-sensitivity (ts) [12.05]	0.0001882	CDC28 SEC20 SEC3 BEM2 PRP43 SRB5 CBF2 RPN1 NUP159 GEA1 SBA1 VPS1 CDC3 VPS33 ERO1 RPC31 SLA2 CTR9 SCD5 HSP82 PRE2	21	313
other cell cycle defects [22.99]	0.0007327	BEM2 CDC14 SAE2 CBF2 PAN1 VPS1 NAP1 DYN1 CDC3 SIR3 BUB2 CLA4 SIN3 CTR9 PRE2	15	207
other aminoacid analogs and other drugs [92.99]	0.002972	PTR3 YOR1 IXR1 ERO1 DDR48 TOP2	6	51
MIPS Subcellular Localization (48 categories)				
cytoplasm [725]	0.000101	NTG1 SHP1 RER2 AKL1 CNS1 CDC28 EHT1 PCS60 MRC1 VAC17 ABP1 PHO2 NRP1 RBS1 KIN1 SWI5 EKI1 STB3 GCN2 SSD1 MSN5 UTP5 PRB1 SEC3 GCD11 GAL83 DOT6 BEM2 DNF1 BCK2 PUF4 HEM2 SDS23 HUL5 SAE2 ECT1 CBF2 YOR1 YAP3 RPL8A THR1 VMA16 RPN1 PIH1 AAP1 KEL1 SET5 IRR1 ARC15 HOS4 RPS14B TDH2 POL32 TAH11 URA8 NNF1 DEF1 SBA1 PGM1 LOT5 VPS1 NAP1 DYN1 PXL1 MHT1 YPS1 TOS4 IMH1 CDC3 KAP95 VPS33 CNA1 ECM30 GSF2 CMP2 AEP1 CTF18 DDR48 GFD1 DSK2 PUB1 ARK1 ARP5 RPL9B RHO5 UBP10 SLA2 CLA4 EMW1 SSK2 SOL1 TRM112 SIN3 CTR9 SLG1 DFG16 CUE5 CDC21 GPB1 VPS28 YTA6 SEC16 FRK1 RPL7B HSP82 TIP41 PRE2	107	2879
actin cytoskeleton [730.01]	0.0001214	ABP1 ENT1 RVS167 ARC15 PAN1 ARP3 ARK1 SLA2	8	54
nucleus [750]	0.0003389	NTG1 SAS3 SHP1 SPT7 CDC28 MRC1 RSC6 PRP11 PHO2 SWI5 HDA2 YCG1 MSN5 GAL83 DOT6 CHD1 BCK2 CDC14 HEM2 SDS23 SEH1 PRP43 HUL5 INO80 SAE2 ECT1 SRB5 CLB1 DAM1 CBF2 YAP3 RPN1 PIH1 AAP1 YNG2 RTT107 SET5 DOT5 IRR1 HOS4 NUP159 SET2 RPS14B TDH2 POL32 TAH11 NNF1 IXR1 DEF1 MPE1	78	1976

Ontology	p- value	Genes in ontology category	k	f
		SBA1 LOT5 NAP1 DYN1 SRP40 TOS4 SIR3 POB3 UTP14 BUB2 CTF18 DSK2 PUB1 ARP5 TOP2 RPC31 RHO5 UBP10 VPS75 EMW1 SOL1 TRM112 SIN3 CTR9 CDC21 SFL1 TIP41 PRE2		
cytoskeleton [730]	0.0008464	ABP1 RVS167 DAM1 ARC15 PAN1 ARP3 CDC3 ARP5 SLA2 CTR9	10	107
plasma membrane [720]	0.005824	KIN1 ITR1 SEC3 FTR1 DNF1 GSC2 YOR1 TRK1 YPS1 RHO5 SLA2 SLG1	12	184
spindle pole body [730.05]	0.008289	SDS23 CBF2 NNF1 DYN1 TEM1 BUB2 NUD1	7	82
MIPS Protein Complexes (1142 categories)				
Complex Number 135, probably RNA metabolism [550.1.135]	0.0001453	BEM2 PRP43 VPS1 TOP2 CTR9	5	19
Complex Number 170, probably signalling [550.1.170]	0.001737	YOR1 KEL1 HOS4 TDH2 KAP95 PRE2	6	46
Calcineurin B [100]	0.002349	CNA1 CMP2	2	3
Complex Number 208 [550.2.208]	0.002349	NTG1 PRB1	2	3
Complex Number 34 [550.2.34]	0.003118	RPN1 CDC3 TOP2	3	11
Complex Number 46, SPT16 (8) [550.3.46]	0.003118	CHD1 POB3 CTR9	3	11
Complex Number 284 [550.2.284]	0.003118	NTG1 PRB1 PGM1	3	11
Complex Number 203, probably transcription/DNA maintanance/chromatin structure [550.1.203]	0.004245	RSC6 INO80 VPS1 SIN3	4	24
Complex Number 239 [550.2.239]	0.00461	AKL1 ABP1	2	4
Complex Number 20, probably cell polarity and structure [550.1.20]	0.00461	EDE1 SLA2	2	4
Complex Number 551 [550.2.551]	0.00461	TOP2 YTA6	2	4
Complex Number 128 [550.2.128]	0.00461	PRB1 SSK2	2	4
Complex Number 25 [550.2.25]	0.00461	GAL83 NAP1	2	4
Complex Number 66 [550.2.66]	0.00461	CNA1 CMP2	2	4
Actin-associated proteins [140.20.20]	0.004943	ABP1 RVS167 PAN1 SLA2	4	25
Complex Number 102 [550.2.102]	0.007541	INO80 SIN3	2	5
Complex Number 80, probably membrane biogenesis and traffic [550.1.80]	0.007541	ERV46 ERO1	2	5

Gene ontology analysis of differentially expressed genes in *Δfpr3Δfpr4Δtrf5* triple mutants

Ontologies enriched among the differentially expressed genes in *Δfpr3Δfpr4Δtrf5* triple mutant yeast are presented in the tables below (Table 17 and Table 18).

Lists of ontologies were generated by the FunSpec web-based cluster interpreter for yeast (http://funspec.med.utoronto.ca/)[372]. This program outputs a summary of ontologies significantly enriched in a given input list of yeast genes using ontology annotations from the Gene Ontology Consortium (GO) database[421] and from the Munich Information Center for Protein Sequences (MIPS) database[422].

Ontologies in this analysis were classified by molecular function, biological process, cellular component, MIPS functional classification, MIPS phenotypes, MIPS subcellular localization, and MIPS protein complexes. The *p*-values associated with each ontology were calculated automatically by FunSpec using hypergeometric distribution, they represent the probability that the intersection of a given list of genes with any ontology occurs by chance.

Only ontology categories with *p*-values≤0.01 are presented in the following lists. Bonferroni correction was not applied.

k: number of input genes in ontology category
f: total number of genes in ontology category

Table 17. Ontologies enriched among the 967 genes upregulated in *Δfpr3Δfpr4Δtrf5* triple mutant yeast

Ontology	p- value	Genes in ontology category	k	f
GO Molecular Function (1646 categories)				
structural constituent of ribosome [GO:0003735]	1.91E-10	MRPL16 RPL19A MRPL36 RPL21A MRPS5 MRPL37 RPS14A IMG2 RPS29B RPL31A RPP1A RPP1B RPL41B RPS13 RPP2B MRPL28 RPL27B RPL37B RSM18 RPL34A RPS26B RPL22B RPL29 RPL28 RPS26A RPS25A RPS27B RPL42B RPL40A RPS21B RPL17B RPL39 RPS22A RPS14B RPL43B MRPL31 RPS27A MRP49 RPL17A MRPL13 RPL15A RPL37A RPS28B RPS30A RPL38 RPL26A RPS29A RPS16A MRPS8 RPL36A RPS10B RPL20A MRPL33 RLP7 RPL16B SWS2 MRPL50 MRPS12 RPP2A RPS28A RPS30B RPS9A MRP51 RPL5 RPL33A MRPL40 RTC6 RPL43A	68	218
2 iron, 2 sulfur cluster binding [GO:0051537]	1.21E-05	GRX7 GRX3 RIP1 DRE2 SDH2 ISU2 GRX5 ISU1 YAH1	9	13
structural constituent of cell wall [GO:0005199]	1.47E-05	TIP1 SED1 HSP150 CWP1 CWP2 PIR3 YPS3 CCW14 KRE1 TIR2	10	16
RNA binding [GO:0003723]	4.16E-05	CCR4 LSM2 MAK5 NGR1 MRPS5 SRO9 SRP14 TRM8 WHI4 CTH1 SSD1 LSM6 NPL3 PUF6 RPL37B SNU13 EDC2 LSM4 LCP5 CCA1 SPB4 SMX2 TIF4632 RPL28 NAB2 MPT5 TAN1 TAD1 RRP46 PET54 RRP3 NOP10 LRP1 RPF1 IMP3 SUI2 TMA22 LSM8 PRP40 SRP21 UTP30 RPL15A SMD3 RPL37A SMD2 RPL26A RPL36A RNT1 NGL2 RLP7 HRB1 RPL16B SWS2 NOP15 DBP2 NAF1 WHI3 SSU72 CSL4 NRD1 DBP6 THP1 RRP40 NOP8 DCP1 PNO1 PUS7 CLP1 HSH49	76	337

Ontology	p- value	Genes in ontology category	k	f
		VTS1 RPS9A RPL5 NOP53 MEX67 PUS1 YTH1		
glucosidase activity [GO:0015926]	5.89E-05	SKN1 SCW4 DSE2 SCW10 HPF1 KRE6	6	7
DNA bending activity [GO:0008301]	0.000127	NHP6B HMO1 ABF1 MCM1 ABF2 CEP3 RLM1 NHP6A ROX1	9	16
sequence-specific DNA binding [GO:0043565]	0.000151	OAF1 HAP3 TOD6 NHP6B REI1 HMRA1 STP4 UGA3 LYS14 NRG1 GIS1 GCN4 MIG3 YER130C BUR6 AFT1 MIG2 STP2 RSC30 SKN7 YAP5 DLS1 RSF2 PUT3 IXR1 MSN4 ABF1 STP3 YAP1 SOK2 STB4 MSN2 ARG80 MCM1 CEP3 RGM1 MBF1 TYE7 RLM1 SUT2 NHP6A ROX1	42	165
disulfide oxidoreductase activity [GO:0015036]	0.000206	GRX1 TRX3 GRX3 GRX2 TRX1 GRX5	6	8
threonine-type endopeptidase activity [GO:0004298]	0.000267	PRE7 PRE4 SCL1 PUP2 PRE3 PRE8 PRE5 PRE6	8	14
iron-sulfur cluster binding [GO:0051536]	0.000426	GRX7 GRX3 RIP1 LEU1 NFU1 PRI2 DRE2 ISA1 SDH2 ISU2 GRX5 ISU1 YAH1	13	33
ubiquinol-cytochrome-c reductase activity [GO:0008121]	0.000543	COR1 QCR7 RIP1 QCR6 QCR9 QCR8	6	9
tubulin binding [GO:0015631]	0.001072	GIM4 PAC10 YKE2 GIM5 RBL2	5	7
endopeptidase activity [GO:0004175]	0.001076	PRE7 SOM1 PRE4 SCL1 PUP2 PRE3 PRE8 PRE5 PRE6	9	20
electron carrier activity [GO:0009055]	0.001357	GRX7 GRX1 TRX3 GRX3 GRX2 YEL047C AIM14 CIR1 SDH3 DRE2 SDH2 FRE6 TRX1 ERG5 GRX5 PRM4 YAH1 AIM45	18	59
protein disulfide oxidoreductase activity [GO:0015035]	0.001438	GRX7 GRX1 TRX3 GRX3 GRX2 TRX1 GRX5 PRM4	8	17
cytochrome-c oxidase activity [GO:0004129]	0.001865	COX9 COX13 MTC3 COX8 YMR244C-A COX7 COX5A	7	14
thiosulfate sulfurtransferase activity [GO:0004792]	0.002005	YCH1 TUM1 RDL1 RDL2	4	5
UDP-glycosyltransferase activity [GO:0008194]	0.002005	GPI1 GPI15 GPI2 SPT14	4	5
RNA polymerase II core binding [GO:0000993]	0.002005	RTT103 NPL3 ESS1 ELF1	4	5
phosphatidylinositol N-acetylglucosaminyltransferase activity [GO:0017176]	0.002005	GPI1 GPI15 GPI2 SPT14	4	5
snoRNA binding [GO:0030515]	0.00226	UTP6 UTP8 IMP3 UTP9 DIP2 IMP4 NAF1 BUD21	8	18
rRNA primary transcript binding [GO:0042134]	0.003113	RPF1 IMP4 BRX1	3	3
enzyme regulator activity [GO:0030234]	0.004763	ILV6 PMP1 RPN3 COX13 RAI1 SDS22 TSL1	7	16
metal ion binding [GO:0046872]	0.005945	CCR4 OAF1 COR1 PRS4 GRX7 YSA1 PTC4 REI1 MAL33 PTC1 STP4 RPS29B VCX1 UGA3 AIR2 LYS14 NRG1 GIS1 GRX3 CTH1 SDH4 FMN1 INM2 UBA2 PFA5 RIB3 IZH1 RPL37B AGE1 TIM9 RIP1 UTR4 MIG3 PTC2 YER130C SAD1 LEU1 PNC1 RPB9 AFT1 NAB2 MIG2 TAD1 RAI1 SPT4 TIM13 PRS3 AIM17 TIM10 STP2 RPS27B RSC30 DMA1 AGE2 PEX2 BNA1 RPA12 RPL43B CPA2 STE24 RSF2 TIM8	117	647

Ontology	p- value	Genes in ontology category	k	f
		PUT3 PAN3 TUL1 PRI2 MSN4 ABF1 CMC1 SDH3 RPS27A ELF1 KAE1 CCP1 DRE2 SDH2 FRE6 IZH3 XDJ1 RPL37A MAP1 STP3 REH1 RPS29A GLO1 PPZ1 CMP2 ARG81 ADI1 ERG5 STB4 MAC1 MSN2 MOT3 RCO1 MUB1 CEP3 RGM1 SCS7 NCE103 AAH1 GIS2 VPS27 PFA4 IZH4 YOR052C RPB10 ISU2 PDE2 GRX5 IDI1 ISU1 YAH1 RPL43A FCY1 YTH1 BET2		
DNA-directed RNA polymerase activity [GO:0003899]	0.006995	RPB5 RPC53 RPA14 RPB9 RPC17 RPB4 RPA12 PRI2 RPC19 RPB11 RPB10	11	34
hydrolase activity, hydrolyzing O-glycosyl compounds [GO:0004553]	0.00709	SCW11 CRH1 SCW4 BGL2 CTS1 EXG1 SCW10	7	17
phosphoprotein phosphatase activity [GO:0004721]	0.008202	PTC4 PTC1 PHO13 PTC2 YVH1 PSR1 PPZ1 CMP2 FCP1 SIW14 MSG5 OCA1 SSU72	13	44
GO Biological Process (2062 categories)				
rRNA processing [GO:0006364]	1.14E-08	LSM2 MAK5 POP7 RRP7 RPS14A SAS10 RRP8 BFR2 LSM6 NPL3 UTP6 SNU13 LSM4 NSA2 LCP5 SPB4 CGR1 RAI1 POP6 SLX9 RRP46 UTP8 RRP3 NOP10 LRP1 RPF1 IMP3 UTP9 RPS21B RPS14B LSM8 URB2 MRT4 UTP30 SOF1 GRC3 NOC3 SDO1 FCF2 REX3 DIP2 RMP1 RNT1 NGL2 IMP4 NOP15 DBP2 NAF1 SSU72 CSL4 DBP6 RRP40 BUD21 PUS7 RPS9A NOP53 RVB2 TIF6 RRP15	59	195
ribosome biogenesis [GO:0042254]	5.77E-08	MAK5 REI1 RRP7 RPS14A SAS10 NPL3 UTP6 SNU13 NSA2 LCP5 SPB4 LOC1 CGR1 SLX9 UTP8 RRP3 SSF1 NOP10 RPF1 IMP3 UTP9 RPL40A ALB1 RPS14B URB2 MRT4 MAK11 UTP30 SOF1 NOC3 SDO1 FCF2 DIP2 RLP7 IMP4 NOP15 DBP2 NAF1 DBP6 NOG2 RCL1 BRX1 NOP8 BUD21 RIO1 PNO1 PUS7 RPS9A NOP53 RTC6 RSA1 RRP15	52	170
cellular response to oxidative stress [GO:0034599]	2.29E-07	PRX1 UGA2 GRX7 GPX2 GRX1 TRX3 GRX3 GRX2 HSP12 MTL1 ERV1 ASK10 HYR1 TMA19 MSN4 MCR1 CCP1 TRX1 AHP1 MSN2 NCE103 OCA1 TIM18 GRX5 POS5 OXR1 YAR1	27	67
fungal-type cell wall organization [GO:0031505]	2.97E-06	ECM15 ECM13 PRS4 TIP1 PST1 SED1 SBE2 HKR1 MPT5 MTL1 SKN1 CRH1 BGL2 PRS3 SLT2 SVP26 HSP150 GPI14 CWP1 CWP2 PIR3 CCW12 YPS1 YPS3 EXG1 MID2 ECM19 CCW14 ARG7 ROT1 WSC2 KRE1 ZEO1 HPF1 SRL1 KTR6 RLM1 TCO89 KRE6	39	128
ribosomal large subunit biogenesis [GO:0042273]	2.39E-05	MAK5 REI1 YDL063C PUF6 NSA2 LOC1 ALB1 MRT4 MAK11 SDO1 REH1 RLP7 NOP15 NOP8 TIF6 JIP5	16	37
electron transport chain [GO:0022900]	2.74E-05	COR1 GRX1 TRX3 SDH4 GRX2 QCR7 RIP1 QCR6 QCR9 CIR1 QCR8 SDH3 ACP1 SDH2 FRE6 TRX1 SCS7 YAH1 AIM45	19	49
translation [GO:0006412]	3.17E-05	MRPL16 RPL19A RPL21A MRPS5 SRO9 RPS14A IMG2 RPS29B RPL31A RPP1A RPP1B RPL41B SES1 RPS13 GIR2 GCD6 RPP2B RPL27B RPL37B RSM18 RPL34A RPS26B RPL22B RPL29 TIF4632	73	318

Ontology	p- value	Genes in ontology category	k	f
		RPL28 RPS26A RPS25A RPS27B RPF1 MSR1 RPL42B RPL40A RPS21B RPL17B RPL39 RPS22A RPS14B SUI2 RPL43B TMA19 RPS27A RPL17A RPL15A RPL37A RPS28B RPS30A RPL38 RPL26A RPS29A RPS16A MRPS8 RPL36A RPS10B RPL20A MRPL33 RLP7 RPL16B IMP4 SWS2 MRPS12 RPP2A BRX1 RPS28A RPS30B AIM41 RPS9A RPL5 RPL33A MRPL40 RTC6 TIF6 RPL43A		
proteasomal ubiquitin-independent protein catabolic process [GO:0010499]	0.000267	PRE7 PRE4 SCL1 PUP2 PRE3 PRE8 PRE5 PRE6	8	14
maturation of 5.8S rRNA from tricistronic rRNA transcript (SSU-rRNA, 5.8S rRNA, LSU-rRNA) [GO:0000466]	0.000267	MAK5 NSA2 RAI1 RPF1 MAK11 RMP1 TIF6 RRP15	8	14
cellular cell wall organization [GO:0007047]	0.000279	ECM13 FIG2 SBE2 DSE1 SCW11 GSC2 SKN1 CRH1 SCW4 BGL2 DSE2 HSP150 GPI14 PIR3 UTH1 CCW12 CTS1 EXG1 ECM19 SCW10 WSC2 KRE1 GAS5 HPF1 SRL1 KRE6	26	89
tubulin complex assembly [GO:0007021]	0.000348	GIM4 PAC10 YKE2 GIM5 RBL2	5	6
maturation of LSU-rRNA from tricistronic rRNA transcript (SSU-rRNA, 5.8S rRNA, LSU-rRNA) [GO:0000463]	0.00041	MAK5 NSA2 RAI1 RPF1 MAK11 RLP7 NOP53 TIF6 RRP15	9	18
proteolysis involved in cellular protein catabolic process [GO:0051603]	0.00041	PRE7 PRE4 SCL1 PUP2 PRE3 PRE8 PRE5 PRE6 PEP4	9	18
iron-sulfur cluster assembly [GO:0016226]	0.001076	ISD11 QCR9 NFU1 DRE2 ISA1 ISU2 GRX5 ISU1 YAH1	9	20
maturation of SSU-rRNA from tricistronic rRNA transcript (SSU-rRNA, 5.8S rRNA, LSU-rRNA) [GO:0000462]	0.00168	RPS14A SAS10 RPS13 UTP6 SNU13 SLX9 UTP8 RPS27B RRP3 UTP9 RPS14B RPS27A SOF1 DIP2 RPS16A BUD21 RIO1 RPS9A	18	60
transcription, DNA-dependent [GO:0006351]	0.001806	CCR4 OAF1 RRN6 HAP3 NHP6B RPB5 MED8 MAL33 HMRA1 BDF2 RPC53 UGA3 LYS14 NRG1 GIS1 TAF12 RPA14 SAC3 HMO1 RVB1 RTT103 SRB7 GCN4 NPR2 MIG3 BUR6 EPL1 PGD1 RPB9 AFT1 SUT1 MIG2 RAI1 TFG2 SPT4 ASK10 SRB5 UTP8 TFG1 RTT102 RSC30 MED6 EGD2 UTP9 SKN7 VHR1 SDS3 POG1 RRT14 YAP5 RPC17 DLS1 RPB4 RPA12 EAF6 PUT3 IXR1 PRI2 MSN4 HAP4 ABF1 ELF1 KAE1 IES3 RRN5 BUR2 YAP1 RRN11 ARG81 CTK3 TAF8 TAF4 SOK2 STB4 MAC1 MSN2 ARG80 MCM1 MOT3 RCO1 MED11 CEP3 RGM1 SAP30 YAF9 RPC19 CAF40 RPB11 INO4 RPB10 MBF1 TYE7 TFC8 LGE1 GCR1 RLM1 RVB2 HFI1 SUT2 CCL1 NHP6A ROX1 NOT5	103	540
cAMP-mediated signaling [GO:0019933]	0.002005	SOK1 YVH1 SGT1 PDE2	4	5
regulation of cell size [GO:0008361]	0.002326	WHI4 RPA14 PRS3 SLT2 SSF1 SCH9 SKN7 VPS51 WHI3 LGE1 RHO1	11	30
protein targeting to ER [GO:0045047]	0.003061	SRP14 SEC11 SPC1 SRP21 SRP102 SPC3 SPC2	7	15
protein targeting to mitochondrion [GO:0006626]	0.004023	TIM9 MSP1 TIM13 TIM10 TIM8 TOM5	6	12

Ontology	p- value	Genes in ontology category	k	f
proteasomal ubiquitin-dependent protein catabolic process [GO:0043161]	0.004161	PRE7 VID24 SEM1 PRE4 SCL1 PUP2 PRE3 PRE8 PRE5 PRE6 CDC31	11	32
response to acid [GO:0001101]	0.004981	SPI1 SLT2 MID2 TIM18 RLM1	5	9
protein import into mitochondrial inner membrane [GO:0045039]	0.004981	TIM9 TIM13 TIM10 TIM8 TIM18	5	9
aerobic respiration [GO:0009060]	0.005214	COR1 DLD1 PET100 RIB3 QCR7 RIP1 QCR6 RMD9 COX13 QCR9 QCR8 PET10 COQ9 MIC17 ALG6 MCT1 PET20	17	61
GPI anchor biosynthetic process [GO:0006506]	0.006049	GPI18 PER1 GPI1 GWT1 GPI14 GPI15 PGA1 GPI2 SPT14 DPM1	10	29
mRNA 3'-end processing [GO:0031124]	0.006558	SAC3 SWD2 PAN3 CTK3 THP1 CLP1	6	13
ER to Golgi vesicle-mediated transport [GO:0006888]	0.009585	ERP1 TRS20 RER1 BUG1 SHR3 SLY1 AGE1 YOS1 ERV14 COG2 GOS1 SVP26 AGE2 BET4 BET3 TRX1 BET5 YIP3 SLY41 BET2	20	80
transport [GO:0006810]	0.009857	SYN8 FLC2 ERP1 MST28 COR1 BAP2 SEC18 VID24 YSY6 TRS20 STP22 GRX1 TRX3 ATP16 NPC2 YET3 BUG1 VCX1 GGC1 SHR3 SSS1 ENT5 SAC3 SDH4 SLY1 MSC2 ATP5 BFR2 HXT3 SBE2 VPS60 PUF6 GRX2 AGE1 QCR7 YEA4 TIM9 RIP1 VMA3 AVT2 SIT1 NTF2 PIC2 YOS1 GET2 CAF16 LOC1 QCR6 VPS45 COG1 TAM41 COG2 FHN1 TPO2 TIM13 QCR9 MVB12 CIR1 GOS1 OSH7 TIM10 VMA16 VMA10 HXT4 CTR2 EGD2 YIA6 YKE4 QDR2 SYS1 APS3 KHA1 PAM16 ALB1 QCR8 TIM8 SFT1 ATP7 OAC1 SDH3 TPO5 ZRT3 MTR2 ACP1 VPS51 PAM17 BET3 POM33 TPO1 SDH2 FRE6 TRX1 PER33 NDL1 SEC72 ATP14 IMH1 VAC14 BET5 VPS20 SEC14 GFD1 SCS7 SAM50 COG6 COG5 AQR1 TOM22 PGA2 PDR16 PHO91 THP1 MCH4 BSC6 NRT1 PNS1 GET4 GSP2 ODC2 CDC31 TIM18 SLY41 DGK1 SNX3 VTS1 FIT2 SNF8 SEC62 ATG5 MEX67 FLC1 YAH1 APM1 ATP15 AIM45 ATP20 VMA13 TOM5 NCE102 TPO3 TDA6 SGE1	142	815
GO Cellular Component (625 categories)				
ribonucleoprotein complex [GO:0030529]	1.94E-13	LSM2 MRPL16 RPL19A MRPL36 RPL21A MRPS5 MRPL37 RPS14A IMG2 RPS29B RPL31A RPP1A SRP14 RPP1B RPL41B SAS10 RPS13 LSM6 RPP2B NPL3 UTP6 MRPL28 RPL27B RPL37B SNU13 RSM18 RPL34A LSM4 LCP5 RPS26B SMX2 RPL22B SAD1 RPL29 RPL28 RPS26A RPS25A UTP8 RPS27B NOP10 RPL42B IMP3 UTP9 RPL40A RPS21B RPL17B RPL39 RPS22A RPS14B TMA22 LSM8 RPL43B PRP40 SRP21 MRPL31 RPS27A MRP49 RPL17A MRPL13 SOF1 RPL15A DIP2 SMD3 RPL37A RPS28B SMD2 RPS30A RPL38 RPL26A RPS29A RPS16A MRPS8 RPL36A RPS10B RPL20A MRPL33 RPL16B IMP4 SWS2 NOP15 NAF1 MRPL50 MRPS12 RPP2A BUD21 RPS28A RPS30B RPS9A MRP51 RPL5 RPL33A MRPL40 RTC6 RPL43A	94	307

Ontology	p- value	Genes in ontology category	k	f
intracellular [GO:0005622]	6.76E-10	GEM1 HAP3 MRPL16 RPL19A RPL21A MRPS5 TRS20 REI1 RPS14A IMG2 STP4 RPS29B RPL31A RPP1A RPP1B NRG1 RPS13 GIS1 RPP2B UTP6 SDC1 RPL27B RPL37B NTF2 MIG3 RSM18 RPL34A YER130C RPS26B BUR6 GYP8 RPL22B RPL29 RPL28 RPS26A MIG2 TWF1 MDR1 OCA5 STP2 RPS27B FUR1 RPL42B IMP3 HIS5 RPL40A HYR1 DLS1 RPS21B RPL17B RPL39 RPS22A RPS14B RPL43B RSF2 MRT4 MSN4 RPS27A RPL17A IRC25 RPL15A REX3 RPL37A PNP1 CDC42 RPS28B RPS30A CDC25 RPL38 RPL26A STP3 REH1 RPS29A MSN2 BUB2 MOT3 SEC14 RPS16A MRPS8 RGM1 RPL36A RNT1 FCP1 NGL2 MRPL33 RLP7 SWS2 MRPS12 NOG2 RPP2A GYP1 RPS28A RPS30B RPS9A RPL5 RPL33A MRPL40 RTC6 RPL43A RHO1	100	381
extracellular region [GO:0005576]	1.02E-09	TIP1 FIG2 PST1 SED1 MFA1 SPI1 SCW11 CRH1 SCW4 BGL2 DSE2 PRY3 PRY1 HSP150 CWP1 CWP2 PIR3 PRY2 UTH1 YLR040C CCW12 CTS1 EXG1 CCW14 SCW10 KSH1 MFA2 YGP1 TOS6 KRE1 AGA1 PLB3 GAS5 HPF1 TIR2 SRL1 FIT2 THI22	38	95
fungal-type cell wall [GO:0009277]	1.87E-09	TIP1 FIG2 PST1 SED1 SPI1 SCW11 AGA2 CRH1 SCW4 BGL2 DSE2 PRY3 HSP150 CWP1 CWP2 PIR3 UTH1 YLR040C CCW12 YPS1 CTS1 EXG1 CCW14 HOR7 SCW10 TOS6 KRE1 AGA1 GAS5 ZPS1 HPF1 TIR2 SRL1 FIT2 SVS1	35	85
cell wall [GO:0005618]	3.84E-09	TIP1 FIG2 PST1 SED1 SPI1 SCW11 CRH1 SCW4 BGL2 DSE2 PRY3 HSP150 CWP1 CWP2 PIR3 UTH1 YLR040C CCW12 CTS1 EXG1 CCW14 SCW10 TOS6 KRE1 AGA1 GAS5 HPF1 TIR2 SRL1 FIT2	30	68
nucleolus [GO:0005730]	5.12E-09	RRN6 LSM2 YBR141C MAK5 RRP7 RPS14A SAS10 AIR2 RRP8 RPA14 HMO1 BFR2 LSM6 NPL3 UTP6 PUF6 SNU13 EDC2 LSM4 NSA2 LCP5 SPB4 LOC1 CGR1 SLX9 RRP46 UTP8 RRP3 SSF1 NOP10 RPF1 IMP3 UTP9 RRT14 RPS14B LSM8 URB2 RPA12 MRT4 MAK11 UTP30 SOF1 GRC3 NOC3 FCF2 DIP2 RRN5 RMP1 RRN11 CTK3 RNT1 RLP7 IMP4 NOP15 RPC19 CSL4 DBP6 TRM112 NOG2 TOP1 RCL1 BRX1 RRP40 NOP8 BUD21 PNO1 RPB10 RPS9A NOP53 TIF6 RRP15 JIP5	72	253
nucleus [GO:0005634]	5.51E-09	CCR4 OAF1 ECM15 HTB2 RRN6 FUS3 HAP3 LSM2 PRE7 TOD6 AAR2 HHF1 HHT1 HMT1 NHP6B YSA1 YBR141C MAK5 RPB5 SLI15 UBS1 POP7 UMP1 SWD3 MED8 GPX2 MAL33 RRP7 GRX1 KAR4 RPS14A HMRA1 PTC1 STP4 PBP4 YDL063C BDF2 SRP14 HNT1 RPC53 SAS10 UGA3 AIR2 TRM8 HEM3 PHO13 SOK1 LYS14 ARO3 NRG1 CDC34 PDC2 RRP8 GIS1 GRX3 MTQ2 TAF12 CTH1 RPA14 SAC3 NBP2 HMO1 RVB1 MSC2 HTB1 RTT103 BFR2 SRB7 SEM1 CDC40 LSM6 UBA2 NPL3 UTP6 RMT2 SDC1 SLD5 PUF6 GCN4 SNU13 UTR4 HPA3 MIG3 CHZ1 EDC2 PHM8 HOR2 PTC2 IES5 RAD51 LSM4 SCS2 NSA2 LCP5 YER130C BUR6 CCA1 SPB4 WWM1	364	1965

Ontology	p- value	Genes in ontology category	k	f
		HSP12 SMX2 EPL1 CAF16 LOC1 SAD1 CDC26 BNA6 PRE4 SCL1 PGD1 CGR1 PNC1 SDS23 RPB9 AFT1 MMS2 RPL28 NAB2 CWC23 ARI1 SUT1 TOS3 MIG2 SKI8 FRA2 TAN1 TAD1 RAI1 CUL3 TFG2 PRP18 POP6 NQM1 PEF1 SPT4 SLX9 RRP46 SRB5 UTP8 LSB1 RTS3 TFG1 PCT1 YCH1 PUP2 RTT102 CAB4 STP2 SLT2 FSH1 RSC30 MED6 RRP3 SSF1 PCL5 NOP10 LRP1 RTC3 RPF1 ARO9 IMP3 CTF8 EGD2 UTP9 SCH9 SKN7 NAS2 APQ12 VHR1 SDS3 POG1 RRT14 RPL40A STS1 YAP5 YVH1 PRE3 RPC17 DLS1 PSF2 ALB1 GCD14 RPB4 TPK1 RPS14B POL31 ESS1 LSM8 BNA1 URB2 ISY1 RPA12 RFC2 EAF6 NNF1 RSF2 TTI2 MRT4 PRP40 PUT3 SWD2 SPT23 MAK11 IXR1 PRI2 MSN4 YJU2 HAP4 ABF1 SRP21 ELF1 MTR2 SDS22 KAE1 UTP30 LAS1 SOF1 POM33 GRC3 UBI4 NOC3 CMS1 SDO1 TRX1 FCF2 IES3 PER33 XDJ1 SEN2 REX3 DIP2 RRN5 RMP1 SMD3 YKE2 CLB4 TUB4 BUR2 NDL1 SMD2 CDC25 NKP2 TMA10 STP3 CAR2 GLO1 YAP1 PPZ1 RRN11 SML1 PRE8 ARG81 CTK3 TAF8 MIC17 TAF4 ADI1 SOK2 STB4 MAC1 MSN2 ARG80 MCM1 SEN15 UBX4 MOT3 ABF2 RCO1 MED11 CEP3 RGM1 YMR244C-A GFD1 SAP30 FCP1 NGL2 GLC8 PRE5 RLP7 HRB1 HHT2 NCE103 MSG5 IMP4 YAF9 NOP15 DBP2 RPC19 NAF1 SPC98 FPR1 AAH1 ALF1 PGA2 IGO1 PGA1 SSU72 ELA1 CSL4 NRD1 RTC4 YNL260C ORC5 CAF40 CLA4 DBP6 TRM112 NOG2 RPB11 TOP1 RCL1 PRE6 THP1 BRX1 RFC4 INO4 MDY2 SKM1 RRP40 NOP8 PSF3 GRE2 YOR052C BUD21 RGS2 RIO1 PNO1 GSP2 RPB10 PUS7 CLP1 CDC31 MBF1 DGK1 HSH49 TYE7 VTS1 PDE2 TFC8 SKS1 DIG1 LGE1 GCR1 RPS9A RLM1 IDI1 NOP53 MEX67 RSA1 PUS1 RVB2 HFI1 SUT2 TIF6 THP3 NHP6A FCY1 ROX1 NOT5 SNT309 YTH1 RRP15 PIN3 JIP5		
ribosome [GO:0005840]	8.70E-08	MRPL16 RPL19A MRPL36 RPL21A MRPS5 MRPL37 RPS14A IMG2 RPS29B RPL31A RPP1A RPP1B RPL41B RPS13 SED1 RPP2B MRPL28 RPL27B RPL37B YEL047C RSM18 RPL34A RPS26B RPL22B RPL29 TIF4632 RPL28 AIM14 RPS26A RPS25A YPP1 RPS27B RPL42B RPL40A ALB1 RPS21B RPL17B RPL39 RPS22A RPS14B SUI2 TMA22 RPL43B TMA19 MRPL31 RPS27A MRP49 RPL17A MRPL13 POM33 RPL15A RPL37A RPS28B RPS30A RPL38 TMA10 RPL26A RPS29A RPS16A MRPS8 RPL36A RPS10B RPL20A MRPL33 RLP7 RPL16B SWS2 MRPL50 MRPS12 RPP2A MDY2 RPS28A RPS30B RPS9A MRP51 RPL5 RPL33A MRPL40 RTC6 RPL43A	80	310
cytosolic large ribosomal subunit [GO:0022625]	3.00E-07	RPL19A RPL21A REI1 RPL31A RPP1A RPP1B RPL41B RPP2B RPL27B RPL37B RPL34A RPL22B RPL29 RPL28 RPL42B RPL40A RPL17B RPL39 RPL43B RPL17A RPL15A RPL37A RPL38 RPL26A REH1 RPL36A RPL20A RPL16B RPP2A RPL5 RPL33A RPL43A	32	88

Ontology	p- value	Genes in ontology category	k	f
membrane [GO:0016020]	2.27E-06	SYN8 GEM1 FLC2 ERP1 MST28 COR1 GPI18 TCM62 YRO2 TIP1 BAP2 YBR074W VID24 ALG1 YSY6 YPC1 OM14 AIM5 RER1 STP22 MGR1 YCL057C-A PMP1 PER1 FIG2 ATP16 TSC13 PEX19 COX9 YET3 SNA4 VCX1 DLD1 GGC1 SHR3 OST4 RCR2 PST1 IPT1 SED1 PET100 SSS1 TVP15 ENT5 SDH4 SLY1 MSC2 RTN1 FMN1 PMP3 SUR2 ATP5 YDR319C HXT3 ATP22 YDR352W STE14 DFM1 HKR1 PFA5 MFA1 VPS60 IZH1 FPR2 SNA2 QCR7 IRC22 YEA4 VAC8 PMP2 TIM9 RIP1 VMA3 MTC7 SOM1 AVT2 SIT1 FMP52 ERG28 PIC2 YOS1 GET2 SCS2 COX15 SPI1 WWM1 STE2 FMP32 QCR6 YGL010W ERG4 OCH1 ERV14 FMP37 VPS45 RMD9 AIM14 COX13 YIP4 KEX1 COG1 EMC4 MTL1 MSP1 GSC2 TAM41 SCM4 VOA1 COG2 FHN1 TPO2 SKN1 TIM13 QCR9 CRH1 YPP1 PCT1 MVB12 GPI1 PET54 SPG1 COQ6 COS6 GOS1 TIM10 STP2 VMA16 HXT4 NSG1 DSE2 CTR2 SVP26 YHR192W YIA6 YKE4 KRE27 APQ12 AIM19 SLM1 PRM5 QDR2 COA1 SEC11 SYS1 APS3 COA3 PRY3 GWT1 KHA1 PAM16 PRM10 YUR1 SNA3 QCR8 ASG7 ELO1 SPC1 GPI14 STE18 STE24 TIM8 SFT1 LAC1 ATP7 MAK11 TUL1 SFK1 CWP1 CWP2 OAC1 CMC1 SDH3 MCR1 SRP102 TPO5 ZRT3 AIM27 VPS51 UTH1 PET10 PAM17 TVP38 PSR1 EMC6 POM33 TPO1 SDH2 FRE6 IZH3 YLR040C TRX1 PER33 SPC3 XDJ1 SEN2 CCW12 YPS1 YPS3 RMP1 COQ9 QRI5 CDC42 ATP14 IMH1 CDC25 MID2 ORM2 ATG33 VAC14 ECM19 CCW14 COX8 FLD1 YLR413W PUN1 SUR7 SPC2 VAN1 ADI1 SEN15 VPS20 SEC14 PKR1 OSW5 ICY1 ROT1 GFD1 COX7 SCS7 SAM50 GPI15 COG6 YIP3 COG5 COX5A AQR1 TOM22 MFA2 PGA2 PGA1 PDR16 WSC2 TOS6 BXI1 KRE1 COS1 VPS27 PHO91 COQ2 AGA1 PFA4 COQ10 PLB3 GAS5 YOL092W IZH4 ZEO1 MCH4 BSC6 PEX11 HPF1 ALG6 TIR2 IRC23 YOR059C NRT1 ATX2 OST2 PIN2 PNS1 LCB4 ODC2 TIM18 SLY41 DGK1 SNX3 FIT2 SNF8 KTR6 GPI2 SEC62 MGR2 ATG5 PRM4 SPT14 TCO89 PGC1 FLC1 APM1 ATP15 ATP20 YOP1 VMA13 ERV2 PIS1 TOM5 NCE102 TPO3 TDA6 KRE6 RHO1 DPM1 SGE1	303	1671
endoplasmic reticulum [GO:0005783]	2.47E-06	FLC2 ERP1 MST28 GPI18 ALG1 YSY6 YPC1 TRS20 PER1 TSC13 PEX19 YET3 SHR3 OST4 SSS1 SLY1 MSC2 GTB1 RTN1 FMN1 SUR2 CPR5 DFM1 IZH1 FPR2 IRC22 YEA4 AVT2 FMP52 ERG28 YOS1 GET2 SCS2 YGL010W ERG4 OCH1 ERV14 EMC4 VOA1 NSG1 SVP26 YKE4 KRE27 APQ12 SEC11 PRY1 GWT1 SPC1 GPI14 STE24 LAC1 SRP102 AIM27 BET3 EMC6 POM33 IZH3 PER33 SPC3 CTS1 ORM2 FLD1 SPC2 BET5 CUE4 VAN1 ERG5 PKR1 ROT1 HOR7 SCS7 SCW10 YIP3 PGA2 PDR16 BXI1 PFA4 IZH4 PEX11 ALG6 IRC23 LCB4 RDL1 SLY41 DGK1 GPI2 SEC62 SPT14 PGC1 FLC1 YOP1 ERV2 PIS1	95	416

Ontology	p- value	Genes in ontology category	k	f
		NCE102 DPM1		
anchored to membrane [GO:0031225]	6.92E-06	TIP1 FIG2 PST1 SED1 SPI1 CRH1 DSE2 PRY3 CWP1 CWP2 YLR040C CCW12 YPS1 YPS3 CCW14 TOS6 KRE1 AGA1 PLB3 GAS5 HPF1 TIR2 FIT2	23	61
endoplasmic reticulum membrane [GO:0005789]	1.70E-05	FLC2 ERP1 PRE7 GPI18 ALG1 YSY6 YPC1 PER1 TSC13 PEX19 YET3 SHR3 OST4 SSS1 MSC2 RTN1 SUR2 STE14 DFM1 IZH1 FPR2 IRC22 YEA4 ERG28 YOS1 GET2 SCS2 PRE4 YGL010W OCH1 ERV14 EMC4 VOA1 NSG1 YKE4 KRE27 SEC11 PRE3 GWT1 SPC1 GPI14 STE24 LAC1 SRP102 AIM27 EMC6 POM33 IZH3 PER33 SPC3 SEC72 ORM2 FLD1 SPC2 VAN1 PKR1 ROT1 SCS7 PGA2 PDR16 PFA4 IZH4 ALG6 IRC23 LCB4 DGK1 SEC62 SPT14 PGC1 FLC1 YOP1 ERV2 PIS1 DPM1	74	318
mitochondrion [GO:0005739]	8.34E-05	GCV3 GEM1 ERP1 FUS3 MRPL16 COR1 PRX1 GPI18 TCM62 YRO2 YSA1 MRPL36 EXO5 OM14 MRPS5 AIM5 MRPL37 ILV6 MGR1 YCL057C-A RIM1 IMG2 TRX3 ATP16 TSC13 STP4 COX9 DLD1 DLD2 INH1 GGC1 GCV1 ARO3 TPS2 SED1 PET100 GIS1 SDH4 MFB1 RTN1 FMN1 ATP5 ATP22 MRPL28 GRX2 QCR7 TIM9 RIP1 YEL047C SOM1 FMP52 ISD11 RSM18 PIC2 COX15 CCA1 PDA1 WWM1 FMP32 QCR6 HXK1 SCL1 FMP37 RMD9 COX13 NIF3 MTC3 MSP1 ERV1 TAM41 SCM4 TIM13 QCR9 CIR1 PET54 YGR235C SPG1 PUP2 COQ6 AIM17 YHR003C TIM10 MSR1 COX23 YHR162W AIM18 BAT1 YIA6 MMF1 AIM19 FMC1 SLM1 COA1 YIR024C COA3 KHA1 PAM16 NCA3 QCR8 TES1 TIM8 ATP7 NFU1 TMA19 OAC1 CMC1 MRPL31 SDH3 MCR1 MRP49 ACP1 MRPL13 UTH1 LAS1 PAM17 CCP1 DRE2 COX19 ISA1 SDH2 XDJ1 SEN2 COQ9 QRI5 ATP14 TMA10 ATG33 ARC18 ECM19 CCW14 COX8 SUR7 CPR3 PRE8 MIC17 SEN15 ARG7 ABF2 NDE1 MRPS8 YMR244C-A COX7 MRPL33 PRE5 SAM50 COX5A SWS2 LEU4 DBP2 TOM22 FPR1 BXI1 MRPL50 MRPS12 COQ2 COQ10 PRE6 NGL1 GPD2 ZEO1 GYP1 LSC1 GEP3 AIM41 MCT1 ODC2 ISU2 TUM1 RDL1 RDL2 TIM18 MBF1 RRG7 FAA1 ALD4 LSP1 GRX5 MRP51 ISU1 PPT2 PEP4 PET20 MRPL40 RTC6 POS5 OXR1 PGC1 YAH1 FUM1 ATP15 AIM45 ATP20 CCL1 PIS1 TOM5 NCE102 RHO1 DPM1	198	1072
proteasome storage granule [GO:0034515]	0.000118	PRE7 RPN5 SEM1 RPN9 PRE4 RPN12 SCL1 PUP2 PRE3 PRE8 PRE5 PRE6	12	26
mitochondrial inner membrane [GO:0005743]	0.000205	COR1 TCM62 MGR1 ATP16 COX9 DLD1 GGC1 PET100 SDH4 FMN1 ATP5 ATP22 QCR7 TIM9 SOM1 PIC2 COX15 QCR6 RMD9 COX13 TAM41 TIM13 QCR9 PET54 COQ6 TIM10 YIA6 COA1 COA3 PAM16 QCR8 TIM8 ATP7 OAC1 CMC1 SDH3 PAM17 SDH2 COQ9 QRI5 ATP14 COX8 COX7 COX5A COQ2 COQ10 ODC2 TIM18 ATP15	49	204

Ontology	p- value	Genes in ontology category	k	f
Golgi membrane [GO:0000139]	0.000226	YPC1 RER1 TVP15 SLY1 YOS1 GET2 OCH1 ERV14 VPS45 YIP4 COG1 COG2 GOS1 SYS1 YUR1 SFT1 TUL1 TPO5 TVP38 TRX1 IMH1 VAN1 SEC14 COG6 YIP3 COG5 ATX2 LCB4 DGK1 SNX3 YOP1 KRE6	32	117
preribosome, large subunit precursor [GO:0030687]	0.000282	REI1 NSA2 LOC1 CGR1 RPF1 YVH1 MRT4 SDO1 REH1 RLP7 NOP15 DBP6 NOG2 BRX1 TIF6 RRP15	16	44
cytoplasm [GO:0005737]	0.000446	CCR4 FLC2 ECM15 RRN6 FUS3 LSM2 PRE7 TOD6 PRS4 AAR2 YBL107C UGA2 HMT1 SEC18 RPL19A YSA1 PTC4 SHE3 ARA1 SLI15 UMP1 RPL21A NGR1 GPX2 REI1 STP22 GRX1 SRO9 KAR4 RVS161 RPS14A CTR86 PTC1 TSC13 STP4 PBP4 RPS29B YDL063C PEX19 BDF2 RPL31A RPP1A SRP14 BUG1 HNT1 RPP1B RPL41B HEM3 WHI4 PHO13 RCR2 KCS1 GCV1 SES1 ARO3 CDC34 RPS13 TPS2 MTQ2 GIR2 ENT5 NBP2 HMO1 SLY1 VHS1 SSD1 CPR5 GIC2 LSM6 RPP2B NPL3 APT2 RMT2 RPL27B VPS60 RPL37B GRX2 AGE1 SNA2 GIM4 UTR4 YEL047C HPA3 NTF2 MIG3 EDC2 PHM8 HOM3 RPL34A HOR2 PTC2 LSM4 RPS26B CCA1 TMT1 WWM1 HSP12 CAF16 RPL22B RPL29 BNA6 PRE4 HXK1 SCL1 PNC1 TIF4632 SDS23 AFT1 MMS2 VPS45 RPL28 GPG1 NAB2 CWC23 ARI1 SUT1 MPT5 TOS3 RPS26A SKI8 FRA2 NIF3 TAN1 CUL3 RPS25A NQM1 PEF1 PAC10 TWF1 RRP46 ASK10 MDR1 LSB1 RTS3 YPP1 YCH1 MVB12 PUP2 CAB4 PRS3 OCA5 OSH7 STP2 RPS27B SLT2 FSH1 NMD2 RTC3 MSR1 DMA1 COX23 ARO9 RPL42B YHR192W EGD2 SCH9 NAS2 CAP2 AGE2 VHR1 SLM1 TPM2 RPL40A DJP1 YAP5 YVH1 HYR1 PRE3 RPE1 ALB1 RPS21B RPB4 TPK1 RPL17B RPL39 RPS22A RPS14B SUI2 TMA22 ESS1 LSM8 BNA1 ISY1 STE18 RPL43B CPA2 TTI2 ARC19 PAN3 TMA19 MSN4 SRP21 MRP8 RPS27A RPL17A SDS22 EAP1 SAP190 KAE1 DRE2 TVP38 SRL3 COX19 UBI4 SDO1 RPL15A TRX1 YLR063W REX3 AHP1 YLR143W RMP1 SMD3 RPL37A YKE2 CLB4 TUB4 NDL1 GSY2 RPS28B RPS30A SEC72 IMH1 CDC25 RPL38 TMA10 RPL26A NMD4 ARC18 REH1 RPS29A PUN1 CAR2 GLO1 YAP1 PPZ1 CMP2 SML1 PRE8 GIM5 ARG81 TSL1 CUE4 CTK3 MIC17 ADI1 MSN2 BUB2 UBX4 VPS20 SEC14 SNO1 MUB1 JLP2 RPS16A RPL36A RPS10B RPL20A YMR244C-A GFD1 NGL2 SCW10 GLC8 PRE5 HRB1 SIW14 NCE103 MSG5 RPL16B TPM1 SWS2 OCA1 LEU4 YAF9 NOP15 DBP2 NCS2 SPC98 FPR1 AAH1 ALF1 IGO1 BNI5 WHI3 PDR16 CSL4 RTC4 GIS2 YNL260C WSC2 CAF40 TRM112 PRE6 RPP2A DDR2 GPD2 YOL092W MDY2 PFK27 RRP40 DCP1 GRE2 RGS2 RIO1 PFY1 PNO1 GET4 RPS28A RPS30B RCN2 SRL1 TUM1 NAT5 CDC31 RBL2 PLP2 MBF1 SNX3 VTS1 PDE2 SNF8 LSP1 SKS1 MUK1 RPS9A IDI1 RPL5 RPL33A	341	2026

Ontology	p- value	Genes in ontology category	k	f
		ATG5 MEX67 RTT10 YAR1 FUM1 TIF6 RPL43A FCY1 UBA3 NOT5 NAT3 NCE102 PIN3		
signal peptidase complex [GO:0005787]	0.000454	SEC11 SPC1 SPC3 SPC2	4	4
proteasome core complex [GO:0005839]	0.0005	PRE7 PRE4 SCL1 PUP2 PRE3 PRE8 PRE5 PRE6	8	15
proteasome complex [GO:0000502]	0.000504	PRE7 UBC4 UMP1 RPN5 UBC5 SEM1 RPN9 RPN3 PRE4 RPN12 SCL1 PUP2 PRE3 PRE8 PRE5 PRE6	16	46
cytosolic small ribosomal subunit [GO:0022627]	0.000949	RPS14A RPS29B RPS13 RPS26B RPS26A RPS25A RPS27B RPS21B RPS22A RPS14B RPS27A RPS28B RPS30A RPS29A RPS16A RPS10B RPS28A RPS30B RPS9A	19	62
proteasome core complex, alpha-subunit complex [GO:0019773]	0.001072	SCL1 PUP2 PRE8 PRE5 PRE6	5	7
Golgi apparatus [GO:0005794]	0.001097	MST28 GRX7 YPC1 TRS20 RER1 TVP15 RTN1 SBE2 YOS1 GET2 OCH1 ERV14 YIP4 COG1 COG2 PCT1 GOS1 SVP26 AGE2 SYS1 APS3 KHA1 YUR1 SFT1 TUL1 TPO5 VPS51 BET3 TVP38 TRX1 IMH1 BET5 VAN1 SEC14 KSH1 COG6 YIP3 COG5 BSC6 GYP1 ATX2 LCB4 DGK1 SNX3 YOP1 PIS1 KRE6 RHO1	48	213
mitochondrial respiratory chain complex III [GO:0005750]	0.001189	COR1 QCR7 RIP1 QCR6 QCR9 QCR8	6	10
integral to membrane [GO:0016021]	0.001256	SYN8 GEM1 FLC2 ERP1 MST28 COR1 GPI18 GRX7 TCM62 YRO2 BAP2 YBR074W ALG1 YSY6 YPC1 OM14 AIM5 RER1 MGR1 YCL057C-A PMP1 PER1 ATP16 TSC13 PRM7 COX9 YET3 SNA4 VCX1 GGC1 SHR3 OST4 RCR2 IPT1 PET100 SSS1 TVP15 SDH4 MSC2 RTN1 PMP3 SUR2 ATP5 YDR319C HXT3 YDR352W STE14 DFM1 HKR1 PFA5 IZH1 SNA2 QCR7 IRC22 YEA4 PMP2 TIM9 VMA3 MTC7 AVT2 SIT1 NTF2 ERG28 PIC2 YOS1 GET2 SCS2 COX15 WWM1 STE2 FMP32 QCR6 YGL010W ERG4 OCH1 ERV14 FMP37 AIM14 COX13 YIP4 KEX1 EMC4 MTL1 MSP1 GSC2 SCM4 VOA1 FHN1 TPO2 SKN1 TIM13 QCR9 GPI1 SPG1 COS6 GOS1 OSH7 TIM10 VMA16 HXT4 NSG1 CTR2 SVP26 YHR192W YIA6 YKE4 KRE27 APQ12 AIM19 PRM5 QDR2 COA1 SEC11 SYS1 COA3 GWT1 KHA1 PRM10 YUR1 SNA3 QCR8 ASG7 ELO1 SPC1 GPI14 STE24 TIM8 SFT1 LAC1 ATP7 TUL1 SFK1 OAC1 SDH3 MCR1 SRP102 TPO5 ZRT3 MTR2 AIM27 PAM17 TVP38 EMC6 POM33 TPO1 FRE6 IZH3 PER33 SPC3 RMP1 ATP14 CDC25 MID2 ORM2 ATG33 ECM19 COX8 FLD1 YLR413W PUN1 SUR7 SPC2 VAN1 PKR1 OSW5 ROT1 GFD1 COX7 SCS7 HRB1 SAM50 GPI15 YIP3 COX5A AQR1 TOM22 PGA2 PGA1 ELA1 WSC2 BXI1 KRE1 COS1 PHO91 COQ2 PFA4 GAS5 YOL092W IZH4 MCH4 BSC6 ALG6 IRC23 YOR059C NRT1 ATX2 OST2 PIN2 PNS1 GSP2 ODC2 CDC31 TIM18 SLY41 DGK1 KTR6 GPI2 SEC62	226	1303

Ontology	p- value	Genes in ontology category	k	f
		MGR2 PRM4 MEX67 SPT14 PGC1 FLC1 ATP15 YOP1 VMA13 ERV2 PIS1 TOM5 NCE102 TPO3 TDA6 KRE6 DPM1 SGE1		
mitochondrial intermembrane space protein transporter complex [GO:0042719]	0.002005	TIM9 TIM13 TIM10 TIM8	4	5
integral to endoplasmic reticulum membrane [GO:0030176]	0.002586	GPI18 SHR3 RTN1 SCS2 SVP26 STE24 SPT23 SRP102 PKR1 PGA1 DGK1 SEC62 KRE6	13	39
cytoplasmic mRNA processing body [GO:0000932]	0.004547	CCR4 LSM2 NGR1 SSD1 LSM6 LSM4 RPB4 IGO1 DCP1 VTS1	10	28
respiratory chain [GO:0070469]	0.004763	COR1 QCR7 RIP1 QCR6 QCR9 QCR8 ACP1	7	16
glycosylphosphatidylinositol-N-acetylglucosaminyltransferase (GPI-GnT) complex [GO:0000506]	0.005317	GPI1 GPI15 GPI2 SPT14	4	6
ER membrane protein complex [GO:0072546]	0.005317	EMC4 KRE27 AIM27 EMC6	4	6
proteasome regulatory particle, lid subcomplex [GO:0008541]	0.008773	RPN5 SEM1 RPN9 RPN3 RPN12	5	10
fungal-type vacuole lumen [GO:0000328]	0.008773	NPC2 SNA4 PRB1 SNA3 PEP4	5	10
small nucleolar ribonucleoprotein complex [GO:0005732]	0.008773	LSM2 LSM6 LSM4 LCP5 SOF1	5	10
MIPS Functional Classification (459 categories)				
ribosomal proteins [12.01.01]	3.21E-12	MRPL16 RPL19A MRPL36 MAK5 RPL21A MRPS5 MRPL37 RRP7 RPS14A IMG2 RPS29B RPL31A RPP1A RPP1B RPL41B RPS13 RPP2B MRPL28 RPL27B RPL37B RSM18 RPL34A RPS26B SPB4 RPL22B RPL29 RPL28 RPS26A RPS25A RPS27B SSF1 RPF1 RPL42B RPL40A RPS21B RPL17B RPL39 RPS22A RPS14B RPL43B MRPL31 MRP8 RPS27A MRP49 RPL17A MRPL13 RPL15A RPL37A RPS28B RPS30A RPL38 RPL26A RPS29A RPS16A MRPS8 RPL36A RPS10B RPL20A MRPL33 RPL16B SWS2 MRPL50 MRPS12 DBP6 RPP2A BRX1 NOP8 RPS28A RPS30B RPS9A MRP51 RPL5 RPL33A MRPL40 RTC6 RSA1 RPL43A RRP15	78	246
electron transport [20.01.15]	6.12E-08	GRX1 TRX3 ATP16 COX9 INH1 GRX3 SDH4 ATP5 GRX2 VMA3 YEL047C COX13 VMA16 VMA10 ATP7 SDH3 MCR1 CCP1 SDH2 TRX1 ATP14 COX8 NDE1 COX7 COX5A SIA1 GRX5 YAH1 ATP15 AIM45 ATP20 VMA13	32	83
rRNA processing [11.04.01]	3.30E-07	LSM2 MAK5 POP7 RRP7 SAS10 RRP8 NPL3 UTP6 SNU13 LSM4 LCP5 SPB4 CGR1 RAI1 POP6 RRP46 UTP8 RRP3 NOP10 LRP1 RPF1 IMP3 UTP9 LSM8 MRT4 UTP30 SOF1 GRC3 NOC3 SDO1 DIP2 RMP1 RNT1 NGL2 RLP7 IMP4 DBP2 SSU72 CSL4 DBP6 RCL1 RRP40 NOP8 BUD21 RIO1 PNO1 NOP53 RVB2 TIF6 RRP15	50	169
RNA binding [16.03.03]	2.26E-06	SHE3 NGR1 SRO9 RPS14A SAS10 WHI4 SSD1 NPL3 UTP6 EDC2 LCP5 LOC1 RPL28 NAB2 MPT5 TAN1 UTP8 PET54 SSF1 NOP10	52	189

Ontology	p- value	Genes in ontology category	k	f
		RPF1 IMP3 UTP9 RPS14B TMA22 RSF2 PRP40 UTP30 SOF1 RPL15A DIP2 RRN5 SMD3 RPL26A RPL36A RNT1 RLP7 HRB1 RPL16B IMP4 NAF1 WHI3 NRD1 BRX1 DCP1 BUD21 CLP1 HSH49 VTS1 RPL5 MEX67 YTH1		
electron transport and membrane-associated energy conservation [02.11]	2.52E-06	COR1 ATP16 COX9 INH1 SDH4 ATP5 QCR7 RIP1 QCR6 COX13 QCR9 QCR8 ATP7 SDH3 MCR1 SDH2 ATP14 COX8 NDE1 COX7 COX5A ATP15 ATP20	23	58
oxidative stress response [32.01.01]	3.51E-06	PRX1 UGA2 GPX2 GRX1 TRX3 GRX3 GRX2 HSP12 ASK10 SCH9 SKN7 HYR1 MCR1 CCP1 TRX1 AHP1 YAP1 OCA1 GRE2 GRX5 POS5 OXR1	22	55
modification with fatty acids (e.g. myristylation, palmitylation, farnesylation) [14.07.01]	9.96E-05	STE14 PFA5 GPI1 BET4 GWT1 GPI14 RAM2 GPI15 PFA4 FAA1 GPI2 SPT14 BET2 DPM1	14	33
DNA binding [16.03.01]	0.000114	OAF1 HTB2 HHF1 HHT1 RPB5 NGR1 RIM1 RPC53 NRG1 RPA14 HMO1 HTB1 SLD5 GCN4 MIG3 RPB9 RSC30 RPC17 PSF2 RPB4 RPA12 RFC2 IXR1 MSN4 ABF1 STB4 MSN2 ARG80 MCM1 MOT3 ABF2 CEP3 HHT2 RPC19 RPB11 RFC4 PSF3 RPB10 GCR1 RLM1 ROX1	41	158
protein processing (proteolytic) [14.07.11]	0.000141	PRE7 APE3 STE14 PRE4 RPN12 SCL1 KEX1 PUP2 SEC11 PRE3 SPC1 STE24 RAM2 SPC3 YPS1 MAP1 SPC2 PRE8 PRE5 PRE6 PEP4	21	63
general transcription activities [11.02.03.01]	0.000188	RRN6 RPB5 MED8 HMRA1 UGA3 PDC2 HMO1 RVB1 SRB7 BUR6 PGD1 RPB9 SUT1 MIG2 SRB5 STP2 MED6 POG1 YAP5 RPB4 PUT3 RRN5 RRN11 ARG81 TAF8 TAF4 MAC1 ARG80 MCM1 MED11 RGM1 RPB11 INO4 RPB10 MBF1 TFC8 HFI1 SUT2	38	146
mitochondrion [42.16]	0.000304	MRPL16 MRPL36 NGR1 MRPS5 MRPL37 MGR1 IMG2 PTC1 DLD1 DLD2 GGC1 MRPL28 TIM9 SOM1 RSM18 ERV1 TIM10 MMF1 PAM16 NCA3 MRPL31 MRP49 MRPL13 UTH1 PAM17 CCP1 SML1 ABF2 NDE1 MRPS8 MRPL33 SAM50 MRPL50 MRPS12 ALD4 GRX5 MGR2 MRP51 MRPL40 RTC6 FUM1 AIM45	42	170
transcriptional control [11.02.03.04]	0.000477	CCR4 HTB2 TOD6 HHF1 HHT1 NHP6B MED8 MAL33 KAR4 HMRA1 BDF2 SAS10 UGA3 SOK1 KCS1 PDC2 GIS1 TAF12 CTH1 SAC3 RVB1 HTB1 SRB7 SCS2 YER130C BUR6 EPL1 CAF16 PGD1 AFT1 SUT1 MIG2 NIF3 TFG2 SPT4 ASK10 MDR1 SRB5 TFG1 STP2 RSC30 MED6 EGD2 SKN7 SDS3 YAP5 TPK1 ESS1 RSF2 PUT3 IXR1 MSN4 ABF1 BUR2 YAP1 CMP2 ARG81 CTK3 SOK2 STB4 MAC1 MSN2 ARG80 MCM1 MED11 RGM1 SAP30 HHT2 YAF9 SSU72 NRD1 GIS2 ORC5 CAF40 TOP1 INO4 PLP2 MBF1 TYE7 SKS1 MUK1 RVB2 HFI1 SUT2 CCL1 NHP6A NOT5	87	426
homeostasis of protons [34.01.01.03]	0.000663	PMP1 ATP16 VCX1 ATP5 PMP2 VMA3 VMA16 VMA10 VMA22 KHA1 ATP7 CWP2 ATP14 SIA1 ATP15 VMA13	16	47

Ontology	p- value	Genes in ontology category	k	f
peroxidase reaction [32.07.07.05]	0.001072	GPX2 GRX1 GRX2 HYR1 CCP1	5	7
aerobic respiration [02.13.03]	0.001114	COR1 COX9 DLD1 PET100 SDH4 RIB3 QCR7 RIP1 QCR6 COX13 QCR9 COX23 QCR8 SDH3 PET10 SDH2 COQ9 COX8 NDE1 COX7 COX5A MCT1	22	77
protein binding [16.01]	0.001201	MST28 FUS3 TCM62 UBC4 UMP1 MED8 STP22 RVS161 SRP14 DLD2 TRM8 SHR3 OST4 CDC34 UBC5 PET100 ENT5 SAC3 SLY1 MFB1 HSP31 GIM4 VAC8 TIM9 NTF2 SCS2 CDC26 AGA2 MMS2 VPS45 CUL3 PRP18 PAC10 TWF1 COG2 PEX4 TIM10 VMA22 NMD2 NSG1 SVP26 EGD2 CAP2 SDS3 TPM2 DJP1 PAM16 PEX2 CAP1 SRP21 SRP102 MTR2 VPS51 PAM17 UBI4 NOC3 YKE2 YLR243W SPC2 GIM5 SNZ1 TPM1 ALF1 VPS27 AGA1 THP1 SGT1 PFY1 PNO1 RBL2 CIN1 SNX3 DIG1 SEC62 ISU1 NOP53 MEX67 APM1 YOP1	79	391
cell wall [42.01]	0.001953	ECM15 ECM13 TIP1 IPT1 SED1 SSD1 SBE2 HKR1 YEA4 GET2 DSE1 SPI1 MPT5 MTL1 GSC2 SKN1 GPI1 BGL2 SLT2 DSE2 CAP2 YUR1 HSP150 CAP1 PAN3 CWP1 CWP2 PIR3 CCW12 EXG1 MID2 ECM19 CCW14 VAN1 ARG7 ROT1 WSC2 KRE1 GAS5 ZEO1 HPF1 CDC31 KTR6 RLM1 SPT14 KRE6 RHO1	47	213
homeostasis of metal ions (Na, K, Ca etc.) [34.01.01.01]	0.003041	SRO9 PER1 VCX1 GGC1 MSC2 IZH1 VMA3 SIT1 AFT1 AIM14 ERV1 CTR2 NFU1 ZRT3 ISA1 FRE6 IZH3 AHP1 CDC25 PPZ1 MAC1 IZH4 ATX2 ISU2 ISU1	25	98
stress response [32.01]	0.003074	YRO2 TIP1 UBC4 KCS1 TPS2 SED1 SSD1 FPR2 WWM1 RPN12 CWC23 MPT5 MDR1 PUP2 SLT2 PRE3 RPB4 HSP150 MSN4 KDX1 PIR3 UTH1 PSR1 UBI4 PPZ1 TSL1 MAC1 MSN2 MCM1 SNO1 SNZ1 HOR7 SIW14 YGP1 DDR2 ZEO1 TIR2	37	162
enzymatic activity regulation / enzyme regulator [18.02.01]	0.003192	ILV6 PMP1 COX13 YIP4 RAI1 YCH1 PCL5 YVH1 RFC2 SDS22 CLB4 BUR2 CMP2 TSL1 MAC1 SIW14 OCA1 SSU72 RFC4 CCL1 UBA3	21	78
ribosome biogenesis [12.01]	0.003688	NSA2 LOC1 CGR1 IMP3 URB2 MRT4 MAK11 TMA19 RLP7 MSG5 NOP15 NCS2 FPR1 GIS2 NOG2 RRP40 NOP53 TIF6	18	64
intra Golgi transport [20.09.07.05]	0.005434	AGE1 COG1 COG2 GOS1 SVP26 AGE2 SFT1 TPO5 COG6 COG5 VPS27	11	33
regulation of amino acid metabolism [01.01.13]	0.005434	CCR4 LYS14 CDC34 SAC3 GCN4 ARO9 PUT3 ABF1 ARG81 ARG80 MCM1	11	33
RNA degradation [01.03.16.01]	0.005978	CCR4 EDC2 MPT5 SKI8 RAI1 RRP46 NMD2 MRT4 REX3 NMD4 DBP2 CSL4 RRP40 DCP1 NOT5	15	52
protein kinase [30.01.05.01]	0.00791	TOS3 YCH1 YVH1 SAP190 PPZ1 CMP2 SIW14 MSG5 OCA1 SSU72	10	30
MIPS Phenotypes (142 categories)				
Respiratory deficiency [42.25.20]	0.000883	HTB2 TCM62 RVS161 IMG2 ATP16 PTC1 PET100 SDH4 ATP5 QCR7 RIP1 SOM1 COX15 PDA1 QCR6 COX13 QCR9 PET54	41	173

Ontology	p- value	Genes in ontology category	k	f
		EGD2 MMF1 IXR1 HAP4 SRP102 MRP49 ACP1 SDH2 ATP14 CPR3 MAC1 ABF2 NDE1 COX7 PEX11 MCT1 HEM4 MRP51 PPT2 HFI1 ATP15 TOM5 SGE1		
other nitrogen utilization defects [42.30.99]	0.003113	SHR3 GLY1 SLT2	3	3
Inappropriate sporulation [32.15]	0.005317	KAR4 RVS161 RIM1 VAN1	4	6
MIPS Subcellular Localization (48 categories)				
ER [735]	1.27E-10	FLC2 PRE7 TIP1 UBC4 ALG1 YSY6 UMP1 RER1 PER1 TSC13 YET3 SRP14 SNA4 VCX1 RPN5 SHR3 OST4 PST1 IPT1 SED1 SSS1 MSC2 GTB1 RTN1 SUR2 CPR5 STE14 DFM1 RPN9 IZH1 FPR2 HSP31 IRC22 VMA3 AVT2 FMP52 RPN3 ERG28 GET2 SCS2 PRE4 RPN12 YGL010W SCL1 ERG4 AGA2 OCH1 ERV14 KEX1 EMC4 PCT1 GPI1 PUP2 BGL2 VMA16 VMA22 CTR2 SVP26 KRE27 APQ12 DJP1 SEC11 PRE3 SYS1 DLS1 PRY3 PRY1 GWT1 HSP150 ELO1 SPC1 GPI14 STE24 RSF2 LAC1 CWP1 CWP2 SRP21 SRP102 EMC6 POM33 TPO1 IZH3 PER33 SPC3 CCW12 YPS1 CTS1 SEC72 EXG1 ORM2 STP3 ECM19 CCW14 SPC2 PRE8 CUE4 ERG5 VPS20 SEC14 PKR1 ROT1 HOR7 SCS7 SCW10 PRE5 YIP3 PGA2 CLA4 TOS6 KRE1 PHO91 AGA1 GAS5 PRE6 IZH4 ALG6 IRC23 OST2 HEM4 RDL1 SLY41 DGK1 FAA1 KTR6 GPI2 SEC62 SPT14 YOP1 PIS1 NCE102 DPM1	132	537
nucleus [750]	2.02E-09	SYN8 CCR4 OAF1 ECM15 HTB2 RRN6 FUS3 HAP3 LSM2 PRE7 TOD6 PRX1 AAR2 YBL107C HHF1 HHT1 HMT1 UBC4 NHP6B VID24 CMD1 YSA1 MAK5 ARA1 RPB5 SLI15 YSY6 UBS1 POP7 UMP1 SWD3 MED8 GPX2 MAL33 RRP7 GRX1 KAR4 MAK31 HMRA1 STP4 PBP4 YDL063C BDF2 HNT1 RPN5 RPC53 SAS10 UGA3 AIR2 TRM8 HEM3 WHI4 PHO13 RCR2 SOK1 LYS14 ARO3 NRG1 CDC34 UBC5 PDC2 RRP8 GIS1 GRX3 MTQ2 TAF12 RPA14 SAC3 HMO1 RVB1 HTB1 PMP3 RTT103 SRB7 SEM1 CDC40 LSM6 UBA2 RPN9 NPL3 MFA1 RMT2 SDC1 RIB3 SLD5 PUF6 GRX2 HSP31 GCN4 SNU13 UTR4 GLY1 YEL047C HPA3 NTF2 RPN3 MIG3 CHZ1 EDC2 PHM8 HOR2 PTC2 IES5 RAD51 LSM4 NSA2 LCP5 BUR6 CCA1 SPB4 WWM1 HSP12 SMX2 EPL1 CAF16 LOC1 SAD1 CDC26 BNA6 PRE4 RPN12 LEU1 SCL1 PGD1 CGR1 SDS23 RPB9 AFT1 FMP37 MMS2 NAB2 CWC23 ARI1 SUT1 KEX1 MIG2 FRA2 TAN1 TAD1 RAI1 CUL3 TFG2 PRP18 POP6 NQM1 PEF1 SPT4 SLX9 RRP46 ASK10 SRB5 LSB1 RTS3 TFG1 YCH1 PUP2 COQ6 RTT102 STP2 SLT2 FSH1 MED6 RRP3 SSF1 PCL5 NOP10 LRP1 RTC3 ARO9 UTP9 SKN7 VHR1 SDS3 SLM1 POG1 RRT14 RPL40A STS1 YAP5 PRE3 RPC17 DLS1 PSF2 RPE1 ALB1 GCD14 RPB4 TPK1 RPS22A RPS14B POL31 ESS1	368	1976

Ontology	p- value	Genes in ontology category	k	f
		LSM8 BNA1 ISY1 RPA12 RFC2 EAF6 NNF1 RSF2 SFT1 MRT4 PRP40 PUT3 SPT23 MAK11 IXR1 PRI2 MSN4 YJU2 HAP4 ABF1 SRP21 ELF1 ZRT3 MTR2 SDS22 MRPL13 PRY2 KAE1 UTP30 LAS1 SOF1 COX19 GRC3 UBI4 NOC3 CMS1 SDO1 RPL15A YLR040C TRX1 FCF2 IES3 XDJ1 SEN2 REX3 AHP1 DIP2 RRN5 RMP1 SMD3 YKE2 PNP1 CLB4 TUB4 BUR2 MAP1 NDL1 GSY2 SMD2 TMA10 STP3 CAR2 GLO1 YAP1 PPZ1 RRN11 SML1 PRE8 ARG81 CTK3 TAF8 MIC17 TAF4 ADI1 ERG5 SOK2 STB4 MAC1 MSN2 ARG80 MCM1 BUB2 SEN15 UBX4 MOT3 RCO1 SEC14 MED11 OSW5 CEP3 RGM1 RNT1 YMR244C-A SAP30 FCP1 GLC8 PRE5 RLP7 HRB1 HHT2 NCE103 IMP4 TPM1 YAF9 NOP15 DBP2 RPC19 NAF1 SPC98 FPR1 AAH1 ALF1 IGO1 SSU72 ELA1 CSL4 NRD1 RTC4 GIS2 ORC5 DBP6 TRM112 NOG2 PFA4 RPB11 TOP1 RCL1 GAS5 PRE6 GPD2 BRX1 RFC4 INO4 PFK27 RRP40 NOP8 PSF3 GRE2 YOR052C SGT1 BUD21 RGS2 PFY1 GSP2 RPB10 PUS7 CLP1 CDC31 MBF1 HSH49 TYE7 PDE2 TFC8 DIG1 LGE1 GCR1 RLM1 IDI1 NOP53 PRM4 MEX67 RSA1 PUS1 HFI1 TIF6 CCL1 THP3 NHP6A FCY1 ROX1 SNT309 YTH1 RRP15 PIN3 TDA6 JIP5		
cell wall [710]	9.95E-08	TIP1 FIG2 SED1 SCW11 AGA2 CRH1 SCW4 BGL2 DSE2 HSP150 CWP1 CWP2 PIR3 CTS1 CCW14 SCW10 YNL260C TOS6 KRE1 TIR2 SVS1	21	43
nucleolus [750.05]	9.63E-06	RRN6 YBR141C MAK5 POP7 RRP7 SOK1 RRP8 RPA14 HMO1 BFR2 UTP6 PUF6 SNU13 LCP5 SPB4 LOC1 POP6 SLX9 RRP46 UTP8 RRP3 SSF1 NOP10 UTP9 RRT14 RPS22A RPS14B URB2 RPA12 MRT4 MAK11 UTP30 SOF1 NOC3 FCF2 RRN5 RMP1 RRN11 RNT1 NOP15 RPC19 CSL4 DBP6 TOP1 RCL1 BRX1 RRP40 NOP8 BUD21 RPB10 NOP53 TIF6 RRP15 JIP5	54	208
vacuole [770]	2.19E-05	GEM1 GRX7 BAP2 APE3 PER1 NPC2 VCX1 RCR2 CPR5 HXT3 VAC8 PMP2 VMA3 PRB1 SIT1 PIC2 SPI1 STE2 AGA2 ERV14 VPS45 SCW4 BGL2 COS6 VMA16 VMA10 PRM5 PRY1 SNA3 RAM2 ZRT3 PRY2 UTH1 FRE6 CTS1 EXG1 IMH1 VAC14 VAN1 SCW10 AQR1 BXI1 COS1 VPS27 PLB3 DDR2 ZPS1 SRL1 KTR6 ATG5 PEP4 SVS1 FLC1 VMA13 ERV2 KRE6	56	224
mitochondrial matrix [755.07]	3.71E-05	GCV3 MRPL16 PRX1 MRPL36 MRPS5 MRPL37 RIM1 IMG2 DLD2 MRPL28 GRX2 RSM18 NFU1 ISA1 ARG7 ABF2 MRPS8 MRPL50 LSC1 GRX5 MRP51 ISU1 YAH1 FUM1	24	71
mitochondrial inner membrane [755.05]	0.000159	COR1 TCM62 ATP16 COX9 DLD1 INH1 GGC1 SDH4 FMN1 ATP5 ATP22 QCR7 RIP1 SOM1 COX15 QCR6 COX13 QCR9 PET54 YIA6 QCR8 ATP7 OAC1 SDH3 PAM17 CCP1 SDH2 COQ9 ATP14 COX8 COX7 COX5A COQ2 COQ10 ODC2 TIM18 ATP15 AIM45 ATP20	39	150

Ontology	p- value	Genes in ontology category	k	f
extracellular [701]	0.000321	TIP1 FIG2 MFA1 AGA2 CRH1 BGL2 DSE2 HSP150 CWP1 CWP2 PIR3 CTS1 EXG1 MFA2 YGP1 KRE1 GAS5 TIR2	18	53
cytoplasm [725]	0.001367	SYN8 CCR4 OAF1 FLC2 ECM15 RRN6 FUS3 HAP3 LSM2 PRE7 TOD6 PRX1 PRS4 AAR2 YBL107C UGA2 HMT1 SEC18 UBC4 RPL19A VID24 CMD1 YSA1 PTC4 SHE3 ARA1 UMP1 SWD3 RPL21A NGR1 GPX2 RIB5 REI1 STP22 GRX1 SRO9 GLK1 KAR4 RVS161 PMP1 RPS14A CTR86 PTC1 NPC2 STP4 PBP4 RPS29B YDL063C PEX19 BDF2 RPL31A RPP1A SRP14 BUG1 SNA4 HNT1 RPP1B RPL41B RPC53 SAS10 UGA3 AIR2 DLD2 HEM3 WHI4 PHO13 RCR2 KCS1 SES1 LYS14 ARO3 NRG1 CDC34 UBC5 RPS13 IPT1 TPS2 PDC2 GRX3 MTQ2 GIR2 ENT5 NBP2 SLY1 RVB1 GCD6 RTN1 FMN1 VHS1 INM2 SSD1 CPR5 SRB7 GIC2 CDC40 LSM6 RPP2B PPM1 APT2 MFA1 RMT2 RPL27B VPS60 RIB3 RPL37B GRX2 AGE1 HSP31 IRC22 GIM4 GCN4 UTR4 GLY1 YEL047C SOM1 PRB1 NPR2 HPA3 FMP52 NTF2 RPN3 MIG3 EDC2 PHM8 HOM3 RPL34A HOR2 PTC2 RAD51 LSM4 NSA2 RPS26B SPI1 BUR6 CCA1 TMT1 WWM1 HSP12 CAF16 RPL22B FMP32 SAD1 GCN20 RPL29 QCR6 BNA6 PRE4 HXK1 LEU1 SCL1 PNC1 TIF4632 SDS23 AFT1 MMS2 RPL28 GPG1 CWC23 ARI1 SUT1 MPT5 TOS3 RPS26A KEX1 MIG2 SKI8 FRA2 NIF3 COG1 TAN1 CUL3 RPS25A POP6 SCM4 PEF1 PAC10 TWF1 RRP46 ASK10 MDR1 VOA1 COG2 LSB1 RTS3 CRH1 YPP1 YCH1 PUP2 RTT102 CAB4 PRS3 OCA5 OSH7 STP2 ARG4 RPS27B VMA16 SLT2 FSH1 MED6 VMA22 RRP3 NMD2 RTC3 DMA1 COX23 FUR1 ARO9 RPL42B DSE2 YHR192W EGD2 SCH9 NAS2 YKE4 CAP2 APQ12 VHR1 FMC1 SLM1 HIS5 TPM2 RPL40A DJP1 STS1 YAP5 YVH1 HYR1 BET4 PRY3 NCA3 RPE1 GCD14 RPS21B RPB4 SNA3 HSP150 TPK1 RPL17B RPL39 RPS22A RPS14B SUI2 TMA22 ESS1 LSM8 BNA1 ISY1 EAF6 STE18 RPL43B CPA2 NNF1 TTI2 SFT1 ARC19 PUT3 SWD2 RAM2 SPT23 PAN3 TUL1 SFK1 TMA19 MSN4 CWP1 CWP2 HAP4 SRP21 MRP8 RPS27A KDX1 RPL17A MTR2 SDS22 EAP1 KAE1 PET10 DRE2 SRL3 PSR1 COX19 TPO1 UBI4 SDO1 RPL15A TRX1 FCF2 YLR063W SPC3 RFU1 REX3 AHP1 CCW12 YPS1 DIP2 RKM5 YLR143W RMP1 SMD3 RPL37A YKE2 COQ9 TUB4 YLR243W MAP1 NDL1 GSY2 RPS28B SMD2 RPS30A IMH1 CDC25 RPL38 TMA10 RPL26A ATG33 NMD4 REH1 RPS29A PUN1 CAR2 GLO1 YAP1 PPZ1 CMP2 SML1 GIM5 ARG81 TSL1 CUE4 CTK3 VAN1 MIC17 ADI1 ERG5 MAC1 MSN2 UBX4 RCO1 VPS20 SEC14 SNO1 SNZ1 MED11 JLP2 RPS16A RGM1 RPL36A RPS10B RPL20A YMR244C-A GFD1 SCS7 NGL2 SCW10 GLC8 PRE5 SIW14 NCE103 YIP3 MSG5 RPL16B IMP4 TPM1 SWS2 OCA1 LEU4 YAF9 DBP2 NCS2 SPC98 FPR1 AAH1	464	2879

Ontology	p- value	Genes in ontology category	k	f
		ALF1 IGO1 YGP1 BNI5 WHI3 SSU72 ELA1 PDR16 CSL4 RTC4 GIS2 WSC2 CAF40 CLA4 BXI1 KRE1 TRM112 COQ10 PRE6 RPP2A DDR2 GPM3 GPD2 YOL092W INO4 ZEO1 MDY2 PFK27 PEX11 GRE2 ZPS1 HPF1 IRC23 YOR052C SGT1 GYP1 RGS2 RIO1 PFY1 PNO1 GET4 RPS28A LCB4 DCI1 RPS30B GSP2 GEP3 RCN2 SRL1 TUM1 NAT5 CDC31 RBL2 PLP2 RDL1 MBF1 FAA1 HSH49 TYE7 SNX3 VTS1 PDE2 LSP1 SKS1 MUK1 GCR1 RPS9A RLM1 IDI1 RPL5 RPL33A SVS1 RTT10 RSA1 OXR1 FLC1 YAR1 FUM1 TIF6 VMA13 RPL43A FCY1 UBA3 NOT5 YTH1 NAT3 NCE102 PIN3 KRE6 MLC2		
mitochondria [755]	0.001707	GCV3 FLC2 ERP1 FUS3 MRPL16 COR1 PRX1 GPI18 GRX7 HMT1 TCM62 YRO2 YSA1 MRPL36 EXO5 OM14 MRPS5 AIM5 MRPL37 ILV6 MGR1 RIM1 IMG2 TRX3 ATP16 TSC13 STP4 COX9 DLD1 DLD2 INH1 GGC1 GCV1 ARO3 TPS2 PET100 GIS1 SDH4 MFB1 RTN1 ATP5 MRPL28 GRX2 QCR7 TIM9 RIP1 YEL047C SOM1 FMP52 ISD11 RSM18 PIC2 COX15 CCA1 PDA1 WWM1 GYP8 FMP32 QCR6 SCL1 FMP37 RMD9 COX13 NIF3 MTC3 CUL3 MSP1 ERV1 TAM41 SCM4 TIM13 QCR9 CIR1 PET54 YGR235C SPG1 COQ6 CAB4 AIM17 YHR003C TIM10 MSR1 YHR162W AIM18 BAT1 MMF1 AIM19 FMC1 SLM1 PRM5 COA1 YIR024C COA3 KHA1 PAM16 QCR8 TES1 TIM8 ATP7 NFU1 OAC1 MRPL31 SDH3 MRP8 MCR1 MRP49 ACP1 MRPL13 LAS1 PAM17 CCP1 COX19 ISA1 SDH2 XDJ1 SEN2 YPS3 COQ9 QRI5 PNP1 ATP14 ATG33 ECM19 COX8 SUR7 CPR3 SEN15 ARG7 ABF2 NDE1 MRPS8 COX7 MRPL33 SAM50 COX5A SWS2 LEU4 DBP2 TOM22 YNL260C MRPL50 MRPS12 COQ2 NGL1 GPD2 ZEO1 GYP1 LSC1 PNS1 GEP3 AIM41 MCT1 ODC2 ISU2 TUM1 RDL1 RDL2 TIM18 MBF1 RRG7 FAA1 ALD4 LSP1 GRX5 MUK1 MRP51 ISU1 PEP4 PET20 MRPL40 RTC6 POS5 PGC1 YAH1 FUM1 ATP15 AIM45 ATP20 CCL1 ERV2 TOM5 NCE102 RHO1 DPM1	184	1042
ER membrane [735.01]	0.003678	PRE7 ALG1 UMP1 RER1 RPN5 SHR3 SSS1 SUR2 STE14 RPN9 FPR2 RPN3 YOS1 SCS2 PRE4 RPN12 SCL1 PUP2 VMA22 SEC11 PRE3 SRP102 SEC72 PRE8 ERG5 PRE5 PRE6 OST2 GPI2 SEC62 DPM1	31	131
MIPS Protein Complexes (1142 categories)				
cytoplasmic ribosomal large subunit [500.40.10]	4.44E-07	RPL19A RPL21A RPL31A RPP1A RPP1B RPL41B RPP2B RPL27B RPL37B RPL34A RPL22B RPL29 RPL28 RPL42B RPL40A RPL17B RPL39 RPL43B RPL17A RPL15A RPL37A RPL38 RPL26A RPL36A RPL20A RPL16B RPP2A RPL5 RPL33A RPL43A	30	81
20S proteasome [360.10.10]	6.39E-05	PRE7 UMP1 PRE4 SCL1 PUP2 PRE3 PRE8 PRE5 PRE6	9	15
cytoplasmic ribosomal small subunit [500.40.20]	0.00029	RPS14A RPS29B RPS13 RPS26B RPS26A RPS25A RPS27B RPS21B RPS22A RPS14B RPS27A RPS28B RPS30A RPS29A RPS16A RPS10B	19	57

Ontology	p- value	Genes in ontology category	k	f
		RPS28A RPS30B RPS9A		
Complex Number 60, 20S Proteosome (13) [550.3.60]	0.001066	PRE7 SCL1 PUP2 PRE3 PRE8 PRE5 PRE6	7	13
Cytochrome bc1 complex (Ubiquinol-cytochrome c reductase complex, complex III) [420.30]	0.001189	COR1 QCR7 RIP1 QCR6 QCR9 QCR8	6	10
Gim complexes [177]	0.002005	GIM4 PAC10 YKE2 GIM5	4	5
Nucleosomal protein complex [320]	0.002515	HTB2 HHF1 HHT1 HTB1 HHT2	5	8
Complex Number 238 [550.2.238]	0.003061	PRE7 SCL1 PUP2 PRE3 PRE8 PRE5 PRE6	7	15

Table 18. Ontologies enriched among the 354 genes downregulated in *Δfpr3Δfpr4Δtrf5* triple mutant yeast

Ontology	p- value	Genes in ontology category	k	f
GO Molecular Function (1646 categories)				
ATP binding [GO:0005524]	<1e-14	SSA1 CDC19 URA7 ILS1 YPK3 AKL1 GRS1 VMA2 PYC2 HIS4 PGK1 SUB2 GET3 CDC9 VMA1 SSB1 SNQ2 MSH6 YCF1 ADK1 SAM2 EMI2 SPF1 AFG3 HIS1 FRS2 INO80 PMR1 MCM6 GUS1 HXK2 ADE6 VAS1 ASN2 ADE3 PFK1 MES1 MYO1 SSZ1 THS1 SSL2 SLN1 CYR1 CCT3 KAR2 BCK1 CCT7 YAK1 SSC1 TAH11 PTK2 URA8 URA6 LHS1 TOR2 UBA1 DPS1 SSA2 ACS2 SAM1 MDL1 RCK2 YEF3 HSP60 VIP1 YTA12 HSC82 PFK2 YDJ1 SSB2 ACC1 WRS1 GLN4 MYO2 ALA1 SSE1 CDC60 HSP82 HTS1 ASN1	80	622
nucleotide binding [GO:0000166]	2.77E-13	SSA1 FUN12 CDC19 PEP1 URA7 ILS1 YPK3 AKL1 GRS1 PYC2 HIS4 PGK1 PSA1 SUB2 GET3 CDC9 VMA1 SHS1 SSB1 SNQ2 MSH6 YCF1 ADK1 SAM2 EMI2 SPF1 AFG3 HIS1 FRS2 INO80 PMR1 MCM6 GUS1 HXK2 ADE6 VAS1 ASN2 ADE3 PFK1 MES1 MYO1 SSZ1 THS1 SSL2 SLN1 CYR1 CCT3 KAR2 BCK1 CCT7 YAK1 SSC1 PTK2 URA8 URA6 LHS1 TOR2 UBA1 VPS1 DPS1 SSA2 ACS2 SAM1 MDL1 RCK2 YEF3 HSP60 VIP1 TUB1 YTA12 HSC82 PFK2 POL1 SSB2 ADE12 ACC1 WRS1 EFT1 SEY1 GLN4 MYO2 ALA1 SSE1 CDC60 HSP82 HTS1 ASN1 TIF3	88	778
ligase activity [GO:0016874]	3.90E-10	URA7 ILS1 LYS2 GRS1 PYC2 CDC9 UFD2 FRS2 GUS1 ADE6 VAS1 ASN2 ADE3 MES1 THS1 URA8 UBA1 DPS1 ACS2 ADE12 ACC1 WRS1 GLN4 ALA1 CDC60 HTS1 ASN1	27	130
aminoacyl-tRNA ligase activity [GO:0004812]	8.04E-08	ILS1 GRS1 FRS2 GUS1 VAS1 MES1 THS1 DPS1 WRS1 GLN4 ALA1 CDC60 HTS1	13	41
binding [GO:0005488]	2.40E-07	LYS2 SEC7 SEC26 MSN5 SXM1 KAP123 SPT15 BLM10 PUF4 KAP122 CHC1 PPT1 ADE3 SDA1 ECM29 RPN1 GND1 AYR1 TDH2	38	300

Ontology	p- value	Genes in ontology category	k	f
		HOM6 MAE1 TOR2 UBA1 HRD3 YEF3 CLU1 PDS5 ADH3 RRP5 SRV2 BNI1 SEC21 EMW1 LYS9 STI1 GDH1 RRP12 FAS2		
transferase activity [GO:0016740]	7.68E-07	PMT2 CDC19 SCT1 YPK3 AKL1 PGK1 NOP1 PSA1 PMT5 PMT1 TRM3 LYS20 LCB2 ADK1 SAM2 EMI2 RML2 HIS1 MET6 STT3 HXK2 CHO2 PFK1 BIO2 LAG1 DYS1 SLN1 ARG3 BCK1 YAK1 ERG20 SET2 MNN5 PTK2 PMT4 BAT2 URA6 UGP1 MCD4 FAS1 TOR2 PDC1 SAM1 RCK2 VIP1 ERG6 ERG13 ADE17 PFK2 POL1 RIB4 LEU9 RPO31 RPB2 ALE1 RPA190 REV1 ERG10 FAS2 TKL1	60	611
catalytic activity [GO:0003824]	1.56E-06	CDC19 FAT1 LYS2 PYC2 HIS4 LYS20 LCB2 PHO8 SPF1 DLD3 SEC53 CWH41 PMR1 HXK2 ADE6 CYS4 ADE3 PFK1 BIO2 GND1 AYR1 CYR1 TDH2 HOM6 BAT2 MAE1 FBA1 MCD4 FAS1 UBA1 URA1 PDC1 ACS2 BNA5 ADE13 IMD4 ALO1 ERG13 ADH3 ADE17 PFK2 ACC1 LYS9 LEU9 GDH1 ERG10 FAS2 TKL1	48	455
ATPase activity [GO:0016887]	4.33E-06	SSA1 GET3 SSB1 SNQ2 MSH6 YCF1 SPF1 AFG3 INO80 KAR2 SSC1 LHS1 SSA2 MDL1 YEF3 HSP60 YTA12 HSC82 SSB2	19	112
unfolded protein binding [GO:0051082]	7.38E-06	SSA1 SSB1 SSZ1 CCT3 KAR2 CCT7 PHO86 SSC1 LHS1 SSA2 HSP60 HSC82 YDJ1 SSB2 SEC63 HSP82	16	86
ligase activity, forming aminoacyl-tRNA and related compounds [GO:0016876]	0.000101	GUS1 THS1 GLN4 ALA1	4	6
metal ion binding [GO:0046872]	0.000156	CDC19 PYC2 LEU2 HIS4 GET3 CDC9 HO RSC3 PHO8 SAM2 SPF1 AFG3 MET6 GRX4 RSC8 PPT1 YHB1 PFK1 BIO2 ERG11 AAP1 ENO2 SLN1 DAL81 CYR1 FAR1 ERG20 VPS70 MAE1 UGP1 RGT1 MPE1 FBA1 PXL1 PDC1 RPS31 SAM1 FRE1 ACO1 IMD4 TCB3 ADH3 YTA12 YDJ1 ADE12 ACC1 ADH1 TCB1 RPO31 RPB2 ALA1 RPA190 REV1 ERG10 TKL1	55	647
dolichyl-phosphate-mannose-protein mannosyltransferase activity [GO:0004169]	0.000226	PMT2 PMT5 PMT1 PMT4	4	7
calmodulin binding [GO:0005516]	0.000344	SSB1 CLC1 RCK2 MYO2 SSE1	5	13
acid phosphatase activity [GO:0003993]	0.000748	PHO11 PHO5 PHO12 VIP1	4	9
rRNA binding [GO:0019843]	0.000757	RPS11A RPL2A RPL9A RPS4B RPS4A YEF3 RPL9B EFT1	8	39
oxidoreductase activity [GO:0016491]	0.000904	RFS1 LYS2 LEU2 HIS4 DLD3 ADE3 YHB1 ERG11 TRR2 GND1 AYR1 TDH2 HOM6 MAE1 FAS1 URA1 ERG3 FRE1 IMD4 ALO1 ERO1 ADH3 LYS9 ADH1 GDH1 ALD6 FAS2	27	272
magnesium ion binding [GO:0000287]	0.001131	CDC19 LEU2 HIS1 ENO2 CYR1 PDC1 ADE12 REV1 FAS2	9	51
structural molecule activity [GO:0005198]	0.001425	COP1 SEC26 NUP157 SEC27 CHC1 CLC1 NSP1 TUB1 PDS5 SEC21	10	63
lipid binding [GO:0008289]	0.001479	SWH1 IST2 OSH2 TCB3 TCB2 TCB1	6	25

Ontology	p- value	Genes in ontology category	k	f
CTP synthase activity [GO:0003883]	0.002722	URA7 URA8	2	2
myo-inositol transmembrane transporter activity [GO:0005365]	0.002722	ITR1 ITR2	2	2
fatty-acyl-CoA synthase activity [GO:0004321]	0.002722	FAS1 FAS2	2	2
G-protein alpha-subunit binding [GO:0001965]	0.002722	SCP160 ASC1	2	2
6-phosphofructokinase activity [GO:0003872]	0.002722	PFK1 PFK2	2	2
methionine adenosyltransferase activity [GO:0004478]	0.002722	SAM2 SAM1	2	2
calcium-dependent phospholipid binding [GO:0005544]	0.002722	TCB3 TCB1	2	2
actin binding [GO:0003779]	0.003611	SLA1 MYO1 PAN1 SRV2 SLA2 BNI1 MYO2	7	39
lyase activity [GO:0016829]	0.00767	FDC1 ARO2 CYS4 ENO2 CYR1 FBA1 FAS1 PDC1 ACO1 ADE13	10	79
fatty acid synthase activity [GO:0004312]	0.007884	FAS1 FAS2	2	3
asparagine synthase (glutamine-hydrolyzing) activity [GO:0004066]	0.007884	ASN2 ASN1	2	3
cyclin-dependent protein kinase inhibitor activity [GO:0004861]	0.007884	PHO81 FAR1	2	3
phosphotransferase activity, phosphate group as acceptor [GO:0016776]	0.007884	ADK1 URA6	2	3
nucleobase, nucleoside, nucleotide kinase activity [GO:0019205]	0.007884	ADK1 URA6	2	3
nucleotide kinase activity [GO:0019201]	0.007884	ADK1 URA6	2	3
phosphatidylinositol-4-phosphate phosphatase activity [GO:0043812]	0.007884	SAC1 INP53	2	3
ATPase activity, coupled [GO:0042623]	0.007884	HSC82 HSP82	2	3
protein kinase inhibitor activity [GO:0004860]	0.007884	SPL2 FAR1	2	3
translation elongation factor activity [GO:0003746]	0.008078	ANB1 TEF4 YEF3 EFT1	4	16
GO Biological Process (2062 categories)				
translation [GO:0006412]	1.53E-09	SSA1 FUN12 ILS1 RPG1 GRS1 RPS6B SSB1 RPS11A RML2 FRS2 RPL2A RPS2 RPL9A GUS1 VAS1 RPS23A RPS0A MES1 RPL8A SSZ1 RPS4B THS1 ANB1 RPS4A TEF4 DPS1 RPS31 YEF3 RPP0 RPS22B RPL9B SSB2 RPL18B WRS1 RPS19A RPS7A EFT1 GLN4 ALA1 TAE2 RPS6A CDC60 HTS1 TIF3	44	318
metabolic process [GO:0008152]	7.78E-08	CDC19 SCT1 FAT1 LYS2 PYC2 HIS4 LYS20 LCB2 PHO8 SPF1 SEC53 CWH41 PMR1 HXK2 CYS4 ADE3 PFK1 BIO2 GND1 AYR1 TDH2	49	425

Ontology	p- value	Genes in ontology category	k	f
		HOM6 BAT2 MAE1 UGP1 FBA1 MCD4 FAS1 UBA1 URA1 PDC1 ACS2 BNA5 ACO1 ERG6 IMD4 ERG13 PLB2 ADH3 ADE17 PFK2 ACC1 LYS9 LEU9 GDH1 ERG10 ALD6 FAS2 TKL1		
tRNA aminoacylation for protein translation [GO:0006418]	9.61E-08	ILS1 GRS1 FRS2 GUS1 VAS1 MES1 THS1 DPS1 WRS1 GLN4 CDC60 HTS1	12	35
glycolysis [GO:0006096]	7.51E-07	CDC19 PGI1 PGK1 EMI2 HXK2 PFK1 ENO2 TDH2 FBA1 PFK2	10	28
protein refolding [GO:0042026]	7.60E-06	SSA1 SSC1 HSP60 HSC82 YDJ1 SSE1 HSP82	7	16
polyphosphate metabolic process [GO:0006797]	1.86E-05	VTC1 VTC2 VTC4 PHO84 VTC3	5	8
tRNA aminoacylation [GO:0043039]	1.86E-05	FRS2 GUS1 THS1 GLN4 ALA1	5	8
cellular amino acid biosynthetic process [GO:0008652]	4.07E-05	LYS2 LEU2 HIS4 LYS20 HIS1 MET6 ARO2 ASN2 CYS4 ADE3 ARG3 HOM6 BAT2 LYS9 LEU9 ASN1	16	98
actin cytoskeleton organization [GO:0030036]	4.28E-05	AKL1 GEA2 BEM2 GRX4 SDA1 BBC1 VPS1 APP1 BNI1	9	34
vacuolar transport [GO:0007034]	9.98E-05	PEP1 VTC1 VTC2 VTC4 VPS1 VTC3	6	16
'de novo' protein folding [GO:0006458]	0.000101	HSP60 HSC82 YDJ1 HSP82	4	6
protein folding [GO:0006457]	0.000119	SSA1 CCT3 CCT7 PHO86 SSC1 SSA2 HSP60 FPR4 ERO1 HSC82 YDJ1 STI1 SEC63 SSE1 HSP82	15	96
gluconeogenesis [GO:0006094]	0.000212	PGI1 PYC2 PGK1 ENO2 TDH2 FBA1	6	18
purine nucleotide biosynthetic process [GO:0006164]	0.000212	ADE6 ADE3 ADE13 IMD4 ADE17 ADE12	6	18
oxidation-reduction process [GO:0055114]	0.000904	RFS1 LYS2 LEU2 HIS4 DLD3 ADE3 YHB1 ERG11 TRR2 GND1 AYR1 TDH2 HOM6 MAE1 FAS1 URA1 ERG3 FRE1 IMD4 ALO1 ERO1 ADH3 LYS9 ADH1 GDH1 ALD6 FAS2	27	272
ergosterol biosynthetic process [GO:0006696]	0.000921	ERG11 ERG20 ERG3 ERG6 ERG13 ERG10	6	23
microautophagy [GO:0016237]	0.001196	VTC1 VTC2 VTC4 VTC3	4	10
regulation of translational fidelity [GO:0006450]	0.001196	SSB1 RPS23A SSZ1 SSB2	4	10
phosphate transport [GO:0006817]	0.001196	PHO88 PHO89 PHO86 PHO84	4	10
lipid biosynthetic process [GO:0008610]	0.001306	LAG1 ERG11 ERG20 FAS1 ERG3 ERG6 ERG13 ACC1 FAS2	9	52
pyrimidine nucleotide biosynthetic process [GO:0006221]	0.001803	URA7 URA8 URA6 URA1	4	11
response to stress [GO:0006950]	0.002318	SSA1 UFD2 SSB1 TIR1 ARO2 YHB1 KAR2 SSC1 SSA2 HSP60 HSC82 YDJ1 SSB2 STI1 SEY1 SSE1 HSP82	17	152
protein import into mitochondrial intermembrane space [GO:0045041]	0.002513	AFG3 HSP60 YTA12	3	6
phospholipid biosynthetic process [GO:0008654]	0.002644	SCT1 URA7 INO2 CHO2 URA8 PAH1 ALE1	7	37

Ontology	p- value	Genes in ontology category	k	f
myo-inositol transport [GO:0015798]	0.002722	ITR1 ITR2	2	2
protein splicing [GO:0030908]	0.002722	VMA1 HO	2	2
intein-mediated protein splicing [GO:0016539]	0.002722	VMA1 HO	2	2
negative regulation of Rho protein signal transduction [GO:0035024]	0.002722	BEM2 BEM3	2	2
ER-associated misfolded protein catabolic process [GO:0071712]	0.002722	PMT2 PMT1	2	2
branched chain family amino acid biosynthetic process [GO:0009082]	0.003594	LEU2 HOM6 BAT2 LEU9	4	13
glutamine metabolic process [GO:0006541]	0.003844	URA7 ADE6 ASN2 URA8 ASN1	5	21
translational elongation [GO:0006414]	0.004765	ANB1 TEF4 YEF3 RPP0 EFT1	5	22
establishment of cell polarity [GO:0030010]	0.004826	SHS1 BOI2 BEM2 BCK1 SPA2 MSB1 BEM3	7	41
pentose-phosphate shunt [GO:0006098]	0.004827	PGI1 GND1 RKI1 TKL1	4	14
cellular protein metabolic process [GO:0044267]	0.004827	VMA1 CCT3 CCT7 HSP60	4	14
methionine metabolic process [GO:0006555]	0.004827	SAM2 SAH1 HOM6 SAM1	4	14
nucleobase, nucleoside, nucleotide and nucleic acid metabolic process [GO:0006139]	0.005833	ADK1 SPT6 URA6 POL1 RAT1	5	23
proteasome assembly [GO:0043248]	0.006315	BLM10 ECM29 HSC82 HSP82	4	15
one-carbon metabolic process [GO:0006730]	0.006315	SAM2 SAH1 ADE3 SAM1	4	15
lysine biosynthetic process [GO:0009085]	0.006505	LYS2 LYS20 LYS9	3	8
lysine biosynthetic process via aminoadipic acid [GO:0019878]	0.006505	LYS2 LYS20 LYS9	3	8
phosphate metabolic process [GO:0006796]	0.006505	PHO11 PHO5 PHO81	3	8
pyruvate metabolic process [GO:0006090]	0.006505	CDC19 MAE1 PDC1	3	8
nucleotide phosphorylation [GO:0046939]	0.007884	ADK1 URA6	2	3
pyrimidine base biosynthetic process [GO:0019856]	0.007884	URA7 URA8	2	3
S-adenosylmethionine biosynthetic process [GO:0006556]	0.007884	SAM2 SAM1	2	3
CTP biosynthetic process [GO:0006241]	0.007884	URA7 URA8	2	3
asparagine biosynthetic process [GO:0006529]	0.007884	ASN2 ASN1	2	3
protein O-linked glycosylation [GO:0006493]	0.008078	PMT2 PMT5 PMT1 PMT4	4	16

Ontology	p- value	Genes in ontology category	k	f
steroid biosynthetic process [GO:0006694]	0.008454	ERG11 ERG20 ERG3 ERG6 ERG13	5	25
posttranslational protein targeting to membrane, translocation [GO:0031204]	0.009383	KAR2 LHS1 SEC63	3	9
maintenance of cell polarity [GO:0030011]	0.009383	SWH1 OSH2 PXL1	3	9
'de novo' IMP biosynthetic process [GO:0006189]	0.009383	ADE6 ADE13 ADE17	3	9
endocytosis [GO:0006897]	0.009922	SWH1 SLA1 EDE1 OSH2 CHC1 CLC1 PAN1 VPS1 SLA2 INP53	10	82
GO Cellular Component (625 categories)				
cytoplasm [GO:0005737]	<1e-14	SSA1 AIM2 SWH1 SLA1 EDE1 ILS1 YPK3 RFS1 AKL1 RPG1 LYS2 GRS1 VMA2 RPS6B PGI1 PYC2 LEU2 PGK1 PSA1 GET3 TRM3 COP1 LYS20 UFD2 SSB1 RPS11A LCB2 SEC7 ADK1 SEC26 ASP1 MSN5 SVF1 SXM1 PHO8 EMI2 FDC1 GEA2 DLD3 SAH1 HIS1 MET6 KAP123 BOI2 BEM2 BLM10 FRS2 SEC53 LSB3 RPL2A PUF4 KAP122 RPS2 SEC27 RPL9A ARO2 MCM6 GUS1 ADE6 VAS1 RPS23A PPT1 ASN2 CYS4 ADE3 RPS0A PHO81 YHB1 PFK1 MES1 ECM29 RPL8A RPN1 AAP1 SSZ1 DYS1 SFB3 TRR2 SPL2 KEL1 ENO2 GND1 RPS4B THS1 AYR1 UBP7 PAN1 CCT3 BBC1 MHP1 ARG3 BCK1 CCT7 LSM1 YAK1 FAR1 ERG20 UBP12 TDH2 TAH11 ANB1 PTK2 URA8 HOM6 RPS4A HMS2 BAT2 URA6 UGP1 RGT1 FBA1 TEF4 FAS1 DPH2 UBA1 URA1 VPS1 PXL1 DPS1 SSA2 PDC1 ARP6 ACS2 RPS31 SAM1 TOS4 BNA5 RCK2 YEF3 HSP60 ACO1 RPP0 NIT3 RPS22B IKI3 VIP1 PSP2 IMD4 TUB1 CLU1 EIS1 MIH1 YTA12 ASC1 PAH1 HSC82 PFK2 YDJ1 RPL9B MKT1 APP1 SRV2 SSB2 VID27 ADE12 SLA2 BNI1 SEC21 RPL18B EMW1 ACC1 LYS9 MDM20 ADH1 WRS1 RPS19A RIB4 STI1 RKI1 RPS7A INP53 EFT1 SEY1 GLN4 ALA1 GDH1 TAE2 RRP12 ERG10 ALD6 RPS6A SSE1 BEM3 CDC60 FAS2 HSP82 HTS1 TKL1 ASN1	189	2026
plasma membrane enriched fraction [GO:0001950]	1.59E-06	SSA1 CDC19 ECM33 PGI1 PGK1 SSB1 MET6 ENO2 TDH2 UGP1 SSA2 ADE17 HSC82 SSB2 BNI1 ADH1 TCB1	17	86
cytosol [GO:0005829]	1.97E-06	CDC19 URA7 ILS1 PGI1 PYC2 SEC7 ADK1 ASP1 GEA2 SEC53 HXK2 YHB1 ARG3 URA8 FBA1 FAS1 SSA2 PDC1 ACS2 ACO1 ADE17 YDJ1 ADH1 GLN4 ERG10 ALD6 FAS2	27	192
cytosolic small ribosomal subunit [GO:0022627]	2.56E-06	FUN12 RPS6B RPS11A RPS2 RPS23A RPS0A RPS4B RPS4A RPS31 RPS22B ASC1 RPS19A RPS7A RPS6A	14	62
vacuolar transporter chaperone complex [GO:0033254]	7.33E-06	VTC1 VTC2 VTC4 VTC3	4	4
endoplasmic reticulum [GO:0005783]	2.23E-05	PMT2 ERV46 SWH1 SCT1 FAT1 OSH2 PMT5 PMT1 GET3 LCB2 VTC1 VTC2 CWH41 GUP1 LAG1 ERG11 RPN1 SFB3 GPI16 AYR1 VTC4 KAR2 SCP160 PHO86 ERG20 GEF1 PMT4 LHS1 MCD4 SAC1	42	416

Ontology	p- value	Genes in ontology category	k	f
		ERG3 HRD3 ERG6 ERG13 ERO1 MID1 ACC1 SEY1 ALE1 SEC63 VTC3 SEC16		
mating projection tip [GO:0043332]	2.62E-05	SLA1 EDE1 SHS1 SEC3 BEM2 SFB3 KEL1 PAN1 BCK1 FAR1 PXL1 SPA2 SRV2 SLA2 BNI1 MYO2 BEM3	17	105
polysome [GO:0005844]	4.74E-05	SSA1 SSB1 SSZ1 SCP160 SSA2 MKT1 SSB2 SSE1	8	27
incipient cellular bud site [GO:0000131]	5.90E-05	RPG1 SEC3 BEM2 MYO1 PXL1 SPA2 BNI4 SLA2 BNI1 MYO2 BEM3	11	52
COPI vesicle coat [GO:0030126]	0.000434	COP1 SEC26 SEC27 SEC21	4	8
cellular bud tip [GO:0005934]	0.000453	EDE1 NUM1 SEC3 BEM2 KEL1 PXL1 SPA2 SLA2 BNI1 MSB1 MYO2 BEM3	12	75
cellular bud neck [GO:0005935]	0.000729	EDE1 AKL1 BUD3 OSH2 SHS1 SEC3 BOI2 LSB3 MYO1 KEL1 BUD4 PXL1 SPA2 BNI4 BNI1 MSB1 MYO2	17	137
COPI coated vesicle membrane [GO:0030663]	0.001196	COP1 SEC26 SEC27 SEC21	4	10
90S preribosome [GO:0030686]	0.001456	NOP1 RPS11A RPS0A RPS4B RPS4A NOP56 RPP0 RRP5 RPS7A RRP12 RPS6A	11	74
chaperonin-containing T-complex [GO:0005832]	0.001803	SSA1 CCT3 CCT7 SSA2	4	11
m-AAA complex [GO:0005745]	0.002722	AFG3 YTA12	2	2
dolichyl-phosphate-mannose-protein mannosyltransferase complex [GO:0031502]	0.002722	PMT2 PMT1	2	2
fatty acid synthase complex [GO:0005835]	0.002722	FAS1 FAS2	2	2
clathrin coat of trans-Golgi network vesicle [GO:0030130]	0.002722	CHC1 CLC1	2	2
intrinsic to vacuolar membrane [GO:0031310]	0.002722	VTC1 VTC4	2	2
clathrin coat of coated pit [GO:0030132]	0.002722	CHC1 CLC1	2	2
6-phosphofructokinase complex [GO:0005945]	0.002722	PFK1 PFK2	2	2
plasma membrane [GO:0005886]	0.004728	SLA1 ECM33 IST2 PHO89 OSH2 SNQ2 MKC7 ITR1 FDC1 BEM2 GUP1 AVT7 SLN1 PAN1 CYR1 OPT1 GEF1 PTK2 TOR2 FRE1 TCB3 EFR3 TCB2 SLA2 BNI1 MID1 ITR2 TCB1 DIP5 CTR1	30	350
intracellular [GO:0005622]	0.00485	RPS6B BUD3 HIS4 RPS11A SEC7 ASP1 GEA2 RML2 HIS1 BEM2 RPL2A RPS2 RPL9A RPS23A RPS0A RTT107 RPS4B BCK1 RPS4A RPS31 RPP0 RPS22B MIH1 RRP5 RPL9B RPL18B RPS19A RAT1 RPS7A REV1 RPS6A BEM3	32	381
ribosome [GO:0005840]	0.00585	RPS6B NOP1 RPS11A RML2 RPL2A RPS2 RPL9A RPS23A RPS0A RPL8A RPS4B RPS4A TEF4 RPS31 YEF3 RPP0 RPS22B RPL9B RPL18B RPS19A RPS7A EFT1 ALE1 TAE2 RRP12 RPS6A TIF3	27	310
methionyl glutamyl tRNA synthetase complex [GO:0017102]	0.007884	GUS1 MES1	2	3

Ontology	p- value	Genes in ontology category	k	f
mitochondrial inner boundary membrane [GO:0097002]	0.007884	AFG3 YTA12	2	3
luminal surveillance complex [GO:0034099]	0.007884	KAR2 HRD3	2	3
membrane coat [GO:0030117]	0.008078	COP1 SEC26 SEC27 SEC21	4	16
mitochondrion [GO:0005739]	0.008081	FUN12 ECM33 PHO88 GRS1 PGI1 PGK1 CDC9 LYS20 SNQ2 NUM1 ADK1 CFT1 YSP2 SPF1 RML2 AFG3 BEM2 LSB3 GUS1 HXK2 VAS1 SPT6 CYS4 YHB1 PFK1 BIO2 TRR2 ENO2 GND1 THS1 AYR1 CYR1 TDH2 SSC1 CBF1 MAE1 FBA1 TEF4 FAS1 TOR2 SAC1 SSA2 TOS4 MDL1 HSP60 ACO1 NIT3 ERG6 TCB3 ALO1 EIS1 ADH3 YTA12 HSC82 PFK2 EFR3 YHM2 ZRC1 POL1 ACC1 MDM38 RAT1 TCB1 LEU9 RPB2 GLN4 MSB1 SEC63 ALA1 REV1 ALD6 FAS2 HTS1	73	1072
actin cortical patch [GO:0030479]	0.008976	SLA1 EDE1 PAN1 BBC1 APP1 SRV2 SLA2 INP53	8	57
MIPS Functional Classification (459 categories)				
aminoacyl-tRNA-synthetases [12.10]	4.08E-08	ILS1 GRS1 FRS2 GUS1 VAS1 MES1 THS1 DPS1 WRS1 GLN4 ALA1 CDC60 HTS1	13	39
phosphate metabolism [01.04]	4.68E-05	SSA1 CDC19 PHO11 YPK3 AKL1 PHO5 PPS1 HIS4 PGK1 GET3 SSB1 MSH6 ADK1 PHO8 GDA1 AFG3 VTC2 INO80 HXK2 PPT1 PFK1 PHO12 SLN1 KAR2 BCK1 YAK1 SSC1 PTK2 URA6 UGP1 TOR2 SAC1 MDL1 RCK2 MIH1 YTA12 PFK2 SSB2 INP53 HSP82	40	401
sugar, glucoside, polyol and carboxylate catabolism [01.05.02.07]	6.48E-05	CDC19 PGI1 PGK1 PSA1 SEC53 PFK1 ENO2 TDH2 UGP1 FBA1 ACO1 PFK2 RKI1 TKL1	14	81
protein folding and stabilization [14.01]	8.18E-05	SSA1 CCT3 KAR2 CCT7 SSC1 LHS1 SSA2 HSP60 FPR4 ERO1 HSC82 YDJ1 STI1 SSE1 HSP82	15	93
glycolysis and gluconeogenesis [02.01]	0.000207	CDC19 PGI1 PYC2 PGK1 PFK1 ENO2 TDH2 FBA1 PFK2	9	41
unfolded protein response (e.g. ER quality control) [32.01.07]	0.000802	SSA1 SSB1 SSZ1 CCT3 KAR2 CCT7 LHS1 HSC82 SSB2 STI1 SSE1	11	69
ATP binding [16.19.03]	0.000923	SSA1 PGK1 SUB2 GET3 SSB1 SNQ2 MSH6 AFG3 INO80 MCM6 KAR2 SSC1 URA6 UBA1 SSA2 MDL1 HRD3 VBA1 YTA12 SSB2 HSP82	21	191
C-compound and carbohydrate metabolism [01.05]	0.001291	PMT2 PHO11 PHO5 PYC2 PMT5 PMT1 LYS20 EMI2 DLD3 GUP1 HXK2 DYS1 ENO2 GND1 PHO12 AYR1 PMT4 MAE1 RGT1 PDC1 ALO1 ADH3 ADH1	23	223
phosphate transport [20.01.01.07.07]	0.001803	PHO88 PHO89 PHO86 PHO84	4	11
cytoskeleton/structural proteins [42.04]	0.002137	SHS1 BOI2 MYO1 CCT3 CCT7 FAR1 TOR2 SAC1 TUB1 SRV2 BNI4 MDM20 MSB1 BEM3	14	113
tetracyclic and pentacyclic triterpenes (cholesterin, steroids and hopanoids) metabolism [01.06.06.11]	0.002242	OSH2 ERG11 ERG20 ERG3 ERG6 ERG13 ERG10	7	36

Ontology	p- value	Genes in ontology category	k	f
small GTPase mediated signal transduction [30.01.05.05.01]	0.00287	BOI2 BEM2 RPI1 CYR1 TOR2 SPA2 SRV2 BNI1 BEM3	9	58
purine nucleotide/nucleoside/nucleobase anabolism [01.03.01.03]	0.003325	HIS4 ADE6 ADE3 ADE13 ADE17 ADE12	6	29
protein binding [16.01]	0.003941	SSA1 SLA1 PEP1 SUB2 UFD2 SSB1 NUM1 MSN5 SEC3 PHO81 ECM29 SSZ1 SLN1 PAN1 CCT3 BBC1 KAR2 CCT7 FAR1 LHS1 TOR2 UBA1 PXL1 SPA2 HRD3 HSC82 SRV2 SSB2 BNI4 SLA2 BNI1 STI1 SSE1	33	391
actin cytoskeleton [42.04.03]	0.00404	SLA1 AKL1 BEM2 LSB3 SDA1 PAN1 BBC1 SPA2 VIP1 APP1 SLA2 BNI1	12	96
S-adenosyl-methionine - homocysteine cycle [01.05.13.01]	0.004228	SAM2 SAH1 SAM1	3	7
pentose-phosphate pathway [02.07]	0.005833	PGI1 GND1 FBA1 RKI1 TKL1	5	23
protein targeting, sorting and translocation [14.04]	0.006039	SSA1 PEP1 MSN5 NUP157 KAP123 VTC2 SEC53 PUF4 KAP122 CHC1 LAG1 VPS29 KAR2 NSP1 SSC1 VPS70 LHS1 VPS1 SSA2 ARP6 HSP60 YDJ1 VPS75 ACC1 SEC63	25	281
O-directed glycosylation, deglycosylation [14.07.02.01]	0.006315	PMT2 PMT5 PMT1 PMT4	4	15
biosynthesis of leucine [01.01.11.04.01]	0.006505	LEU2 BAT2 LEU9	3	8
vacuole or lysosome [42.25]	0.007195	VTC1 VTC2 VPS29 VTC4 VBA1 MYO2 VTC3	7	44
structural protein binding [16.07]	0.008072	NUP157 CHC1 CLC1 NSP1 SPA2 PDS5 BNI1 SEC16	8	56
phospholipid metabolism [01.06.02.01]	0.008404	SCT1 URA7 INO2 CHO2 AYR1 URA8 MCD4 SAC1 PLB2	9	68
homeostasis of phosphate [34.01.03.03]	0.009383	PHO89 PHO86 PHO84	3	9
aminoadipic acid pathway [01.01.06.06.01.03]	0.009383	LYS2 LYS20 LYS9	3	9
cell growth / morphogenesis [40.01]	0.009601	SLA1 SHS1 BOI2 CLC1 PHO81 MYO1 YAK1 FAR1 TOR2 PAH1 EFR3 APP1 SRV2 BNI4 SLA2 BNI1 STI1 MSB1	18	189
MIPS Phenotypes (142 categories)				
Actin cytoskeleton mutants [52.30.10]	0.000147	SLA1 BEM2 PAN1 CCT3 TOR2 SRV2 SLA2 BNI1 MDM20 MYO2	10	48
Heat-sensitivity (ts) [12.05]	0.000177	SLA1 RPG1 VMA2 NOP1 COP1 VMA1 SEC3 BEM2 SEC53 STT3 SEC27 CHC1 SPT6 RPN1 THS1 RPI1 CYR1 NSP1 BCK1 YAK1 VPS1 NOP56 ERO1 SRV2 SLA2 SEC21 MDM20 SEC63 MYO2 SSE1 HSP82 HTS1	32	313
other cell cycle defects [22.99]	0.002543	PGI1 CDC9 INO2 NUM1 RSC3 BEM2 SPT16 MYO1 DYS1 BAR1 PAN1 CCT3 VPS1 ERG3 ERG6 MIH1 POL1 BNI1 SIN3 BUB3 SEC63	21	207
Slow-growth (slg) [12.15]	0.002872	FUN12 SUB2 ADK1 BEM2 ZRT1 CLC1 RPS0A MYO1 SSZ1 DYS1 SFB3 ENO2 SCP160 ERG20 ERG6 ASC1 SSB2 MDM20 BUB3 ALD6 SSE1 SPN1 TIF3	23	237

Ontology	p- value	Genes in ontology category	k	f
Secretory mutants [52.45]	0.004073	COP1 SEC7 SEC3 SEC53 SEC27 PMR1 ERO1 SEC21 MYO2	9	61
Cold-sensitivity (cs) [12.10]	0.008295	VMA2 VMA1 SSB1 RPS11A NUM1 SSZ1 CCT3 LHS1 TUB1 ASC1 SSB2 TIF3	12	105
Bud localization [52.10.05]	0.008728	BUD3 MYO1 BUD4 SPA2 SRV2 BNI1	6	35
MIPS Subcellular Localization (48 categories)				
cytoplasm [725]	<1e-14	SSA1 FUN12 CDC19 AIM2 SWH1 SLA1 URA7 ILS1 YPK3 AKL1 RPG1 PHO88 LYS2 GRS1 VMA2 RPS6B PGI1 PYC2 LEU2 HIS4 PGK1 OSH2 PSA1 PMT5 GET3 TRM3 COP1 CDC9 VMA1 UFD2 SSB1 RPS11A SEC7 ADK1 RSC3 ASP1 MSN5 SVF1 SXM1 PHO8 SAM2 EMI2 FDC1 GEA2 SPF1 RML2 DLD3 SEC3 SAH1 MET6 KAP123 BOI2 BEM2 GRX4 VTC2 BLM10 FRS2 SEC53 LSB3 RPL2A PUF4 KAP122 RPS2 RPL9A ARO2 MCM6 CHC1 SPT16 GUS1 HXK2 ADE6 VAS1 RPS23A PPT1 ASN2 CYS4 CHO2 CLC1 ADE3 RPS0A PHO81 YHB1 PFK1 SDA1 MES1 ECM29 RPL8A VPS29 RPN1 AAP1 SSZ1 DYS1 SPL2 KEL1 ENO2 GND1 GPI16 RPS4B THS1 RPI1 AYR1 SSL2 UBP7 DAL81 CYR1 VTC4 CCT3 BBC1 MHP1 SCP160 ARG3 BCK1 CCT7 LSM1 YAK1 FAR1 ERG20 UBP12 TDH2 TAH11 ANB1 PTK2 URA8 HOM6 RPS4A HMS2 BAT2 URA6 UGP1 RGT1 FBA1 TEF4 FAS1 DPH2 UBA1 SAC1 URA1 VPS1 PXL1 DPS1 SPA2 SSA2 PDC1 ARP6 RPS31 SAM1 TOS4 FRE1 BNA5 RCK2 YEF3 ACO1 RPP0 NIT3 RPS22B IKI3 VIP1 ERG6 PSP2 IMD4 TUB1 CLU1 MIH1 VBA1 YTA12 ASC1 ADE17 PAH1 HSC82 PFK2 YDJ1 RPL9B MKT1 APP1 POL1 SSB2 VID27 ADE12 BNI4 SLA2 BNI1 RPL18B EMW1 ACC1 LYS9 SIN3 MDM38 MDM20 ADH1 WRS1 RPS19A RIB4 BUB3 STI1 RKI1 RPS7A EFT1 RPB2 GLN4 MSB1 MYO2 ALA1 REV1 GDH1 TAE2 RRP12 ERG10 ALD6 SEC16 RPS6A SSE1 BEM3 CDC60 FAS2 HSP82 HTS1 TKL1 ASN1 TIF3	219	2879
cell periphery [715]	2.08E-07	AKL1 ECM33 IST2 SHS1 SNQ2 ITR1 SEC3 BOI2 LSB3 CRP1 KEL1 SLN1 PAN1 CYR1 PHO86 UGP1 SAC1 PXL1 SPA2 TCB3 EFR3 RSN1 TCB2 SRV2 BNI4 SLA2 MID1 TCB1 MYO2 DIP5 CTR1	31	216
neck [705.03]	1.69E-05	EDE1 AKL1 BUD3 SHS1 SEC3 BOI2 BEM2 LSB3 MYO1 KEL1 BUD4 PXL1 SPA2 BNI4 BNI1 MSB1 MYO2 BEM3	18	112
cytoskeleton [730]	0.000405	SLA1 BUD3 LSB3 SDA1 MYO1 PAN1 MHP1 SPA2 ARP6 TUB1 SRV2 BNI4 SLA2 BNI1 MYO2	15	107
ER [735]	0.000483	PMT2 ERV46 SCT1 ECM33 PHO88 PHO89 PMT1 GET3 COP1 LCB2 SPF1 TIR1 VTC1 VTC2 STT3 CWH41 GUP1 PMR1 ZRT1 CHO2 LAG1 ERG11 RPN1 AVT7 AYR1 KAR2 NSP1 SCP160 PHO86 MNN5 OPT1 PMT4 LHS1 MCD4 SAC1 ERG3 ACS2 FRE1 HSP60 ERG6 ERO1 YDJ1	46	537

Ontology	p- value	Genes in ontology category	k	f
		ACC1 ALE1 SEC63 SEC16		
golgi [740]	0.000738	ERV46 PEP1 RPG1 COP1 SEC7 SEC26 TRS120 GEA2 GDA1 SEC27 PMR1 VPS29 MNN5 SAC1 VPS1 SEC21	16	125
plasma membrane [720]	0.003297	FAT1 IST2 SNQ2 MKC7 ITR1 SEC3 VTC1 SLN1 CYR1 GEF1 FRE1 PHO84 PLB2 ZRC1 SLA2 MID1 ITR2 DIP5 CTR1	19	184
transport vesicles [745]	0.006326	RPG1 COP1 SEC7 SEC26 SEC27 SEC21 SEC16	7	43
ER lumen [735.05]	0.009383	AYR1 KAR2 LHS1	3	9
MIPS Protein Complexes (1142 categories)				
Complex Number 341 [550.2.341]	1.33E-10	SAH1 MET6 FRS2 SEC53 GUS1 CYS4 PFK1 GND1 THS1 CYR1 SCP160 TEF4 UBA1 ACO1 ERG6 ERG13 CLU1 RSN1	18	55
Complex Number 244 [550.2.244]	7.12E-09	ILS1 GRS1 ADE6 ADE3 SSZ1 SCP160 ERG20 UBA1 DPS1 ACS2 CLU1 ADE17 PFK2 ALA1 ERG10	15	47
Complex Number 41, probably intermediate and energy metabolism [550.1.41]	6.53E-07	URA7 PSA1 KAP123 SEC27 GUS1 VAS1 SAM1 CLU1 ACC1 TCB1 RPB2	11	34
Complex Number 214, probably transcription/DNA maintanance/chromatin structure [550.1.214]	1.05E-06	NOP1 KAP123 SPT15 VAS1 MES1 MYO1 TEF4 VPS1 CLU1 PFK2 SIN3 ADH1 RPB2	13	50
Complex Number 79, probably membrane biogenesis and traffic [550.1.79]	4.48E-06	TOS1 PGK1 COP1 SEC26 SEC27 SAM1 SEC21	7	15
cytoplasmic ribosomal small subunit [500.40.20]	5.21E-06	RPS6B RPS11A RPS2 RPS23A RPS0A RPS4B RPS4A RPS31 RPS22B ASC1 RPS19A RPS7A RPS6A	13	57
Complex Number 379 [550.2.379]	5.30E-06	ILS1 RPG1 GRS1 SSZ1 ERG20 ACS2 ALA1 ERG10 CDC60	9	27
Complex Number 68, probably membrane biogenesis and traffic [550.1.68]	7.29E-06	CHC1 CLC1 YHB1 ASC1 SSE1	5	7
Complex Number 195, probably transcription/DNA maintanance/chromatin structure [550.1.195]	1.26E-05	KAP123 GUS1 YHB1 PFK1 CLU1 HSC82 MKT1 RPB2	8	23
Complex Number 171, probably signalling [550.1.171]	1.86E-05	LYS2 SXM1 KAP123 HSC82 ADH1	5	8
Complex Number 134 [550.2.134]	1.89E-05	ECM33 SEC27 PFK1 ECM29 RPN1 BBC1 MKT1 MYO2 RPA190	9	31
Complex Number 135, probably RNA metabolism [550.1.135]	2.92E-05	FUN12 RPG1 NOP1 BEM2 SPT16 VPS1 CLU1	7	19
Complex Number 192, probably transcription/DNA maintanance/chromatin structure [550.1.192]	2.92E-05	SPT15 RSC8 VPS1 PDC1 YEF3 SIN3 ADH1	7	19
Complex Number 316 [550.2.316]	3.28E-05	ILS1 PYC2 KAP122 SEC27 GUS1 ECM29 GND1 ACC1 RPO31 RPA190 CDC60	11	49
Complex Number 123, probably protein/RNA transport [550.1.123]	4.29E-05	LCB2 SAM2 GEA2 KAP123 ECM29 SAM1 CLU1	7	20
Complex Number 17, probably cell polarity and structure [550.1.17]	6.52E-05	KAP123 MYO1 YEF3 HSC82 ADH1 MYO2	6	15

Ontology	p- value	Genes in ontology category	k	f
Complex Number 196, probably transcription/DNA maintanance/chromatin structure [550.1.196]	6.52E-05	SPT15 VPS1 PDC1 YEF3 PFK2 ADH1	6	15
Complex Number 535 [550.2.535]	9.98E-05	EDE1 RPG1 COP1 BEM2 LHS1 SRV2	6	16
Complex Number 27, probably intermediate and energy metabolism [550.1.27]	0.000142	PGK1 SPF1 ENO2	3	3
Complex Number 175, probably signalling [550.1.175]	0.000142	PPT1 HSC82 HSP82	3	3
Complex Number 266 [550.2.266]	0.000142	SSL2 MKT1 STI1	3	3
Complex Number 103 [550.2.103]	0.000148	ADE3 SSZ1 THS1 URA1 PFK2 ALA1	6	17
Complex Number 69 [550.2.69]	0.000221	COP1 SEC26 SEC27 PHO86 SEC21	5	12
Complex Number 329 [550.2.329]	0.000226	ECM29 UBP7 HOM6 PHO84	4	7
Complex Number 211, probably transcription/DNA maintanance/chromatin structure [550.1.211]	0.000277	COP1 VMA1 SEC27 PDC1 SAM1 POL1 FAS2	7	26
Complex Number 388 [550.2.388]	0.000281	ADK1 SEC53 GUS1 CYS4 YHB1 PFK1 TEF4 CLU1	8	34
Complex Number 156 [550.2.156]	0.000344	SLA1 PEP1 RPN1 PHO84 YHM2	5	13
Complex Number 231, probably transcription/DNA maintanance/chromatin structure [550.1.231]	0.000344	VMA1 ECM29 CLU1 ASC1 YDJ1	5	13
Complex Number 86, probably protein synthesis turnover [550.1.86]	0.000344	FUN12 RPL2A ADE3 RAT1 TAE2	5	13
Complex Number 34, probably intermediate and energy metabolism [550.1.34]	0.000344	ENO2 FBA1 PDC1 HSC82 ADH1	5	13
Complex Number 70, probably membrane biogenesis and traffic [550.1.70]	0.000404	SEC7 KAP123 ECM29 SAM1 SRV2 ADH1	6	20
COPI [260.30.10]	0.000434	COP1 SEC26 SEC27 SEC21	4	8
Complex Number 167, probably signalling [550.1.167]	0.000544	PHO81 CYR1 SRV2	3	4
Complex Number 149, probably RNA metabolism [550.1.149]	0.000587	RPG1 NOP1 SEC7 BEM2 CYS4 SDA1 CYR1 NOP56 YEF3 FPR4 CLU1 RPA190 RRP12	13	88
Complex Number 54, probably intermediate and energy metabolism [550.1.54]	0.001307	HIS4 PDC1 SAM1	3	5
Complex Number 474 [550.2.474]	0.001307	SCP160 CLU1 MKT1	3	5
Complex Number 18, probably cell polarity and structure [550.1.18]	0.001389	SLA1 VMA1 LSB3 CHC1 SLA2	5	17
Complex Number 106, probably protein synthesis turnover [550.1.106]	0.001803	BEM2 SSZ1 SCP160 ASC1	4	11
Complex Number 230, probably transcription/DNA	0.001803	VPS1 PDC1 ADH1 WRS1	4	11

Ontology	p- value	Genes in ontology category	k	f
maintanance/chromatin structure [550.1.230]				
Complex Number 212, probably transcription/DNA maintanance/chromatin structure [550.1.212]	0.001889	PGK1 SHS1 MSH6 RSC8 VAS1 VPS1 HSC82	7	35
Complex Number 338 [550.2.338]	0.002333	COP1 SEC26 SEC27 AYR1 MAE1 SEC21 STI1 CTR1	8	46
Complex Number 170, probably signalling [550.1.170]	0.002333	BLM10 GUS1 PFK1 KEL1 TDH2 TEF4 YEF3 ERG13	8	46
Complex Number 283 [550.2.283]	0.002394	BEM2 SEC53 SEC27 TEF4 UBA1	5	19
Complex Number 396 [550.2.396]	0.002513	SPT16 ACO1 CLU1	3	6
Complex Number 136, probably RNA metabolism [550.1.136]	0.002594	PGI1 PDC1 YEF3 ADH1	4	12
Complex Number 48, probably intermediate and energy metabolism [550.1.48]	0.002722	CYS4 SSC1	2	2
Complex Number 3 [550.2.3]	0.002722	AKL1 HTS1	2	2
Complex Number 121, probably protein/RNA transport [550.1.121]	0.002722	ILS1 GET3	2	2
Complex Number 235 [550.2.235]	0.002722	PPS1 ADE13	2	2
Complex Number 359 [550.2.359]	0.002722	COP1 SLN1	2	2
Complex Number 61, probably intermediate and energy metabolism [550.1.61]	0.002722	PFK1 PFK2	2	2
Fatty acid synthetase, cytoplasmic [170]	0.002722	FAS1 FAS2	2	2
Clathrin [260.10]	0.002722	CHC1 CLC1	2	2
Phosphofructokinase [340]	0.002722	PFK1 PFK2	2	2
m-AAA protease complex [350.10.10]	0.002722	AFG3 YTA12	2	2
Complex Number 520 [550.2.520]	0.003611	SAH1 MET6 SEC53 GUS1 GND1 ACO1 FPR4	7	39
Complex Number 94 [550.2.94]	0.003611	SAH1 MET6 SEC53 GUS1 GND1 ACO1 FPR4	7	39
Complex Number 267 [550.2.267]	0.003844	YSP2 SEC53 ERG20 TEF4 ACO1	5	21
Complex Number 99 [550.2.99]	0.004228	COP1 FAR1 CLU1	3	7
Complex Number 224 [550.2.224]	0.004228	ADK1 PHO81 YHB1	3	7
Complex Number 35, probably intermediate and energy metabolism [550.1.35]	0.004228	VMA1 KAP123 EMW1	3	7
Complex Number 53, probably intermediate and energy metabolism [550.1.53]	0.004228	GEA2 KAP123 ADH1	3	7
Complex Number 250 [550.2.250]	0.004228	COP1 ECM29 TCB1	3	7

Ontology	p- value	Genes in ontology category	k	f
Complex Number 150 [550.2.150]	0.004765	BUD3 CCT3 NOP56 CLU1 RRP12	5	22
Complex Number 9, probably cell cycle [550.1.9]	0.004827	PDC1 BNI1 RPO31 RPA190	4	14
Complex Number 103, probably protein synthesis turnover [550.1.103]	0.004827	KAP123 SEC27 GUS1 TEF4	4	14
Complex Number 240 [550.2.240]	0.006315	COP1 ADK1 SEC27 CLU1	4	15
Complex Number 35 [550.2.35]	0.006315	MET6 SEC53 GUS1 IMD4	4	15
Complex Number 39, probably intermediate and energy metabolism [550.1.39]	0.006505	KAP123 SAM1 CLU1	3	8
Complex Number 454 [550.2.454]	0.006505	SAH1 SRV2 STI1	3	8
Complex Number 203, probably transcription/DNA maintanance/chromatin structure [550.1.203]	0.007059	RSC8 INO80 VPS1 SIN3 ADH1	5	24
Complex Number 222 [550.2.222]	0.007884	PFK1 PFK2	2	3
Complex Number 498 [550.2.498]	0.007884	NOP1 SEC27	2	3
Nop56p/Nop1p complex [440.12.30]	0.007884	NOP1 NOP56	2	3
Complex Number 65, probably membrane biogenesis and traffic [550.1.65]	0.007884	PGI1 ADH1	2	3
Complex Number 175 [550.2.175]	0.007884	CLU1 STI1	2	3
Complex Number 91, probably protein synthesis turnover [550.1.91]	0.007884	SSA1 RPB2	2	3
Complex Number 109, probably protein synthesis turnover [550.1.109]	0.008728	NOP1 BEM2 SWI3 SAM1 ADH1 RRP12	6	35
Complex Number 304 [550.2.304]	0.009383	DLD3 ACS2 ERG10	3	9
Complex Number 194, probably transcription/DNA maintanance/chromatin structure [550.1.194]	0.009383	NET1 YEF3 ADH1	3	9
Complex Number 23, probably intermediate and energy metabolism [550.1.23]	0.009383	SWH1 OSH2 NUM1	3	9

Yeast Strains

Table 19. Yeast strains

Strains	Genotype	Source	Note (Reference)
Strains used for strain construction			
BY4741	*MATa his3Δ1 leu2Δ0 met15Δ0 ura3Δ0*	Thermofisher/Dharmacon	[423]
UCC1188	*MATα his3Δ200 trp1(Δ901 or ::HIS3) leu2Δ1 lys2-801 ura2(-52 or -167) RDN1::URA3 hht1-hhf1::LEU2 Δhht2-hhf2::HIS3 pMP9 (HHT2-HHF2-LYS2-CEN ARS)*	Daniel E. Gottschling	[406]
Y7092	*MATα* can1Δ::STE2pr-Sp_his5 lyp1Δhis3Δ1 leu2Δ0 ura3Δ0 met15Δ0	Charlie Boone	[364]
YDB19	*MATα can1Δ::STE2pr-Sp_his5 lyp1Δhis3Δ1 leu2Δ0 ura3Δ0 met15Δ0 fpr4Δ::NATMX4*	This study	From Y7092
YNS3	*MATa his3Δ1 leu2Δ0 met15Δ0 ura3Δ0 fpr3Δ::KANMX4*	Open Biosystems	[424]
YNS5	*MATa his3Δ1 leu2Δ0 met15Δ0 ura3Δ0 fpr4Δ::KANMX4*	Open Biosystems	[424]
YNS6	*MATa his3Δ1 leu2Δ0 met15Δ0 ura3Δ0 fpr3Δ::URA3 fpr4Δ::NATMX4*	This study	Generated from BY4741 by transformation
Strains used for synthetic genetic array analysis			
The MAT a yeast deletion collection	*MATa his3Δ1 leu2Δ0 met15Δ0 ura3Δ0 xxxΔ::KANMX4*	Thermofisher Dharmacon	[424]
YNS35	*MATα can1Δ::STE2pr-Sp_his5 lyp1Δhis3Δ1 leu2Δ0 ura3Δ0 met15Δ0 fpr4Δ::NATMX4 fpr3Δ::LEU2 (prs316 FPR4)*	This study	From YDB19
Strains used for sequencing			
BY4741 (YNS1)	*MATa his3Δ1 leu2Δ0 met15Δ0 ura3Δ0*	Open Biosystems	Open Biosystems
YNS3	*MATa his3Δ1 leu2Δ0 met15Δ0 ura3Δ0 fpr3Δ::KANMX4*	Open Biosystems	[424]
YNS5	*MATa his3Δ1 leu2Δ0 met15Δ0 ura3Δ0 fpr4Δ::KANMX4*	Open Biosystems	[424]
YNS11	*MATa his3Δ1 leu2Δ0 met15Δ0 ura3Δ0 fpr3Δ::KANMX4 fpr4Δ::NATMX4*	This study	Generated from DMA FPR3 KO by transformation
YNS8	*MATa his3Δ1 leu2Δ0 met15Δ0 ura3Δ0 sir2Δ::KANMX4*	Thermofisher Dharmacon	[424]
UCC1188	*MATα his3Δ200 trp1(Δ901 or ::HIS3) leu2Δ1 lys2-801 ura2(-52 or -167) RDN1::URA3 hht1-hhf1::LEU2 Δhht2-hhf2::HIS3 pMP9 (HHT2-HHF2-LYS2-CEN ARS)*	Daniel E. Gottschling	[406]
YNS13	*MATα his3Δ200 leu2Δ1 lys2-801 ura2(-52 or -167) RDN1::URA3 hht1-hhf1::LEU2*	This study	Generated from a cross of

Strains	Genotype	Source	Note (Reference)
	Δhht2-hhf2::HIS3 pMP9 (HHT2-HHF2-LYS2-CEN ARS) fpr4Δ::KAN		UCC1188 and YNS5
Strains used for Northern blots			
UCC1188	*MATα his3Δ200 trp1(Δ901 or ::HIS3) leu2Δ1 lys2-801 ura2(-52 or -167) RDN1::URA3 hht1-hhf1::LEU2 Δhht2-hhf2::HIS3 pMP9 (HHT2-HHF2-LYS2-CEN ARS)*	Daniel E. Gottschling	[406]
YNS22	*MATα his3Δ200 leu2Δ1 lys2-801 ura2(-52 or -167) RDN1::URA3 hht1-hhf1::LEU2 Δhht2-hhf2::HIS3 pMP9 (HHT2-HHF2-LYS2-CEN ARS) fpr3Δ::KAN*	This study	Generated from a cross of UCC1188 and YNS11
YNS13	*MATα his3Δ200 leu2Δ1 lys2-801 ura2(-52 or -167) RDN1::URA3 hht1-hhf1::LEU2 Δhht2-hhf2::HIS3 pMP9 (HHT2-HHF2-LYS2-CEN ARS) fpr4Δ::KAN*	This study	Generated from a cross of UCC1188 and YNS5
YNS20	*MATα his3Δ200 leu2Δ1 lys2-801 ura2(-52 or -167) RDN1::URA3 hht1-hhf1::LEU2 Δhht2-hhf2::HIS3 pMP9 (HHT2-HHF2-LYS2-CEN ARS) sir2Δ::KAN*	This study	Generated from transformation of UCC1188
Strains used for spotting assays			
UCC1188	*MATα his3Δ200 trp1(Δ901 or ::HIS3) leu2Δ1 lys2-801 ura2(-52 or -167) RDN1::URA3 hht1-hhf1::LEU2 Δhht2-hhf2::HIS3 pMP9 (HHT2-HHF2-LYS2-CEN ARS)*	Daniel E. Gottschling	[406]
YNS22	*MATα his3Δ200 leu2Δ1 lys2-801 ura2(-52 or -167) RDN1::URA3 hht1-hhf1::LEU2 Δhht2-hhf2::HIS3 pMP9 (HHT2-HHF2-LYS2-CEN ARS) fpr3Δ::KAN*	This study	Generated from a cross of UCC1188 and YNS11
YNS13	*MATα his3Δ200 leu2Δ1 lys2-801 ura2(-52 or -167) RDN1::URA3 hht1-hhf1::LEU2 Δhht2-hhf2::HIS3 pMP9 (HHT2-HHF2-LYS2-CEN ARS) fpr4Δ::KAN*	This study	Generated from a cross of UCC1188 and YNS5
YNS31	*MATα his3Δ200 leu2Δ1 lys2-801 ura2(-52 or -167) RDN1::URA3 hht1-hhf1::LEU2 Δhht2-hhf2::HIS3 pMP9 (HHT2-HHF2-LYS2-CEN ARS) fpr3Δ::KAN fpr4Δ::NAT*	This study	Generated from transformation of YNS22
YNS20	*MATα his3Δ200 leu2Δ1 lys2-801 ura2(-52 or -167) RDN1::URA3 hht1-hhf1::LEU2 Δhht2-hhf2::HIS3 pMP9 (HHT2-HHF2-LYS2-CEN ARS) sir2Δ::KAN*	This study	Generated from transformation of UCC1188
UCC1369	*MATa ade2Δ::HIS3 his3Δ200 leu2Δ0 lys2Δ0 met15Δ0 trp1Δ63 ura3Δ0 adh4::URA3-TEL (VII-L) ADE2-TEL (VR) Δhhf2-hht2::MET15 Δhhf1-hht1::LEU2pMP9 (LYS2 CEN ARS)-HHF2-HHT2*	Daniel E. Gottschling	[406]
YNS45	*MATa ade2Δ::HIS3 his3Δ200 leu2Δ0 lys2Δ0 met15Δ0 trp1Δ63 ura3Δ0 adh4::URA3-TEL (VII-L) ADE2-TEL (VR) Δhhf2-hht2::MET15 Δhhf1-hht1::LEU2pMP9 (LYS2 CEN ARS)-HHF2-HHT2 fpr3Δ::KAN*	This study	Generated from transformation of UCC1369
YNS44	*MATa ade2Δ::HIS3 his3Δ200 leu2Δ0 lys2Δ0 met15Δ0 trp1Δ63 ura3Δ0 adh4::URA3-TEL (VII-L) ADE2-TEL (VR) Δhhf2-hht2::MET15 Δhhf1-hht1::LEU2pMP9 (LYS2 CEN ARS)-HHF2-HHT2 fpr4Δ::KAN*	This study	Generated from transformation of UCC1369
YNS64	*MATa ade2Δ::HIS3 his3Δ200 leu2Δ0 lys2Δ0 met15Δ0 trp1Δ63 ura3Δ0 adh4::URA3-TEL (VII-L) ADE2-TEL (VR) Δhhf2-hht2::MET15 Δhhf1-hht1::LEU2pMP9 (LYS2 CEN ARS)-HHF2-HHT2 fpr3Δ::KAN fpr4Δ::NAT*	This study	Generated from transformation of YNS45

Strains	Genotype	Source	Note (Reference)
YNS47	*MATa ade2Δ::HIS3 his3Δ200 leu2Δ0 lys2Δ0 met15Δ0 trp1Δ63 ura3Δ0 adh4::URA3-TEL (VII-L) ADE2-TEL (VR) Δhhf2-hht2::MET15 Δhhf1-hht1::LEU2pMP9 (LYS2 CEN ARS)-HHF2-HHT2 sir2Δ::KAN*	This study	Generated from transformation of UCC1369
UCC7266	*MATa ade2? his3? leu2? lys2? ura3? ADE2-TEL (VR) hml@::URA3 hhf2-hht2::MET15 hhf1-hht1::LEU2 pMP9 (LYS2 CEN ARS)-HHF2-HHT2*	Daniel E. Gottschling	[406]
YNS50	*MATa ade2? his3? leu2? lys2? ura3? ADE2-TEL (VR) hml@::URA3 hhf2-hht2::MET15 hhf1-hht1::LEU2 pMP9 (LYS2 CEN ARS)-HHF2-HHT2 fpr3Δ::KAN*	This study	Generated from transformation of UCC7266
YNS52	*MATa ade2? his3? leu2? lys2? ura3? ADE2-TEL (VR) hml@::URA3 hhf2-hht2::MET15 hhf1-hht1::LEU2 pMP9 (LYS2 CEN ARS)-HHF2-HHT2 fpr4Δ::NAT*	This study	Generated from transformation of UCC7266
YNS57	*MATa ade2? his3? leu2? lys2? ura3? ADE2-TEL (VR) hml@::URA3 hhf2-hht2::MET15 hhf1-hht1::LEU2 pMP9 (LYS2 CEN ARS)-HHF2-HHT2 fpr3Δ::KAN fpr4Δ::NAT*	This study	Generated from transformation of YNS52
YNS54	*MATa ade2? his3? leu2? lys2? ura3? ADE2-TEL (VR) hml@::URA3 hhf2-hht2::MET15 hhf1-hht1::LEU2 pMP9 (LYS2 CEN ARS)-HHF2-HHT2 sir2Δ::KAN*	This study	Generated from transformation of UCC7266
Strains used for propagation assays			
UCC1188	*MATα his3Δ200 trp1(Δ901 or ::HIS3) leu2Δ1 lys2-801 ura2(-52 or -167) RDN1::URA3 hht1-hhf1::LEU2 Δhht2-hhf2::HIS3 pMP9 (HHT2-HHF2-LYS2-CEN ARS)*	Daniel E. Gottschling	[406]
YNS190	*MATα his3Δ200 leu2Δ1 lys2-801 ura2(-52 or -167) RDN1::URA3 hht1-hhf1::LEU2 Δhht2-hhf2::HIS3 pMP9 (HHT2-HHF2-LYS2-CEN ARS) fpr3Δ::KAN*	This study	Generated from UCC1188 by transformation
YNS193	*MATα his3Δ200 leu2Δ1 lys2-801 ura2(-52 or -167) RDN1::URA3 hht1-hhf1::LEU2 Δhht2-hhf2::HIS3 pMP9 (HHT2-HHF2-LYS2-CEN ARS) fpr4Δ::KAN*	This study	Generated from UCC1188 by transformation
YNS245	*MATα his3Δ200 trp1(Δ901 or ::HIS3) leu2Δ1 lys2-801 ura2(-52 or -167) RDN1::URA3 hht1-hhf1::LEU2 Δhht2-hhf2::HIS3 pMP9 (HHT2-HHF2-LYS2-CEN ARS) fpr3Δ::NAT fpr4Δ::KAN*	This study	Generated from UCC1188 by transformation
YNS182	*MATα his3Δ200 trp1(Δ901 or ::HIS3) leu2Δ1 lys2-801 ura2(-52 or -167) RDN1::URA3 hht1-hhf1::LEU2 Δhht2-hhf2::HIS3 pMP9 (HHT2-HHF2-LYS2-CEN ARS) sir2Δ::KAN*	This study	Generated from UCC1188 by transformation
Strains used for rescue qRT-PCR			
YNS99	*MATα his3Δ200 leu2Δ1 lys2-801 ura2(-52 or -167) RDN1::URA3 hht1-hhf1::LEU2 Δhht2-hhf2::HIS3 pMP9 (HHT2-HHF2-LYS2-CEN ARS) fpr4Δ::NAT trp1Δ::KAN pRS414*	This study	Generated from transformation of YNS13
YNS99	*MATα his3Δ200 leu2Δ1 lys2-801 ura2(-52 or -167) RDN1::URA3 hht1-hhf1::LEU2 Δhht2-hhf2::HIS3 pMP9 (HHT2-HHF2-LYS2-CEN ARS) fpr4Δ::NAT trp1Δ::KAN pRS414(FPR4)*	This study	Generated from transformation of YNS13

Strains	Genotype	Source	Note (Reference)
YNS99	*MATα his3Δ200 leu2Δ1 lys2-801 ura2(-52 or -167) RDN1::URA3 hht1-hhf1::LEU2 Δhht2-hhf2::HIS3 pMP9 (HHT2-HHF2-LYS2-CEN ARS) fpr4Δ::NAT trp1Δ::KAN pRS414(FLAG-FPR4)*	This study	Generated from transformation of YNS13
YNS93	*MATα his3Δ200 leu2Δ1 lys2-801 ura2(-52 or -167) RDN1::URA3 hht1-hhf1::LEU2 Δhht2-hhf2::HIS3 pMP9 (HHT2-HHF2-LYS2-CEN ARS) 3XFLAG-FPR4Δ1-180*	This study	Generated from transformation of YNS13
YNS95	*MATα his3Δ200 leu2Δ1 lys2-801 ura2(-52 or -167) RDN1::URA3 hht1-hhf1::LEU2 Δhht2-hhf2::HIS3 pMP9 (HHT2-HHF2-LYS2-CEN ARS) 3XFLAG-FPR4Δ181-392*	This study	Generated from transformation of UCC1188

Primers

Table 20. Primers

Gene	Forward/ Reverse	Sequence (5'-3')
qRT PCR primers used for validating differentially expressed genes in WT, Δfpr3, Δfpr4, Δfpr3Δfpr4 cells (Figure 28)		
PHO5	forward	TTGTAACTCATGTCCTGCTTGG
PHO5	reverse	TCAATCTCTTGGCAATGTCATC
PHO84	forward	TCTGTACCATTCTGCAAACCAC
PHO84	reverse	AGTCACCACCGATACCAATACC
SIT1	forward	TCTATTAGGTTTCGGTGCAGGT
SIT1	reverse	GAGGTTACTACCGCCATTCTTG
TCM1	forward	ACCTCCATTAACCACAAGATTTACA
TCM1	reverse	AGTCGTTCTTAATTTCACCGTAGTG
GPD1	forward	AGAAACGTCAAGGTTGCTAGGC
GPD1	reverse	GGCCATTCAACAACTCCTTTTC
qRT PCR primers used for validating incomplete elongation Δfpr3Δtrf5 and Δfpr3Δfpr4Δtrf5 cells (Figure 30 D)		
UTP9 (5' end)	forward	TTTGGATTTGGTGGCGAGCTTC
UTP9 (5' end)	reverse	ATTGTTCTTTTGTGCGACGCTT
UTP9 (3' end)	forward	AGAAATGTTGAGGAGGCAAGCA
UTP9 (3' end)	reverse	TCAAGCTTTTCAACAGGCGATG
SSF1 (5' end)	forward	ATGGCCAAGAGAAGACAAAAGA
SSF1 (5' end)	reverse	GATTTGGCGGAAGTCCTTTACT
SSF1 (3' end)	forward	AAGAAGAAAAGCTAGAGCAGCAGA
SSF1 (3' end)	reverse	GCTACCATAATGTTCGCTGTCA
ACT1 (5' end)	forward	AGGTTGCTGCTTTGGTTATTGA
ACT1 (5' end)	reverse	CTACCGACGATAGATGGGAAGA
ACT1 (3' end)	forward	TGGTGGTTCTATCTTGGCTTCT
ACT1 (3' end)	reverse	AACACTTGTGGTGAACGATAGATG
GPD1	forward	AGAAACGTCAAGGTTGCTAGGC
GPD1	reverse	GGCCATTCAACAACTCCTTTTC
genomic PCR primers used for validating rDNA reporter loss (Figure 35 C)		
mTRP-URA	forward	AGAAAAGGAGAGGGCCAAGA
mTRP-URA	reverse	AATGCGTCTCCCTTGTCATC
qRT PCR primers for rDNA reporter rescue (Figure 36 D and Figure 37)		
mTRP	forward	AGAAAAGGAGAGGGCCAAGA

Gene	Forward/ Reverse	Sequence (5'-3')
mTRP	reverse	ATCTCCAAGCTGCCTTTGTG
Primers used for Northern analysis probes		
URA3	forward	TGCACGAAAAGCAAACAAAC
URA3	reverse	AATGCGTCTCCCTTGTCATC
NTS1	forward	CGTTGCAAAGATGGGTTG
NTS1	reverse	CTAGTTTCTTGGCTTCCTATGC
NTS2	forward	TTTAACGGAAACGCAGGTGA
NTS2	reverse	CCTCCCAACTACTTTTCCTCA
ADE2	forward	TATGGCGGAATGTGAACAAA
ADE2	reverse	AATCATAAGCGCCAAGCAGT